Facultad de Ciencias
Departamento de Química Orgánica

Synthesis and Characterization of Subporphyrazines and Subnaphthalocyanines: Optical Properties and Applications in Molecular Photovoltaics

Memoria presentada por
DAVID GUZMAN RIOS
Para optar al grado de
DOCTOR EN QUÍMICA ORGÁNICA

Madrid, 2019

La presente Tesis Doctoral ha sido realizada en el Departamento de Química Orgánica de la Universidad Autónoma de Madrid bajo la dirección de los Profesores Tomás Torres Cebada y M. Salomé Rodríguez Morgade.

Abbreviations and acronyms

We have used standard Organic Chemistry abbreviations and acronyms following the recommendation of the "guidelines for authors", *J. Org. Chem.* **2016**, which can be found in the journal webpage:
http://pubs.acs.org/paragonplus/submission/joceah/joceah_authguide.pdf

A	Acceptor
AcOH	Acetic acid
CB	Conduction band
CR	Charge recombination
CS	Charge separation
CSR	Charge separation rate
CSS	Charge separation state
CT	Charge transfer
CuTC	Copper(I) thiophene-2-carboxylate
D	Donor
DFT	Density functional theory
DPV	Differential pulse voltammetry
DMAP	4-Dimethylaminopyridine
DMI	1,3-Dimethyl-2-imidazolidinone
dppf	Diphenylphosphinoferrocene
DSSC	Dye-sensitized solar cell
ε	Molar extinction coefficient
EDC	1-Ethyl-3-(3-dimethylaminopropyl)carbodiimide
EQE	External Quantum Efficiency
Fc	Ferrocene
FF	Fill factor
FTO	Fluorine-doped tin oxide
G	Guest
H	Host
HMDS	Hexamethyldisilazane
IPCE	Incident photon to current efficiency
ITO	Indium tin oxide
IVCT	Intervalence charge transfer
J_{SC}	Short-circuit current density
k_a	Association constant

λ	Wavelength
L	Linker
o-DCB	*o*-Dichlorobenzene
OTFT	Organic thin-film transistor
φ	Quantum Yield
Pc	Phthalocyanine
PCE	Power conversion efficiency
PDA	Perylenedianhydride
PET	Photoelectron transfer
PSC	Perovskite solar cell
p-TSA	*para*-Toluensulfonic acid
Pz	Porphyrazine
η	Efficiency or Yield
SubNc	Subnaphthalocyanine
SubP	Subporphyrin
SubPc	Subphthalocyanine
SubPz	Subporphyrazine
SWV	Square-wave voltammetry
τ	Lifetime
TCO	Transparent conductive oxide
$TBAPF_6$	Tetrabutylammonium hexafluorophosphate
TBP	*tert-B*utylpyridine
V_{OC}	Open-circuit voltage

Index

Introduction 1

Contracted Porphyrinoids as Organic Molecular Materials 3

Frontier Molecules of the Subphthalocyanines 21

Applications of Subphthalocyanines and Related Compounds 27

General Objectives 35

Chapter 1 ***Subporphyrazines with Extended Conjugation*** 39

1.1 State of the art on Subporphyrazines 41

1.2 Specific Objectives 48

1.3 Results and Discussion 50

1.3.1. Synthesis of the hexasulfanyl-SubPz precursors 50

1.3.2. Synthesis of oligophenylene-SubPzs 54

1.3.3. Synthesis of hexavinylene-SubPz 57

1.3.4. Optical properties of oligophenylene and vinylene SubPzs 59

1.3.5. Crystal and molecular structures 67

1.3.6. Electrochemical studies of SubPzs 5 - 13 75

1.3.7. Calculation of HOMO-LUMO levels 81

1.4 Summary and Conclusions 87

1.5 Experimental Section 89

1.5.1. Synthesis of the hexasulfanyl-SubPz precursors 91

1.5.2. Synthesis of oligophenylene-SubPzs 99

1.5.3. Synthesis of hexavinylene-SubPz 109

Chapter 2 ***Symmetrically Dodecafunctionalized Subnaphthalocyanines*** 113

2.1 State of the art on Subnaphthalocyanines 115

2.2 Specific Objectives 121

2.3 Results and Discussion 123

2.3.1. Synthesis of tetrasubstituted 2,3-naphthalenedicarbonitrile precursors .123

2.3.2. Synthesis of dodecafunctionalized subnaphthalocyanines 128

2.3.3. Optical properties of dodecafunctionalized subnaphthalocyanines 143

2.3.4. Electrochemical studies and energy levels of dodecafunctionalized SubNcs 149

2.4 Summary and Conclusions.....155

2.5 Experimental Section 156

2.5.1. Synthesis of tetrasubstituted 2,3-naphthalenedicarbonitrile precursors .156

2.5.2. Synthesis of dodecafunctionalized subnaphthalocyanines 170

Chapter 3 ***Applications of Subnaphthalocyanines and Subporphyrazines in Photovoltaic Devices*** 181

3.1 Solar Energy and Photovoltaic Devices 183

3.1.1. Inorganic solar cells 185

3.1.2. Organic photovoltaics (OPV) 186

3.1.3. Dye-Sensitized Solar Cells (DSSCs) 189

3.1.4. Hybrid solar cells 192

3.1.5. Characteristic parameters of solar cells 194

3.1.6. Fundaments of electron transfer 197

3.1.7. Photoinduced electron transfer (PET) in artificial systems 200

3.1.8. Singlet fission 202

3.2 Specific Objectives 206

3.3 Results and Discussion.....209

3.3.1. Photovoltaic studies of SubNc as electron acceptors in bulk-heterojunction polymer solar cells 209

3.3.2. Hexavinylester-SubPzs as new electron-acceptor molecules 218

3.3.3. Subporphyrazine based molecular sensitizers for DSSCs 226

3.3.4. Activating Intramolecular Singlet Fission on SubPz-Pnc_2 conjugate 242

3.4 Summary and Conclusions 251

3.5 Experimental Section 254

3.5.1 Device fabrication and photovoltaic characterization 255

3.5.2 Hexavinylester-SubPzs as new electron-acceptor molecules 259

3.5.3 Subporphyrazine based molecular sensitizers for DSSCs 264

3.5.4 Activating intramolecular Singlet Fission on SubPz-Pnc_2 conjugate 276

Resumen y Conclusiones 281

INTRODUCTION

Contracted Porphyrinoids as Organic Molecular Materials

Organic molecular materials enjoy a number of characteristics that make them very attractive for application in nanoscale optoelectronic devices.[1] These molecular materials are constituted by molecular units from organic or metal-organic origins, which can be synthesized individually and arranged in a second stage in some kind of condensed phase (e.g., crystals, liquid crystals, and thin films). Their functional versatility and the possibility of influencing their properties by modification of the molecular structure have prompted synthetic chemists to investigate novel, reliable and efficient methods for their functionalization. Key issues for their optimal performance are their molecular electronic characteristics, their supramolecular organizations, their interaction with other molecules, or the processability of the bulk material, in order to provide unconventional electrical, optical, and magnetic properties, similar to those of inorganic compounds with technological applications.[2]

Organic molecular materials are generally characterized by their lightweight, flexibility, ease of molecular design, and potential low-cost, compared with inorganic materials. Among these organic compounds, **porphyrins** (P),[3] together with their

[1] Y. Shirota, H. Kageyama, Organic Materials for Optoelectronic Applications: Overview. In *Handbook of Organic Materials for Electronic and Photonic Devices*, 2nd ed.; O. Ostroverkhova, Eds.; Elsevier-Woodhead Publishing: Oxford, U.K., **2019**, pp 1–33.

[2] a) T. J. Marks, *Science* **1985**, *227*, 881; b) V. Coropceanu, J. Cornil, D. A. da Silva Filho, Y. Olivier, R. Silbey, J.-L. Brédas, *–Rev.* **2007**, *107*, 926–952; c) N. Koch, *ChemPhysChem* **2007**, *8*, 1438–1455; d) H. Liu, J. Xu, Y. Li, Y. Li, *Acc. Chem. Res.* **2010**, *43*, 1496–1508.

[3] a) *The Porphyrin Handbook*; K. M. Kadish, K. M. Smith, R. Guilard, Eds.; Academic Press: Burlington, MA, **2000**; Vols. 1−10; **2003**, Vols. 11−14; b) *Handbook of Porphyrin Science*; K. M. Kadish, K. M. Smith, R. Guilard, Eds.; World Scientific: Singapore, **2010**; Vols. 1−15; c) T. Tanaka, A. Osuka, *Chem. Soc. Rev.* **2015**, *44*, 943–969; d) R. Paolesse, S. Nardis, D. Monti, M. Stefanelli, C. Di Natale, *Chem. Rev.* **2017**, *117*, 2517–2583.

synthetic structural relatives **phthalocyanines** (Pc),[4] **porphyrazines** (Pz),[5] and **tetrabenzoporphyrins** (BP)[6] (Figure 1), constitute a class of macrocyclic tetrapyrrolic or tetraisoindolic systems with unique physicochemical properties, which represent valuable building blocks in materials science. These families of compounds, categorized as *Porphyrinoids*, are planar macrocycles that have a two-dimensional 18 π-electron aromatic system, established on the inner perimeter of the structure, wherein its main electronic delocalization takes place (Figure 1b). The highly delocalized π-electron system defines the spectroscopic features. In particular, these compounds absorb radiation from the visible light region of the solar spectrum, thus functioning as molecular antennae.

[4] a) *The Porphyrin Handbook*; K. M. Kadish, K. M. Smith, R. Guilard, Eds.; Academic Press: Burlington, MA, **2003**; Vols. 15–20; b) G. de la Torre, G. Bottari, U. Hahn, T. Torres, Functional Phthalocyanines: Synthesis, Nanostructuration, and Electro-Optical Applications. In *Functional Phthalocyanine Molecular Materials*; J. Jiang, Eds.; Springer: Berlin, Ger., **2010**; Vol. 135, pp 1–44; c) G. de la Torre, C. G. Claessens, T. Torres, *Chem. Commun.* **2007**, 2000–2015; d) C. G. Claessens, U. Hahn, T. Torres, *Chem. Rec.* **2008**, *8*, 75–97; e) G. Bottari, G. de la Torre, D. M. Guldi, T. Torres, *Chem. Rev.* **2010**, *110*, 6768–6816; f) J. Mack, N. Kobayashi, *Chem. Rev.* **2011**, *111*, 281–321.

[5] a) N. Kobayashi, Meso-Azaporphyrins and their Analogues. In *The Porphyrin Handbook*; K. M. Kadish, K. M. Smith, R. Guilard, Eds.; Academic Press: San Diego, CA, **2000**; Vol. 2, pp 301–360; b) S. L. J. Michel, B. M. Hoffman, S. M. Baum, A. G. M. Barrett, Peripherally Functionalized Porphyrazines: Novel Metallomacrocycles with Broad, Untapped Potential. In *Progress in Inorganic Chemistry*; K. D. Karlin, Eds.; J. Wiley & Sons: New York, **2001**; Vol. 50, pp 473–590; c) P. A. Stuzhin, C. Ercolani, Porphyrazines with Annulated Heterocycles. In *The porphyrin Handbook*; K. M. Kadish, K. M. Smith, R. Guilard, Eds.; Academic Press: New York, **2003**; Vol. 15, pp 263–364; d) M. S. Rodríguez-Morgade, P. A. Stuzhin, *J. Porphyrins Phthalocyanines* **2004**, *8*, 1129.

[6] a) T. D. Lash, B. H. Novak, *Angew. Chem. Int. Ed.* **1995**, *34*, 683–685; b) N. Ono, H. Hironaga, K. Ono, S. Kaneko, T. Murashima, T. Ueda, C. Tsukamura, T. Ogawa, *J. Chem. Soc. Perkin Trans. 1* **1996**, 417–423; c) P. Chandrasekar, T. D. Lash, *Tetrahedron Lett.* **1996**, *37*, 4873–4876; d) S. Ito, T. Murashima, N. Ono, H. Uno, *Chem. Commun.* **1998**, 1661–1662; e) H. Mori, T. Tanaka, A. Osuka, *J. Mater. Chem. C* **2013**, *1*, 2500–2519; f) Y. Zhen, K. Inoue, Z. Wang, T. Kusamoto, K. Nakabayashi, S. Ohkoshi, W. Hu, Y. Guo, K. Harano, E. Nakamura, *J. Am. Chem. Soc.* **2018**, *140*, 62–65.

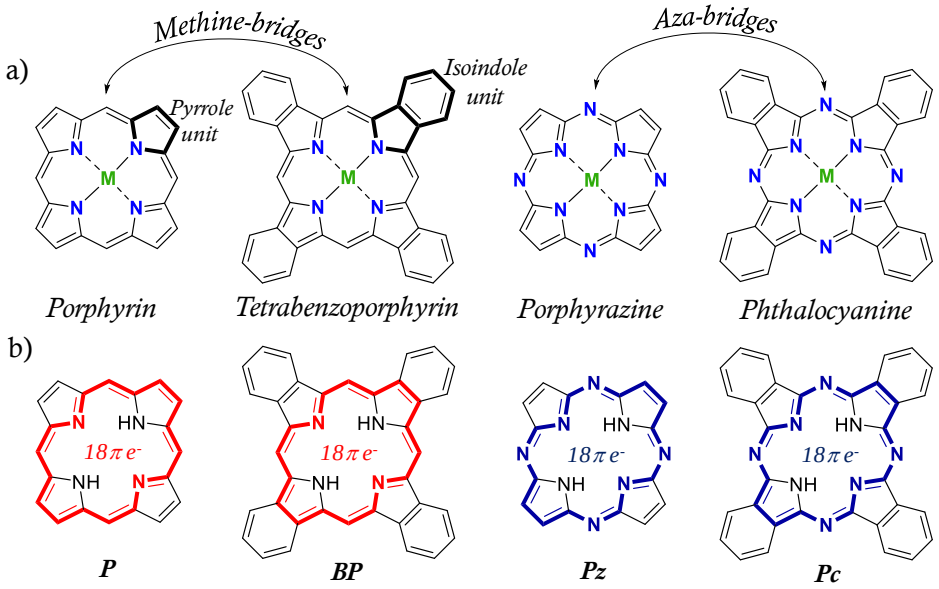

Figure 1. Porphyrinoid molecular structures: (a) Metalloporphyrinoids and (b) free-base porphyrinoids showing their main 18 π-electron delocalization.

Porphyrinoids in general are synthetically versatile compounds, in which the two hydrogen atoms of the central cavity can be replaced by more than 70 different elements of the periodic table. In addition, a wide range of substituents can be incorporated in their structure, either at the axial and/or peripheral positions of these macrocycles. These structural modifications allow tuning of some of the physical parameters of these macrocycles, such as their aggregation status or their reducing/oxidizing characteristics. The scientific interest in porphyrinoids mainly arises from their unique electronic absorptive and electrochemical properties. The latter are very suitable for their application in electronics, catalysis, sensing, light energy conversion, and in artificial photosynthetic devices, among others.

Over the last decades, there has been a growing interest in the synthesis and preparation of new structural porphyrinoid congeners, such as expanded, contracted, and isomeric analogues, by changing the number of pyrrole/isoindole units and/or of *meso*-carbon/nitrogen atoms in their structure, or also, by replacing the ring units with

other heteroaromatic rings.[7] These porphyrinoid analogues have been the subject of considerable work and remain an expanding topic, due to the marked modification of the optical, redox, and ion-coordination properties related to that of the typical macrocycles.[8]

Expanded porphyrinoids, consist of macrocycles containing more than four ring units, thus possessing larger conjugated systems than the 18 π-electron circuit of the porphyrin family. Besides, their larger central core is able to coordinate unusual ions such as actinides or anions. In addition, expanded macrocycles may provide new structural features such as Möbius aromaticity or antiaromaticity.[9] A key factor encouraging the study of expanded porphyrinoids is that they often display absorbance bands that are considerably red-shifted relative to those of tetramers, owing to their extended π-conjugation pathway.[10]

Among representative examples of expanded porphyrinoids are s*apphyrin*,[11] a pentapyrrolic macrocycle serendipitously discovered by R. B. Woodward and co-

[7] a) J. L. Sessler, S. J. Weghorn, *Expanded, Contracted, and Isomeric Porphyrins*; Pergamon Press: New York, **1997**,Vol. 15; b) J. L. Sessler, Z. Gross, H. Furuta, *Chem. Rev.* **2017**, *117*, 2201–2202; c) J. Mack, *Chem. Rev.* **2017**, *117*, 3444–3478.

[8] Heteroporphyrins, Expanded Porphyrins and Related Macrocycles. In *The Porphyrin Handbook*; K. M. Kadish, K. M. Smith, R. Guilard, Eds.; Academic Press: San Diego, **1999**; Vol. 2.

[9] a) A. Jasat, D. Dolphin, *Chem. Rev.* **1997**, *97*, 2267–2340; b) J. L. Sessler, D. Seidel, *Angew. Chem. Int. Ed.* **2003**, *42*, 5134–5175; c) J. L. Sessler, E. Tomat, *Acc. Chem. Res.* **2007**, *40*, 371–379; d) S. Saito, A. Osuka, *Angew. Chem. Int. Ed.* **2011**, *50*, 4342–4373; e) A. Osuka, S. Saito, *Chem. Commun.* **2011**, *47*, 4330–4339; f) T. Tanaka, A. Osuka, *Chem. Rev.* **2017**, *117*, 2584–2640; g) B. Szyszko, M. J. Białek, E. Pacholska-Dudziak, L. Latos-Grażyński, *Chem. Rev.* **2017**, *117*, 2839–2909.

[10] Y. M. Sung, J. Oh, W.-Y. Cha, W. Kim, J. M. Lim, M.-C. Yoon, D. Kim, *Chem. Rev.* **2017**, *117*, 2257–2312.

[11] R. Paolesse, S. Nardis, D. Monti, M. Stefanelli, C. Di Natale, *Chem. Rev.* **2017**, *117*, 2517–2583.

workers,[12] *superphthalocyanine*,[13] obtained for the first time from a template synthesis employing phthalonitrile and uranyl salts, and the *hexaphyrin*,[14,9f] which represents the benchmark molecule of *meso*-aryl-substituted expanded porphyrins, due to many considerable works on these structures (Figure 2).

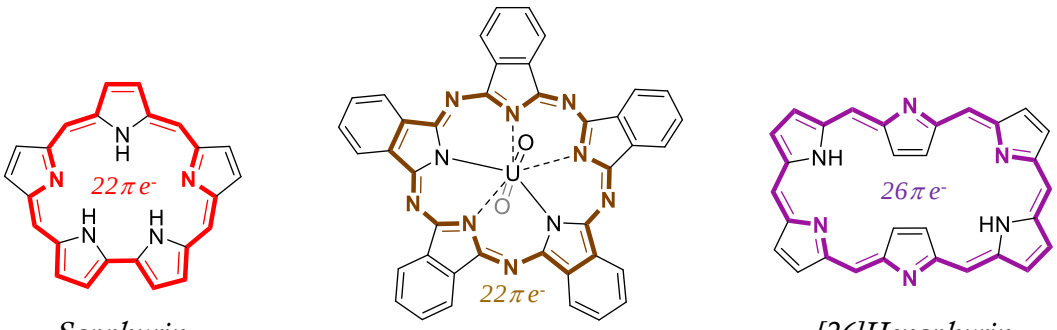

Sapphyrin (1.1.1.1.0) — *Superphthalocyanine* — *[26]Hexaphyrin (1.1.1.1.1.1)*

Figure 2. Representative examples of expanded porphyrinoids with their main electronic delocalization: Sapphyrin, Superphthalocyanine, and Hexaphyrin.

On the other hand, contracted porphyrinoids are becoming an important family of chromophores that exhibit outstanding physicochemical and optical properties, together with high molecular stability and robustness. Among them, *Subporphyrinoids* namely –**subporphyrin** (SubP), **tribenzosubporphyrin** (BzSubP), **subporphyrazines** (SubPz), and **subphthalocyanines** (SubPc)– are conjugated macrocycles containing three pyrrole or isoindole units that are bound together by three methine or aza-

[12] V. J. Bauer, D. L. J. Clive, D. Dolphin, J. B. Paine, F. L. Harris, M. M. King, J. Loder, S. W. C. Wang, R. B. Woodward, *J. Am. Chem. Soc.* **1983**, *105*, 6429–6436.

[13] a) V. W. Day, T. J. Marks, W. A. Wachter, *J. Am. Chem. Soc.* **1975**, *97*, 4519–4527; b) T. J. Marks, D. R. Stojakovic, *J. Am. Chem. Soc.* **1978**, *100*, 1695–1705; c) T. Furuyama, Y. Ogura, K. Yoza, N. Kobayashi, *Angew. Chem. Int. Ed.* **2012**, *51*, 11110–11114; d) T. Furuyama, T. Sato, N. Kobayashi, *J. Am. Chem. Soc.* **2015**, *137*, 13788–13791.

[14] a) R. Charrière, T. A. Jenny, H. Rexhausen, A. Gossauer, *Heterocycles* **1993**, *36*, 1561–1575; b) J. S. Lindsey, I. C. Schreiman, H. C. Hsu, P. C. Kearney, A. M. Marguerettaz, *J. Org. Chem.* **1987**, *52*, 827–836; c) M. G. P. M. S. Neves, R. M. Martins, A. C. Tomé, A. J. D. Silvestre, A. M. S. Silva, V. Félix, J. A. S. Cavaleiro, M. G. B. Drew, *Chem. Commun.* **1999**, 385–386; d) L. Simkhovich, I. Goldberg, Z. Gross, *Org. Lett.* **2003**, *5*, 1241–1244.

bridges. These compounds have in common an aromatic core constituted by 14 π-electrons, delocalized primarily on the inner ring, and a boron(III) ion, which is also linked to an axial ligand (Figure 3).[15]

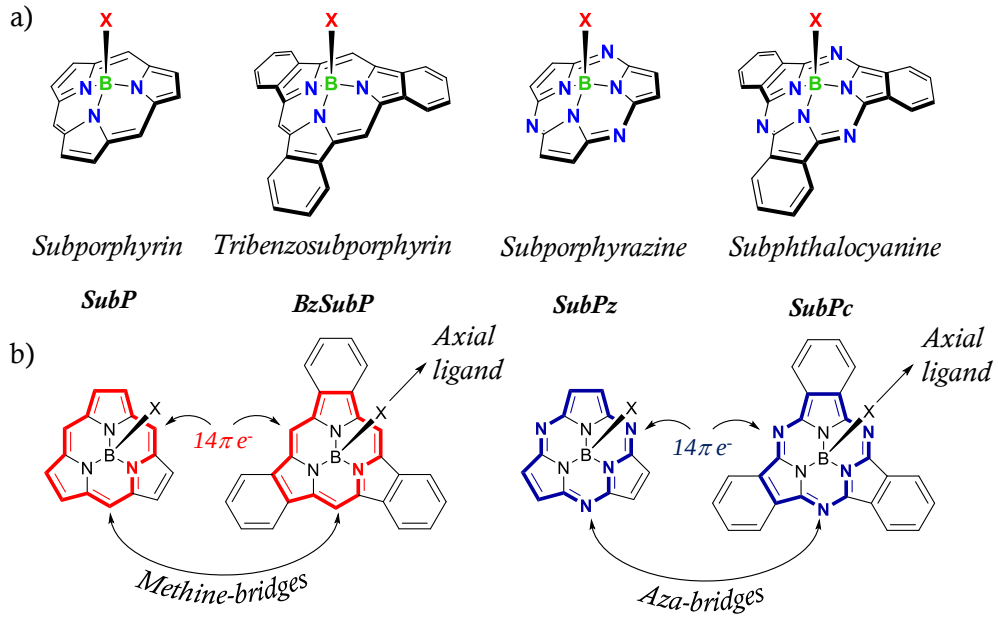

Figure 3. Contracted porphyrinoid systems: (a) Boron-derivative subporphyrinoid structures and (b) their main 14 π-electron aromatic core delocalization.

Another common feature of these contracted porphyrinoids, is that they adopt a nonplanar cone-shaped conformation, established by the tetrahedral geometry of the boron central atom. Thus, these compounds represent appealing examples of nonplanar aromaticity, and are characterized by rather unique spectral and electronic features (Figure 4).[16]

[15] a) C. G. Claessens, D. González-Rodríguez, T. Torres, *Chem. Rev.* **2002**, *102*, 835–854; b) A. Osuka, E. Tsurumaki, T. Tanaka, *Bull. Chem. Soc. Jpn.* **2011**, *84*, 679; c) C. G. Claessens, D. González-Rodríguez, M. S. Rodríguez-Morgade, A. Medina, T. Torres, *Chem. Rev.* **2014**, *114*, 2192–2277; d) S. Shimizu, *Chem. Rev.* **2017**, *117*, 2730–2784.

[16] a) Y. Inokuma, Z. S. Yoon, D. Kim, A. Osuka, *J. Am. Chem. Soc.* **2007**, *129*, 4747–4761; b) Y. Inokuma, J. H. Kwon, T. K. Ahn, M.-C. Yoo, D. Kim, A. Osuka, *Angew. Chem. Int. Ed.* **2006**, *45*, 961–964; c) M. S. Rodríguez-Morgade, C. G. Claessens, A. Medina, D. González-Rodríguez, E. Gutiérrez-Puebla, A. Monge, I. Alkorta, J. Elguero, T. Torres, *Chem. Eur. J.* **2008**, *14*, 1342–1350.

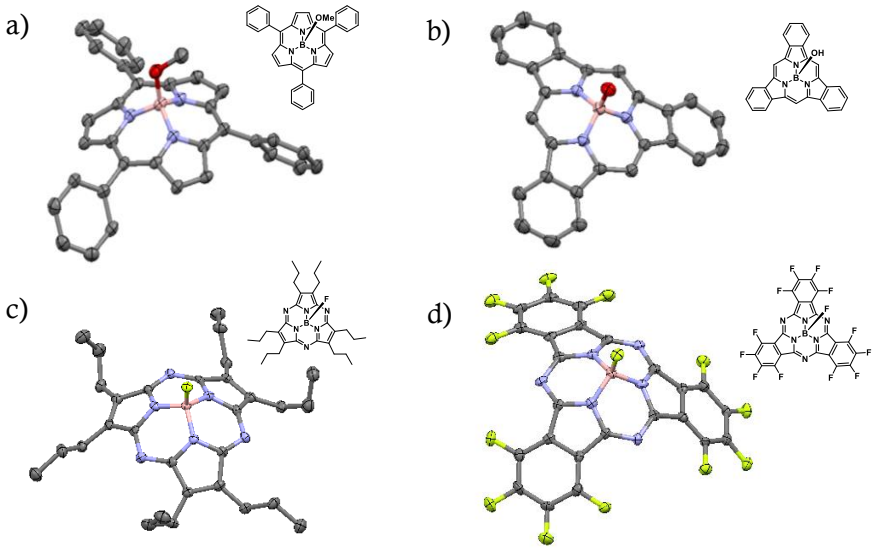

Figure 4. X-ray single-crystal structures of representative subporphyrinoids: (a) Subporphyrin,[16a] (b) tribenzosubporphyrin,[16b] (c) subporphyrazine,[16c] and (d) subphthalocyanines.[16c] The thermal ellipsoid are set at 50% probability level.

The curved nature of the subporphyrinoids makes these molecules particularly interesting as building blocks in supramolecular systems, as the concave and convex π-surfaces can interact in different ways with other electroactive moieties that are attached to the axial or peripheral positions.[17]

The optical properties of subporphyrinoids are analogous to those of their corresponding four-membered partners, even though there are obvious important differences arising from molecular symmetry and size. Generally, the subporphyrinoids display strong absorbance bands in the UV/Vis spectral region that are considerably blue-shifted with respect to those of their corresponding tetramers, as

[17] a) D. González-Rodríguez, T. Torres, D. M. Guldi, J. Rivera, L. Echegoyen, *Org. Lett.* **2002**, *4*, 335–338; b) D. González-Rodríguez, T. Torres, D. M. Guldi, J. Rivera, M. Á. Herranz, L. Echegoyen, *J. Am. Chem. Soc.* **2004**, *126*, 6301–6313; c) D. González-Rodríguez, T. Torres, M. M. Olmstead, J. Rivera, M. Á. Herranz, L. Echegoyen, C. A. Castellanos, D. M. Guldi, *J. Am. Chem. Soc.* **2006**, *128*, 10680–10681; d) D. González-Rodríguez, E. Carbonell, G. de M. Rojas, C. A. Castellanos, D. M. Guldi, T. Torres, *J. Am. Chem. Soc.* **2010**, *132*, 16488–16500.

a result of their smaller π-conjugated cores.[15,16a,18] Moreover, they display high fluorescence quantum yields, low Stokes shifts and reorganization energies, and have only a small tendency to aggregate in solution. Similar to the tetramers, subporphyrinoids are intensively coloured, from orange to deep red, this making them potentially applicable in high-density optical data storage.[15]

Subphthalocyanines[15a,c,19] were discovered serendipitously by Meller and Ossko in 1972, as they were trying to obtain boron-phthalocyanine complex. The condensation reaction of phthalonitrile in the presence of boron trichloride, in chloronaphthalene at 200 °C, did not lead to the expected cyclotetramerization product. Instead, they observed the formation of a purple compound, whose analysis was consistent with the formation of chloro-subphthalocyanine.[20]

SubPcs are synthesized nowadays in good yield, sometimes higher than 90%, by one-step cyclotrimerization reaction of phthalonitrile precursors, in the presence of a boron-based Lewis acid, at high temperatures and using high-boiling point aromatic solvents (Scheme 1). The most common boron reagents that have been employed so far in the synthesis of these macrocycles are BCl_3 and BBr_3, which are readily available and reactive enough.[21] Both boron reagents are commercially available in *p*-xylene solution, which provides certain advantages. First of all, it helps to maintain control over the stoichiometry of the process, avoiding an excess of a strong Lewis acid. On the other hand, *p*-xylene is a high-boiling point solvent that allows to completely

[18] a) S. Saito, K. S. Kim, Z. S. Yoon, D. Kim, A. Osuka, *Angew. Chem. Int. Ed.* **2007**, *46*, 5591–5593; b) Y. Inokuma, S. Easwaramoorthi, Z. S. Yoon, D. Kim, A. Osuka, *J. Am. Chem. Soc.* **2008**, *130*, 12234–12235; c) S. Easwaramoorthi, J.-Y. Shin, S. Cho, P. Kim, Y. Inokuma, E. Tsurumaki, A. Osuka, D. Kim, *Chem. Eur. J.* **2009**, *15*, 12005–12017.

[19] a) A. Medina, C. G. Claessens, *J. Porphyrins Phthalocyanines* **2009**, *13*, 446–454; b) S. Shimizu, N. Kobayashi, *Chem. Commun.* **2014**, *50*, 6949–6966.

[20] A. Meller, A. Ossko, *Monatsh. Chem.* **1972**, *103*, 150.

[21] C. G. Claessens, D. González-Rodríguez, B. del Rey, T. Torres, G. Mark, H.-P. Schuchmann, C. von Sonntag, J. G. MacDonald, R. S. Nohr, *Eur. J. Org. Chem.* **2003**, *2003*, 2547–2551.

dissolve the phthalonitrile derivative and helps to reduce the possible chlorination processes of the macrocycle at their peripheral positions.

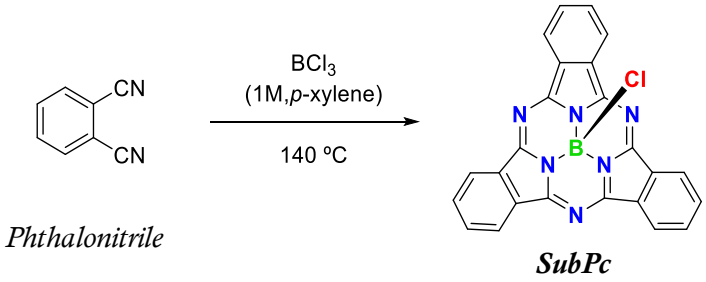

Phthalonitrile ***SubPc***

Scheme 1. General procedure for the synthesis of SubPcs.

The synthesis of SubPcs as free bases or with other metal centers continues to be a challenge for organic chemists. However, theoretical calculations confirm the possibility that these macrocycles can accommodate other central atoms, a carbon or beryllium atom being good candidates, since this would not produce a distortion of the tetrahedral geometry.[22]

A mechanistic study of the formation of chloro-boron SubPc from phthalonitrile derivative and BCl_3 in aromatic solvents suggests that the process begins with the rearrangement of the initial dicarbonitrile-BCl_3 adduct, which leads to an isoindole derivative (**2**) (Scheme 2). The latter would cyclotrimerize to afford the dichlorosubstituted macrocycle (**3**), followed by a concerted elimination reaction in a second step, whereby molecular chlorine is liberated. Quantum-chemical computation shows that the postulated elementary reaction steps leading to the formation of the SubPc-precursor macrocycle are indeed exothermic, or at least kinetically allowed, and

[22] a) Y. Yang, Z. M. Su, *Int. J. Quantum Chem.* **2005**, *103*, 54; b) Y. Yang, *Chem. Phys. Lett.* **2011**, *511*, 51; c) M. M. Montero-Campillo, A. M. Lamsabhi, O. Mó, M. Yáñez, *ChemPhysChem* **2013**, *14*, 915–922; d) M. M. Montero-Campillo, A. M. Lamsabhi, O. Mó, M. Yáñez, *J. Phys. Chem. A* **2016**, *120*, 4845–4852.

that the catalytic effect of BCl_3 is most probably essential to explain the final formation of Cl-B-SubPc structure.[23]

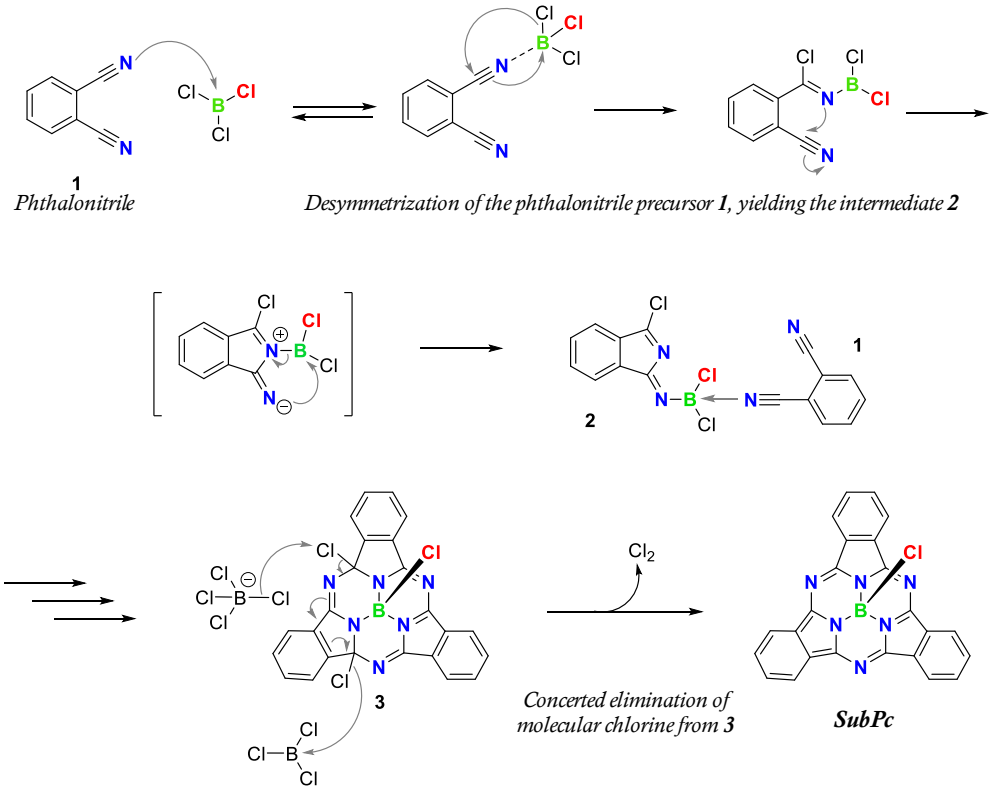

Scheme 2. Proposed mechanism for the synthesis of SubPcs by cyclotrimerization.

One of the main versatilities of SubPcs is that they present different sites of reactivity in their molecular structure. The reactivity may be classified in four main types (Figure 5):

1. *Axial reactivity*. Axial substitution of the chlorine or bromine atom with a wide range of nucleophiles at the central boron atom; the π-conjugated macrocycle maintains its electronic characteristics.[17b,d,24]

[23] a) C. G. Claessens, D. González-Rodríguez, C. M. McCallum, R. S. Nohr, H.-P. Schuchmann, T. Torres, *J. Porphyrins Phthalocyanines* **2007**, *11*, 181–188; b) R. S. Nohr, C. M. McCallum, H.-P. Schuchmann, *J. Porphyrins Phthalocyanines* **2010**, *14*, 271–277.

[24] a) E. Palomares, M. V. Martínez-Díaz, T. Torres, E. Coronado, *Adv. Funct. Mater.* **2006**, *16*, 1166–1170; b) D. González-Rodríguez, T. Torres, M. Á. Herranz, L. Echegoyen, E. Carbonell,

2. *Peripheral reactivity.* Any reaction that produces a chemical modification of the substituents placed at the macrocycle rings. Metal-catalyzed cross coupling reactions are the most used procedures, since they allow access to a large number of new substituents incompatible with the BCl_3 used in the cyclotrimerization reaction.[15a,c,25]
3. *Ring-expansion reaction.* The geometrically constrained SubPc core can readily cleave in the presence of a diiminoisoindoline unit, which is then incorporated into its framework to form an A_3B type phthalocyanine derivative. This reaction has proved very selective and efficient in some cases, allowing to prepare previously unattainable Pcs.[26]
4. *Metal π coordination.* It consists in the formation of ruthenoarene π-complexes of SubPcs and SubPzs by reaction of the aromatic rings in the macrocycle with $[Cp^*Ru(MeCN)_3]PF_6$ (Cp* = pentamethylcyclopentadienyl). Here, the Ru atom can coordinate either to the axial ligand, the SubPc concave side, or the SubPc convex side.[27]

The intrinsic chirality of subphthalocyanines with C_3 or C_1 symmetries is an additional aspect that promises to enhance their utility as building blocks for the construction of complex molecules (Figure 6).[28]

D. M. Guldi, *Chem. Eur. J.* **2008**, *14*, 7670–7679; c) M. E. El-Khouly, D. K. Ju, K.-Y. Kay, F. D'Souza, S. Fukuzumi, *Chem. Eur. J.* **2010**, *16*, 6193–6202; d) J. Guilleme, D. González-Rodríguez, T. Torres, *Angew. Chem. Int. Ed.* **2011**, *50*, 3506–3509.

[25] a) D. González-Rodríguez, T. Torres, *Eur. J. Org. Chem.* **2009**, *2009*, 1871; b) D. González-Rodríguez, M. V. Martínez-Díaz, J. Abel, A. Perl, J. Huskens, L. Echegoyen, T. Torres, *Org. Lett.* **2010**, *12*, 2970–2973.

[26] a) N. Kobayashi, R. Kondo, S. Nakajima, T. Osa, *J. Am. Chem. Soc.* **1990**, *112*, 9640–9641, b) C. Penglei, W. Xiaobing, T. Daihua, Z. Zhen, Z. Jiancheng, L. Xinhou, *Dyes Pigments* **2001**, *48*, 85–92; c) S. M. S. Chauhan, P. Kumari, *Tetrahedron* **2009**, *65*, 2518–2524.

[27] E. Caballero, J. Fernández-Ariza, V. M. Lynch, C. Romero-Nieto, M. S. Rodríguez-Morgade, J. L. Sessler, D. M. Guldi, T. Torres, *Angew. Chem. Int. Ed.* **2012**, *51*, 11337–11342.

[28] a) C. G. Claessens, T. Torres, *Tetrahedron Lett.* **2000**, *41*, 6361; b) N. Kobayashi, *Coord. Chem. Rev.* **2001**, *99*, 219–221; c) N. Kobayashi, T. Nonomura, *Tetrahedron Lett.* **2002**, *43*, 4253.

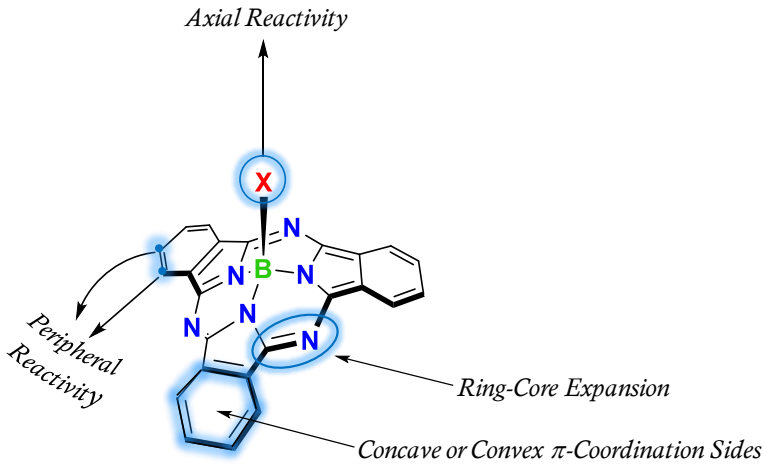

Figure 5. Generalized structure of SubPc showing their main different reactivity and functionalization sites.

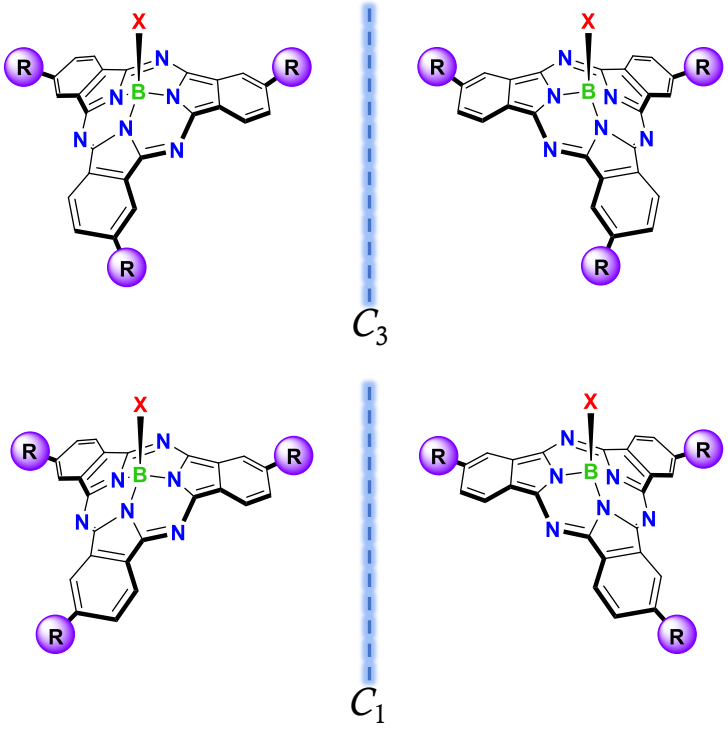

Figure 6. C_3 and C_1 symmetries of *meta*-substituted SubPc regioisomers.

The optical absorption spectra of SubPcs are comparable to those exhibited by Pcs, in that they show two main transition bands, the lowest energy band in the near red region of the spectrum, and the more energetic one in the near UV. These bands are designated, respectively, Q (corresponds to the transition $S_o \rightarrow S_1$) and B (Soret band corresponds to the transition $S_o \rightarrow S_2$) by analogy with porphyrins within Gouterman's four-orbital model (Figure 7).[15a,c]

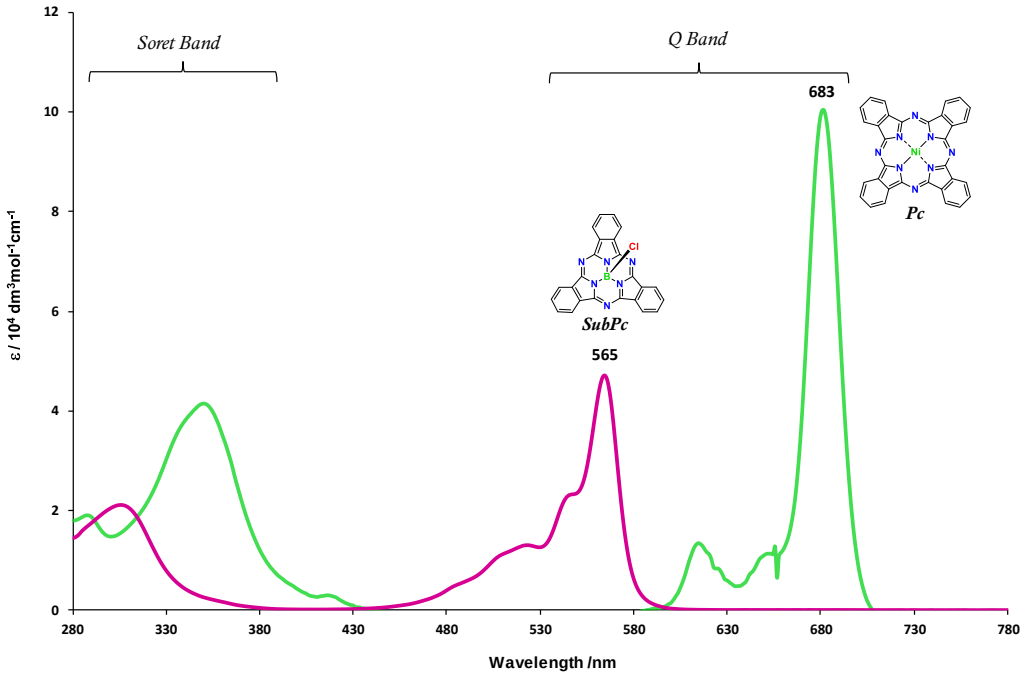

Figure 7. Comparative UV/vis spectra of SubPc (pink line) and Ni(II) Pc (green line) in toluene.

The axial substituents have none or only a very small effect on the position of the absorption bands. On the contrary, peripheral donor and acceptor substituents shift the Q band toward longer wavelengths. The effect is particularly dramatic when the macrocycle is substituted with π-donor atoms, such as sulphur, oxygen, or nitrogen, and sometimes it goes along with broadening of the Q bands, as an attributable

consequence of $n \rightarrow \pi^*$ transitions between the heteroatom lone pair and the macrocycle.[17b,25a,29]

In a similar way to the ground-state, the substitution model around the SubPcs, may tune the properties of their excited states. Particularly, diverse fluorescence emission maxima (λ_{max} = 575−670 nm) have been recorded, their shifts paralleling those of the absorption Q band. The emission spectra of most SubPc analogues are a mirror image of the Q-absorption band. Fluorescence emission only takes place from the lowest singlet excited state, where the SubPcs, as their parent Pcs, exhibit very small Stokes shifts (typically around 10−15 nm) and unusually narrow widths at half of the maximum intensity (60−80 nm). This indicates very small geometric distortion of the excited state with respect to the ground state and a narrow density of states of the HOMO and LUMO levels.[30] Fluorescence quantum yields (φ_F) of these macrocycles are typically around 0.2−0.5, but they can reach up to 0.95 for certain compounds.[31] A good correlation was established between this radiative parameter and the measured fluorescence lifetimes. That is, higher fluorescence quantum yields coincide always with longer lifetimes. Thus, singlet excited state lifetimes (τ_s) in SubPcs have been evaluated to be around 2−4 ns, again similar to those measured for monomeric Pcs.[15c]

In the redox properties of SubPcs, the first oxidative or reductive half-wave potentials are both one electron processes. The reduction is frequently reversible on the cyclic voltammetry time scale, while on the other hand, oxidation processes appear to give rise to less stable charged species. Scanning at more positive or negative potentials

[29] a) N. Kobayashi, *J. Chem. Soc. Chem. Commun.* **1991**, 1203–1205; b) N. Kobayashi, T. Ishizaki, K. Ishii, H. Konami, *J. Am. Chem. Soc.* **1999**, *121*, 9096–9110; c) E. Ohno-Okumura, K. Sakamoto, T. Kato, T. Hatano, K. Fukui, T. Karatsu, A. Kitamura, T. Urano, *Dyes Pigments* **2002**, *53*, 57–65.

[30] D. D. Díaz, H. J. Bolink, L. Cappelli, C. G. Claessens, E. Coronado, T. Torres, *Tetrahedron Lett.* **2007**, *48*, 4657.

[31] N. Shibata, B. Das, E. Tokunaga, M. Shiro, N. Kobayashi, *Chem. Eur. J.* **2010**, *16*, 7554–7562.

typically reveals several redox events, some of them multi-electronic, which usually are electrochemically irreversible or quasi-reversible. This irreversibility is thought to be due to chemical transformations, or to the deposition of the redox species on the electrodes. The electrochemical features of the resulting products may be sometimes detected in the reverse scan.[17b,25b]

The first oxidative or reductive half-wave potential of SubPcs, and hence their electron-donor/acceptor ability, can be predictably tuned by the peripheral substitution pattern on the macrocycle. On the other hand, although the nature of the axial ligand affects to a much lower extent the position of the redox peaks, it does have a strong influence on the reversibility of the different redox processes. For instance, axial phenoxy ligands seem to efficiently stabilize charged species, phenoxy-SubPcs displaying more reversible events than chloro-SubPcs.[17c] In some cases, up to five consecutive reversible reductions can be detected in the cathodic scan of the voltammograms. In relation to these observations, DFT theoretical studies on charged SubPc species have shown that the polar B–X bond may play an important role in releasing the extra charge from the ring, experiencing a shortening or lengthening upon oxidation or reduction of the macrocycle, respectively.[32]

Subporphyrin[15b,c,d,16a,33] and **tribenzosubporphyrin**[15b,d,16b,34] as members of the subporphyrinoid family, were reported for the first time over the years 2006 and 2008 by Osuka and Kobayashi independently. BzSubPs can be prepared by the thermal self-condensation of isoindolinone-3-acetic acid or from 3-benzalphthalimide, using boric acid as a template (Scheme 3a,b). Although the reaction conditions were drastic, with

[32] V. R. Ferro, L. A. Poveda, C. G. Claessens, R. H. González-Jonte, J. M. García de la Vega, *Int. J. Quantum Chem.* **2003**, *91*, 369–375.

[33] a) N. Kobayashi, Y. Takeuchi, A. Matsuda, *Angew. Chem. Int. Ed.* **2007**, *46*, 758–760; b) Y. Takeuchi, A. Matsuda, N. Kobayashi, *J. Am. Chem. Soc.* **2007**, *129*, 8271–8281; c) Y. Inokuma, A. Osuka, *Chem. Commun.* **2007**, 2938–2940; d) Y. Inokuma, S. Easwaramoorthi, S. Y. Jang, K. S. Kim, D. Kim, A. Osuka, *Angew. Chem. Int. Ed.* **2008**, *47*, 4840–4843.

[34] a) Y. Inokuma, A. Osuka, *Dalt. Trans.* **2008**, 2517–2526; b) E. A. Makarova, S. Shimizu, A. Matsuda, E. A. Luk'yanets, N. Kobayashi, *Chem. Commun.* **2008**, 2109–2111.

heating at 350 °C or use of microwave enhancement, and the reaction yields were rather low, the characterization of this new and important missing member of the subporphyrinoid family represented a significant advance. On the other hand, the synthesis of subporphyrins and *meso*-substituted subporphyrin derivatives is usually carried out by intramolecular cyclization of a trimeric pyrrolyl intermediate. SubPs have mostly been prepared through Adler reaction conditions[35] of a preformed tripyrrolylborane derivative or by the aroylation of a tri-*N*-tripyrromethane precursor, followed by intramolecular cyclization (Scheme 3c).[36]

SubPs show an additional functionalization site, namely the *meso* position, which constitutes a distinctive feature with respect to SubPcs and SubPzs. The distance between the *meso* substituents and the adjacent pyrrole rings is larger compared to that of the corresponding porphyrins. Consequently, freely rotating *meso*-aryl substituents strongly couple to the SubP aromatic core, allowing fine-tuning of SubP electronic properties.[15b,c,d,36a,37]

[35] A. D. Adler, F. R. Longo, J. D. Finarelli, J. Goldmacher, J. Assour, L. A. Korsakoff, *J. Org. Chem.* **1967**, *32*, 476.

[36] a) S. Hayashi, Y. Inokuma, S. Easwaramoorthi, K. S. Kim, D. Kim, A. Osuka, *Angew. Chem. Int. Ed.* **2010**, *49*, 321–324; b) T. Tanaka, M. Kitano, S. Hayashi, N. Aratani, A. Osuka, *Org. Lett.* **2012**, *14*, 2694–2697; c) M. Kitano, S. Hayashi, T. Tanaka, H. Yorimitsu, N. Aratani, A. Osuka, *Angew. Chem. Int. Ed.* **2012**, *51*, 5593–5597.

[37] a) S. Hayashi, J. Sung, Y. M. Sung, Y. Inokuma, D. Kim, A. Osuka, *Angew. Chem. Int. Ed.* **2011**, *50*, 3253–3256; b) M. Kitano, J. Sung, K. H. Park, H. Yorimitsu, D. Kim, A. Osuka, *Chem. Eur. J.* **2013**, *19*, 16523–16527; c) D. Shimizu, H. Mori, M. Kitano, W.-Y. Cha, J. Oh, T. Tanaka, D. Kim, A. Osuka, *Chem. Eur. J.* **2014**, *20*, 16194–16202; d) D. Shimizu, J. Oh, K. Furukawa, D. Kim, A. Osuka, *Angew. Chem. Int. Ed.* **2015**, *54*, 6613–6617; e) Y. Okuda, E. Tsurumaki, J. Oh, J. Sung, D. Kim, A. Osuka, *Angew. Chem. Int. Ed.* **2016**, *55*, 9212–9215; f) Y. Okuda, N. Fukui, J. Kim, T. Kim, H.-W. Jiang, G. Copley, M. Kitano, D. Kim, A. Osuka, *Angew. Chem. Int. Ed.* **2017**, *56*, 12317–12321; g) K. Kise, Y. Hong, N. Fukui, D. Shimizu, D. Kim, A. Osuka, *Chem. Eur. J.* **2018**, *24*, 8306–8310; h) Y. Bekki, D. Shimizu, K. Fujimoto, A. Osuka, *Chem. Eur. J.* **2018**, *24*, 12708–12715; i) K. Kise, K. Yoshida, R. Kotani, D. Shimizu, A. Osuka, *Chem. Eur. J.* **2018**, *24*, 19136–19140.

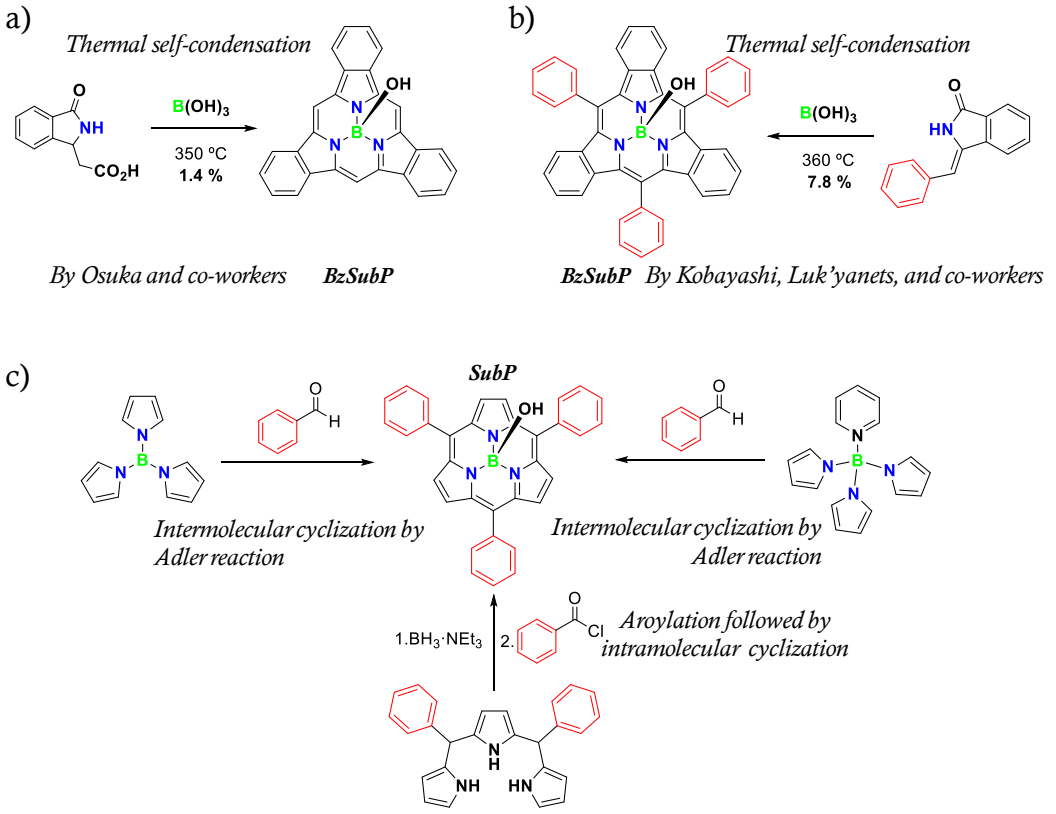

Scheme 3. Synthetic methods of BzSubP and SubP: (a) Synthesis of the first BzSubP and (b) *meso*-phenyl-substituted BzSubP by thermal self-condensation. (c) Synthesis of *meso*-aryl-substituted SubP in three ways.

In the last 15 years, there has been an exponential growth of works in the development of new synthetic routes, X-ray diffraction analysis, electrochemical properties, and new conjugated/fused systems based on subporphyrinoids. Also, they have already begun to have a profound impact in many high-technology areas, finding

applications as active units in artificial photosynthetic systems,[17,24b,c,41c,38] sensors,[24a,39] light-emitting devices,[40] field-effect transistors,[41] supramolecular systems,[42] optical information recording media, among others. As a consequence, these species are attracting the attention of an increasing number of chemists, physicists, and materials scientists.

[38] a) D. González-Rodríguez, C. G. Claessens, T. Torres, S. Liu, L. Echegoyen, N. Vila, S. Nonell, *Chem. Eur. J.* **2005**, *11*, 3881–3893; b) F. Camerel, G. Ulrich, P. Retailleau, R. Ziessel, *Angew. Chem. Int. Ed.* **2008**, *47*, 8876–8880; c) R. Ziessel, G. Ulrich, K. J. Elliott, A. Harriman, *Chem. Eur. J.* **2009**, *15*, 4980–4984; d) D. González-Rodríguez, E. Carbonell, D. M. Guldi, T. Torres, *Angew. Chem. Int. Ed.* **2009**, *48*, 8032–8036; d) C. R. Nieto, J. Guilleme, C. Villegas, J. L. Delgado, D. González-Rodríguez, N. Martin, T. Torres, D. M. Guldi, *J. Mater. Chem.* **2011**, *21*, 15914–15918.; e) C. Romero-Nieto, J. Guilleme, J. Fernández-Ariza, M. S. Rodríguez-Morgade, D. González-Rodríguez, T. Torres, D. M. Guldi, *Org. Lett.* **2012**, *14*, 5656–5659; f) J.-Y. Liu, H.-S. Yeung, W. Xu, X. Li, D. K. P Ng, *Org. Lett.* **2008**, *10*, 5421; g) M. E. El-Khouly, J. B. Ryu, K.-Y. Kay, O. Ito, S. Fukuzumi, *J. Phys. Chem. C* **2009**, *113*, 15444; h) M. E. El-Khouly, *Phys. Chem. Chem. Phys.* **2010**, *12*, 12746; i) M. E. El-Khouly, J.-H. Kim, K.-Y. Kay, S. Fukuzumi, *J. Phys. Chem. C* **2012**, *116*, 19709.

[39] a) S. Xu, K. Chen, H. Tian, *J. Mater. Chem.* **2005**, *15*, 2676; b) J. V. Ros-Lis, R. Martínez-Mañéz, J. Soto, *Chem. Commun.* **2005**, 5260.

[40] a) G. E. Morse, J. S. Castrucci, M. G. Helander, Z.-H. Lu, T. P. Bender, *ACS Appl. Mater. Interfaces* **2011**, *3*, 3538–3544; b) Y.-H. Chen, Y.-J. Cheng, G.-R. Lee, C.-I. Wu, T.-W. Pi, *Org. Electron.* **2011**, *12*, 562–565; c) B. H. Lessard, K. L. Sampson, T. Plint, T. P. Bender, *J. Polym. Sci. Part A Polym. Chem.* **2015**, *53*, 1996–2006; d) T. G. Plint, B. H. Lessard, T. P. Bender, *Opt. Mater. (Amst).* **2018**, *75*, 710–718.

[41] T. Yasuda, T. Tsutsui, *Mol. Cryst. Liq. Cryst.* **2007**, *462*, 3.

[42] a) C. G. Claessens, T. Torres, *J. Am. Chem. Soc.* **2002**, *124*, 14522; b) C. G. Claessens, T. Torres, *Chem. Commun.* **2004**, 1298; c) C. G. Claessens, M. J. Vicente-Arana, T. Torres, *Chem. Commun.* **2008**, 6378; d) C. G. Claessens, I. Sánchez-Molina, T. Torres, *Supramol. Chem.* **2009**, *21*, 44; e) I. Sánchez-Molina, B. Grimm, R. M. Krick Calderon, C. G. Claessens, D. M. Guldi, T. Torres, *J. Am. Chem. Soc.* **2013**, *135*, 10503–10511.

Frontier Molecules of the Subphthalocyanines

The chemistry of subphthalocyanines has been developed over the last two decades as the result of the dedicated efforts, which main interest has been focused from the purely synthetic point of view to the applied physical properties. Major synthetic breakthroughs have been made in this area, like the ring expansion reaction of SubPc to afford phthalocyanines, the synthesis of SubPc dimers and trimers with extended conjugation, the establishment of an efficient methodology for their preparation, and the development of general methods for axial substitution.

The basic peripheral structure of SubPc can also be rationally modified in another way, giving rise to other extraordinary analogues (Figure 8) via the following strategies: a) the nice example of chiral 1,2-subnaphthalocyanines. These molecules possess two diastereomers with respect to the arrangement of the naphthalene moieties (Figure 8a);[43] b) azasubphthalocyanines (Figure 8b);[44] c) dimers or oligomers (fused bi- and trinuclear SubPc systems (Figure 8c). These dimers and related trimers reveal interesting spectroscopic features, including strongly red-shifted Q bands, showing a well-defined curved, fully conjugated π surfaces).[45] All these compounds are available

[43] a) S. Shimizu, A. Miura, S. Khene, T. Nyokong, N. Kobayashi, *J. Am. Chem. Soc.* **2011**, *133*, 17322–17328.

[44] a) R. Münnich, P. Löser, A. Winzenburg, R. Faust, *J. Porphyrins Phthalocyanines* **2016**, *20*, 1277–1283; b) M. Liebold, E. Sharikow, E. Seikel, L. Trombach, K. Harms, P. Zimcik, V. Novakova, R. Tonner, J. Sundermeyer, *Org. Biomol. Chem.* **2018**, *16*, 6586–6599; c) P. A. Stuzhin, I. A. Skvortsov, Y. A. Zhabanov, N. V Somov, O. V Razgonyaev, I. A. Nikitin, O. I. Koifman, *Dyes Pigments* **2019**, *162*, 888–897.

[45] a) C. G. Claessens, T. Torres, *Angew. Chem. Int. Ed.* **2002**, *41*, 2561–2565; b) T. Fukuda, J. R. Stork, R. J. Potucek, M. M. Olmstead, B. C. Noll, N. Kobayashi, W. S. Durfee, *Angew. Chem. Int. Ed.* **2002**, *41*, 2565–2568; c) R. S. Iglesias, C. G. Claessens, T. Torres, G. M. A. Rahman, D. M. Guldi, *Chem. Commun.* **2005**, 2113–2115; d) R. S. Iglesias, C. G. Claessens, T. Torres, M. Á. Herranz, V. R. Ferro, J. M. García de la Vega, *J. Org. Chem.* **2007**, *72*, 2967–2977; e) B. Verreet, B. P. Rand, D. Cheyns, A. Hadipour, T. Aernouts, P. Heremans, A. Medina, C. G. Claessens, T. Torres, *Adv. Energy Mater.* **2011**, *1*, 565–568; f) N. Shibata, S. Mori, M. Hayashi, M. Umeda, E. Tokunaga, M. Shiro, H. Sato, T. Hoshi, N. Kobayashi, *Chem. Commun.* **2014**,

due to the existence of the corresponding phthalonitrile precursors with fused aromatic ring units or functional units, which have sufficient reactivity in the standard SubPc syntheses. These modifications have a strong impact on the electronic features of the macrocycle core.

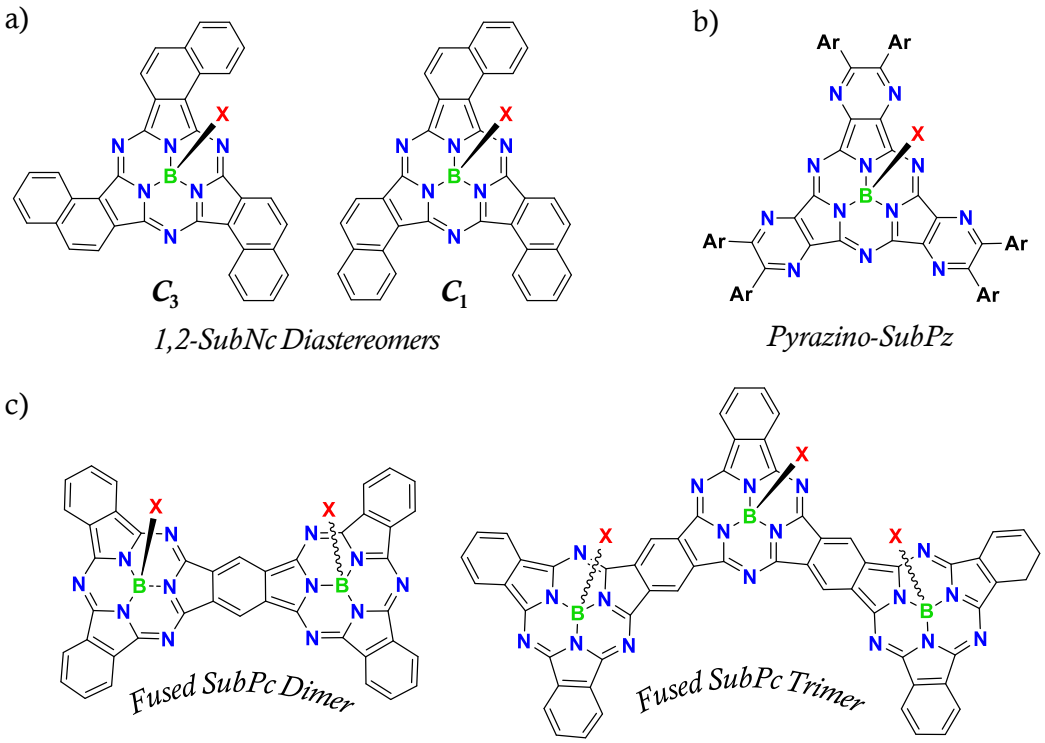

Figure 8. Representative examples of SubPc analogues: (a) chiral 1,2-subnaphthalocyanines; (b) tripyrazino-subporphyrazine; (c) benzo-annulated SubPc dimers and trimers.

If the structure of SubPc is modified by removing or adding fused aromatic ring units at the periphery, another types of analogues are obtained: **Subporphyrazines**

50, 3040–3043; g) G. Zango, J. Zirzlmeier, C. G. Claessens, T. Clark, M. V. Martínez-Díaz, D. M. Guldi, T. Torres, *Chem. Sci.* **2015**, *6*, 5571–5577.

(SubPzs)[15a,c,16c,46] (also referred as subazaporphyrins), in the case of a replacement of the isoindole moieties by pyrrole rings, and **2,3-subnaphthalocyanines** (SubNcs),[15a,19b,29b,46a,47] in the case of conjugate extension by incorporation of three fused benzene ring units (Figure 9).

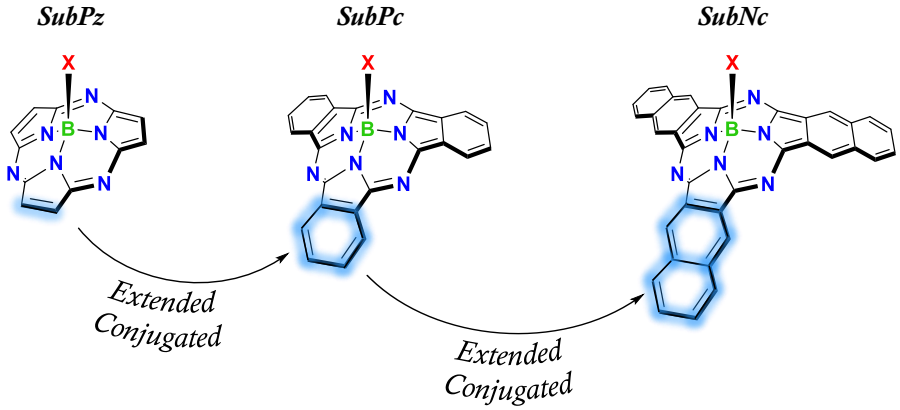

Figure 9. SubPz and SubNc as frontier molecules of the SubPc.

[46] a) J. Rauschnabel, M. Hanack, *Tetrahedron Lett.* **1995**, *36*, 1629–1632; b) N. Kobayashi, *J. Porphyrins Phthalocyanines* **1999**, *3*, 453–467; c) M. S. Rodríguez-Morgade, S. Esperanza, T. Torres, J. Barberá, *Chem. Eur. J.* **2005**, *11*, 354–360; d) J. R. Stork, J. J. Brewer, T. Fukuda, J. P. Fitzgerald, G. T. Yee, A. Y. Nazarenko, N. Kobayashi, W. S. Durfee, *Inorg. Chem.* **2006**, *45*, 6148–6151; e) G. M. Aminur, D. Lüders, M. S. Rodríguez-Morgade, E. Caballero, T. Torres, D. Guldi, *ChemSusChem*. **2009**, *2*, 330–335; f) S. Shimizu, T. Otaki, Y. Yamazaki, N. Kobayashi, *Chem. Commun.* **2012**, *48*, 4100–4102; g) X. Liang, S. Shimizu, N. Kobayashi, *Chem. Commun.* **2014**, *50*, 13781–13784; h) H. Shang, L. Zhao, D. Qi, C. Chen, J. Jiang, *Chem. Eur. J.* **2014**, *20*, 16266–16272.

[47] a) M. Geyer, F. Plenzig, J. Rauschnabel, M. Hanack, B. del Rey, A. Sastre, T. Torres, *Synthesis* **1996**, 1139; b) J. R. Stork, R. J. Potucek, W. S. Durfee, B. C. Noll, *Tetrahedron Lett.***1999**, *40*, 8055–8058; c) S. Nonell, N. Rubio, B. del Rey, T. Torres, *J. Chem. Soc.*, *Perkin Trans.* **2000**, *2*, 1091–1094; d) C. D. Zyskowski, V. O. Kennedy, *J. Porphyrins Phthalocyanines* **2000**, *04*, 707–712; e) G. Martín, G. Rojo, F. Agulló-López, V. R. Ferro, J. M. García de la Vega, M. V. Martínez-Díaz, T. Torres, I. Ledoux, J. Zyss, *J. Phys. Chem. B* **2002,** *106,* 13139–13145; f) N. Rubio, A. Jiménez-Banzo, T. Torres, S. Nonell, *J. Photochem. Photobiol. A* **2007**, *187*, 214-219; g) Y. Takao, T. Masuoka, K. Yamamoto, T. Mizutani, F. Matsumoto, K. Moriwaki, K. Hida, T. Iwai, T. Ito, T. Mizuno, et al., *Tetrahedron Lett.* **2014**, *55*, 4564–4567; h) J. D. Dang, D. S. Josey, A. J. Lough, Y. Li, A. Sifate, Z.-H. Lu, T. P. Bender, *J. Mater. Chem. A* **2016**, *4*, 9566–9577; i) A. Takagi, T. Mizutani, *RSC Adv.* **2017**, *7*, 54235–54245.

Although SubPz derivatives were described for first time by Hanack[46a] and Kobayashi[29b] in the 90's decade, it was only in the year 2005 that they were unambiguously prepared and unequivocally characterized by Rodríguez-Morgade *et al.*[46c] SubPzs were obtained by treating disubstituted maleonitriles with boron trichloride in 8-20% yield. The easier axial substitution by nucleophiles in SubPzs, in comparison with SubPcs, was thought to reflect the stronger interaction of the peripheral substituents with the macrocyclic core. In these macrocycles, some of the SubPc properties (e.g., conical shape and aromatic nature) are preserved, whereas others (e.g., absorption profiles, reactivity, or supramolecular organization) can be tailored. Furthermore, the efficient modulation of SubPz properties through their peripheral substitution with selected specific functions is remarkable, because the substituents are attached directly at the β-positions of the pyrrole moieties. Consequently, a more efficient coupling between the peripheral groups and the azaporphyrinic aromatic core takes place.

2,3-SubNcs are also minor constituents within a broader class of well-known and highly studied SubPcs. Just like in the cases of SubPzs and SubPcs, SubNcs are composed of three nitrogen-bridged benzoisoindoline subunits that chelate a single boron atom within their internal cavity, which is linked to an axial ligand. SubNcs are known to be aromatic, non-planar, and cone-shaped molecules. The total 42 π-electrons of SubNcs are distributed over 36 carbon and 6 nitrogen atoms. But like with SubPcs and SubPzs, the electronic delocalization mainly takes place at the inner ring constituted by 14 π-electrons, while the outer benzene rings maintain their electronic structure.

SubPzs and SubNcs can be prepared using the same synthetic methodology employed in the construction of the SubPc macrocycles, that is, by boron(III)-assisted cyclotrimerization reaction of maleonitrile and 2,3-naphthalenedicarbonitrile derivatives, respectively (Scheme 4).

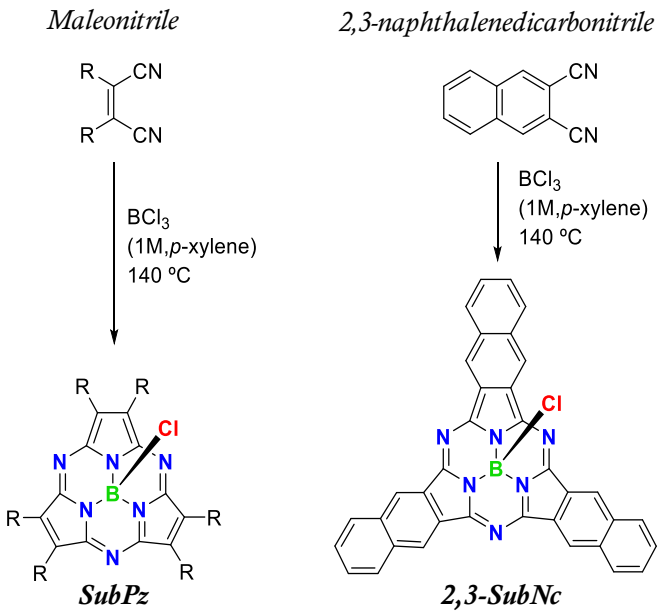

Scheme 4. General procedure for the synthesis of SubPz and SubNc analogues.

However, for the SubPzs sysnthesis, the stereochemistry of the dinitrile precursor has proven crucial. In fact, neither bis(alkyl)- or bis(aryl)fumaronitriles afford SubPzs under the standard reaction conditions.[46c] The only exception has been the use of unsubstituted fumaronitrile in a mixed condensation with tetramethylsuccinonitrile. This gave a mixture of a subazachlorin and unstable non-substituted SubPz.[46f]

The delocalized 14 π-electron heteroaromatic system defines the spectroscopic characteristics of these subporphyrinoids. These evidence their aromatic natures by absorbing radiation corresponding to visible light (Figure 10). The Q band of the 2,3-SubNcs are shifted to lower energies and the strength is enhanced in comparison to those of SubPcs and SubPzs, because of the extended conjugation over the extra fused benzene rings. This also results in an increase of the molar absorption coefficient. The observed red shift agrees with that predicted by theoretical calculations that the gap of the SubNcs is 0.5 eV smaller than the gap of the SubPcs.[47b,c] On the other hand, SubPzs absorb in the green-yellow region of the visible spectrum. The spectroscopic properties of these macrocycles indicate that the removal of the three fused benzene rings from

the SubPc skeleton produces a blue shift of 65-70 nm in the Q band, in addition to a slight reduction in its absorption coefficient. From another point of view, the reduction from 18 to 14 π-electron systems when passing from a Pz to a SubPz causes a hypsochromic displacement of approximately 100 nm in the Q band.[46c]

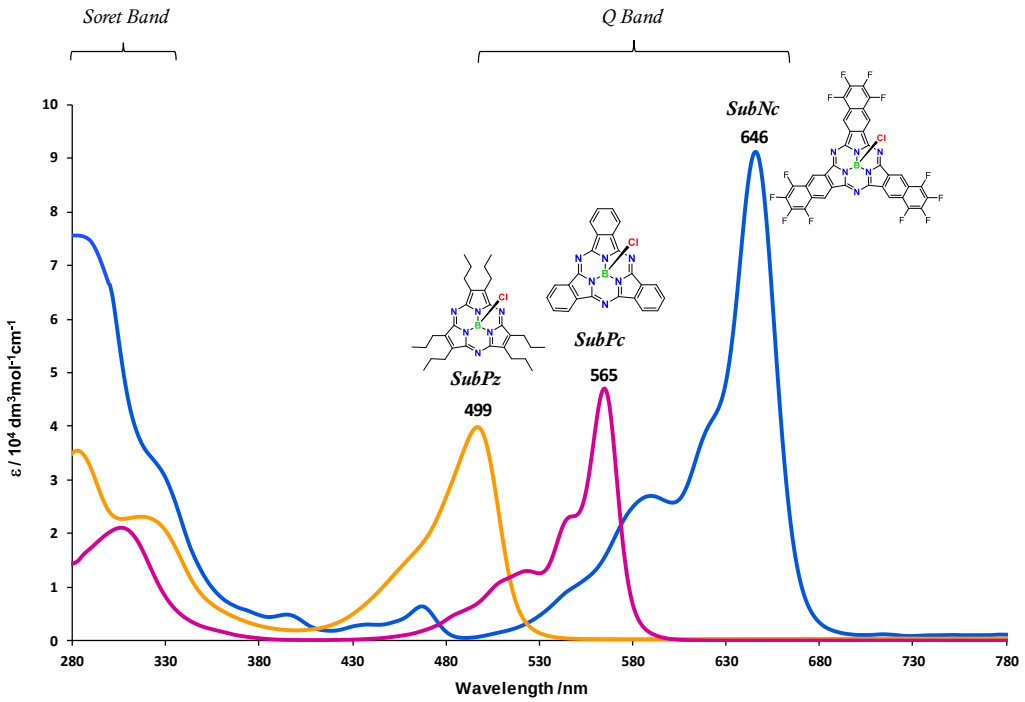

Figure 10. Comparative UV/vis spectra of SubPz (orange line), SubPc (pink line), and SubNc (blue line) in toluene. The color of the lines represents the color in solution for each compound.

SubPzs represents far more than just SubPc derivatives lacking the fused benzene rings. As we will discuss in Chapter 1, the peripheral substituents directly attached to the macrocyclic core exert much stronger influence on the aromatic heteroannulene, related to their SubPc congeners, whose peripheral substituents are appended to the fused benzene rings.[48]

[48] T. Higashino, M. S. Rodríguez-Morgade, A. Osuka, T. Torres, *Chem. Eur. J.* **2013**, *19*, 10353–10359.

Applications of Subphthalocyanines and Related Compounds

SubPcs are being studied and applied in order to construct state-of-the-art technological devices. The electronic and photo-physical features of this family of subporphyrinoids, allow the generation of long-lived excited states. This fact, together with an increasing understanding of the morphology at the nanometer-scale of the SubPc-based molecular materials, are little by little allowing the control of these physical properties in condensed phases, giving rise to practical applications in fields ranging from the optical recording data to molecular photovoltaics.

The first studies in applications of SubPcs as molecular materials were based on nonlinear optics (NLO).[49] Although the third order phenomena were analysed, most of the subsequent investigations focused on second-order effects, since these molecules are intrinsically unsymmetrical. On the other hand, concerning the biological area, SubPc analogues do not tend to form aggregates. Therefore, they have high triplet and singlet oxygen quantum yields, which make them cytotoxic with potential use in photodynamic therapy, as well as in sensing applications.[47c,50]

Organic field effect transistor (OFETs) are the basic building blocks for many integrated circuits and displays, and have attracted much attention due to their merits

[49] a) A. Sastre, T. Torres, M. A. Díaz-García, F. Agulló-López, C. Dhenaut, S. Brasselet, I. Ledoux, J. Zyss, *J. Am. Chem. Soc.* **1996**, *118*, 2746–2747; b) G. Rojo, A. Hierro, M. A. Díaz-Garcia, F. Agulló-Lopez, B. del Rey, A. Sastre, T. Torres, *Appl. Phys. Lett.* **1997**, *70*, 1802–1804; c) G. Rojo, F. Agulló-López, B. del Rey, T. Torres, *J. Appl. Phys.* **1998**, *84*, 6507–6512; d) G. Olbrechts, K. Wostyn, K. Clays, A. Persoons, S. Ho Kang, K. Kim, *Chem. Phys. Lett.* **1999**, *308*, 173–175; e) M. Victoria Martínez-Díaz, B. del Rey, T. Torres, B. Agricole, C. Mingotaud, N. Cuvillier, G. Rojo, F. Agulló-López, *J. Mater. Chem.* **1999**, *9*, 1521–1526; f) G. de la Torre, P. Vázquez, F. Agulló-López, T. Torres, *Chem. Rev.* **2004**, *104*, 3723–3750; g) C. G. Claessens, D. González-Rodríguez, T. Torres, G. Martín, F. Agulló-López, I. Ledoux, J. Zyss, V. R. Ferro, J. M. García de la Vega, *J. Phys. Chem. B* **2005**, *109*, 3800–3806.

[50] E. van de Winckel, M. Mascaraque, A. Zamarrón, Á. Juarranz de la Fuente, T. Torres, A. de la Escosura, *Adv. Funct. Mater.* **2018**, *28*, 1705938.

of mechanical flexibility and high compatibility with the large area electronic devices. These devices are widely used in the fields of electronic nose, memory device, and radio frequency identification. Over the last decades a great effort has been made for the scientific understanding of the fundamental charge transport and injection physics of conjugated polymer and small-molecule organic semiconductors to ensure that organic molecules can compete with silicon derivatives in this field. Thus, examples of OFETs based on SubPcs have recently been described with promising results.[51]

SubPcs are also competent within the field of organic light emitting diodes (OLEDs), where they play the role of orange emitters and have a narrow emission amplitude with excellent electrical performance.[40a,b,c,d,52] A representative example is the case of the axially substituted phthalimido-boron SubPcs, which exhibit a high quantum yield for photoluminescence (Φ), maintain a high molar extinction coefficient (ε) and have bipolar electrochemical stability. Its main role have been extended into simple organic electronic devices with double functionality such as charge transporters and emitters (Figure 11).[47a]

[51] a) C. K. Renshaw, X. Xu, S. R. Forrest, *Org. Electron.* **2010**, *11*, 175–178; b) X. Tong, S. R. Forrest, *Org. Electron.* **2011**, *12*, 1822–1825; c) J. S. Castrucci, M. G. Helander, G. E. Morse, Z.-H. Lu, C. M. Yip, T. P. Bender, *Cryst. Growth Des.* **2012**, *12*, 1095–1100; d) G. E. Morse, T. P. Bender, *ACS Appl. Mater. Interfaces* **2012**, *4*, 5055–5068; e) M. Singh, A. Mahajan, R. K. Bedi, D. K. Aswal, *Electron. Mater. Lett.* **2013**, *9*, 101–106; f) J. Li, W. Shi, L. Shu, J. Yu, *J. Mater. Sci. Mater. Electron.* **2015**, *26*, 8301–8306.

[52] a) Y.-H. Chen, J.-H. Chang, G.-R. Lee, I.-W. Wu, J.-H. Fang, C.-I. Wu, T.-W. Pi, *Appl. Phys. Lett.* **2009**, *95*, 133302; b) Y.-H. Chen, Y.-J. Chang, G.-R. Lee, J.-H. Chang, I.-W. Wu, J.-H. Fang, S.-H. Hsu, S.-W. Liu, C.-I. Wu, T.-W. Pi, *Org. Electron.* **2010**, *11*, 445–449; c) M. G. Helander, G. E. Morse, J. Qiu, J. S. Castrucci, T. P. Bender, Z.-H. Lu, *ACS Appl. Mater. Interfaces* **2010**, *2*, 3147–3152; d) G. E. Morse, M. G. Helander, J. F. Maka, Z.-H. Lu, T. P. Bender, *ACS Appl. Mater. Interfaces* **2010**, *2*, 1934–1944.

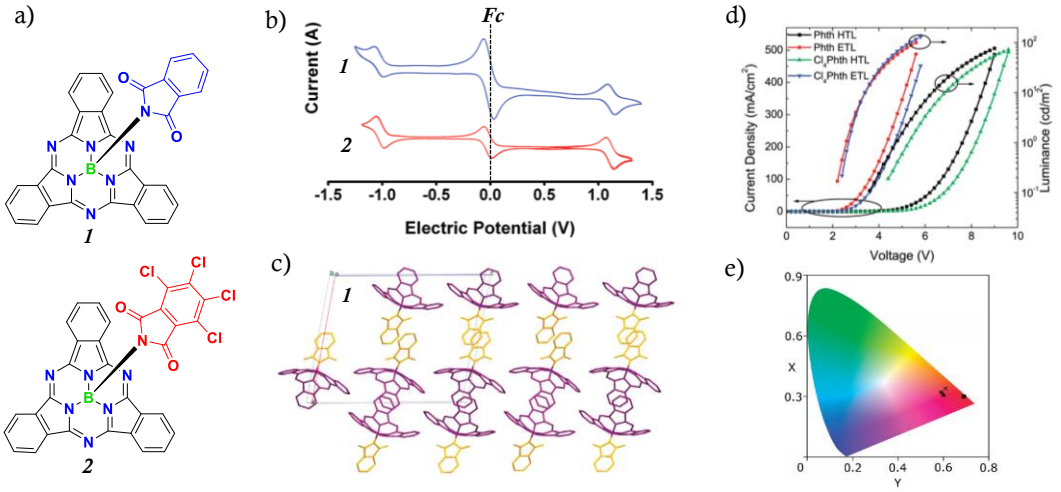

Figure 11. (a) Target phthalimido-boron SubPcs structures; (b) cyclic voltammograms of **1** (blue) and **2** (red) in DCM; (c) unit cell of **1** viewed along the *b* (left) and *c* (right) axis showing the π–π extended stacking pathways; (d) luminance and current density as a function of voltage for OLED devices; (e) CIE color coordinates (symbol; x, y) for the light emission produced by the OLED devices. For HTL devices with compound **1**.[40a]

On the other hand, organic-semiconductor-materials-based bulk heterojunction (BHJ) and planar heterojunction (PHJ) photovoltaic cells have been considered as a promising approach for making large-size, flexible and light-weight solar cell devices.[53] In these devices, a blend film of electron donor (p-type conjugated polymer or small molecule) and electron acceptor (n-type fullerene and their derivatives) acts as the photovoltaic active layer to collect light and generate electricity. Such a BHJ or PHJ structures are useful to overcome the relatively short exciton diffusion length, usually in the order of 10 nm in neat organic films. Recently, there has been a great effort to show that SubPcs are competitive molecules within the field of organic photovoltaic (OPV) devices, proving that they can behave both as electron donors when combined

[53] a) G. Yu, J. Gao, J. C. Hummelen, F. Wuld, A. J. Heeger, *Science*, **1995**, *270*, 1789–1791; b) S. Günes, H. Neugebauer, N. S. Sariciftci, *Chem. Rev.* **2007**, *107*, 1324; c) B. C. Thompson, J. M. J. Fréchet, *Angew. Chem. Int. Ed.* **2008**, *47*, 58–77; d) G. Li, R. Zhu, Y. Yang, *Nature Photon* **2012**, *6*, 153–161.

with fullerenes, or as electron acceptors when they are appropriately substituted.[54] A power conversion efficiency of 4.4% has been obtained using a PHJ organic photovoltaic cell by diluting the electron donor chloro-SubPc into a wide-energy-gap host material, i.e. *p*-bis(triphenylsilyl)benzene (UGH2), as electron donor unit, optimizing the degree of interaction between donor molecules and giving a ~50% increase in the exciton diffusion length.[54h]

The combination of SubPcs and SubNcs has been used as complementary absorbers in tandem (Figure 12),[55] wherein the SubNcs behave as an electron donor in PHJ photovoltaic cells. The dilute donor concept is applied to demonstrate energy-cascade OPVs that utilize a host-guest donor layer.

One of the significant advantages of SubNcs is that they can be thermally evaporated in high vacuum, and they are also soluble in organic solvents, due to their non-planar molecular structure. Thus allows the preparation of SubNc thin films via both vacuum evaporation and solution processes. Organic photovoltaic cells based on SubNcs have proven efficient growth of the power conversion efficiencies.[56] More recently, maximum efficiency has been achieved 8.4% with a fullerene-free organic solar cell, thanks to the combination of chloro-SubNc, chloro-SubPc, and α-6T (polythiophene), in a simple three-layer architecture, in which an energy-relay cascade

[54] a) K. L. Mutolo, E. I. Mayo, B. P. Rand, S. R. Forrest, M. E. Thompson, *J. Am. Chem. Soc.* **2006**, *128*, 8108–8109; b) H. Gommans, D. Cheyns, T. Aernouts, C. Girotto, J. Poortmans, P. Heremans, *Adv. Funct. Mater.* **2007**, *17*, 2653–2658; c) H. Gommans, B. Verreet, B. P. Rand, R. Müller, J. Poortmans, P. Heremans, J. Genoe, *Adv. Funct. Mater.* **2008**, *18*, 3686–3691; d) B. Kippelen, J. L. Bredas, *Energy Environ. Sci*. **2009**, *2*, 251–261; e) W. A. Luhman, R. J. Holmes, *Adv. Funct. Mater.* **2011**, *21*, 764–771; f) N. Beaumont, I. Hancox, P. Sullivan, R. A. Hatton, T. S. Jones, *Energy Environ. Sci.* **2011**, *4*, 1708–1711; g) J. Y. Kim, J. Kwak, S. Noh, C. J. Lee, *Nanosci. Nanotechnol.* **2012**, *12*, 5724–5727; h) S. M. Menke, W. A. Luhman, R. J. Holmes, *Nat. Mater.* **2012**, *12*, 152–157; i) R. Pandey, A. A. Gunawan, K. A. Mkhoyan, R. J. Holmes, *Adv. Funct. Mater*. **2012**, *22*, 617–624; j) C. Kulshreshtha, G.-W. Kim, R. Lampande, D.-H. Huh, M. Chaeb, J.-H. Kwon, *J. Mater. Chem. A* **2013**, *1*, 4077–4082; k) G. E. Morse, J. L. Gantz, K. X. Steirer, N. R. Armstrong, T. P. Bender, *ACS. Appl. Mater. Interfaces* **2014**, *6*, 1515–1524.

[55] S. M. Menke, R. J. Holmes, *ACS Appl. Mater. Interfaces* **2015**, *7*, 2912–2918.

enables an efficient two-step exciton dissociation process.[56e] This result shows that SubNcs are promising materials for photovoltaic applications *via* various processing techniques, such as vacuum deposition and wet coating.

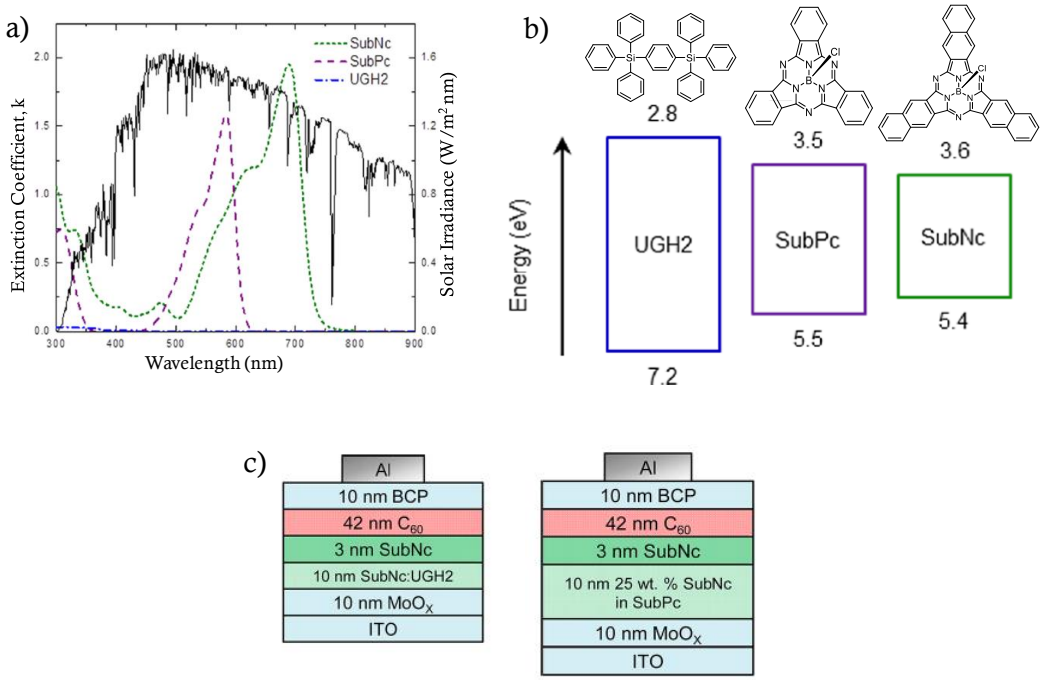

Figure 12. (a) Thin film spectral extinction coefficient for SubPc (violet dashed line), SubNc (green dotted line), and UGH2 (blue dash-dotted line) as compared to the AM1.5G solar spectrum (solid line). (b) Molecular structures and molecular orbital energy levels for UGH2, SubPc, and SubNc. (c) Schematic of a host–guest device based on the pairing of SubNc/UGH2 and of a host–guest OPV incorporating SubPc as a photoactive host.[55]

[56] a) B. Ma, C. H. Woo, Y. Miyamoto, J. M. J. Fréchet, *Chem. Mater.* **2009**, *21,* 1413–1417; b) B. Verreet, S. Schols, D. Cheyns, B. P. Rand, H. Gommans, T. Aernouts, P. Heremans, J. Genoe, *J. Mater Chem.* **2009**, *19*, 5295–5297; c) T. Sano, X.-F. Wang, Z. Hong, J. Kido and Y. Yang, *Nanotechnology*, *2013*, *24*, *484007; d)* B. Verreet, K. Cnops, D. Cheyns, P. Heremans, A. Stesmans, G. Zango, C. G. Claessens, T. Torres, B. P. Rand, *Adv. Energy. Mater.* **2014**, *4*, 1301413; e) K. Cnops, B. P.Rand, D. Cheyns, B. Verreet, M. A. Empl, P. Heremans, P. *Nat. Commun.* **2014**, *5*, 3406.

As mentioned before, SubPcs can behave both as electron donor or acceptor as a function of the counter-partner. Geminal work on the performance of fullerene-free OPVs or "all SubPc based-devices" has been reported. The latter makes use of electron deficient SubPcs as the acceptor material instead of C_{60}, and cloroboron-SubPc, as the donor one.[57]

More recently, another application of supramolecular systems based on SubPcs has been reported for the first time. This consist in the formation of non-centrosymmetric homochiral columnar SubPc assemblies, through a cooperative supramolecular polymerization process, driven by a combination of noncovalent interactions: H-bonding, π–π stacking, and dipolar interactions, between axial dipolar B-F bonds. The latter results in the formation of nanofibers and condensed phases that can be aligned in the presence of electric fields, yielding hierarchically organized nanomaterials and liquid crystalline devices that may show permanent or switchable polarization. The

[57] a) N. Beaumont, J. S. Castrucci, P. Sullivan, G. E. Morse, A. S. Paton, Z.-H. Lu, T. P. Bender, T. S. Jones, *J. Phys. Chem. C* **2014**, *118*, 14813–14823; b) K. Cnops, G. Zango, J. Genoe, P. Heremans, M. V. Martinez-Diaz, T. Torres, D. Cheyns, *J. Am. Chem. Soc.* **2015**, *137*, 8991–8997; c) J. S. Castrucci, R. K. Garner, J. D. Dang, E. Thibau, Z.-H. Lu, T. P. Bender, *ACS Appl. Mater. Interfaces* **2016**, *8*, 24712–24721; d) D. S. Josey, S. R. Nyikos, R. K. Garner, A. Dovijarski, J. S. Castrucci, J. M. Wang, G. J. Evans, T. P. Bender, *ACS Energy Lett.* **2017**, *2*, 726–732; e) C. Duan, G. Zango, M. García-Iglesias, F. J. M. Colberts, M. M. Wienk, M. V. Martínez-Díaz, R. A. J. Janssen, T. Torres, *Angew. Chem. Int. Ed.* **2017**, *56*, 148–152; f) T. G. Plint, B. H. Lessard, T. P. Bender, *Opt. Mater. (Amst).* **2018**, *75*, 710–718; g) R. K. Garner, D. S. Josey, S. R. Nyikos, A. Dovijarski, J. M. Wang, G. J. Evans, T. P. Bender, *Sol. Energy Mater. Sol. Cells* **2018**, *176*, 331–335; h) K. L. Sampson, G. E. Morse, T. P. Bender, *ACS Appl. Energy Mater.* **2018**, *1*, 2490–2501; i) J. D. Dang, D. S. Josey, M. T. Dang, T. P. Bender, *ACS Omega* **2018**, *3*, 2093–2103; j) R. K. Garner, M. T. Dang, J. D. Dang, T. P. Bender, *ACS Appl. Energy Mater.* **2018**, *1*, 1029–1036; k) T. M. Grant, D. S. Josey, K. L. Sampson, T. Mudigonda, T. P. Bender, B. H. Lessard, *Chem. Rec.* **2019**, *0*, DOI 10.1002/tcr.201800178; l) D. S. Josey, G. L. Ingram, R. K. Garner, J. M. Wang, G. J. Evans, Z.-H. Lu, T. P. Bender, *ACS Appl. Energy Mater.* **2019**, DOI 10.1021/acsaem.8b01918.

axial dipole moments generated in these assemblies produces an electric-field-responsive polar materials that may exhibit ferroelectricity (Figure 13).[58]

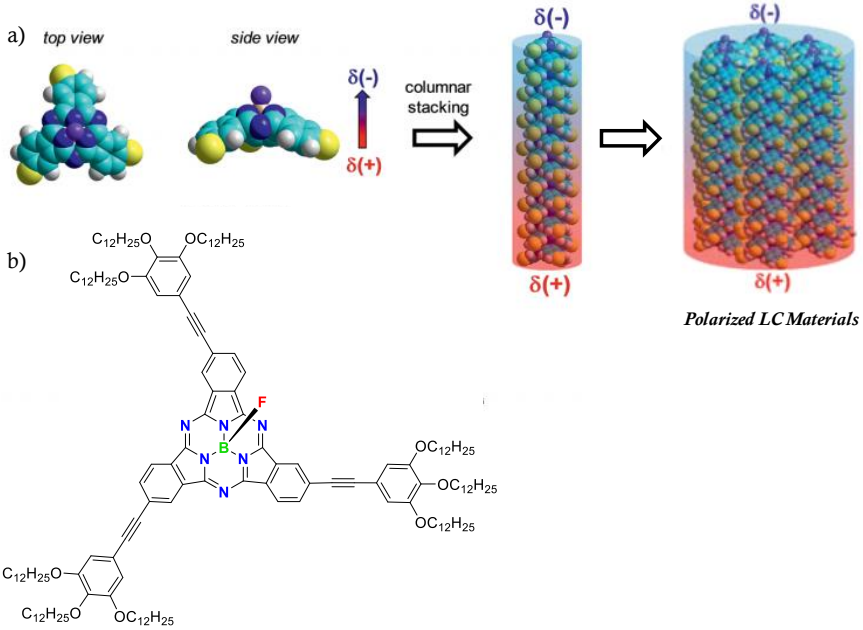

Figure 13. (a) Top and side views of the axial dipolar SubPc(B–F) macrocycle. The yellow spheres represent the arylethynyl substituents. Head-to-tail stacking leads to polarized columnar structures. (b) Target molecule structure of the C_3-symmetric SubPc.[58c]

Apart from the above mentioned, studies on the application of SubNcs in technological areas are scarce, and almost inexistent for SubPzs (as an exception, the liquid crystal behaviour of hexasulfanylated SubPzs has been explored).[46c] In general, SubPzs and SubNcs remain mostly unexplored, in comparison with SubPcs, mainly due to the limited synthetic methodology for the construction of these macrocycles.

[58] a) J. Guilleme, M. J. Mayoral, J. Calbo, J. Aragó, P. M. Viruela, E. Ortí, T. Torres, D. González-Rodríguez, *Angew. Chem. Int. Ed.* **2015**, *54*, 2543–2547; b) J. Guilleme, E. Cavero, T. Sierra, J. Ortega, C. L. Folcia, J. Etxebarria, T. Torres, D. González-Rodríguez, *Adv. Mater.* **2015**, *27*, 4280–4284; c) J. Guilleme, J. Aragó, E. Ortí, E. Cavero, T. Sierra, J. Ortega, C. L. Folcia, J. Etxebarria, D. González-Rodríguez, T. Torres, *J. Mater. Chem. C* **2015**, *3*, 985–989; d) A. V Gorbunov, M. Garcia Iglesias, J. Guilleme, T. D. Cornelissen, W. S. C. Roelofs, T. Torres, D. González-Rodríguez, E. W. Meijer, M. Kemerink, *Sci. Adv.* **2017**, *3*, e1701017.

GENERAL OBJECTIVES

General Objectives

The main goal of this Doctoral Thesis is the development of different synthetic methodologies for the preparation of new molecular materials based on subporphyrazines (SubPzs) and subnaphthalocyanines (SubNcs) as frontier molecules of the well-known and studied subphthalocyanines (SubPcs). These analogues of subphthalocyanines are presented as potential competitors in various emerging fields of physics. This means that exploiting and exploring the chemistry of these derivatives is a necessary task to satisfy the requirements imposed by these possible applications.

More in detail, the objectives of this thesis are defined as follows:

Chapter 1 is devoted to the chemistry of subporphyrazine derivatives. As we will discuss in the next section, SubPzs show exceptional tunability of their properties by peripheral functionalization. We plan to exploit this distinctive feature by exploring in depth the existing strategies for peripheral functionalization of SubPzs and developing new ones. The aim of this chapter is to endow the periphery of SubPzs with carefully selected functional groups as a means to obtain chromophores with, for example, red and/or panchromatic absorption, or particular redox properties. This ability of controlling the physicochemical parameters by chemical manipulation is essential for the application of SubPzs in applied fields.

Chapter 2 is focused on the synthesis and characterization of novel structures based on dodecafunctionalized subnaphthalocyanines. We will focus on a synthetic route for preparing functionalized 2,3-naphthalenedicarbonitrile precursors. Cyclotrimerization reactions will furnish a new series of SubNc derivatives.

Chapter3 is aimed at studying potential applications of SubPzs and SubNcs:

1. SubNcs with electron acceptor features will be prepared and evaluated as active agents in bulk heterojunction solar cells (BHJ).

2. We will use our studies on structure-property relationships to design SubPzs for their specific application in photovoltaics or singlet fission.

CHAPTER 1

Subporphyrazines with Extended Conjugation

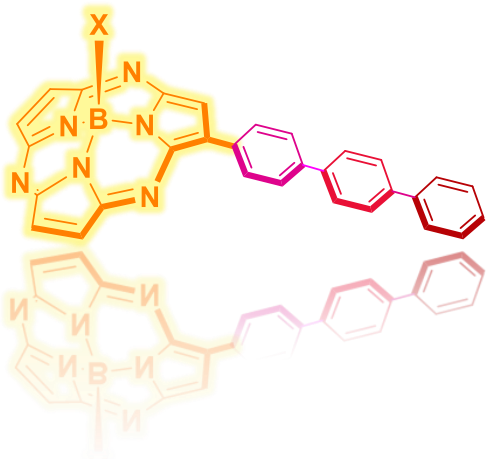

1.1 State of the art on Subporphyrazines

The singular features of SubPzs have attracted our interest in their synthesis and study, in search for dyes displaying unusual optical and electronic properties. SubPzs, which can be regarded as contracted porphyrazines (Pzs), belong to the group of tripyrrolic porphyrinoids, a large family of heteroannulenes categorized as subporphyrinoids.

The SubPz skeleton has always been assembled by treating a maleonitrile derivative with boron trichloride (Scheme 1.1).[46c,d]

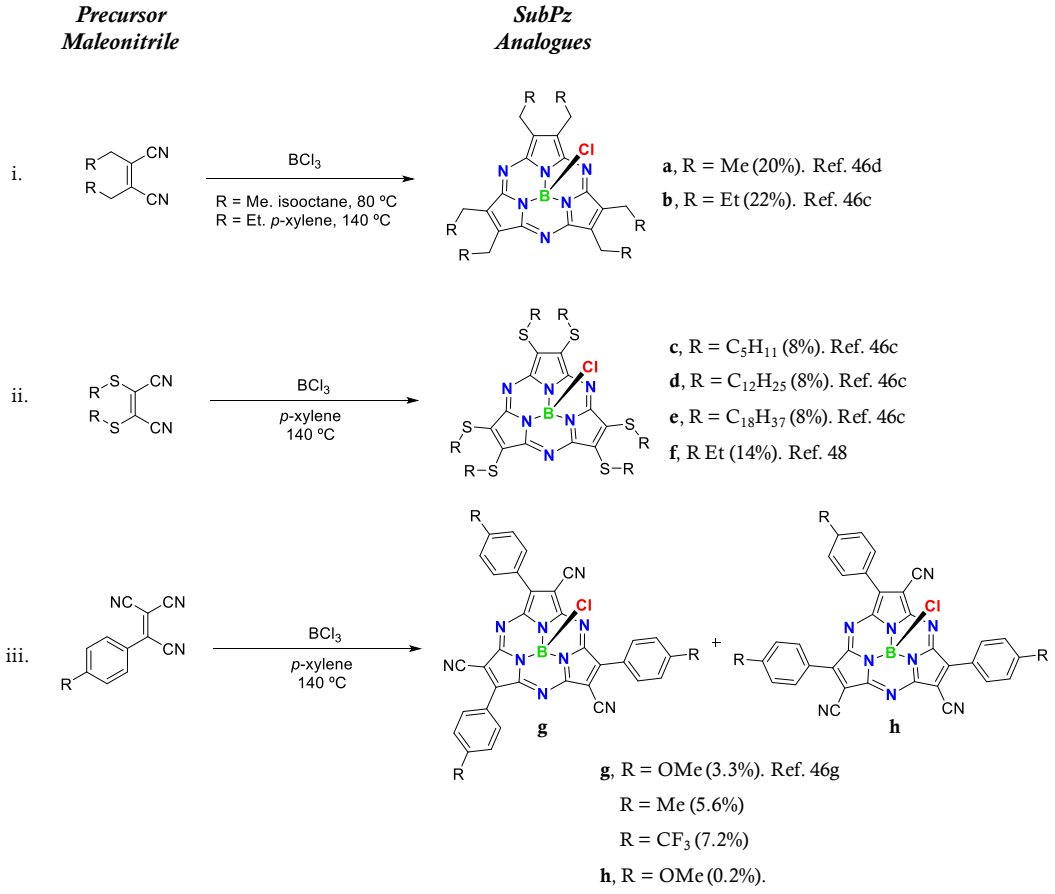

Scheme 1.1. Syntheses of SubPz derivatives through cyclotrimerization reported to date.

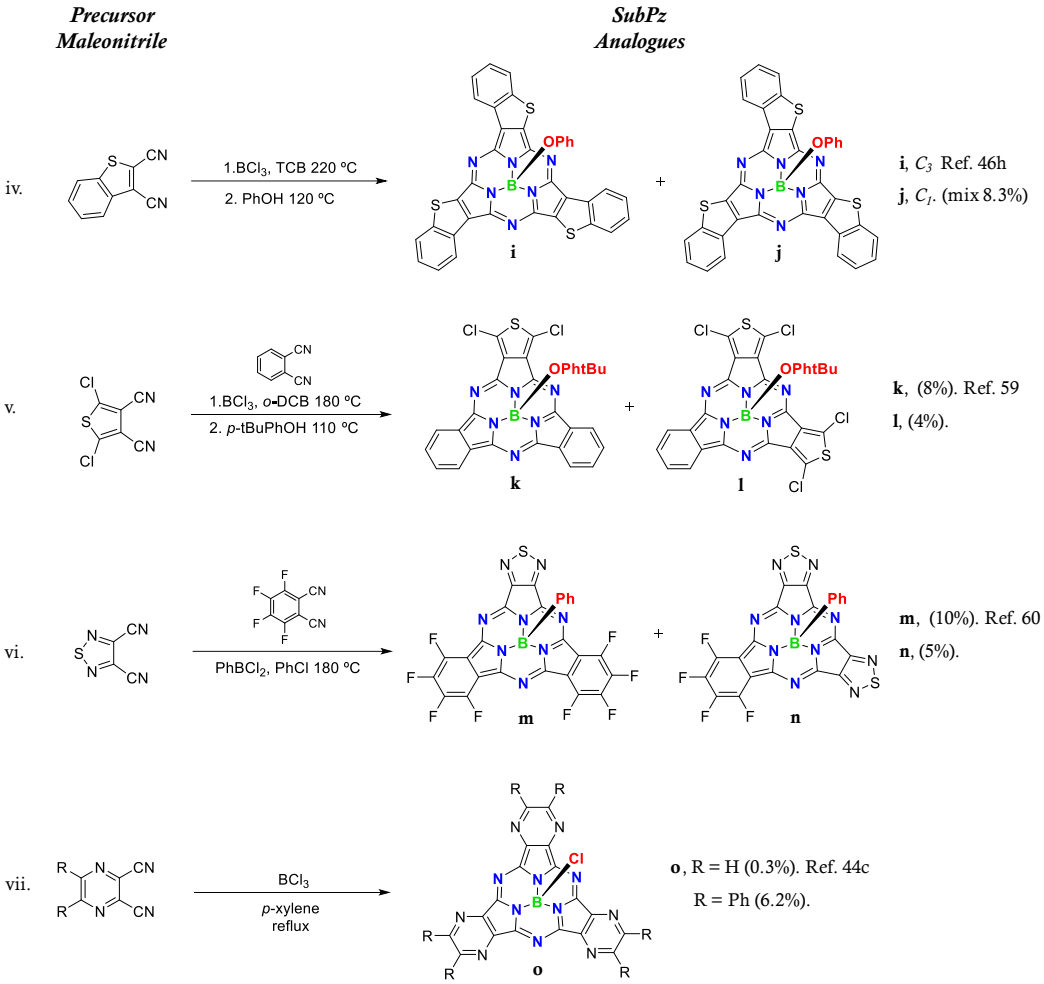

Scheme 1.1 (cont.). Syntheses of SubPz derivatives containing fused heterocycles reported to date.

The only exception was reported by Kobayashi and co-workers, in which unsubstituted fumaronitrile was used as a starting material in a crossover cyclotrimerization reaction with tetramethylsuccinonitrile. A mixture of subazachlorin and peripherally unsubstituted SubPz were obtained (Scheme 1.2).[46f] Unfortunately, chemical manipulation of unsubstituted SubPz (**q**) is not feasible due to its proven instability once formed.

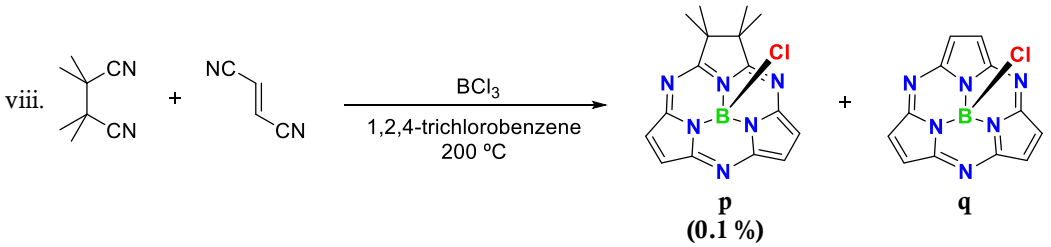

p (0.1 %) **q**

Scheme 1.2. Synthesis of subazachlorin **p** by crossover cyclotrimerization reaction.[46f]

Another limiting synthetic condition is that the use of BCl_3 is incompatible with many functions, in particular, with precursors bearing boron-coordinating heteroatoms such as nitrogen or even oxygen. These synthetic limitations have precluded the development of a variety of SubPz derivatives, parallel to those reported for the SubPc and SubP series.

Basically, the peripheral functionalization at SubPzs depends closely on the functionalization itself imposed by the precursor maleonitrile derivative. To date, very few cases have been reported in direct synthesis of SubPzs, either by the use of precursor maleonitriles, or by heterocycle dicarbonitrile analogues for obtaining SubPzs bearing fused heterocycles at their periphery, namely, thiophene,[59] benzo[*b*]thiophene,[46h] pyrazine,[44c] dibenzoquinoxaline,[44a] and thiadiazole[60] (Schemes 1.1 and 1.2).

The use of BCl_3 leads to the production of macrocycles bearing a chloride ion as the axial ligand. This axial ligand can be replaced by other substituents, thus affording a means of functionalizing the axial position of SubPzs. Typically, this ligand exchange is facile compared to that of SubPcs. For instance, the chloride anion may be replaced by water under mild conditions to afford the corresponding axially substituted hydroxy-SubPzs.[46c,d] Likewise, treating chloro-SubPzs with phenol or $BF_3{\cdot}Et_2O$ gives rise to the corresponding phenoxy- or fluoro-substituted compounds, respectively.[16c]

[59] H. Gotfredsen, F. E. Storm, A. V. Muñoz, M. Santella, A. Kadziola, O. Hammerich, K. V Mikkelsen, M. B. Nielsen, *Chem. Eur. J.* **2017**, *23*, 16194–16198.
[60] M. Hamdoush, I. A. Skvortsov, M. S. Mikhailov, G. Pakhomov, P. A. Stuzhin, *J. Fluor. Chem.* **2017**, *204*, 31–36.

The higher efficiency of both the hydrolysis and fluorination reactions in the case of SubPzs, relative to the same type of conversion with SubPcs, serves to underscore the higher reactivity of SubPzs at the axial positions.

Recently, the axial ligand of a phenoxy-substituted SubPz could be further functionalized by treating it with a Cp^*Ru^+ salt (Cp^*=1,2,3,4,5-pentamethylcyclopentadienyl). This gives rise to the associated SubPz π-complex bearing a ruthenoarene subunit (Figure 1.1a).[27] Conversely, π-coordination could not be performed on the pyrrole subunits. SubPz dimers and trimers in which the macrocycles are connected through their axial positions by phenolic ruthenoarene-linkers also have been prepared (Figure 1.1b, c). The nature of the axial linkers greatly impacts the redox properties of SubPz arrays, and the electrochemical studies reveal strong electronic interactions of SubPz macrocycles in the ground state upon formation of the ruthenoarene-linked dimer and trimer.[61] This approach provides a useful means for modifying the electronic properties of the basic SubPz skeleton by increasing its electron-accepting ability.

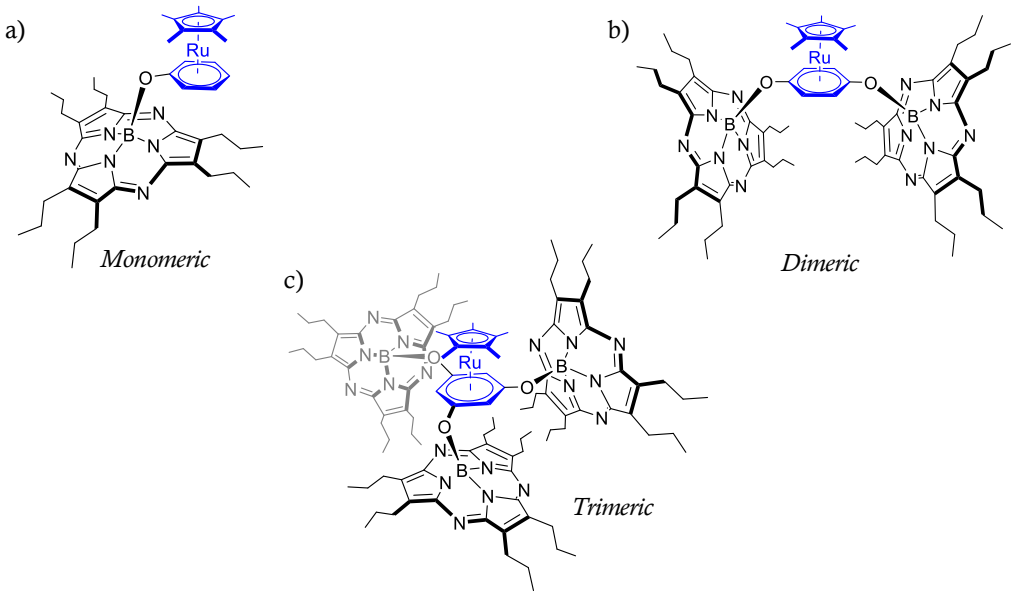

Figure 1.1. Ruthenoarene-linked SubPz arrays: a) monomer, b) dimer, and c) trimer.

[61] E. Caballero, C. Romero-Nieto, V. Strauß, M. S. Rodríguez-Morgade, D. M. Guldi, J. L. Sessler, T. Torres *Chem. Eur. J.* **2014**, *20*, 6518–6525.

What makes SubPzs unique among all the other classes of porphyrinoids is their exceptional electronic tunability by peripheral functionalization. The striking influence of peripheral substituents on the SubPz π-system arises from the combination of three structural features within these macrocycles, namely, their *meso*-aza bridges, their non-fused pyrrolic units and their electron deficient, boron(III) central ions.

Thus, in addition to intense Soret and Q-bands, the absorption spectra of SubPzs peripherally substituted with functions containing *p*- or π-electrons also display strong absorptions in a window that goes from 384 nm to 503 nm.[46c,d,e,48] In particular, the optical spectra of thioether-substituted SubPzs show a strong feature at 438 nm, [46c] which has been attributed to n→π* transitions from nonbonding sulfur electrons to the macrocycle, by analogy with those exhibited by the Pz tetramers.[62] But unlike Pzs, in which these bands are weak (<40% of the Q-band),[63] within SubPzs, peripheral thioethers originate bands that dominate the UV/Vis spectrum (15-25% higher than the Q-band), evincing a higher impact of these peripheral substituents on the electronic properties of the macrocycle within the trimer.

There is only one example of derivatization of peripheral substituents on SubPzs. Peripherally hexaarylated SubPzs have been prepared through a Pd-catalyzed, CuTC-mediated coupling of a hexaethylsulfanylated SubPz with arylboronic acids (Scheme 1.3).[48] The low yields obtained in the preparation of the hexasulfanyl precursors constitute a drawback of this method. The introduced aryl substituents strongly influence the electronic properties of SubPz through effective conjugative interaction. Aryl rings endowed with π-electron-donating groups at the *para* positions produce a remarkable perturbation of the electron density of the SubPz macrocycle. This is reflected through significant red-shifts of the SubPz CT and Q-bands, together with increase of the molar absorptivity of the former, with respect to those exhibited by the

[62] L. Guo, D. E. Ellis, B. M. Hoffman, Y. Ishikawa, *Inorg. Chem.* **1996**, *35*, 5304–5312.

[63] a) C. S. Velazquez, G. A. Fox, W. E. Broderick, K. A. Andersen, O. P. Anderson, A. G. M. Barrett, B. M. Hoffman, *J. Am. Chem. Soc.* **1992**, *114*, 7416–7424; b) S. Lee, A. J. P. White, D. J. Williams, A. G. M. Barrett, B. M. Hoffman, *J. Org. Chem.* **2001**, *66*, 461–465.

hexaphenyl-SubPz (**r**). Moreover, the trend in the first SubPz reduction potentials correlates with the Hammett constants (σ_p) corresponding to the *para* substituents of the aryl. The domed, extended SubPz π-system self-assembles in the solid state to form a dimeric capsule that houses a solvent molecule.

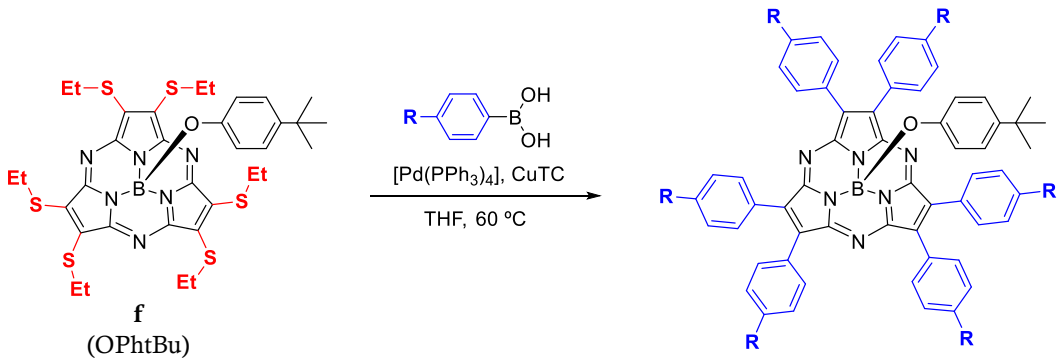

r, R = H (35 %).

s, R = OMe (37 %).

t, R = SMe (34 %).

u, R = NMe_2 (23 %).

v, R = NO_2 (20 %)

w, R = CF_3 (28 %)

x, R = CO_2Me (43 %)

Scheme 1.3. Peripheral arylation of SubPzs by Pd-catalyzed cross coupling reactions.

The striking alteration of the optical properties upon peripheral functionalization is not observed in such a large extent in the corresponding Pzs.[48,63,64,65] Interestingly, only phosphorus (V) octaarylporphyrazines exhibit comparable bathochromic shifts of their Q bands, and strong CT bands arising from the peripheral aryl substituents.[66] The similar absorption spectra of SubPzs and P(V)Pzs point to a possible enhancing effect

[64] a) L. A. Ehrlich, P. J. Skrdla, W. K. Jarrell, J. W. Sibert, N. R. Armstrong, S. S. Saavedra, A. G. M. Barrett, B. M. Hoffman, *Inorg. Chem.* **2000**, *39*, 3963–3969; b) A. Sholto, S. Lee, B. M. Hoffman, A. G. M. Barrett, B. Ehrenberg, *Photochem. Photobiol.* **2008**, *84*, 764–773.

[65] T. Goslinski, E. Tykarska, M. Kryjewski, T. Osmalek, S. Sobiak, M. Gdaniec, Z. Dutkiewicz, J. Mielcarek, *Anal. Sci.* **2011**, 27, 511–515.

[66] a) T. Furuyama, T. Yoshida, D. Hashizume, N. Kobayashi, *Chem. Sci.* **2014**, *5*, 2466–2474; b) T. Yoshida, W. Zhou, T. Furuyama, D. B. Leznoff, N. Kobayashi, *J. Am. Chem. Soc.* **2015**, *137*, 9258–9261.

of the electron deficient phosphorus(V) and boron(III) central ions, in the electronic communication between the peripheral substituents and the macrocycles. Such electronic impact is also higher than for other B(III) containing macrocycles, such as sulfanyl-substituted and arylated SubPcs or SubPs. Obviously, the direct attachment of peripheral substituents to the β-positions of the SubPz pyrrole rings accounts for their stronger interaction with the macrocycle, in comparison with that observed within SubPcs[67] and Pcs.[5d] But the *meso*-aza bridges seem to be also crucial, since SubPs arylated at their pyrrole rings do not show such absorption envelope.[68] Therefore, the combination of *meso*-aza bridges, non-fused pyrrolic units and electron deficient central ions in SubPzs provides an exceptional platform for the development of dyes with tailor-made optical and redox properties.

[67] a) D. Dini, S. Vagin, M. Hanack, V. Amendola, M. Meneghetti, *Chem. Commun.* **2005**, 3796–3798; b) M. Geyer, F. Plenzig, J. Rauschnabel, M. Hanack, B. del Rey, A. Sastre, T. Torres, *Synthesis* **1996**, 1139–1151.

[68] E. Tsurumaki, Y. Inokuma, S. Easwaramoorthi, J. M. Lim, D. Kim, A. Osuka, *Chem. Eur. J.* **2009**, *15*, 237–247.

1.2 Specific Objectives

In this chapter, we aimed at exploring the extent of delocalization of the SubPz π-electron system over conjugated peripheral substituents, consisting in oligophenylene and vinylene moieties. The vinylene moiety should minimize the steric congestion at the SubPz periphery, allowing for a coplanar, extended π-system, which could be used to electronically connect the SubPz core with different chromophores. In this respect, the preparation of these hexaarylene- and hexavinylene-substituted SubPzs by expanding upon our previously developed synthetic methods (Scheme 1.4), allows the increase of the length and/or delocalization degree of the peripheral conjugated systems, as a way to adjust the HOMO/LUMO energies, the absorption and fluorescence wavelengths and intensities, and the electrochemical properties of SubPzs. These fine-tunings should provide a way to panchromatic SubPz chromophores with strong intramolecular charge-transfer, and absorptions over a wide range of the visible region.

The specific objectives of this chapter are:

- Optimization of the synthetic methodology for the preparation of hexaalkylsulfanylated SubPz precursors.

- Preparation of oligophenylene-substituted SubPzs with different substitution patterns and exploration of their impact in the SubPz ground and excited states, as well as their molecular structures.

- Peripheral functionalization of SubPz chromophores with vinylene moieties and investigation of the alterations of the SubPz ground and excited states, as well as their molecular structure.

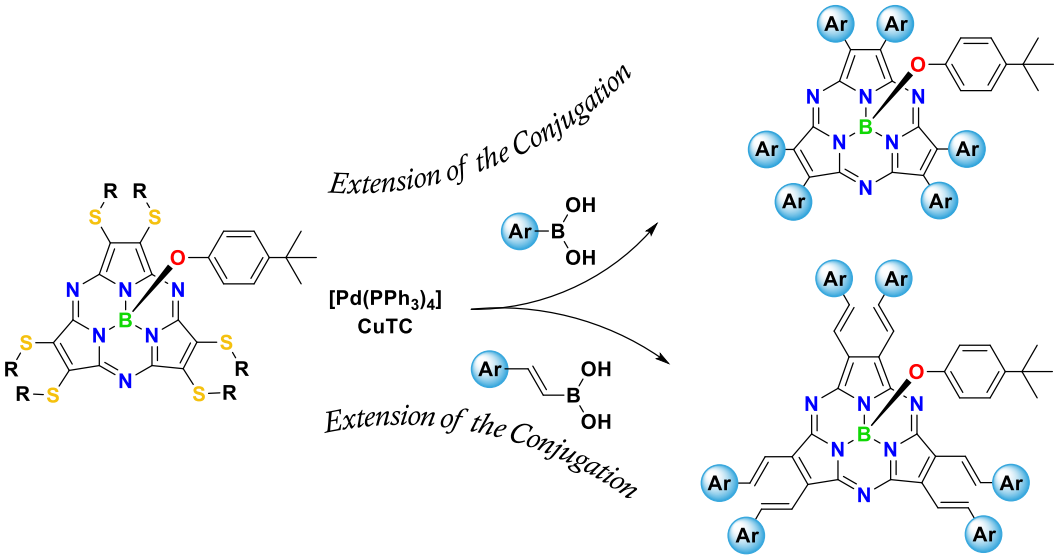

Scheme 1.4. Schematic representation of the general strategy for peripheral functionalization on SubPzs.

1.3 Results and Discussion

1.3.1 Synthesis of the hexasulfanyl-SubPz precursors

As mentioned above, maleonitrile derivatives are essential as starting materials in the synthesis of SubPzs. The preparation of bis-sulfanylated-maleonitriles **1a,b** was carried out following the synthetic route described in Scheme 1.5. Addition of sodium cyanide to carbon disulfide in DMF afforded sodium cyanodithioformate, which spontaneously dimerized in distilled water to yield disodium maleonitrilebisthiolate.[69] The bisthiolate salt was then alkylated by treatment with the corresponding alkyl bromide or iodide, affording **1a,b**.

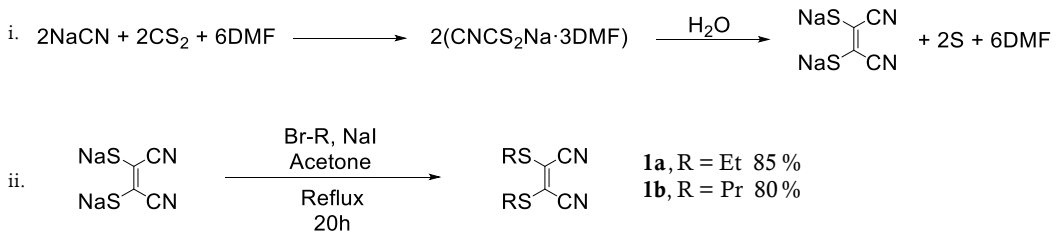

Scheme 1.5. Synthesis of maleonitriles **1a** and **1b**.

The hexaethyl- and hexapropyl-sulfanylated SubPz precursors **2a,b** were prepared by the general procedure of cyclotrimerization reaction, which consists on the treatment of bis-sulfanylated-maleonitriles **1a,b** with boron trichloride in xylenes at 110 ºC during the course of one hour,[46c] followed by axial substitution of the SubPz chloride ligand by *tert*-butylphenoxy, through refluxing in toluene, in the presence of excess *tert*-butylphenol (Scheme 1.6).[16c]. The bulky *tert*-butylphenol group placed on the axial position can guarantee solubility of products in organic solventes.

[69] a) G. Bahr, G. Schleitzer, *Chem. Ber.* **1957**, *90*, 438; b) P. Doppelt, S. Huille, *New. J. Chem.* **1990**, *14*, 607.

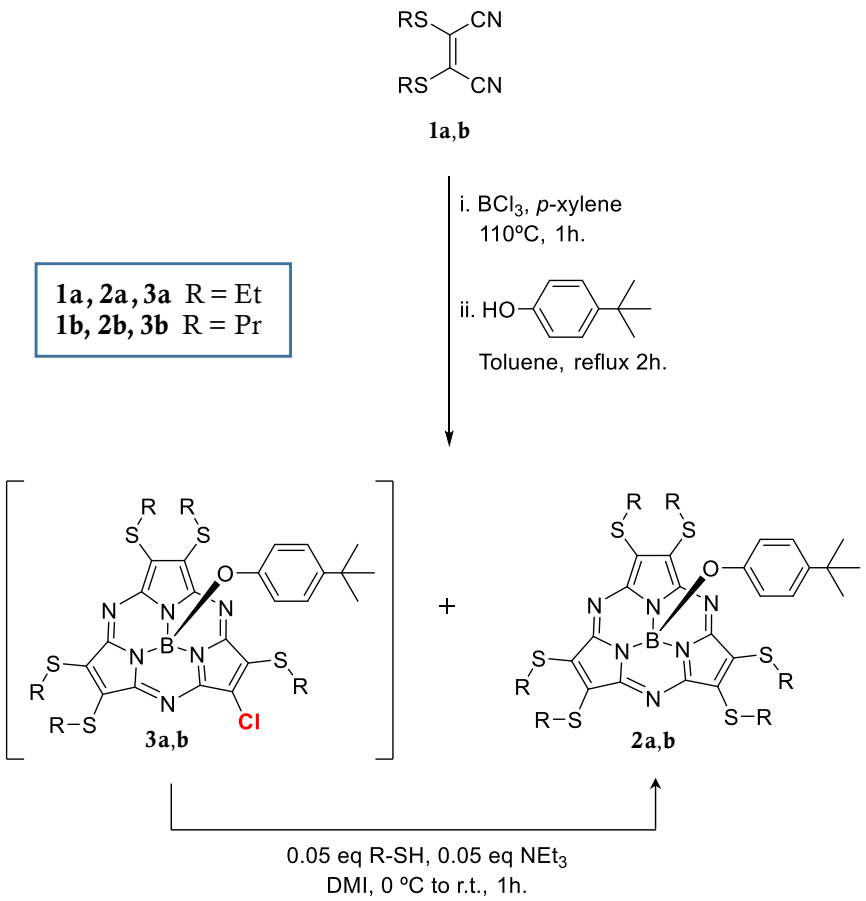

Scheme 1.6. Synthesis of the hexasulfanyl-SubPz precursors **2a** and **2b**.

When this procedure is applied to sulfanylmaleonitriles, a tedious separation of two subporphyrazine products is required, leading to low yields of the desired SubPz. Typically, in the synthesis of hexasulfanyl-SubPzs, two red bands always elute close to each other, detected by TLC and column chromatography. One of them is the hexasulfanyl-SubPz, and the other one is a side product, which turned out to be the chlorinated compound **3a,b** (Scheme 1.6). This compound was enriched after repeated separations on silica gel columns. High-resolution APCI mass spectrometry showed for R= propyl, the molecular ion of **3b** at *m/z*= 798.2377 (calc. 798.2384 $[M+H]^+$), and a less intense borenium cation peak at *m/z*= 648.1334 (calc. 648.1339 $[M - OAr]^+$) (Figure 1.2).

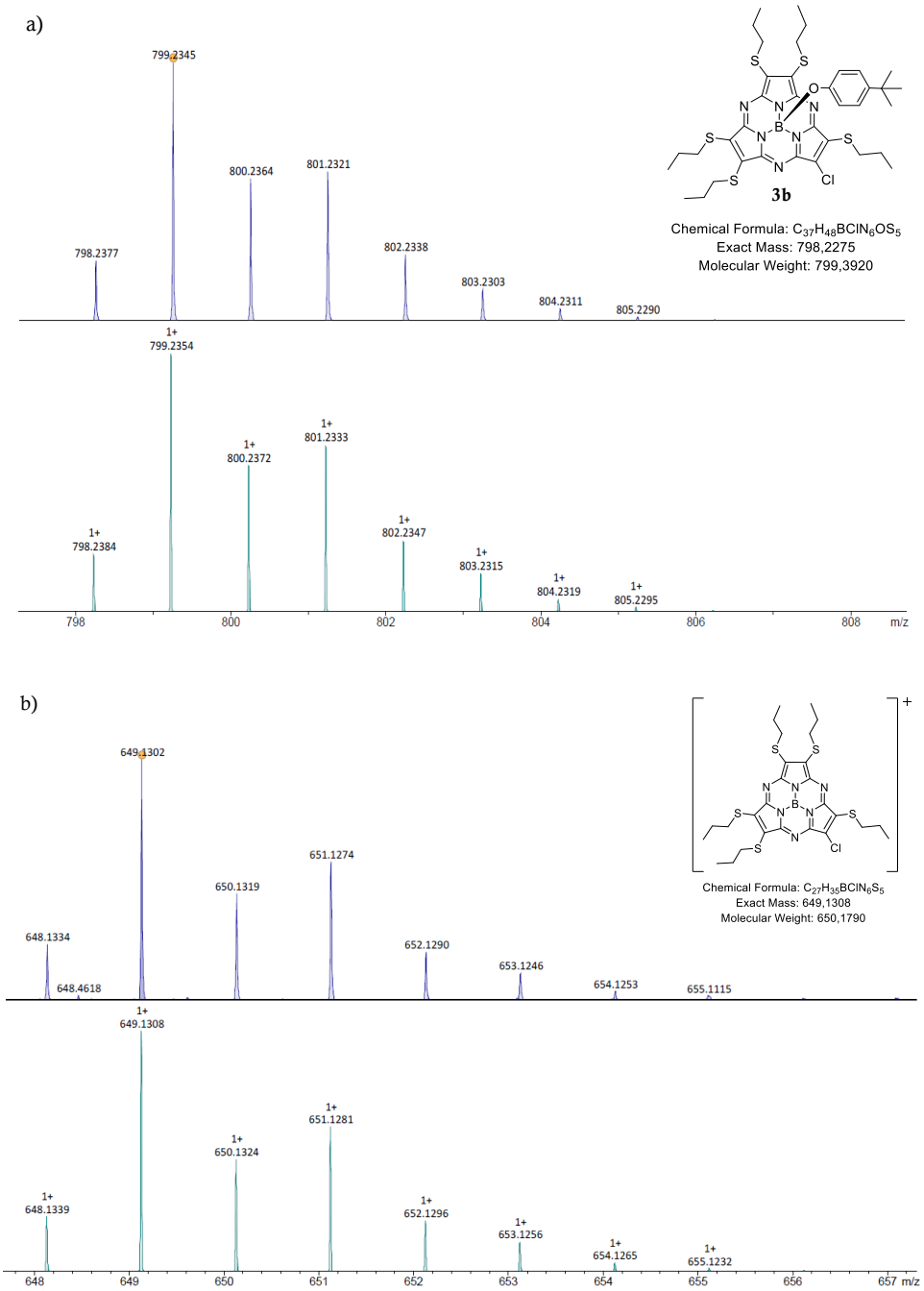

Figure 1.2. Isotopic distribution of the peak of the mass spectrometry: (a) molecular ion of **3b**, (b) borenium cation of **3b**. Upper part–experimental, and lower part–predicted isotopic pattern.

The synthetic procedure to obtain SubPzs substituted with six thioether groups was modified, by treating the mixture of **2a,b** and **3a,b** with the corresponding 1-alkylthiol in 1,3-dimethyl-2-imidazolidinone (DMI) at 0ºC. Under these conditions, the peripheral chlorine atom of **3a,b** was replaced by the corresponding alkylsulfanyl chain, by nucleophilic aromatic substitution reaction, affording the symmetric SubPzs **2a,b** in 15% overall yield (Scheme 1.6). The evolution of this reaction can be monitored by ^{1}H-NMR spectroscopy (Figure 1.3). Compounds **2b** and **3b** display signals of different intensities at 4.1–3.9 ppm and 3.7–3.4 ppm, corresponding to the –SC*H*$_2$– unit, and at 5.3–5.1 ppm, corresponding to the *tert*-butylphenoxy group (Figure 1.3b).

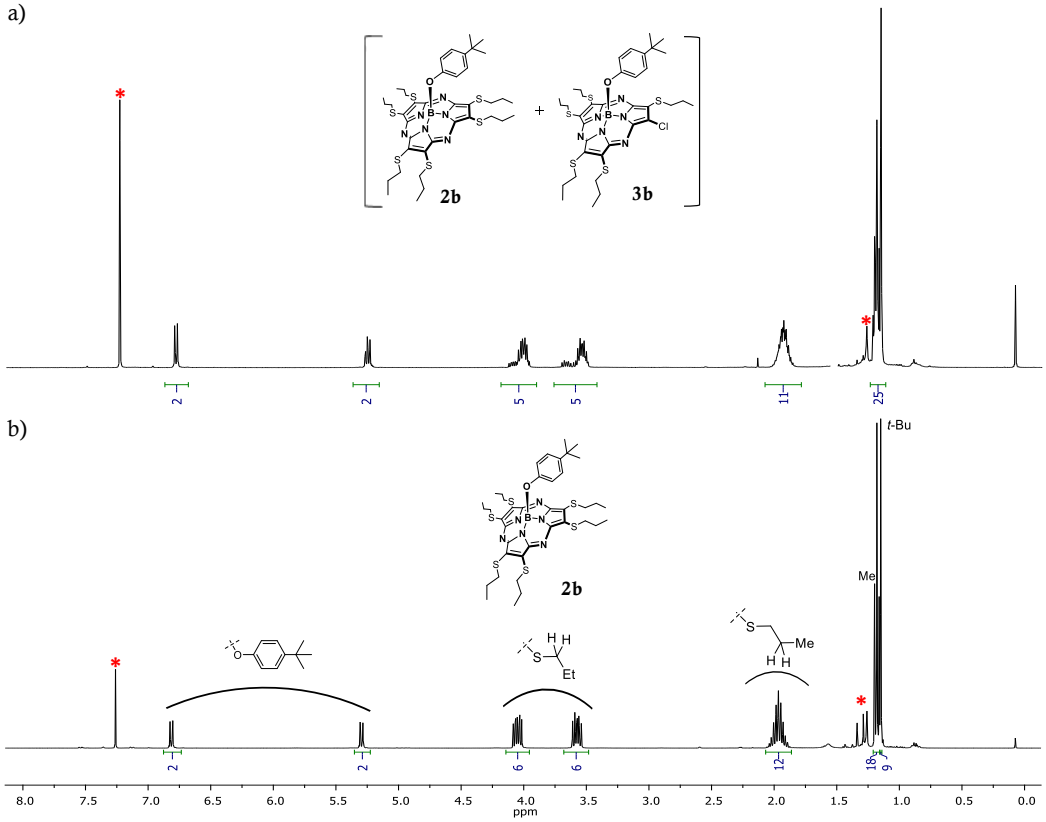

Figure 1.3. ^{1}H-NMR spectra in $CDCl_3$ at 25 ºC of: (a) Mixture **2b** and **3b** and (b) **2b** after nucleophilic aromatic substitution reaction on **3b**. Signals marked with * are due to residual solvents.

1.3.2 Synthesis of oligophenylene-SubPzs

The peripheral arylation and oligophenylation of SubPzs was carried out by applying our previously developed methodology, consisting in the palladium-catalyzed, copper(I) thiophene-2-carboxylate (CuTC)-mediated Liebeskind and Srogl coupling of boronic acids, with heteroaromatic thioethers (Scheme 1.7).[48,70]

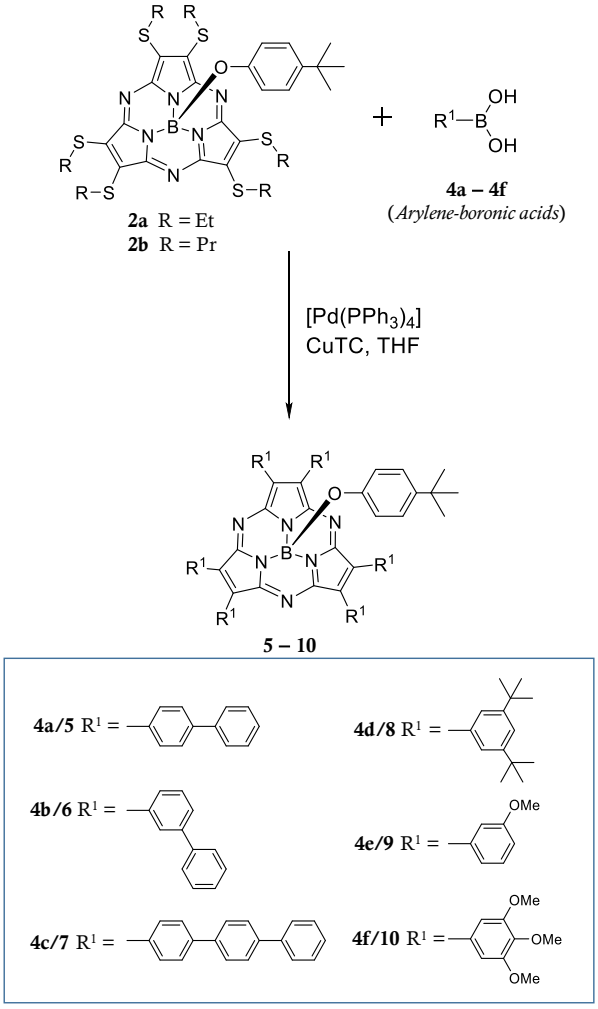

Scheme 1.7. Synthesis of oligophenylene-SubPzs (**5** – **10**).

The CuTC-mediated cross-coupling reaction of SubPz **2a,b** precursors with a variety of arylene-boronic acids at 60 °C afforded the hexaarylated-SubPzs **5**–**10**, with

[70] L. S. Liebeskind, J. Srogl, *Org. Lett.* **2002**, *4*, 979 – 981.

yields of isolated products ranging from 12% to 42% (Chart 1.1). 3,5-di-*tert*-butylphenylboronic acid **4d** afforded the lowest yield of **8** (12%), probably due to steric constraints, arising from the two bulky *tert*-butyl groups located at the two *meta*-positions of the phenylboronic acid. In all cases, the six-fold coupling proceeded smoothly in 20 h, using three equivalents of the arylene-boronic acid and CuTC, and 10% mol of palladium catalyst per thioether unit.

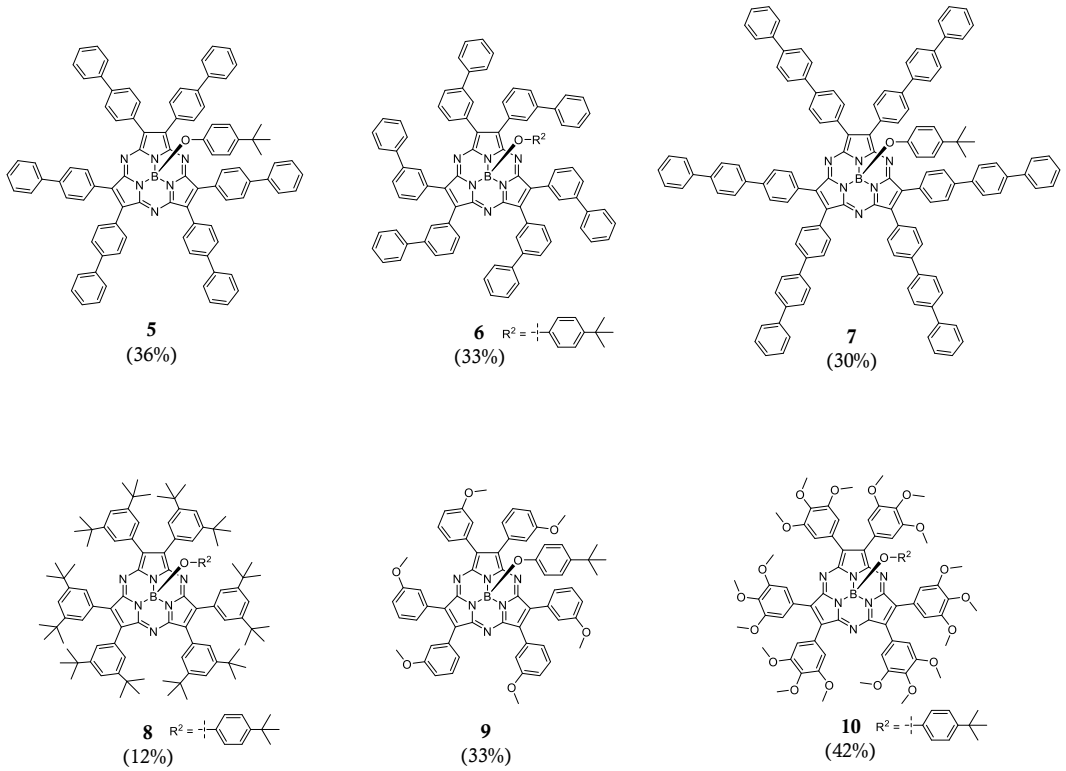

Chart 1.1. Reaction yields for the hexaarylated-SubPzs **5**–**10**.

The ^{1}H-NMR spectra of macrocycles **5** – **10** correspond to SubPzs with C_3-symmetry, indicating free rotation of the peripheral appendages, even for the bulkier substituents of **6**, **8** and **10** (Figure 1.4).

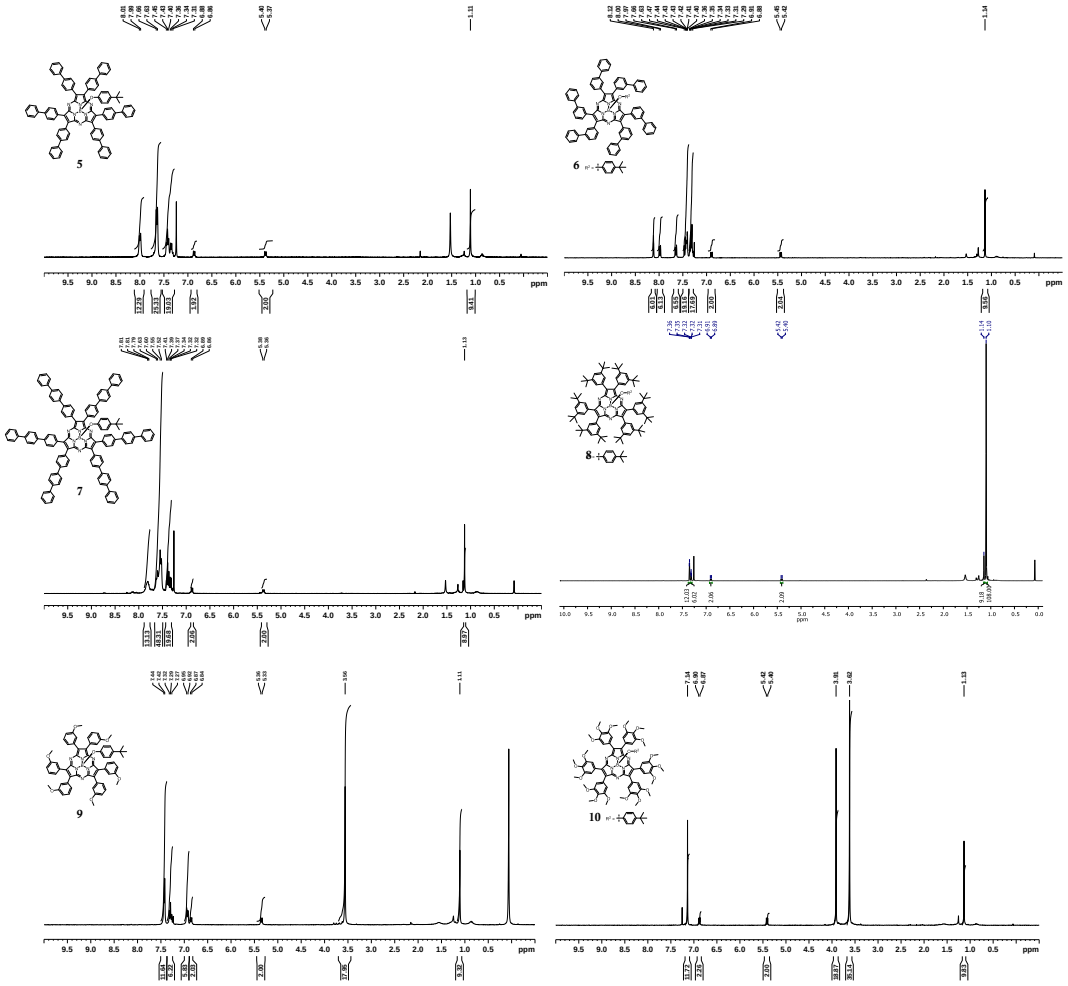

Figure 1.4. ^{1}H-NMR spectra in $CDCl_3$ at 25 ºC of oligophenylene SubPzs (**5**-**10**).

Hexaaryl-SubPzs **5**–**8** exhibit similar ^{1}H-NMR features. Their axial *tert*-butylphenoxy substituent is strongly influenced by the SubPz diamagnetic ring current, appearing as two doublets at 5.31-5.44 ppm and 6.82-6.90 ppm, and a singlet around 1.11-1.14 ppm. In addition, different groups of signals at 7.29-8.12 ppm, account for the protons of the peripheral phenyl rings. SubPzs **9** and **10**, bearing 3-methoxy- and 3,4,5-trimethoxy-substituted phenyl rings show their corresponding aryl resonances at 6.90-7.39 ppm, slightly upfield shifted, as expected for the functionalization with ether groups.

1.3.3 Synthesis of hexavinylene-SubPzs

The synthesis of hexavinylene-substituted SubPzs (**11**-**13**) was performed by applying the same synthetic methodology of coupling reactions on hexasulfanyl-SubPzs, this time with vinylene-boronic acids (**4g-i**), under the above mentioned reaction conditions (Scheme 1.8).

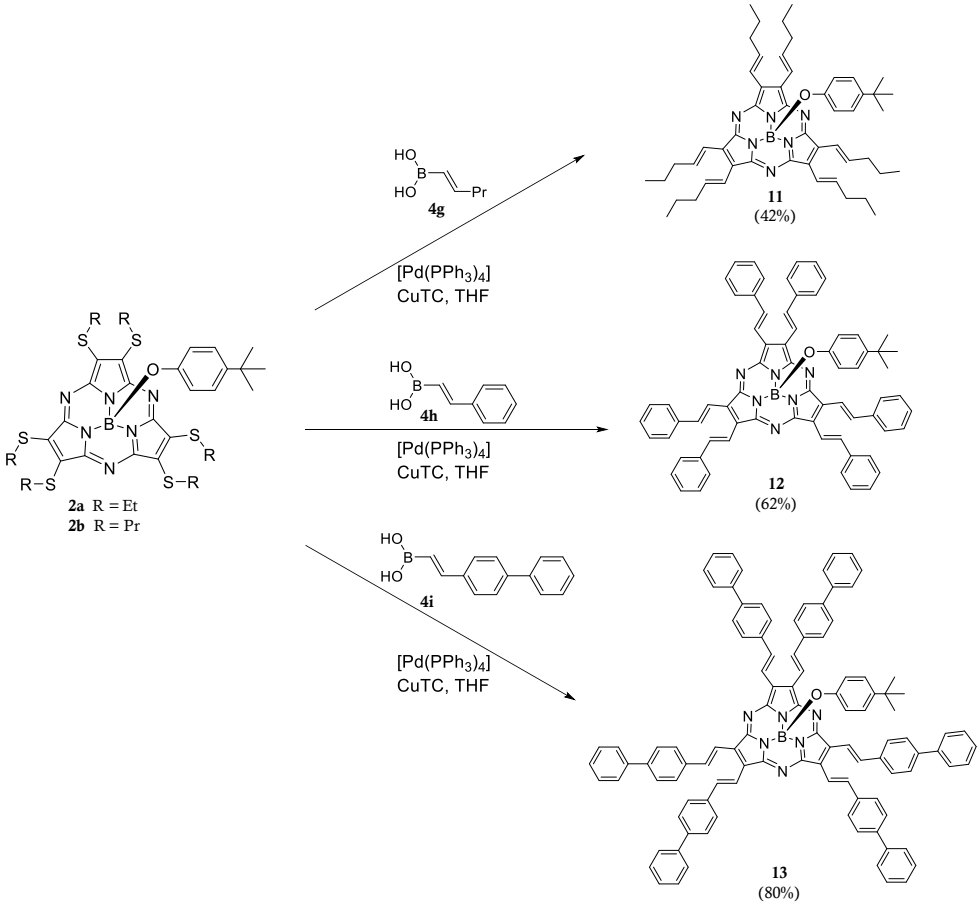

Scheme 1.8. Synthesis of hexavinylene-SubPzs (**11** – **13**).

In this case, higher yields of 62% (**12**) and 80% (**13**) were obtained, probably due to the lower steric hindrance giving by the vinylene moieties.

Substitution of SubPzs with six vinylene-moieties (compounds **11** – **13**) does not produce much impact on the resonances of the axial substituents, apart from that

already observed for the macrocycle by itself. In particular, hexapentenyl-substituted SubPz **11** displays the axial *tert*-butylphenoxy resonances somehow more shielded, at 5.27 ppm, 6.79 ppm and 1.13 ppm, with respect to those of SubPzs **5** – **8** and those of **12** and **13**. The latter show their axial protons at 5.48-5.59 ppm, 6.90-6.96 ppm and 1.15-1.17 ppm. Moreover, the vinylene protons display large coupling constants (J ~ 16 Hz) that denote *trans*-stereochemistry, appearing strongly downfield shifted by the SubPz ring current, at 7.71-8.88 ppm ($H^{2''}$) and 6.81-7.71 ppm ($H^{1''}$) (Figure 1.5).

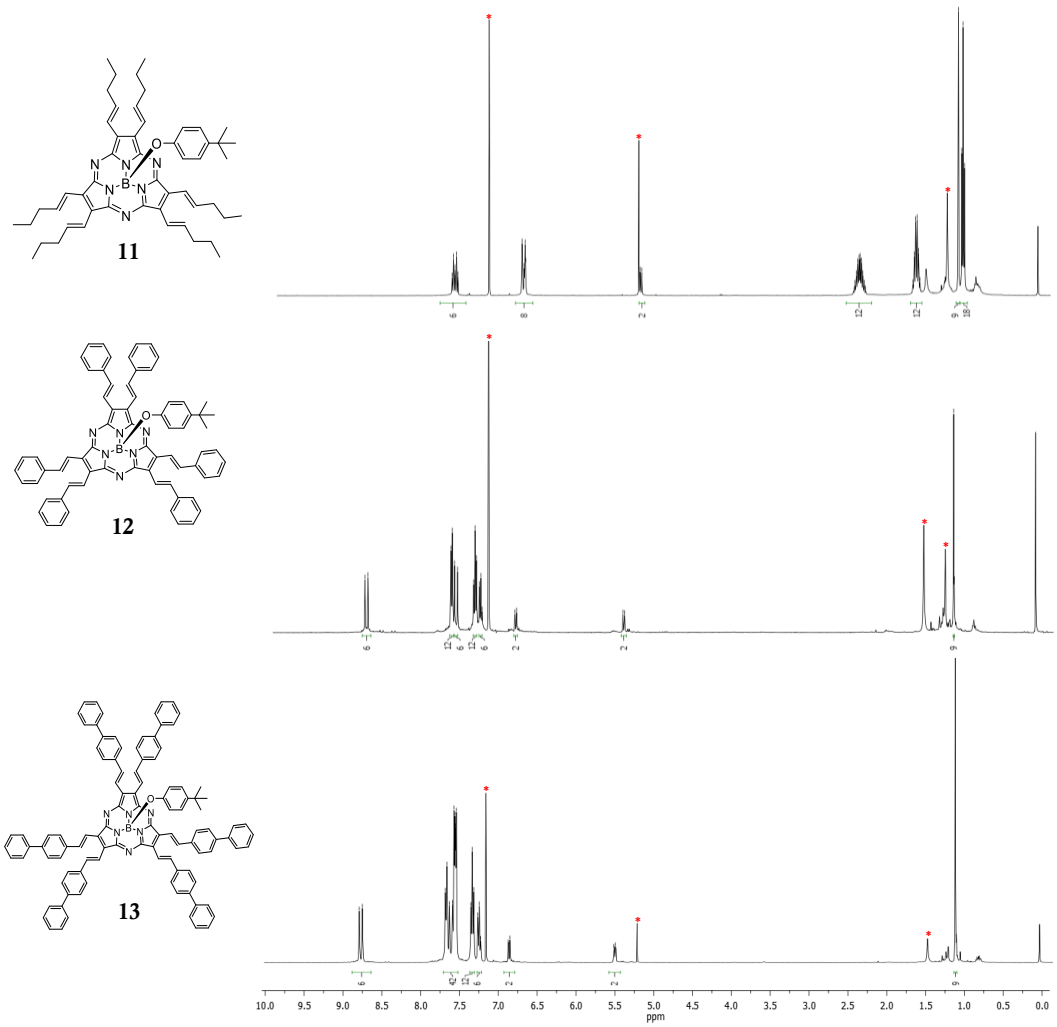

Figure 1.5. ^{1}H-NMR spectra in $CDCl_3$ at 25 °C of vinylene-SubPzs (**11-13**). Signals marked with * are due to residual solvents.

1.3.4 Optical properties of oligophenylene- (5-10) and vinylene- (11-13) SubPzs

Substitution of the SubPz macrocycle with six phenyl rings (SubPz **15**) produces a 40 nm bathochromic shift of the Q-band (λ_{max} = 539 nm), with concomitant egression of a CT band at 395 nm, which is not observed for hexapropyl-SubPz **14** (Figure 1.6).[48] The absorption band of the six benzene rings is visible at 250 nm,[71] accompanied by the typical SubPz Soret band at 304 nm. Q-band excitation of **15** produces fluorescence with a maximum at 563 nm (43 nm red shifted with respect to that of **14**). Based in crystallographic data, all these effects have been attributed to the extended conjugation over the macrocycle and the six peripheral phenyl rings (Figure 1.7).[48]

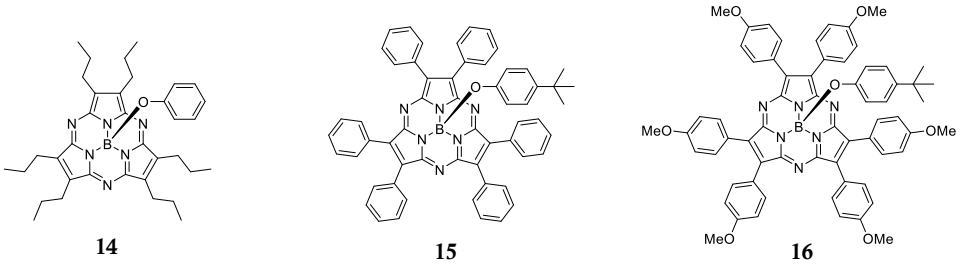

14 **15** **16**

Figure 1.6. SubPz structures for: hexapropyl-SubPz **14**,[16c] hexaphenyl-SubPz **15**,[48] and *p*-methoxyphenyl-SubPz **16**.[48]

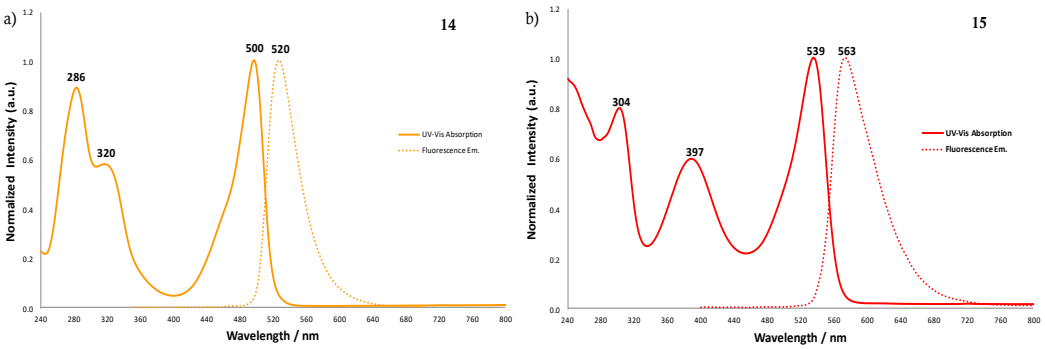

Figure 1.7. Normalized UV/Vis absorption and fluorescence emission spectra of (a)**14**, and (b) **15** in $CHCl_3$.

[71] M.Taniguchi, J. S. Lindsey, *Photochem. Photobiol* **2018**, *94*, 290–327.

The energy of the absorption and fluorescence bands of SubPzs can be modulated independently one from the other by selecting the nature, position and number of substituents at the peripheral phenyl groups. Thus, 4-biphenyl SubPz functionalization (SubPz **5**) shifts the Q and CT bands to 554 and 430 nm, respectively (Figure 1.8, Table 1.1), while substitution with 4-terphenyl moieties (SubPz **7**) does it to 557 and 440 nm, respectively.

Clearly, the effect of the second layer of phenyl rings in the absorption properties of SubPz **5** is weaker (15 nm and 35 nm red shifts of the Q and CT-bands, respectively) than that produced upon conjugating the first layer of phenyl rings in **15**. Although the crystal structure of reported tris(biphenyl)-substituted SubPs has shown small Ph–Ph dihedral angles favourable for π-conjugation,[72] the small red shift of the Q-bands observed here for SubPz **5** suggests a more orthogonal disposition of the two phenyl rings in this molecule.

[72] H. Sugimoto, M. Muto, T. Tanaka, A. Osuka, *Eur. J. Org. Chem.* **2011**, 71–77.

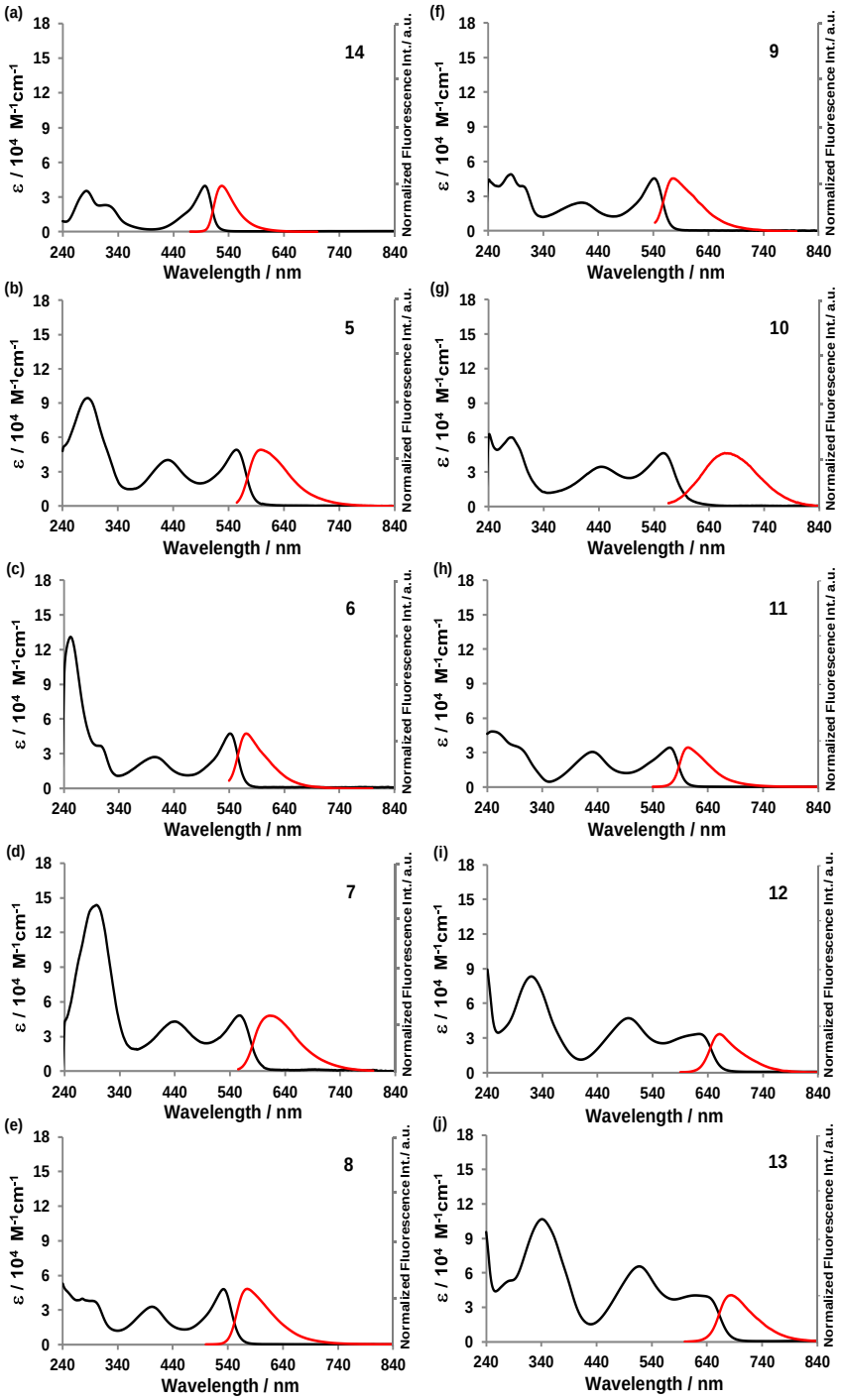

Figure 1.8. UV/Vis absorption (black line) and normalized fluorescence emission (red line) spectra of **14** and **5-13** in $CHCl_3$.

The third layer of phenyl rings produces an even more feeble effect (3 and 10 nm red shift, respectively), evidencing the less efficient electronic delocalization over the phenyl ends as the oligophenylene branch is enlarged. The same trend is observed for the emission bands upon increasing the number of rings of the 4-oligophenylene arms. In particular, the extent of the red shift $\Delta\lambda_{em}$ decreases in the order **14**→**15** (43 nm) > **15**→**5** (36 nm) > **5**→**7** (13 nm), although the Stokes shift decreases in the inverted order: **7** (55 nm) > **5** (45 nm) > **15** (24 nm). Besides, while the fluorescence spectrum of the hexapropyl SubPz **14** follows the mirror image rule, the emission band of **15** somehow broadens,[48] and the broadening increases in the order **15** < **5** < **7**. All of this indicates progressive structural changes between the SubPz ground and excited states upon sequential addition of 4-phenylene units.

SubPz	Absorption λ [nm] (ε[10^4 $M^{-1}cm^{-1}$])	Fluorescence λ_{em} [nm][a]
14[16c]	286 (4.0), 320 (2.6), 500 (4.3)	520[43e]
15[48]	250 (4.4), 304 (4.0), 395 (3.2), 539 (5.2)	563
16[48]	271 (5.9), 434 (3.9), 553 (4.4)	612
5	285 (9.4), 430 (4.0), 554 (4.9)	599
6	252 (13.1), 305 (3.7), 405 (2.7), 541 (4.7)	571
7	298 (14.4), 440 (4.3), 557 (4.8)	612
8	293 (sh), 402 (3.3), 532 (4.8)	575
9	281 (4.9), 301 (3.9), 410 (2.4), 541 (4.5)	575
10	241 (6.3), 281 (6.0), 445 (3.4), 557 (4.6)	668
11	249 (4.9), 295 (sh), 431 (3.1), 571 (3.4)	604
12	320 (8.3), 496 (4.7), 604 (sh), 624 (3.3)	662
13	282 (sh), 341 (10.7), 517 (6.6), 619 (4.0), 639 (sh)	684

[a] Excited at the Q-band.

Table 1.1. Optical properties of SubPzs **14**-**16** and **5**-**13** in $CHCl_3$.

As expected, *meta*-substitution of the peripheral aryl rings brings about little electronic perturbation in the ground state. In particular, substitution with methoxy (SubPz **9**) or phenyl groups (SubPz **6**) produces only 2 nm bathochromic shift of the Q-bands and 15 or 10 nm red shift of the CT bands, respectively. Likewise, substitution at the two *meta*-positions with methoxy- groups (SubPz **10**) produces a bathochromic shift of 4 nm with respect to SubPz **16**, pointing to an additive effect of the two *meta*-substituents in the absorption spectrum of SubPz **10**. Contrasting, the effect of *meta*-substitution on the fluorescence properties is non-additive, so that one *m*-methoxy group per phenyl ring shifts the fluorescence band of SubPz **9** by 12 nm to lower energies, while two *m*-methoxy moieties do it by 56 nm in SubPz **10**. The emission bands of SubPzs **6** and **9** are very similar in shape and Stokes shifts (30 and 34 nm, respectively) to that of hexaphenyl-SubPz **15** (24 nm).

In order to restrict the free rotation of peripheral aryl groups and study the consequences in the absorption and emission properties of these macrocycles, the preparation of compunds bearing aryl groups functionalized at 2 and 6 position was attempted. To this end, the reaction of **2a** or **2b** with the corresponding 2,4,6-triphenyl or 2,4,6-trimethoxyphenylboronic acid was studied in both cases, and a mixture of SubPzs was produced, in which the corresponding hexaarylated compound was not detected (Scheme 1.9). The failure to reach reaction completion in these cases probably arises from the steric hindrance for the coupling reaction of the *ortho*-substituted boronic acids, at the two contiguous β-positions of each of the SubPz pyrrole rings. As an alternative, the 3,5-di-*tert*-butylphenyl substituted SubPz **8** was prepared (Scheme 1.7). As mentioned above, this substitution pattern did not impede aryl rotation, but somehow reduced the electronic coupling of the peripheral moieties with the SubPz macrocycle, judging from the absorption spectrum of **8**. The latter displayed a slightly blue shifted (7 nm with respect to that of **15**) Q-band at 532 nm, while the emission band was red shifted by 12 nm compared to **15**, and the Stokes shift resulted in 43 nm.

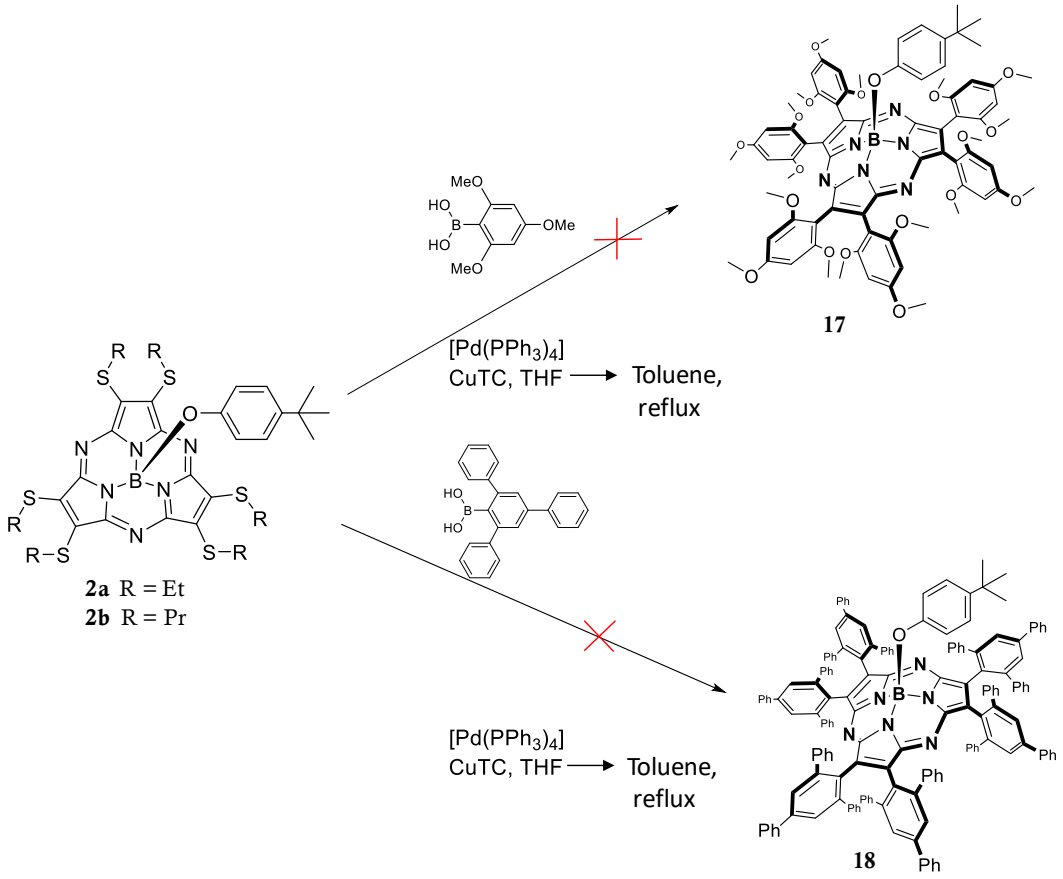

Scheme 1.9. Attempted synthesis of hexaarylated-SubPzs containing substituents at the benzene 2 and 6 positions.

UV/Vis absorption experiments were performed at different temperatures, in order to restrict or further enhance the rotational freedom of di-*tert*-butylphenyl substituents in SubPz **8**, and to detect any blue or red shifts, respectively, of their absorption bands. The measurements were carried out in chloroform selecting a range of temperatures from 50 °C to 0 °C. Nevertheless, no remarkable shift in the absorption bands were detected under these conditions (Figure 1.9).

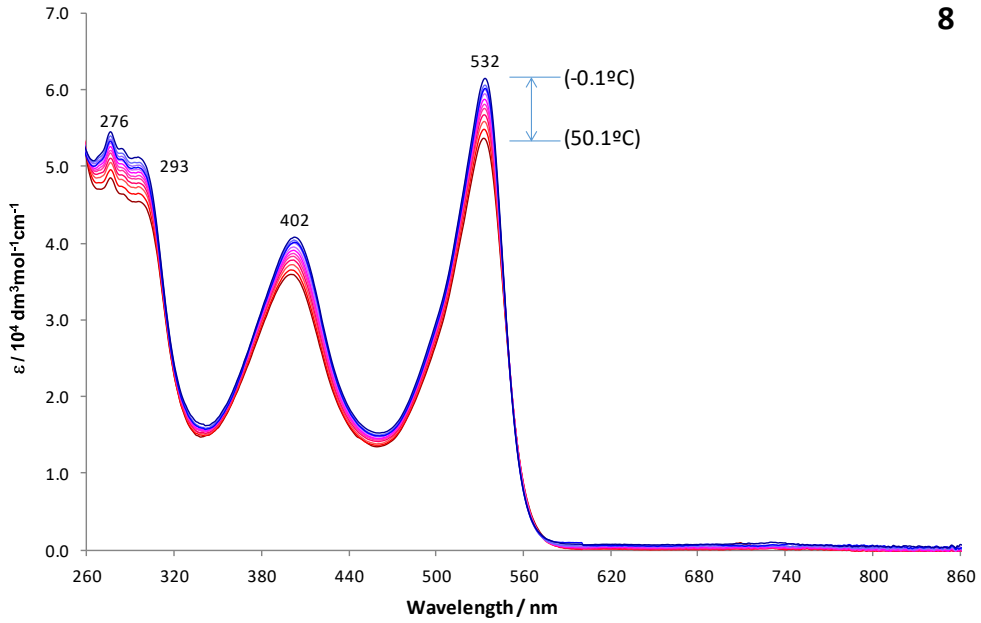

Figure 1.9. Temperature-dependent UV/Vis absorption spectra in $CHCl_3$ for SubPz **8**. Temperature range: from 50 ºC to 0 ºC.

Next, the conjugation of the SubPz core with the less sterically demanding vinylene rests was studied. Substitution of SubPz with six pentenyl groups shifts the SubPz Q-band in **11** to 570 nm, that is, 70 nm red shifted, related to that of hexapropyl SubPz **14**. A strong CT band denoting electronic delocalization over the vinylene moieties emerges at 431 nm, whereas a band at 251 nm, with a shoulder at 295 nm contains the absorption of the vinylene moieties, as well as the SubPz B-band. (Figure 1.8 and Table 1.1). The effect is considerably stronger than that produced upon hexaphenylation, reflecting a more coplanar configuration with respect to the aromatic SubPz core, as we will be discuss in the section 1.3.5. With the attachment of phenyl rings at the other end of the six vinylene linkers, the Q-band of SubPz **12** broadens and develops a shoulder that could be ascribed to an unresolved splitting. Further bathochromic shifts of 54 and 65 nm with respect to **11** are observed for the lowest energy and CT bands, respectively, suggesting a better electronic communication of the terminal phenyl rings with the macrocycle than that produced in the directly attached hexaphenyl-SubPz **15**.

Insertion of six 4-biphenylvinylene branches in SubPz **13** shifts the lowest-energy band additional 15 nm, exactly in the same range as for the directly attached SubPz **5**. All the emission spectra of hexavinylated SubPzs **11**, **12** and **13** are mirror images of the lowest energy absorptions, with λ_{em} = 604, 662 and 684 nm, respectively, and close Stokes shifts of 34, 38 and 45 nm.

As a result of an effective extension of the conjugation on the peripheral substituents, new chromophores based on SubPzs showing a variety of colours, are obtained (Figure 1.10).

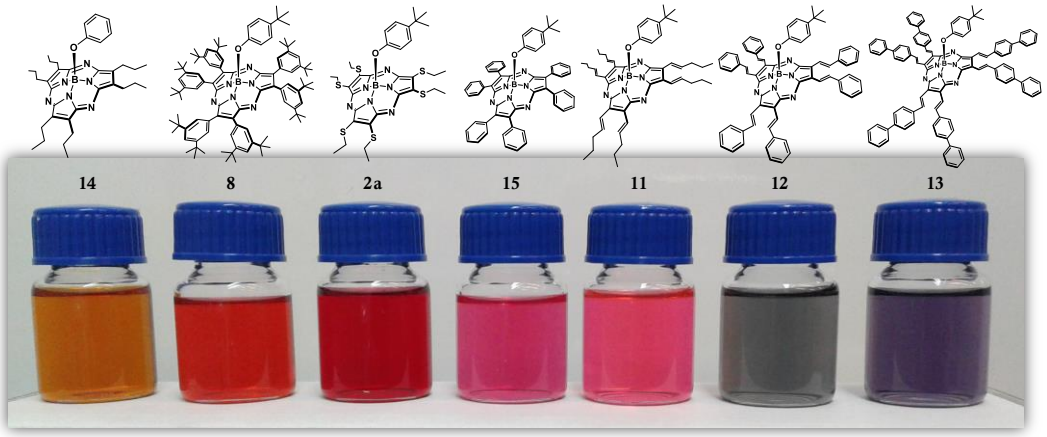

Figure 1.10. Range of colors of SubPzs: **14**, **8**, **2a**, **15**, **11**, **12**, **13** in$CHCl_3$ solutions.

1.3.5 Crystal and molecular structures

Single crystals of the hexaarylated SubPzs **9** and **10** suitable for X-ray diffraction analysis were obtained by vapour diffusion of isooctane and heptane, respectively, into solutions of these SubPzs in 1,2-dichloroethane. The crystal structure[73] of **9** and **10** (Figures 1.11a and 1.11b) revealed the typical curved SubPz shape, with bowl depths (the bowl depth in SubPzs is defined by the distance between the boron atom and the plane defined by the six β-pyrrole carbons) of 1.720 Å and 1.699 Å, respectively, very similar to that of hexaarylated SubPz **16** (1.742 Å)[48] and hexapropyl SubPz-(F) (1.758 Å).[16c]

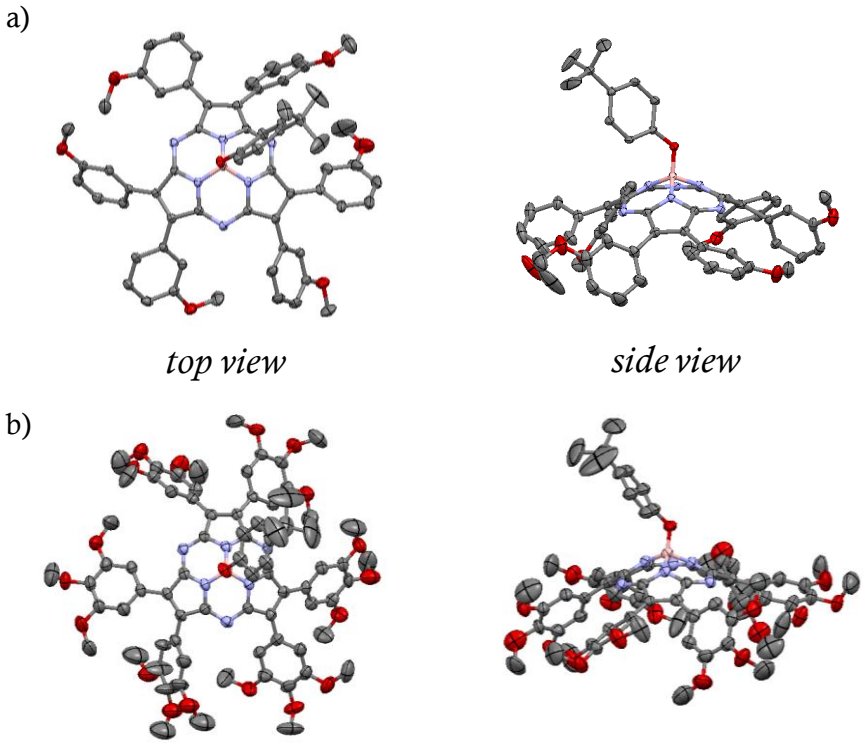

Figure 1.11. Molecular structures showing thermal ellipsoids at the 50% probability level of (a) SubPz **9** and (b) SubPz **10**.

[73] CCDC numbers 1895202-1895205 for **8**, **9**, **10**, and **11**, respectively.

The insertion of methoxy groups at the *meta*-positions of the peripheral phenyl rings does not produce additional tilting between contiguous phenyl rings (4.3(5)º - 13.0(6)º for **9** and 4(1)º - 14(1)º for **10**). The dihedral angles of aryl rings with respect to the plane defined by the pyrrole to which they are attached range from 30.62º to 54.80º for **9** and from 28.45º to 52.02º for **10**, all of this allowing for a similar degree of π-conjugation with the macrocycle to that exhibited by the hexakis(*p*-methoxyphenyl)SubPz **16**.[48] Contrasting, the dihedral angles between two consecutive benzene rings are significantly larger for the sterically more demanding *meta*-substituted compounds than for the *para*-substituted SubPzs, ranging from 54.80º to 58.30º for **9** and from 50.32º to 56.57º for **10** (the largest dihedral angle between two consecutive benzene rings in **16** is of 45.23º).

Single crystals of SubPz **8** were obtained by slow diffusion of methanol into a solution of **8** in chloroform (Figure 1.12).

Figure 1.12. Crystal formation of SubPz **8**. Crystal habit: intense orange prismatic-like. Crystal system: monoclinic.

The obtained crystals diffracted very weakly beyond 1 Å resolution, so the data were cut at this resolution and the refinement of some reflections was omitted. Even so, R, R_1 and wR_2 display high values. In addition, some parts of the two molecules in the asymmetric unit exhibit a high degree of disorder. Therefore, geometric restrictions

were introduced for the bond distances and angles of many of the *tert*-butyl moieties. These disordered carbon atoms have been only isotropically refined, and their location restricted to 50%. The deduced formula does not match the real one because the hydrogen atoms of the disordered CH_3 have been omitted in the model. The asymmetric unit for **8** contains two SubPz macrocycles with bowl depths of 1.715 (Figure 1.13) and 1.737 Å, respectively, in the same range as for the other hexaarylated SubPzs. Similar to the other *meta*-substituted SubPzs, two consecutive benzene rings show a tilting of 0(2)º - 9(2)º to one another, and their corresponding dihedral angles go from 49.90º to 56.48º. But in this case, the two bulky *tert*-butyl groups, located at the two phenyl *meta*-positions, force several of the aryl groups to adopt conformations somehow less coplanar to the plane defined by the pyrrole ring to which they are attached. These, in average, larger dihedral angles range now from 17.85º to 68.12º, and could be responsible for the slightly blue shift of the Q-band observed for the absorption spectrum of **8**.

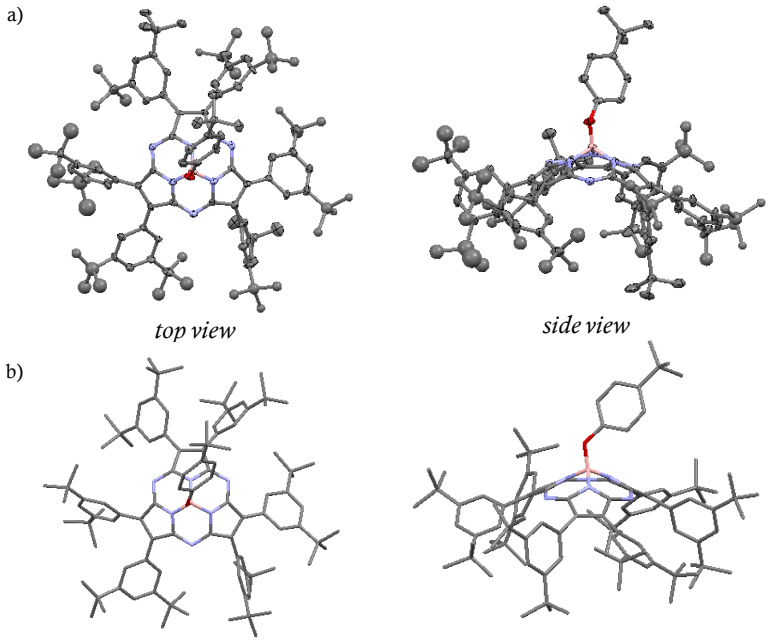

Figure 1.13. (a) Molecular structure showing thermal ellipsoids at the 30% probability level of SubPz **8**. (b) Molecular structure displayed in stick for clarity.

Single crystals of hexavinylene SubPz **12** were obtained by vapour diffusion of isooctane into a solution of **12** in 1,2-dichloroethane. Figure 1.14 shows the *trans* configuration of the six vinylene moieties already anticipated by ^{1}H-NMR spectroscopy. The obtained crystal structure differs markedly from those obtained for hexaarylated compounds, and accounts for the observed differences in the absorption spectra of the two series. Firstly, **12** exhibits a slightly more planar structure, with a bowl depth of 1.600 Å. In addition, the smaller volume of the vinylene moieties related to that of the phenylene rings allows for a more planar configuration and hence, a more effective π-delocalization over the whole structure.

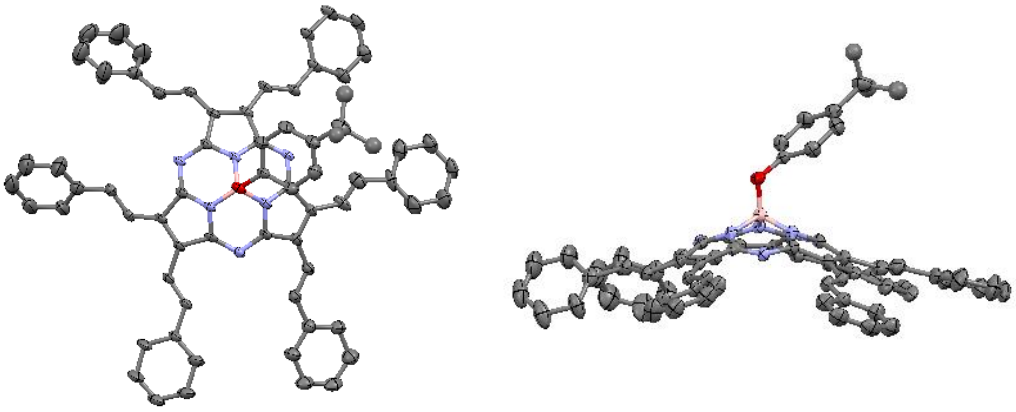

top view *side view*

Figure 1.14. Molecular structure showing thermal ellipsoids at the 30% probability level of SubPz **12**.

Two contiguous pyrrole–vinylene bonds are nearly coplanar (torsion angles between 2(1)º and 5(1)º. Besides, the vinylene C=C bonds lie nearly in the same plane as the pyrrole rings, with small deviation angles ranging from 2.69º to 6.30º, except for one of the C=C moieties, which is tilted by 18.45º. Two of the vinylene C=C linkers also lie in the same plane as the phenyl ring to which they are attached (deviation angles of 1.21º and 1.29º, respectively), while other three C=C moieties are angled with their corresponding phenyl ring by 11.24º to 15.75º, and the sixth vinylene does it by 28.84º. As a result, the dihedral angles between the pyrrole and the phenyl rings are

also much smaller (2.92º to 32.70º) than those of the hexaarylated series, favouring a stronger electronic communication between the macrocycle and the terminal phenyl ring in the former. Such an enlargement of the absorptive and radiative chromophore was evidenced also in UV/Vis spectroscopy by unprecedented (for SubPzs) Q-bands in the yellow-red regions and orange-red emissions for the hexavinylene series.

The organization of SubPzs in the solid state is strongly influenced by the peripheral substituents. SubPzs **9** and **10** stack in columns along the *a* axis, each column arranged by parallel macrocycles in a head–to-tail configuration (Figures 1.15A and 1.15D). B–B distances between two contiguous macrocycles within the same column is of 11.451(5) Å for **9** and 11.60(1) Å for **10**.

The number of "down" columns, formed by "down" molecules (d), is the same as that of "up" columns, formed by "up" molecules (u). The organization of **9** and **10** in the crystal state differs in the relative arrangement of the columns. For **9**, "up" and "down" parallel columns alternate along to the *b* and *c* axes (see Figures 1.15B and 1.15C), with B–B distances between two macrocycles of contiguous columns of 11.139(5) Å (*b* axis) and 13.869(5) Å (*c* axis). For **10**, two columns with alternating "up" and "down" configurations arrange a pair of type **A** (green and yellow colours in Figures 1.15E and 1.15F) or type **B** (cyan and magenta colours in Figures 1.15E and 1.15F). Within a pair, the shortest B–B distance between two macrocycles of contiguous, u and d columns is of 13.83(1) Å. The B–O bonds in a column are nearly parallel to each other. However, within the **A** or **B** pair, B–O bonds of the "up" and "down" columns are angled 15.52º. In addition, B–O bonds of two contiguous macrocycles, each one arising from a different **A** type and **B** type pair, respectively, are angled 49.4(6)º (see Figure 1.15E). Pairs of **A** and **B** type are alternated with a zigzag pattern along the *c* axis (Figure 1.15F), with a non-alternating, u-d-d-u disposition of the SubPz columns, so that the B–B distance of contiguous d and d, or u and u columns is of 11.78(1) Å.

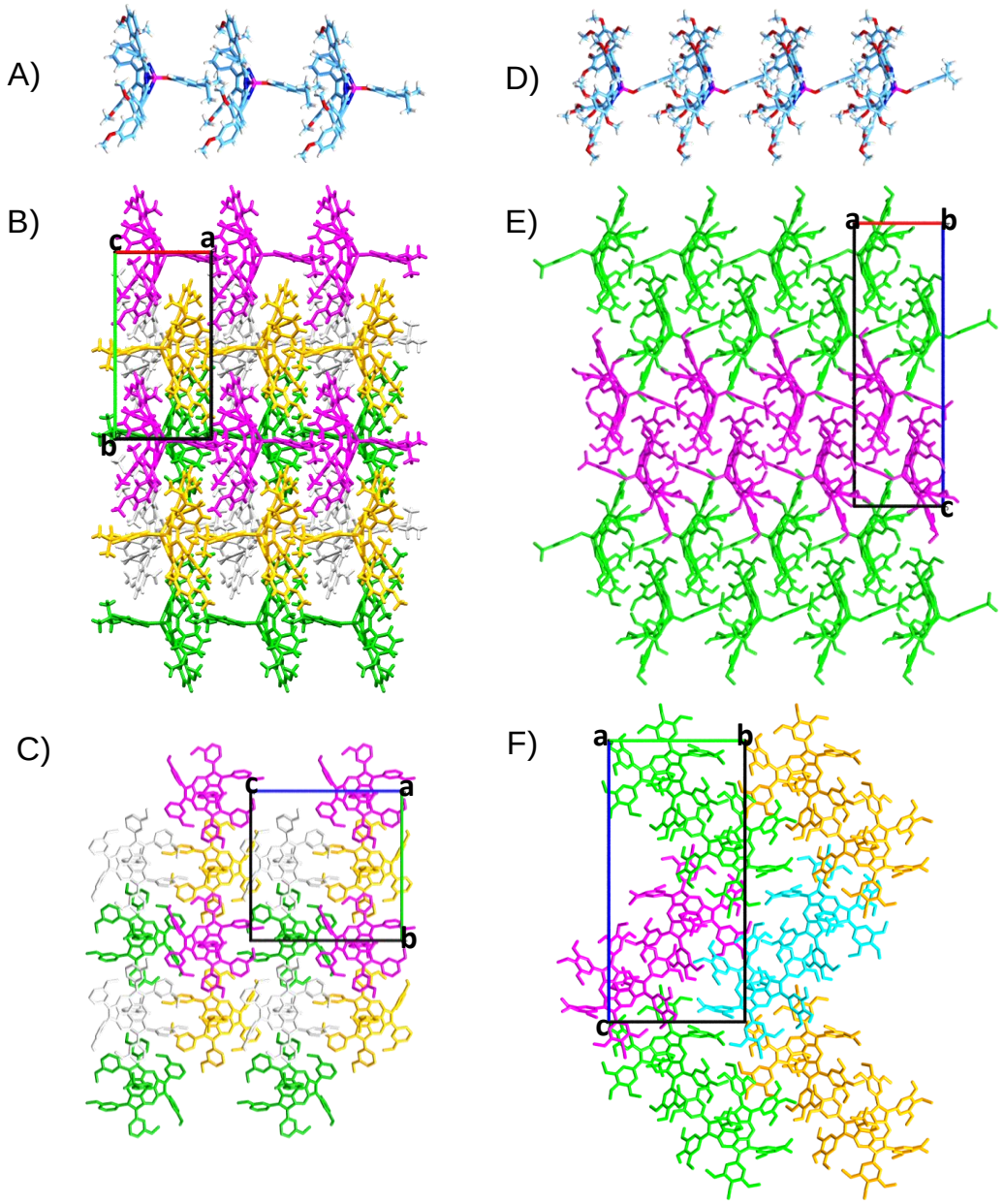

Figure 1.15. Views showing the columns along the *a* axis for **9** (A), and the *b* axis for **10** (D). Views of the column packing (hydrogens have been omitted for clarity) for **9** along the *ab* (B) and *bc* (C) planes, and for **10** along the *ac* (E) and *b*c (F) planes.

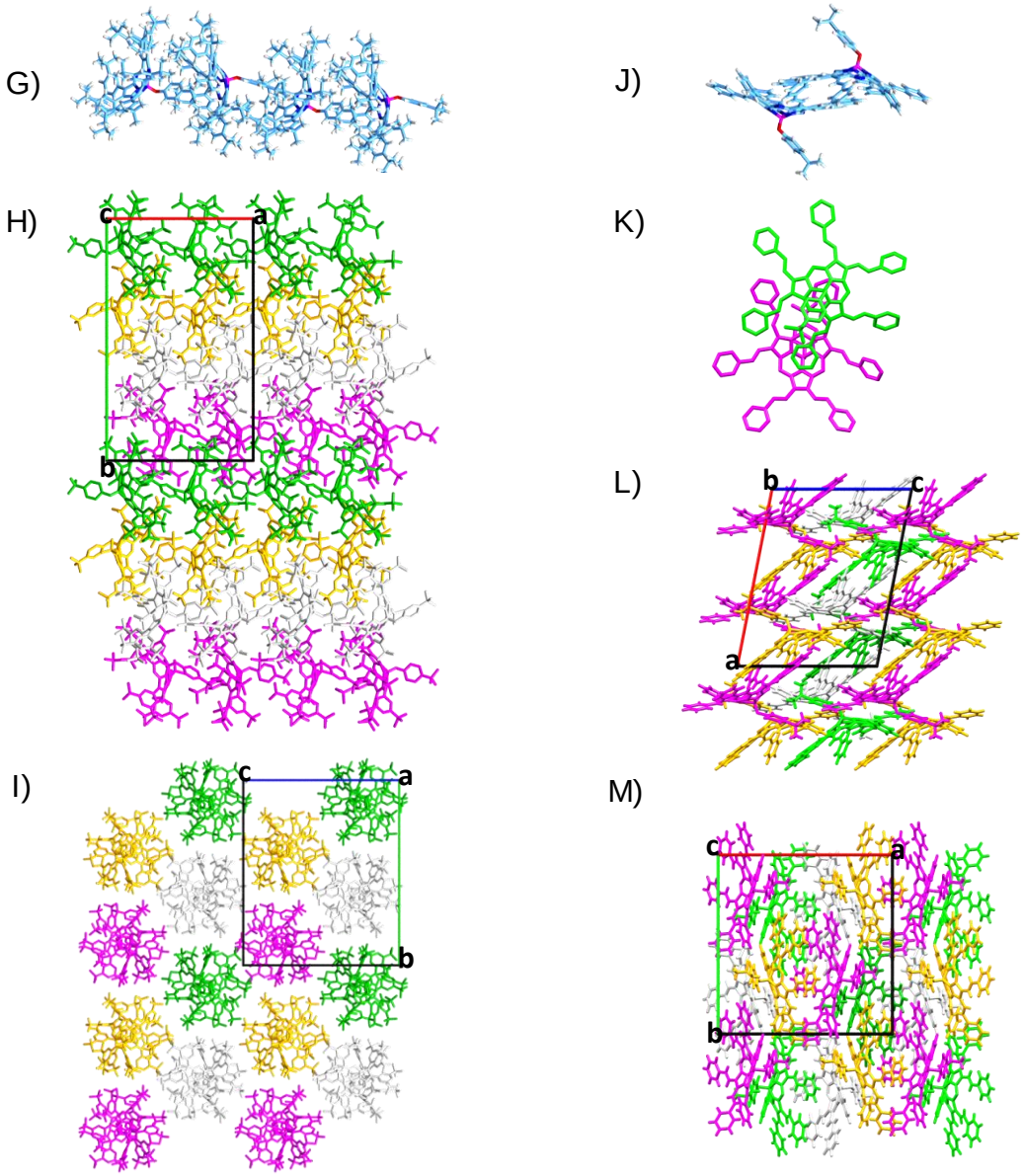

Figure 1.16. Views showing the columns along the *a* axis for **8** (G), and the face-to-face arrangement of **12** (J and K). Views of the column packing (hydrogens have been omitted for clarity) for **8** along the *ab* (H) and *bc* (I) planes, and for **12** along the *ac* (L) and the *ab* (M) planes.

SubPz **8** also stacks in columns along the *a* axis, but here the macrocycles are arranged head to tail in a zigzag fashion (Figure 1.16G), with angles of 39.96º between the planes of two contiguous macrocycles, and B–B alternating distances of 10.97(2) Å and 11.54(2) Å. Two non-symmetrically equivalent macrocycles are rotated by 37.1(6)º - 60.1(7)º (N_{meso}–B–B–N_{meso} torsion angles) within a column. The number of u (magenta and grey) and d (yellow and green) columns is the same (Figures 1.16H and 1.16I). Parallel columns are placed along the *b* axis in alternated configuration, so that each column is surrounded by six alternating u and d columns in hexagonal disposition (Figure 1.16I).

SubPz **12** does not stack into columns but it is arranged in a face-to-face manner (Figure 1.16J), with the centroid of one of the peripheral benzene rings of one SubPz perfectly aligned with the Boron(III) ion of the other SubPz (Figure 1.16K), with a distance of 4.582 Å. The two macrocycles are almost parallel, exhibiting a small angle of 9.78º between their respective planes, and a B–B distance of 11.35(1) Å. All the macrocycles are placed in a parallel configuration with respect to the *b* axis, with the same number of up and down macrocycles (Figures 1.16L and 1.16M).

1.3.6 Electrochemical studies of SubPzs 5 – 13

The electrochemical properties of SubPzs **5** – **13** were studied by cyclic voltammetry (Figure 1.17a) and squarewave voltammetry (Figure 1.17b). Measurements were made in CH_2Cl_2 containing Bu_4NPF_6 as the supporting electrolyte and using a platinum electrode. Tables 1.2 and 1.3 give the redox potentials obtained from these experiments. Unless otherwise specified, Table 1.2 shows the $E_{1/2}$ values from CV at RT. The potentials are given in volts (V) versus the ferrocenium/ferrocene couple (Fc^+/Fc).

All the hexaarylated and hexavinylated SubPzs exhibit three or four reversible reduction peaks and one or two oxidation processes that are irreversible in most of the cases. SubPz **8**, containing bulky substituents at the phenyl rings, constitutes a notable exception, displaying only an oxidation and a reduction process, as observed for hexaalkylated SubPz **14**.[27] Compared to the latter, all of the hexaarylated and hexavinylated SubPzs, including **8**, are by 250 - 560 mV easier to reduce ($E_{1/2}$ = –1.16 - –1.47 V contrasting with –1.72 V for **14**). Here, the most positive reduction potentials correspond to the phenylvinyl (**12**) and biphenylvinyl (**13**) substituted compounds, with values observed at –1.17 and –1.16 V, respectively, as the result of the stronger perturbation of the SubPz π-system by the peripheral phenyl rings, when they are attached through vinylene linkers.

At the other end is the di-*tert*-butylphenyl-substituted compound **8**, which shows its first reduction potential at –1.47 V. This is the least shifted value related to **14**, within the hexaarylated series, and constitutes another evidence for the slightly weaker perturbation of these aryl substituents on the SubPz core.

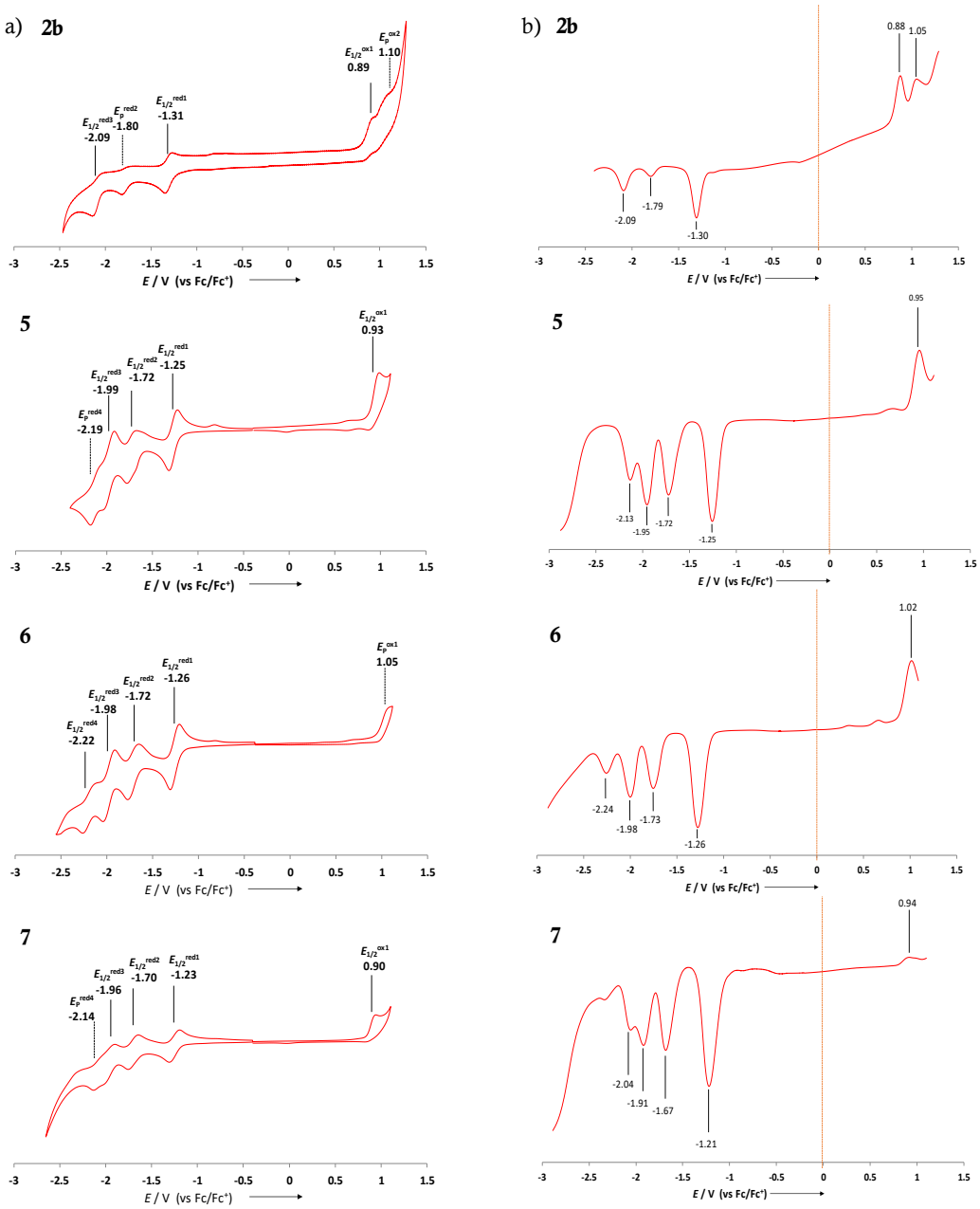

Figure 1.17. (a) Cyclic voltammograms, and (b) SWV of **2b**, **5**, **6**, **7**. . Solvent: CH_2Cl_2 ; scan rate: 100 mVs^{-1}; working electrode: platinum; counter electrode: platinum wire; reference electrode: $Ag/AgNO_3$; electrolyte: Bu_4NPF_6.

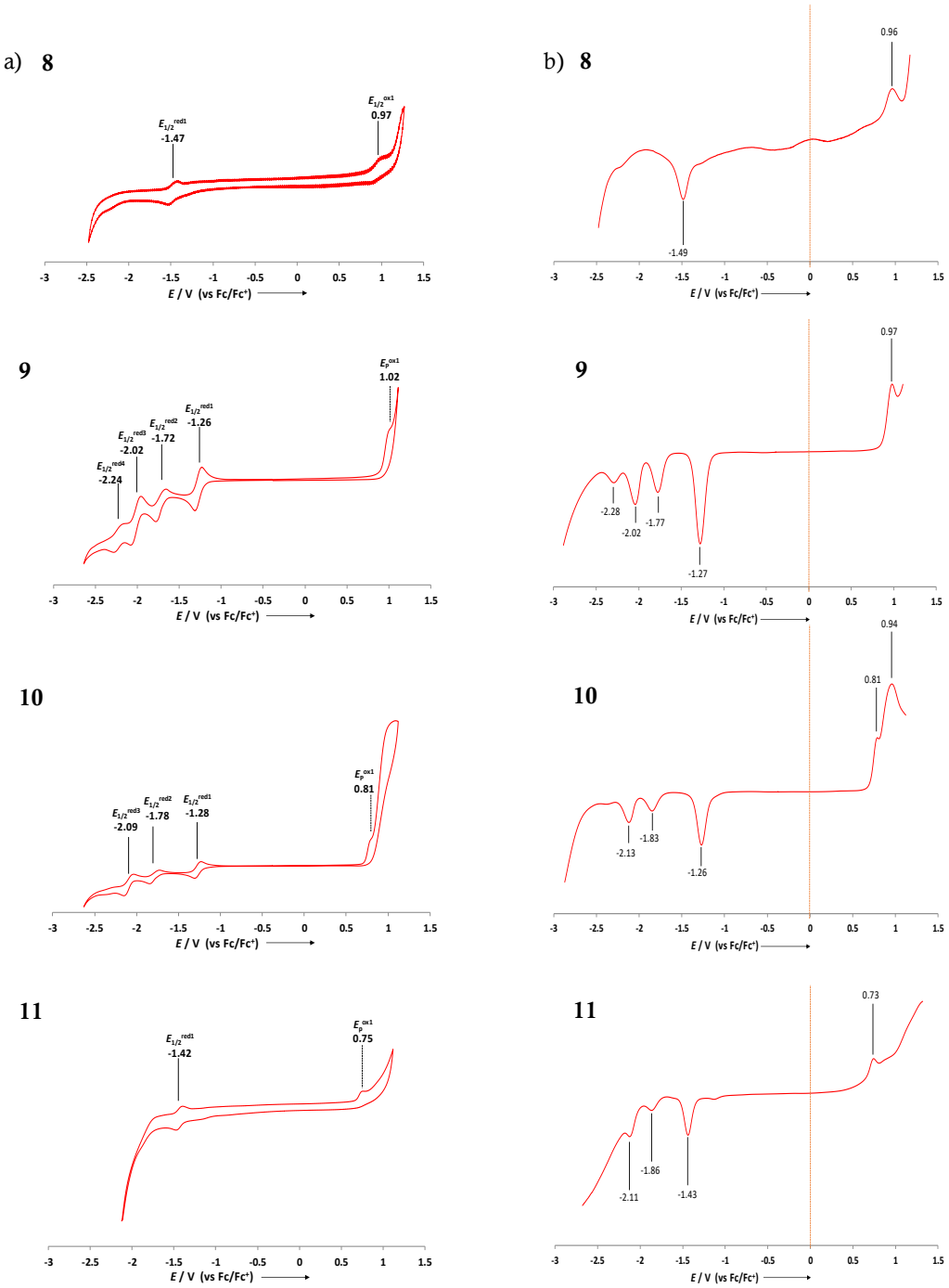

Figure 1.17 (cont). (a) Cyclic voltammograms, and (b) SWV of **8**, **9**, **10**, **11**. . Solvent: CH_2Cl_2 ; scan rate: 100 mVs^{-1}; working electrode: platinum; counter electrode: platinum wire; reference electrode: $Ag/AgNO_3$; electrolyte: Bu_4NPF_6.

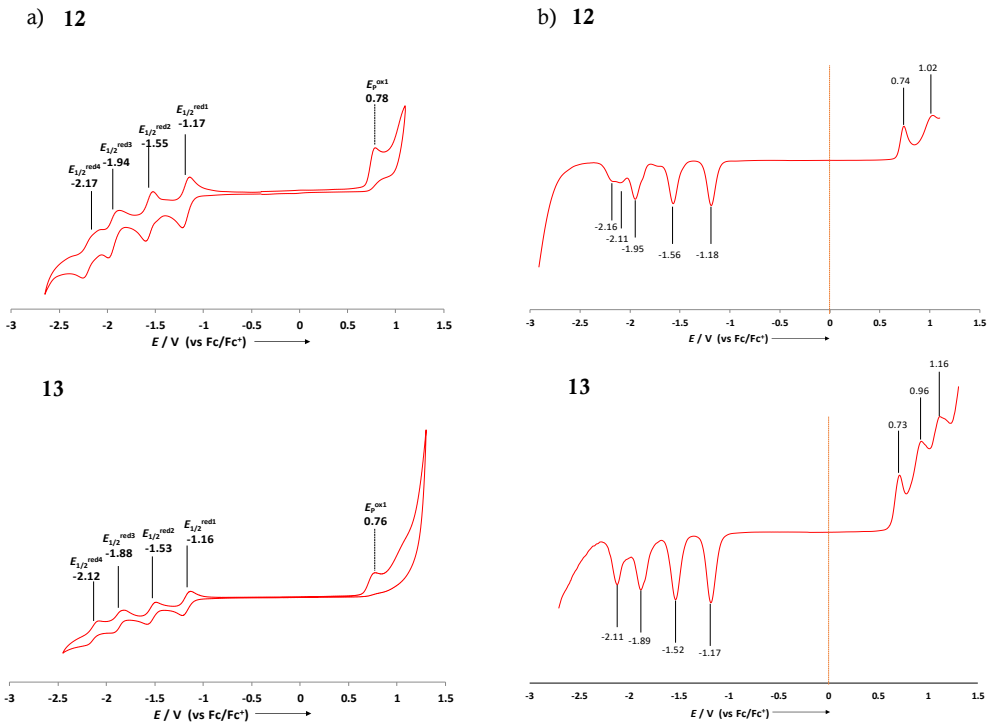

Figure 1.17 (cont.). (a) Cyclic voltammograms, and (b) SWV of **12**, **13**. Solvent: CH_2Cl_2 ; scan rate: 100 mVs^{-1}; working electrode: platinum; counter electrode: platinum wire; reference electrode: $Ag/AgNO_3$; electrolyte: Bu_4NPF_6.

The trend upon conjugation with phenyl rings is parallel to that observed for the optical properties. Hexaphenyl-substitution produces a considerable effect in the reduction ability of SubPz **15** related to **14** (410 mV anodic shift of the first reduction potential).[48] The effect of the second layer of phenyl rings is weaker (further 60 mV and 50 mV anodic shift for the 4-biphenyl- (**5**) and 3-biphenyl-substituted (**6**) SubPzs, respectively), while the third layer causes an even more feeble effect (20 mV anodic shift) in SubPz **7**. Here, *meta-* and *para-* substitution bring about little variations.

SubPz	E_{red4}	E_{red3}	E_{red2}	E_{red1}	E_{ox1}	E_{ox2}
14[60]				–1.72	0.83	
15[48]		–2.02	–1.75	–1.31	0.97	
2b		–2.09	–1.80	–1.31	0.89	1.10[a]
5	–2.19[a]	–1.99	–1.72	–1.25	0.93	-
6	–2.22	–1.98	–1.72	–1.26	1.05	-
7	–2.14	–1.96	–1.70	–1.23	0.90[a,c]	-
8	-			–1.47	0.97[a]	-
9	–2.24	–2.02	–1.72	–1.26	1.02[a]	-
10	-	–2.09	–1.78	–1.28	0.81[a]	1.02[b,c]
11		–2.12[b]	–1.87[b]	–1.42	0.75	-
12	–2.17	–1.94	–1.55	–1.17	0.78[a]	-
13	–2.12	–1.88	–1.53	–1.16	0.76[a]	-

[a] Irreversible process (potential corresponds to the peak potential).

[b] Taken from the SWV. [c] In the window limit.

Table 1.2. Electrochemical oxidation and reduction potentials (in V), $\mathbf{E_{1/2}}$ vs. Fc/Fc^+.

SubPz	E_{red4}	E_{red3}	E_{red2}	E_{red1}	E_{ox1}	E_{ox2}
5	–2.13	–1.95	–1.72	–1.25	0.95	-
6	–2.24	–1.98	–1.73	–1.26	1.02	-
7	–2.04	–1.91	–1.67	–1.21	0.94	-
8	-			–1.49	0.96	-
9	–2.28	–2.02	–1.77	–1.27	0.97	-
10	-	–2.13	–1.83	–1.26	0.81	0.94
11		–2.11	–1.86	–1.43	0.73	0.90
12	–2.16	–1.95	–1.56	–1.18	0.74	1.02
13	–2.11	–1.89	–1.52	–1.17	0.73	0.96

Table 1.3. Electrochemical oxidation and reduction potentials (in V), obtained by **SWV** vs. Fc/Fc^+.

The situation is different for SubPzs containing π-electron donor substituents such as ethers. Thus, depending on the position to which they are attached, the methoxy substituents in SubPzs **16**, **9** and **10** produce opposite effects. In particular, substitution at the *para*-position (SubPz **16**) shifts cathodically the first reduction potential by 90 mV,[48] while substitution at the *meta*-position (SubPz **9**) shifts anodically the same peak by 50 mV. The result of the trimethoxy-substitution on SubPz **10** is an anodic shift of 30 mV, suggesting a nearly additive effect of the three ether groups.

Phenyl and vinylene groups produce contrary effects in the SubPz oxidation window. In particular, vinylene-SubPzs **11** - **13** are by 50-80 mV easier to oxidize, whilst phenylated SubPzs are by 70-192 mV more difficult to oxidize than hexaalkylated SubPz **14**. Here, the electronic perturbation produced by methoxy- or phenyl- substituents diverges as a function of their attachment to the *para*- or *meta*-positions of the peripheral phenyl rings. Specifically, *para*-substituted SubPzs **16**, **10**, **5** and **7** are by 170, 160, 40 and 70 mV, easier to oxidize than **15**, respectively, whereas *meta*-substututed **9** and **6** are by 50, and 80 mV, correspondingly, more difficult.

1.3.7 Calculation of HOMO-LUMO levels

In order to provide some insight into the electronic properties of the arylated and vinylated SubPzs, DFT calculations were performed for **5** - **13**, **15** and **16**, using the GAUSSIAN 09 package. The geometrical parameters were determined with B3LYP/6-31G whereas the orbital energy levels, are corrected at the B3LYP/6-31g (d,p) level. LUMO energies were also estimated from the redox potentials derived from CV data, and calculated using the approximation:[74]

$$E_{LUMO} = -5.1 - E_{1/2red1} \text{ (}vs.\text{ Fc/Fc}^{+}\text{) (eV)}$$

Besides, HOMO energies were obtained from LUMO values and optical band gap E^{g}_{opt} values, which were estimated from the offset wavelength derived from the low energy absorption band.[75]

Figure 1.18 shows the frontier orbitals predicted for the two series of SubPzs and the energy levels obtained by computational studies. Table 1.4 shows the frontier orbital energy values obtained from experimental and from computational data. The trends of calculated energies for the studied SubPzs are consistent by theoretical and experimental methods, although in all cases the values obtained by the former are higher in energy than those arising from the latter. In general, the variation in the $\pi \rightarrow \pi^*$ transition energies observed for the SubPz series also correlate well with the dft calculated trends. As a general tendency, LUMO orbitals are mainly localized at the SubPz macrocycles in the arylated series, while for the vinylated series, contribution from the vinyl moieties is also determined.

[74] C. M. Cardona, W. Li, A. E. Kaifer, D. Stockdale, G. C. Bazan, *Adv. Mater.* **2011**, *23*, 2367–2371.
[75] a) M. V. Fulford, D. Jaidka, A. S. Paton, G. E. Morse, E. R. L. Brisson, A. J. Lough, T. P. Bender, *J. Chem. Eng. Data* **2012**, *57*, 2756–2765. b) A. S. Bhadwal, R. M. Tripathi, R. K. Gupta, N. Kumar, R. P. Singha, A. Shrivastav, *RSC Adv.* **2014**, *4*, 9484–9490.

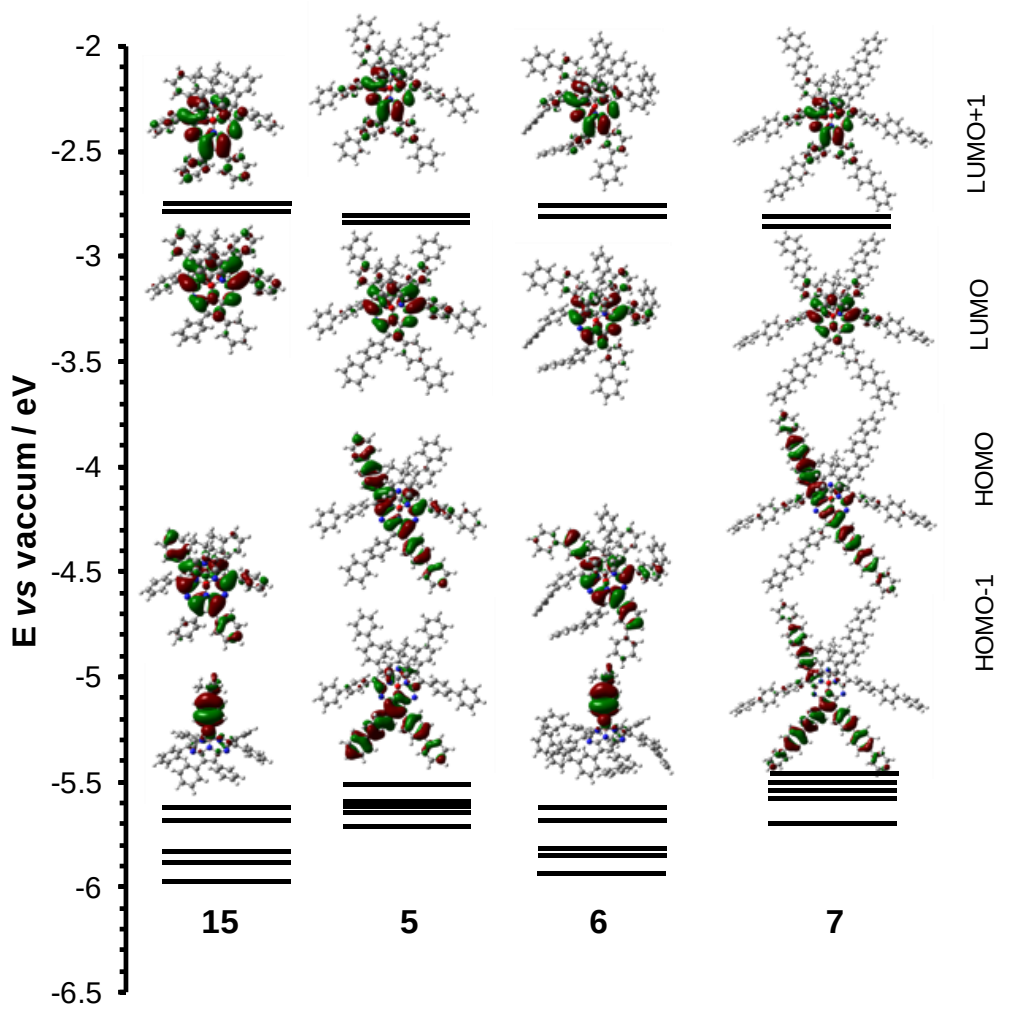

Figure 1.18. DFT predicted HOMO, HOMO–1, LUMO and LUMO+1 orbitals for hexaaryl- and hexavinylene-SubPzs **5** – **7**, and **15**. Predicted frontier orbital energy levels from HOMO–4 to LUMO+1 (B3LYP/6-31G (d,p).

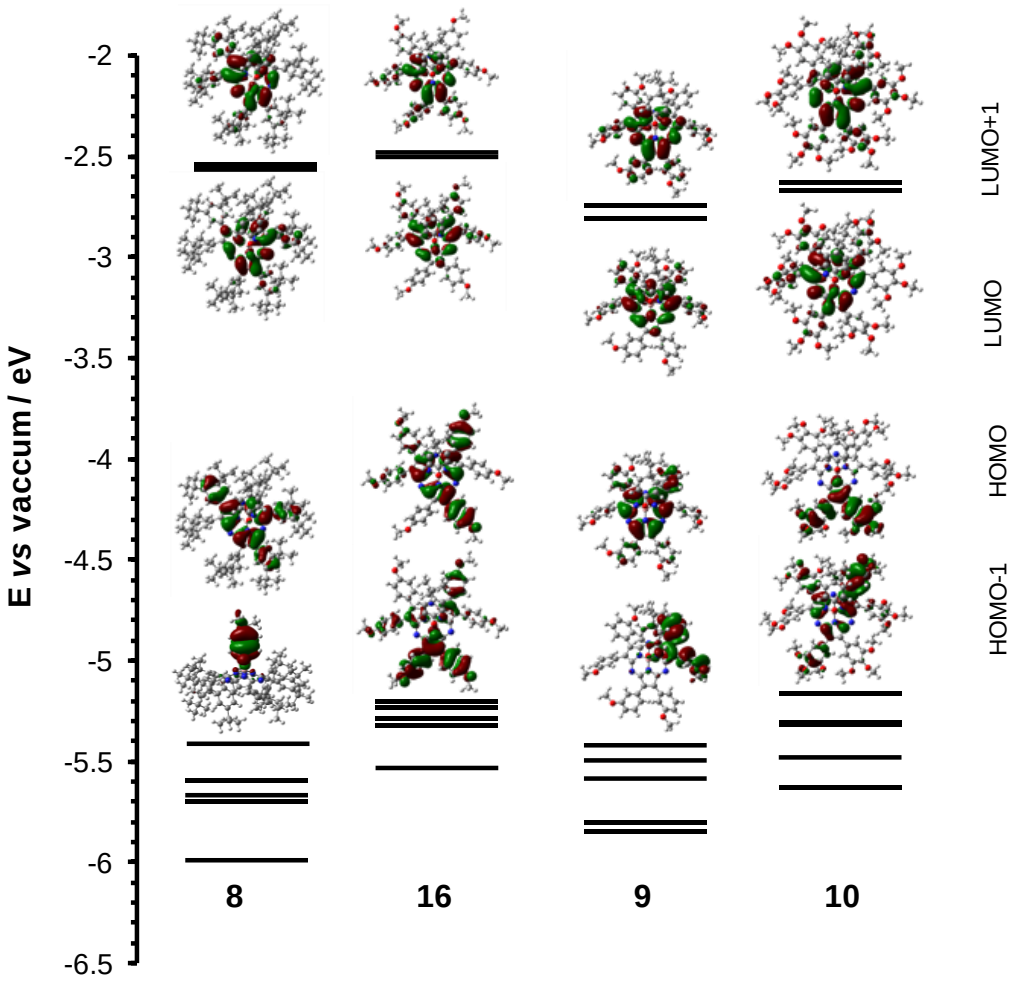

Figure 1.18 (cont.). DFT predicted HOMO, HOMO–1, LUMO and LUMO+1 orbitals for hexaaryl- and hexavinylene-SubPzs **8** – **10**, and **16**. Predicted frontier orbital energy levels from HOMO–4 to LUMO+1 (B3LYP/6-31G (d,p).

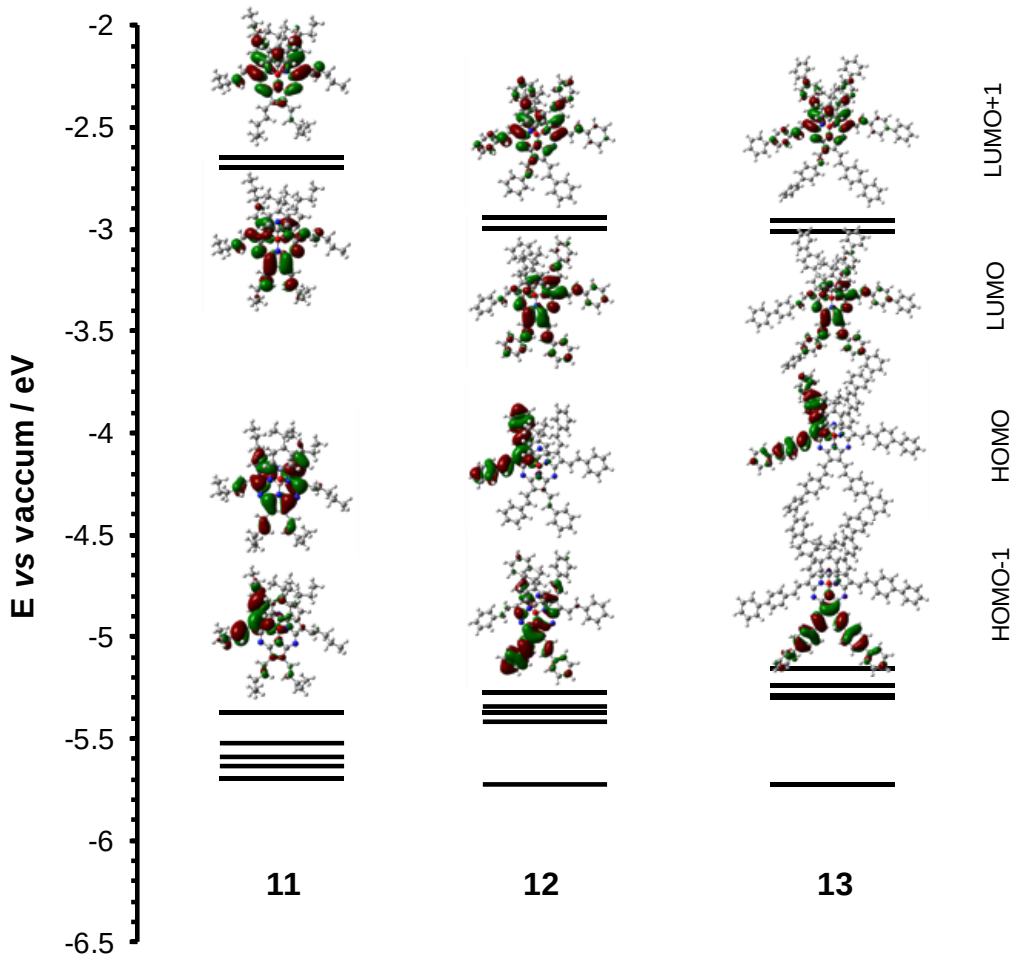

Figure 1.18 (cont.). DFT predicted HOMO, HOMO–1, LUMO and LUMO+1 orbitals for hexaaryl- and hexavinylene-SubPzs **11** – **13**. Predicted frontier orbital energy levels from HOMO–4 to LUMO+1 (B3LYP/6-31G (d,p).

For hexaphenyl-SubPz **15**, DFT predicts the HOMO localized at the macrocycle. The presence of nodes allows only partial contribution from the phenyl substituents. The latter is in contrast with the electronic localization on the SubPz core predicted in recent reports,[76] and is expected to provide important phenyl-to-macrocycle charge-transfer character to the low energy transitions observed in UV/Vis spectroscopy. Consistent with that observed experimentally, extended delocalization over the first and, to a lesser extent, over the second layer of phenyl rings, is predicted for 4-biphenyl-functionalized SubPz **5**, although not for the *meta*-substituted SubPz **6**, whose electronic delocalization on the HOMO is analogue to that of **15**. Similarly, extended delocalization over the first and second and, less significant, the third layer of phenylenes is observed for terphenyl-SubPz **7**. Besides, the DFT-predicted HOMO orbitals of methoxy-substituted SubPzs are suggestive of larger contribution from the peripheral phenyl rings in **16** and **10** than in the *meta*-substituted SubPz **9** or the hexaphenyl-SubPz **15**.

For hexapentenyl-SubPz **11**, extended delocalization over the macrocycle and the six vinylene rests is predicted for the HOMO orbitals. However, the electronic density is mainly localized at the peripheral phenyl rings for **12** and **13**. For the latter, there is only partial delocalization on the second layer of phenyl rings. Besides, delocalization on these moieties is considerably lower for the respective LUMOs of **12** and **13**. This is consistent with significant phenyl-to-macrocycle charge-transfer character in the low energy transitions observed in UV/Vis spectroscopy.

[76] C. Azarias, M. Pawelek, D. Jacquemin, *J. Phys. Chem. A* **2017**, *121*, 4306–4317.

SubPz	$HOMO_{exp}$[a]	$HOMO_{dft}$	$LUMO_{exp}$[b]	$LUMO_{dft}$
15[48]	–5.98	–5.64	–3.79	–2.78
16[48]	–5.80	–5.22	–3.70	–2.49
5	–5.96	–5.54	–3.85	–2.83
6	–6.01	–5.64	–3.84	–2.81
7	–5.95	–5.48	–3.87	–2.84
8	–5.84	–5.43	–3.63	–2.56
9	–6.01	–5.45	–3.84	–2.80
10	–5.88	–5.18	–3.82	–2.65
11	–5.74	–5.34	–3.67	–2.63
12	–5.79	–5.24	–3.93	–2.94
13	–5.75	–5.12	–3.94	–2.95

[a] $E_{HOMO} = E_{LUMO} - E^{g}_{opt}$[74a]

[b] Calculated using the expression $E_{LUMO} = -5.1 - E_{1/2}^{red1}$ (*vs.* Fc/Fc^{+}) (eV)[73]

Table 1.4. Experimental and DFT calculated energy values for frontier orbitals.

1.4 Summary and Conclusions

In this Chapter, the subporphyrazine (SubPz) chromophore has been functionalized at the periphery with six conjugated oligophenylene and vinylene branches, as a way to modulate its electronic properties. The common synthetic strategy used to prepare the two series is based in the implementation of our previously reported Liebeskind-Srogl coupling of hexasulfanyl-SubPzs with boronic acids. Peripheral functionalization with the sterically less demanding vinylene moieties was motivated by the expectation that they would allow for an extended π-system, without losing the typical electronic tunability of SubPzs. This could be used to efficiently transmit to the SubPz dye the electronic features of other chromophores or redox-active systems attached to the vinylene ends.

Within the hexaarylated series, different substitution patterns have been compared, in order to tune the absorption, fluorescence and redox properties independently of one another. *para*-substitution with ether moieties, or sequential addition of 4-phenylene rings, red shift both the SubPz absorption and emission bands. Progressive fading of the effects upon extending the oligophenylene branches from one to three units evidences a less efficient electronic delocalization over the phenyl ends as the oligophenylene branch is enlarged. In contrast, *meta*-substitution produces little perturbation of SubPzs in the ground state, although it does it to higher extent in the excited state. Consequently, the absorption profiles are preserved, while bathochromic shifts of the fluorescence bands are produced upon this substitution pattern. In addition, blue shift of the SubPz Q-band, with concomitant red shift of the emission, is achieved by reducing the conjugation of the aryl moieties with the SubPz core, through introduction of bulky alkyl rests. In line with the experimental results, DFT studies predict for the HOMO orbitals a more significant electronic delocalization through the *para*-substituted aryl moieties than through the *meta*-substituted ones.

Within the hexavinylated series, effective electronic delocalization over the vinylene moieties is evidenced by experimental and DFT studies, reflecting a coplanar configuration with respect to the aromatic SubPz core, which has also been confirmed by X-ray crystallography. This enables a good electronic communication of the macrocycle with other systems attached to the vinylene ends, such as phenyl and biphenyl moieties.

The organization of the macrocycles in the crystalline state is determined by the nature, number and position of peripheral substituents and varies from parallel or zigzag columnar stacking, to face-to face disposition.

Tuning the HOMO/LUMO energies, the absorption and fluorescence features, and the electrochemical properties by chemical design is essential in the search for photosensitizers for different applications, such as photovoltaics, singlet fission or singlet oxygen generation, among others.

1.5 Experimental Section

Materials and general methods

General Experimental Procedures.

All manipulations were carried out under an argon atmosphere using conventional Schlenk Techniques. Column chromatographies were conducted on silica gel Merck-60 (230-400 mesh, 60 Å). TLC was performed on aluminium sheets pre-coated with silica gel 60 F_{254} (E. Merck). Chemicals and boronic acids derivatives were purchased from Aldrich Chemical Co., Alfa Aesar (Thermo Fisher Scientific), and TCI Europe N. V. and used as received without further purification. "Synthetic grade" solvents were used for chemical reactions, column chromatography purifications, and "anhydric grade" for reactions under dry conditions. Additionally, some solvents were further dried by distillation with Sodium/benzophenone (THF) or with solvent purifying system by Innovative Technology Inc. MD-4-PS.

Instrumental Analyses.

^{1}H NMR and **^{13}C NMR** were recorder on a Bruker AC-400 (400 MHz) spectrometer using as deuterated solvent, $CDCl_3$. The temperature was actively controlled at 298 K. Chemical shifts are measured in ppm relative to tetramethylsilane (TMS).

UV/Vis spectra were recorded with a Jasco V-660-Spectrophotometer.

IR spectra were recorded with Agilent Technologies Cary 630 FTIR, or using a Bruker Alpha II spectrometer by attenuated total reflection (ATR).

Mass spectra (**MS**) were acquired by MALDI-TOF technique in SidI, using a Bruker REFLEX III with a nitrogen laser operating at 337 nm, or using Atmospheric Pressure Chemical Ionization (APCI) as ionization method.

Fluorescence was recorded with a JASCO-V8600-Spectrofluorometer.

Electrochemistry. Electrochemical measurements were performed at room temperature in a potentiostat/galvanostat Autolab PGStat30. Measurements were carried out in a home-built one-compartment cell with a three-electrode configuration,

containing 0.1 M tetrabutylammonium hexafluorophosphate ($TBAPF_6$) as supporting electrolyte. A platinum electrode was used as the working electrode, a platinum wire as the counterelectrode, and a $Ag/AgNO_3$ (in CH_3CN) electrode was used as reference. Prior to each voltammetric measurement the cell containing dry DCM was degassed under argon atmosphere for about 20 min. The electrochemical measurements were performed by using a concentration of approximately 0.1-0.2 mmol of the corresponding compound, and ferrocene was added as an internal reference. All the potentials were given relative to the Fc/Fc^+ couple with a scan rate at 100 mV/s.

X-Ray diffraction spectra were done in SidI with a Bruker KAPPA APEX II CCD goniometer with kappa geometry and Mo source (λ= 0.71073 Å). Data were corrected with SADABS program. The intensities were calculated with SAINT program and the structures were resolved with SHELXS and refined with SHELXL.

1.5.1 Synthesis of the hexasulfanyl-SubPz precursors

2,3-Dithioalkylmaleonitrile (1a, b)[68b]

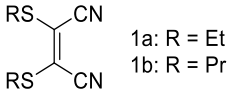

1a: R = Et
1b: R = Pr

To a solution of finely grounded NaCN (29.4 g, 0.6 mol) in 180 mL of dry DMF, carbon disulfide (36.5 mL, 0.6 mol) was added dropwise at 0 ºC. When the addition is over the solution is vigorously stirred at rt for 30 min before adding 500 mL of *i*-BuOH and heating the mixture to reflux for 10 min. The solution was filtered while hot and cooled in ice-salt bath, upon which a brown precipitate appears, that is filtered and washed thoroughly with Et_2O, obtaining 130 g of a yellow solid. The solid is dissolved in 1 L of distilled water and left for one day. The sulphur formed was eliminated by filtration and the water eliminated in the rotary evaporator. Ethanol (400 mL) is added to the remaining oil and heated up to its boiling point and filtered while hot. When the solution cools down again to rt, Et_2O was added until a yellow precipitate appears, which corresponds to the maleonitrile dication (30g).

1a: To a suspension of this solid (20 g, 0.107 mol) in acetone (550 mL), bromoethane (25 g, 0.229 mol) and a tip of spatula of NaI were added, and the mixture was heated to reflux for 20h. After this time the solution was filtered hot and the solvent eliminated in the rotary evaporator. The orange oily residue was purified by column chromatography on silica gel (eluent: hexane/AcOEt 3:1) to yield the compound as a yellow oil (18.07 g, 85 %).

^{1}H NMR (400 MHz, $CDCl_3$): δ = 3.13 (q, J = 7.4 Hz, 4H), 1.39 ppm (t, J = 7.4 Hz, 6H).

1b: To a suspension of disodium maleonitrilebisthiolate (20 g, 0.107 mol) in acetone (550 mL), 1-iodopropane (37.4 g, 0.22 mol) and a tip of spatula of NaI were added, and the mixture was heated to reflux for 20h. After this time the solution was filtered hot and the solvent eliminated in the rotary evaporator. The orange oily residue was

purified by column chromatography on silica gel (eluent: hexane/AcOEt 8:2) to yield the compound as a pale yellow oil (15.24 g, 63 %).

^{1}H NMR (400 MHz, $CDCl_3$): δ= 3.10 (q, J = 8.0 Hz, 4H), 1.81 – 1.72 (m, 4H), 1.05 ppm (t, J = 8.0 Hz, 6H).

***p*-Terphenylboronic acid (4c)[77]**

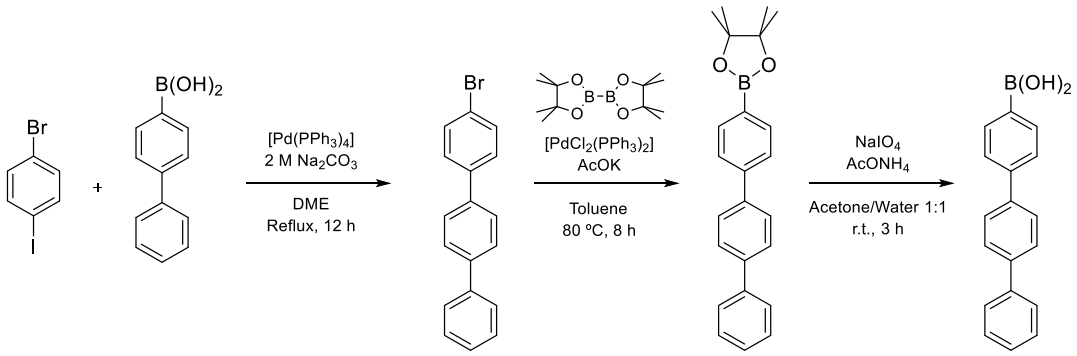

Scheme 1.10. Synthetic route of 4-(4-biphenyl) phenyl boronic acid (**4c**).

p-Bromo-(4-biphenyl)benzene (**19**). A 100 mL two-neck round-bottom flask connected to a condenser and held under argon atmosphere was charged with 1-bromo-4-iodobenzene (800 mg, 2.8 mmol, 1 eq), 5 mol % $[Pd(PPh_3)_4]$ (162 mg, 0.14 mmol), and dissolved by 20 mL of dimethoxyethane (DME). The resulting yellow mixture was stirred for 10 min at room temperature, followed by the addition of 4-biphenylboronic acid (614 mg, 3.1 mmol, 1.1 eq) and 20 mL of 2 M Na_2CO_3. The reaction mixture was refluxed overnight under argon atmosphere, and then cooled to room temperature. The product was extracted with dichloromethane and washed with water, dried over $MgSO_4$, and the solvent was evaporated under reduced pressure. The crude product was recrystallized from dichloromethane giving pure compound (736 mg, 85%) as white needles.

^{1}H NMR (400 MHz, $CDCl_3$): δ= 7.70–7.36 ppm (m, 13H; ArH).

[77] T. J. Dingemans, N. S. Murthy, E. T. Samulski, *Phys. Chem. B* **2001**, *105*, 8845–8860.

^{13}C NMR (100.6 MHz, $CDCl_3$): δ= 141.0, 140.5, 139.7, 138.9, 131.9, 129.0, 128.6, 127.7, 127.3, 127.1, 121.6 ppm.

4-(4-biphenyl)phenylboronic acid pinacolester (**20**). A Schlenk tube of 50 mL held under argon atmosphere was charged with **19** (618 mg, 2.0 mmol, 1 eq), bis(pinacolato)diboron (609 mg, 2.4 mmol, 1.2 eq), potassium acetate (589 mg, 6.0 mmol, 3 eq), and dissolved by 20 mL of toluene. The resulting solution was deoxygenated with an argon reflux for 10 min at room temperature, and the $[PdCl_2(PPh_3)_2]$ (140 mg, 0.2 mmol, 0.1 eq) was added. The reaction mixture was stirred at 80 ºC for 8 h. Once the reaction is completed, the mixture was cooled to room temperature and the solvent was removed under reduced pressure. The crude material was passed through a short pad of compressed celite using toluene, followed by the column chromatography on silica gel (toluene) yielding a pale-blue solid (570 mg, 80%) and fluorescent at 365 nm in solution ($CDCl_3$).

^{1}H NMR (400 MHz, $CDCl_3$): δ= 7.99–7.38 (m, 13H; ArH) 1.42 ppm (s, 12H; 4Me).

^{13}C NMR (100.6 MHz, $CDCl_3$): δ= 140.8, 140.2, 139.7, 135.6, 131.9, 130.4, 128.6, 127.7, 127.3, 127.1, 88.1, 24.7, 24.5 ppm.

4-(4-biphenyl)phenyl boronic acid (**4c**). To a solution of the **20** (400 mg, 1.12 mmol, 1 eq) in 20 mL acetone/water (1:1) was added $AcONH_4$ (432 mg, 5.6 mmol, 5eq) and $NaIO_4$ (1.2 g, 5.6 mmol, 5 eq). The mixture was stirred at room temperature and the reaction was monitored by TLC. Once the reaction is completed, the acetone was removed by evaporation under reduced pressure and the product was extracted with ethyl acetate. The combined organic phases were washed with Brine, dried over $MgSO_4$, and evaporated under reduced pressure giving **4c** (300 mg, quantitative) as a white solid.

^{1}H NMR (400 MHz, DMSO-d_6): δ = 8.09 (s, 2H; ArH), 7.89 (d, J = 8.0 Hz, 2H; ArH), 7.79 (d, J = 8.4 Hz, 2H; ArH), 7.76 (d, J = 8.8 Hz, 2H; ArH), 7.72 (d, J = 8.0 Hz, 2H; ArH), 7.69 (d, J = 8.0 Hz, 2H; ArH), 7.48 (t, J = 7.6 Hz, 2H; ArH), 7.38 ppm

(t, J = 7.6 Hz, 1H; ArH).

^{13}C NMR (100.6 MHz, $CDCl_3$): δ= 141.0, 139.6, 139.2, 139.1, 134.8, 129.0, 127.5, 127.2, 127.1, 126.6, 125.5 ppm.

3,5-Di-*tert*-butylphenylboronic acid (4d)[78]

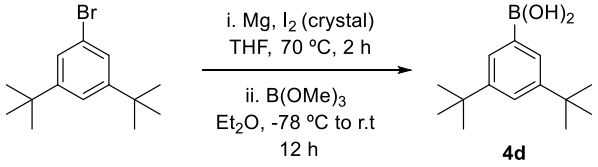

Scheme S2. Synthesis of (3,5-di-*tert*-butyl)phenyl boronic acid (**4d**).

A Schlenk tube of 25 mL held under argon atmosphere was charged with 1-bromo-3,5-di-*tert*-butylbenzene (2.0 g, 7.4 mmol, 1 eq), Mg turnings (200 mg, 8.2 mmol, 1.1 eq), and anhydrous THF (5 mL). The reaction mixture was stirred at 70 °C for 2 h under argon atmosphere. Once all the starting material was consumed, the reaction medium was transferred dropwise via syringe filter into a solution of trimethyl borate (1.15 g, 11.1 mmol, 1.5 eq) in 20 mL of anhydrous Et_2O at -78 °C under argon atmosphere. After complete addition, the reaction mixture was warmed to room temperature and stirred for 12 h. The reaction was quenched by adding 15 mL of aqueous 1 M HCl and stirred for 3 h, followed by extraction with Et_2O. The combined organic phases were washed with Brine, dried over Na_2SO_4, and evaporated under reduced pressure giving **4d** (1.38 g, 80%) as a white solid.

^{1}H NMR (400 MHz, $CDCl_3$): δ= 8.20 (d, J = 2.0 Hz, 2H; ArH), 7.70 (t, J = 2.0 Hz, 1H; ArH), 4.80 (s, 2H; OH), 1.50 ppm (s, 18H, *t*-Bu).

^{13}C NMR (100.6 MHz, $CDCl_3$): δ= 150.3, 129.6, 127.5, 127.1, 35.0, 31.6 ppm.

[78] A. Schöbel, E. Herdtweck, M. Parkinson, B. Rieger, *Chem. Eur. J.* **2012**, *18*, 4174–4178.

Copper (I) thiophene-2-carboxylate (CuTC)[79]

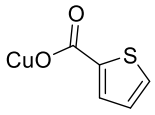

A 50mL round-bottomed flask was charged with thiophene-2-carboxylic acid (10g, 78 mmol), Cu_2O (2.8 g, 19.6 mmol) and dry toluene (30 mL). The flask was then outfitted with Dean-Stark trap and a condenser and the mixture was refluxed overnight with azeotropic removal of water. The yellow/gray suspension was cooled to 60 °C the product was collected by filtration. The solid was washed by methanol (30 mL) to remove excess acid, and with ether until the eluent was colorless, then with a small amount of hexane. The product was dried under vacuum. The product was obtained as a tan powder (5.56 g, 75%).

4-*tert*-Butylphenoxy[2,3,7,8,12,13-hexa(ethylthio)subporphyrazinato]boron(III) (2a)[48]

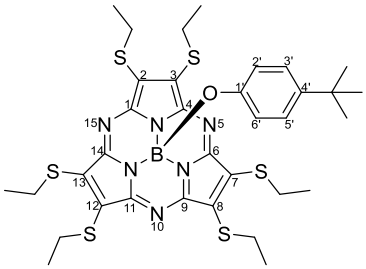

2a

A 1M solution of BCl_3 in xylenes (2.0 mL, 2.0 mmol) was added under a N_2 atmosphere to bis(ethylthio)maleonitrile (396 mg, 2.0 mmol) and the mixture was heated at 100 °C for 45 min. The solvent was removed under reduced pressure. Then, the residue was dissolved in toluene (4 mL) and 4-*tert*-butylphenol (1.50 g, 10 mmol) was added. The resulting solution was stirred at reflux for 2 h and afterwards the solvent was evaporated. Column chromatography on silica gel using a 20:1 mixture of

[79] G. D. Allred, L. S. Liebeskind, *J. Am. Chem. Soc.* **1996**, *118*, 2748–2749.

n-hexane and ethyl acetate gave a red viscous solid, which was dissolved in 20 mL of dry 1,3-dimethyl-2-imidazolidinone (DMI) at 0 °C under argon atmosphere. Then, ethanethiol (8 μL, 0.11 mmol, 0.05 eq respect to **1a**) and freshly distilled triethylamine (15 μL, 0.11 mmol, 0.05 eq respect to **1a**) were added via syringe, and the resulting mixture was stirred heating from 0 °C to room temperature for 1 h. Once the reaction is completed (TLC showed just one red spot in n-hexane/ethyl acetate 20:1) the product was extracted with diethyl ether and washed three times with water, dried over $MgSO_4$, and the solvent was evaporated under reduced pressure. The crude product was chromatographed on silica gel (15:1 mixture of n-hexane/ethyl acetate) giving pure target compound **2a** (70 mg, 14%) as a red viscous solid.

^{1}H NMR (400 MHz, $CDCl_3$): δ = 6.82 (d, J = 8.6 Hz, 2H; $H^{3',5'}$), 5.31 (d, J = 8.6 Hz, 2H; $H^{2',6'}$), 4.03 (m, 6H; -S$CH_2$$CH_3$), 3.66 (m, 6H; -S$CH_2$$CH_3$), 1.60 (t, J = 7.2 Hz, 18H; -SCH_2CH_3) and 1.14 (s, 9H; *t*-Bu) ppm.

^{13}C NMR (100.6 MHz, $CDCl_3$): δ = 154.1, 150.1, 144.5, 151.6, 125.7, 119.2, 34.0, 31.5, 29.4 and 15.8 ppm.

^{11}B NMR (128 MHz, $CDCl_3$): δ = –16.32 ppm.

UV/Vis ($CHCl_3$): λ (log ε, $M^{-1}cm^{-1}$) = 282 (4.3), 438 (4.4) and 556 (4.3) nm.

Fluorescence ($CHCl_3$, λ_{ex} = 530 nm): λ_{max} = 682 nm, Φ_F = 0.001.

HRMS (ESI-TOF, positive) calcd. for $C_{34}H_{44}BN_6OS_6$ $[M+H]^+$ 755.1995; found 755.1987.

4-*tert*-Butylphenoxy[2,3,7,8,12,13-hexa(propylthio)subporphyrazinato]boron(III) (2b)

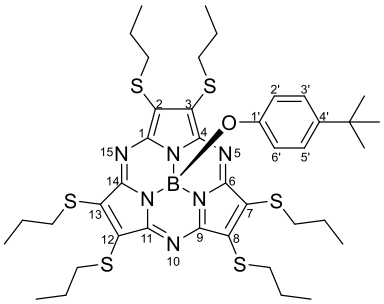

2b

An oven-dried two-neck round-bottom flask connected to a condenser and held under argon atmosphere was charged with bis(propylthio)maleonitrile **1b** (452 mg, 2.0 mmol, 1eq). A 1.0 M solution of BCl_3 in p-xylene (2.0 mL, 2.0 mmol, 1 eq) was then added into the flask via syringe, and the mixture was heated at 110ºC for 1 h under argon. The reaction mixture was cooled to room temperature, and the solvent was removed under reduced pressure. The resulting dark violet crude was dissolved in toluene (4 mL) and 4-*tert*-butylphenol (1.50 g, 10 mmol, 5 eq) was added. The mixture was stirred to reflux for 2 h under argon atmosphere followed by removal of the solvent under reduced pressure once more. The black crude material was passed through a short pad of compressed celite using a 9:1 mixture of n-hexane/ethyl acetate followed by the column chromatography on silica gel (20:1 mixture of n-hexane/ethyl acetate), collecting the two red fractions close to each other. The red viscous solid obtained was dissolved in 20 mL of dry 1,3-dimethyl-2-imidazolidinone (DMI) at 0 ºC under argon atmosphere. Then, 1-propanethiol (10 μL, 0.11 mmol, 0.05 eq respect to **1b**) and freshly distilled triethylamine (15 μL, 0.11 mmol, 0.05 eq respect to **1b**) were added via syringe, and the resulting mixture was stirred heating from 0 ºC to room temperature for 1 h. Once the reaction is completed (TLC showed just one red spot in n-hexane/ethyl acetate 20:1) the product was extracted with diethyl ether and washed three times with water, dried over $MgSO_4$, and the solvent was evaporated under reduced pressure. The crude product was chromatographed on silica gel (15:1 mixture

of n-hexane/ethyl acetate) giving pure target compound **2b** (84 mg, 15%) as a red viscous solid.

^{1}H NMR (400 MHz, $CDCl_3$): δ = 6.86 (d, J = 8.6 Hz, 2H; $H^{3',5'}$), 5.29 (d, J = 8.6 Hz, 2H; $H^{2',6'}$), 4.05 (m, 6H; -S*CH*$_2$Et), 3.57 (m, 6H; -S*CH*$_2$Et), 1.96 (m, 12H; -SCH_2*CH*$_2$$CH_3$), 1.18 (t, J = 7.2 Hz, 18H; -SCH_2CH_2*CH*$_3$), 1.15 ppm (s, 9H; *t*-Bu).

^{13}C NMR (100.6 MHz, $CDCl_3$): δ = 154.1, 150.0, 144.2, 131.6, 125.4, 118.8, 36.9, 33.9, 31.4, 23.7, 13.5 ppm.

MS (APCI, MeOH, +): m/z = 839.2937 $[M + H]^+$; 721.2158 [M – OPh^{t}Bu + OMe]$^+$.

FT-IR (ATR): ν = 2958, 2927, 2869, 1606, 1443, 1241, 1172, 1115, 1025 S*, 895, 838, 749, 575 cm^{-1}.

UV/Vis ($CHCl_3$): λ (log ε/dm^3 mol^{-1} cm^{-1}) = 282 (4.3), 439 (4.4), 557 (4.4) nm.

Fluorescence ($CHCl_3$): λ_{ex} = 552 nm; λ_{em} = 682 nm.

4-*tert*-Butylphenoxy[2-chloro-3,7,8,12,13-penta(propylthio) subporphyrazinato] boron(III) (3b detected)

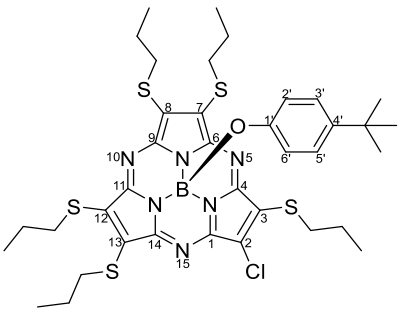

3b

A 1M solution of BCl_3 in xylenes (2.0 mL, 2.0 mmol) was added under a N_2 atmosphere to bis(propylthio)maleonitrile **1b** (452 mg, 2.0 mmol, 1eq). and the mixture was heated at 100 °C for 45 min. The solvent was removed under reduced pressure. Then, the residue was dissolved in toluene (4 mL) and 4-*tert*-butylphenol (1.50 g, 10 mmol) was added. The resulting solution was stirred at reflux for 2 h and afterwards the solvent was evaporated. Column chromatography on silica gel using a

20:1 mixture of *n*-hexane and ethyl acetate gave a red viscous solid (mixture **2b** and **3b**).

^{1}H NMR (400 MHz, $CDCl_3$): δ = 6.81 (d, J = 8.6 Hz, 2H; $H^{3',5'}$), 5.28 (m, 2H; $H^{2',6'}$), 4.15–3.99 (m, 5H; -S*CH*$_2$Et), 3.73–3.53 (m, 5H; -S*CH*$_2$Et), 1.96 (m, 10H; -SCH$_2$*CH*$_2$CH$_3$), 1.18 (m, 15H; -SCH$_2$CH$_2$*CH*$_3$), 1.14 ppm (s, 9H; *t*-Bu).

MS (APCI, MeOH, +): *m/z* = 799.2345 $[M + H]^+$; 649.1302 $[M - OPh^tBu]^+$; 839.2925 $[M_{(\mathbf{2b})}+H]^+$.

HRMS (APCI, MeOH, +): *m/z* calculated for $C_{37}H_{49}BClN_6OS_5$ $[M+H]^+$ 799.2347, found 799.2345.

1.5.2 Synthesis of oligophenylene-SubPzs 5 – 10

General procedure for Liebeskind-Srogl cross-coupling of SubPzs:

An oven-dried flask was over-dried and purged with argon during 10 minutes. Subsequently hexa(ethylthio)subporphyrazine **2a** (15 mg, 19.8 μmol, 1 eq) or **2b** (17 mg, 19.8 μmol, 1 eq), boronic acid (**4a** – **4i**) (18 equiv), $Pd(PPh_3)_4$ (13.9 mg, 12 μmol; 60 mol%) and CuTC (68.6 mg, 360 μmol; 18 equiv) were added into the flask and purged with argon for 10 min, followed by the addition of anhydrous THF (6 mL) *via cannula*. The reaction mixture was stirred at 60 °C for 20 h under argon atmosphere, cooled to room temperature and passed through a short silica gel column using THF as eluent. The solvent was removed and the residue was purified by silica gel column chromatography.

Unless otherwise noted, all reactions were performed according to this typical procedure.

4-*tert*-Butylphenoxy[2,3,7,8,12,13-hexa(4''-biphenyl)subporphyrazinato] Boron(III) (5)

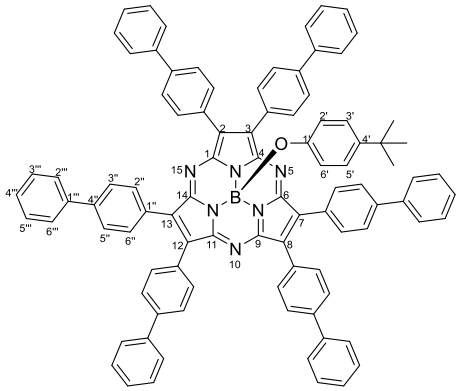

5

The residue was purified by silica gel column chromatography ($CHCl_3$/heptane 2:1). The product was obtained as a red solid (9.3 mg, 36%).

^{1}H NMR (400 MHz, $CDCl_3$): δ = 8.00 (d, J = 8.5 Hz, 12H; $H^{2'', 6''}$), 7.65 (d, J = 8.5 Hz, 24H; $H^{3'', 4'', 2''', 6'''}$), 7.45–7.31 (m, 18H; $H^{3''', 4''', 5'''}$), 6.87 (d, J = 8.5, 2H; $H^{3', 5'}$), 5.39 (d, J = 8.5, 2H, $H^{2', 6'}$), 1.11 ppm (s, 9H; *t*-Bu).

^{13}C NMR (100.6 MHz, $CDCl_3$): δ = 156.8, 150.8, 143.1, 141.1, 140.0, 133.2, 131.8, 130.8, 128.8, 127.5, 127.1, 127.0, 125.7, 116.9, 33.9, 31.4 ppm.

MS (MALDI-TOF, DCTB): *m/z* = 1307.5 $[M + H]^+$; 1345.5 $[M + K]^+$; 1157.5 $[M – OPh^tBu]^+$.

FT-IR (film): ν = 3055, 3030, 2956, 2924, 2853 (C-H), 1605 (C=N), 1500, 1487, 1456, 1390, 1258, 1178, 1124, 1075, 1008, 842, 762, 695 cm^{-1}.

UV/Vis ($CHCl_3$): λ_{max} (log ε/dm^3 mol^{-1} cm^{-1}): 285 (4.8), 429 (4.5), 554 (4.6) nm.

Fluorescence ($CHCl_3$): λ_{ex} = 543 nm; λ_{em} = 599 nm.

4-*tert*-Butylphenoxy[2,3,7,8,12,13-hexa(3''-biphenyl)subporphyrazinato] boron(III) (6)

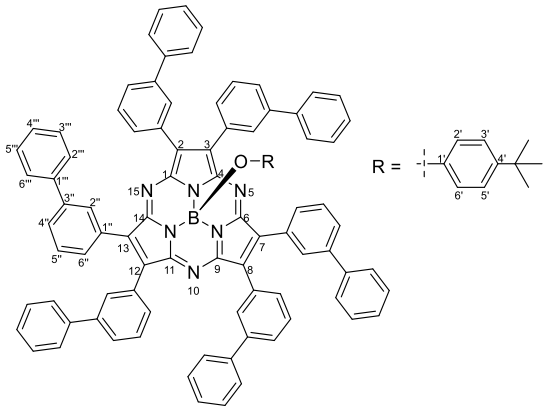

6

The residue was purified by silica gel column chromatography ($CHCl_3$/heptane 2.5:1). The product was obtained as a red solid (8.5 mg, 33%).

^{1}H NMR (400 MHz, $CDCl_3$): δ = 8.12 (s, 6H; $H^{2''}$), 7.99 (d, J = 8.5 Hz, 6H; $H^{4''}$), 7.65 (d, J = 8.5 Hz, 6H; $H^{6''}$), 7.47–7.40 (m, 18H; $H^{5'', 2''', 6'''}$), 7.36–7.29 (m, 18H; $H^{3''', 4''', 5'''}$), 6.90 (d, J = 8.5, 2H; $H^{3', 5'}$), 5.44 (d, J = 8.5, 2H; $H^{2', 6'}$), 1.14 ppm (s, 9H; *t*-Bu).

^{13}C NMR (100.6 MHz, $CDCl_3$): δ = 156.7, 150.6, 143.1, 141.4, 140.7, 133.9, 132.1, 130.2, 130.1, 129.0, 128.6, 127.2, 127.0, 125.8, 117.2, 33.9, 31.4 ppm.

MS (MALDI-TOF, DCTB): m/z = 1307.5 $[M + H]^+$; 1157.5 $[M - OPh^tBu]^+$.

FT-IR (film): ν = 3056, 3030, 2961, 2926, 2857, 1597, 1573, 1511, 1483, 1459, 1383, 1256, 1202, 1172, 1124, 1031, 1018, 896, 842, 801,757, 699 cm^{-1}.

UV/Vis ($CHCl_3$): λ_{max} (log ε/dm^3 mol^{-1} cm^{-1}): 252 (5.1), 305 (4.6), 405 (4.4), 541 (4.7) nm.

Fluorescence ($CHCl_3$): λ_{ex} = 529 nm; λ_{em} = 571 nm.

4-*tert*-Butylphenoxy[2,3,7,8,12,13-hexa(4''-terphenyl)subporphyrazinato] boron(III) (7)

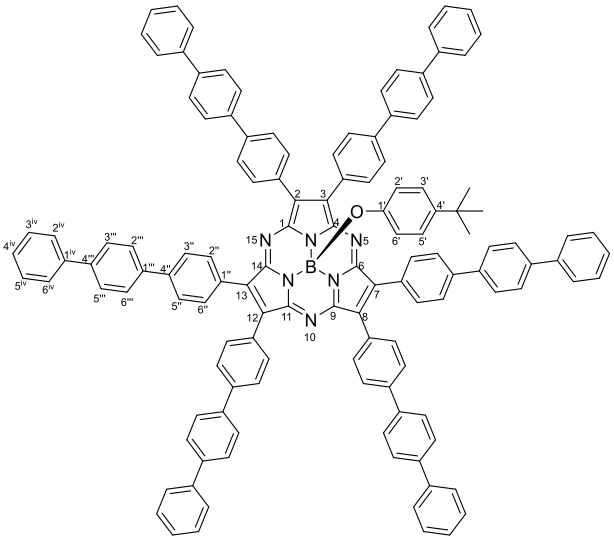

7

The residue was purified by silica gel column chromatography ($CHCl_3$/heptane 2.5:1). The product was obtained as a red solid (10.5 mg, 30%).

^{1}H NMR (400 MHz, $CDCl_3$): δ = 7.81–7.79 (m, 12H; $H^{2iv, 6iv}$), 7.63–7.60 (m, 48H; $H^{2'', 3'', 5'', 6'', 2''', 3''',5''', 6'''}$), 7.41–7.32 (m, 18H; $H^{3iv, 4iv, 5iv}$), 6.88 (d, J = 8.5, 2H; $H^{3', 5'}$), 5.37 (d, J = 8.5, 2H; $H^{2', 6'}$), 1.13 ppm (s, 9H; *t*-Bu).

^{13}C NMR (100.6 MHz, $CDCl_3$): δ = 156.4, 150.7, 143.1, 140.6, 140.5, 140.4, 138.9, 133.3, 131.9, 130.7, 128.7, 127.5, 127.3, 127.0, 120.0, 125.9, 117.0, 33.9, 31.4 ppm.

MS (MALDI-TOF, DCTB): m/z = 1764.6 $[M + 2H]^+$; 1614.6 $[M - OPh^tBu + H]^+$.

FT-IR (film): ν = 3051, 3027, 2960, 2922, 2855, 2831, 1599, 1577, 1513, 1485, 1448, 1387, 1288, 1260, 1200, 1176, 1107, 1075, 1025, 1005, 826, 764,738, 695 cm^{-1}.

UV/Vis ($CHCl_3$): λ_{max} (log ε/dm^3 mol^{-1} cm^{-1}): 298 (5.2), 440 (4.7), 557 (4.8) nm.

Fluorescence ($CHCl_3$): λ_{ex} = 544 nm; λ_{em} = 612 nm.

4-*tert*-Butylphenoxy[2,3,7,8,12,13-hexa(3'',5''-bis(*tert*-butyl) phenyl)subporphyrazinato] boron(III) (8)

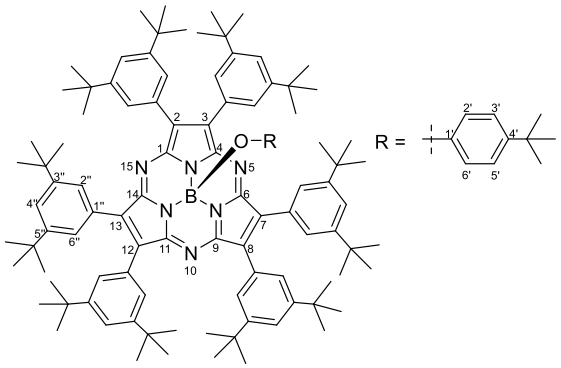

8

The residue was purified by silica gel column chromatography (hexane/ethyl acetate 25:1). The product was obtained as a red solid (3.6 mg, 12%).

^{1}H NMR (400 MHz, $CDCl_3$): δ = 7.35 (d, J = 1.8 Hz, 12H; Ar-$H^{2'', 6''}$), 7.32 (t, J = 1.8 Hz, 6H; $H^{4''}$), 6.90 (d, J = 8.6 Hz, 2H; $H^{3',5'}$), 5.41 (d, J = 8.6 Hz, 2H; $H^{2', 6'}$), 1.14 (s, 9H; OPh *t*-Bu), 1.10 (s, 108H; Ar-*t*-Bu) ppm .

^{13}C NMR (100.6 MHz, $CDCl_3$): δ = 159.1, 158.6, 157.3, 150.3, 136.1, 131.3, 125.9, 125.8, 121.6, 116.9, 34.6, 31.3 ppm.

MS: (MALDI-TOF, DCTB+NaI): m/z = 1546.1 $[M + Na]^+$; 1397.1 $[M - OPh^tBu + Na]^+$; 1374.1 $[M - OPh^tBu]^+$.

FT-IR (ATR): ν = 2959 S*, 2866, 1594, 1470, 1389, 1363, 1252, 1185, 1035, 880, 712 cm^{-1}.

UV/Vis ($CHCl_3$): λ_{max} (log ε/dm^3 mol^{-1} cm^{-1}): 293 (sh), 402 (4.6), 532 (4.8) nm.

Fluorescence ($CHCl_3$): λ_{ex} = 545 nm; λ_{em} = 575 nm.

XRD: Single crystals suitable for X-ray diffraction analysis were obtained by vapor diffusion of methanol into its chloroform solution. Crystallographic data and some refining details are summarized in the following table:

Chemical formula	$C_{95.50}H_{58}BN_6O$	
Formula weight	1316.29 g/mol	
Temperature	200(2) K	
Wavelength	0.71073 Å	
Crystal size	0.096 x 0.141 x 0.198 mm	
Crystal habit	intense orange prismatic	
Crystal system	monoclinic	
Space group	P 1 21/n 1	
Unit cell dimensions	a = 22.030(2) Å	α = 90°
	b = 36.178(4) Å	β = 96.738(2)°
	c = 30.846(3) Å	γ = 90°
Volume	24415.(4) $Å^3$	
Z	8	
Density (calculated)	0.716 g/cm^3	
Absorption coefficient	0.042 mm^{-1}	
F(000)	5488	

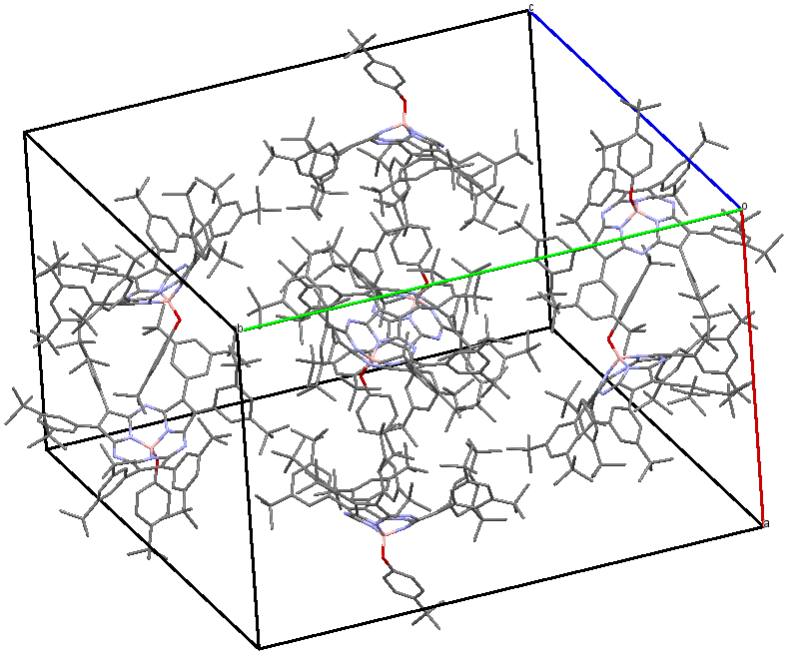

Figure 1.19. Unity cell and crystalline packing of SubPz **8**.

4-*tert*-Butylphenoxy[2,3,7,8,12,13-hexa(3''-methoxyphenyl) subporphyrazinato] boron(III) (9)

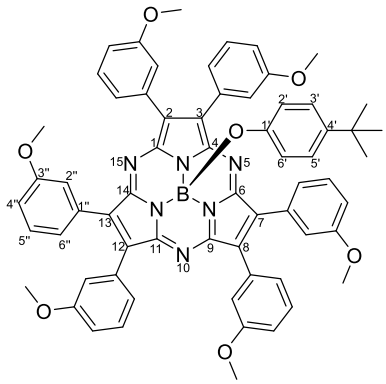

9

The residue was purified by silica gel column chromatography ($CHCl_3$/heptane 2.5:1). The product was obtained as a red solid (6.7 mg, 33%). Single crystals suitable for X-ray diffraction analysis were obtained by vapor diffusion of octane into its 1,2-dichloroethane solution.

^{1}H NMR (400 MHz, $CDCl_3$): δ = 7.39–7.38 (m, 12H; $H^{2'', 4''}$), 7.28–7.22 (m, 6H, $H^{5''}$), 6.90 (d, J = 8.5 Hz, 6H; $H^{6''}$), 6.82 (d, J = 8.5, 2H; $H^{3', 5'}$), 5.31 (d, J = 8.5, 2H; $H^{2', 6'}$), 3.52 (s, 18H; OCH_3), 1.06 ppm (s, 9H; *t*-Bu).

^{13}C NMR (100.6 MHz, $CDCl_3$): δ = 159.7, 156.8, 150.5, 142.9, 133.4, 132.7, 129.3, 125.7, 123.6, 116.8, 115.6, 115.1, 55.0, 33.6, 31.1 ppm.

MS (MALDI-TOF, DCTB): m/z = 1031.4 $[M + H]^+$; 881.4 $[M - OPh^tBu]^+$.

FT-IR (film): ν = 2999, 2960, 2922, 2851, 2831, 1597, 1577, 1511, 1483, 1461, 1422, 1385, 1288, 1254, 1217, 1111, 1081, 1019, 865, 829, 790,719, 691 cm^{-1}.

UV/Vis ($CHCl_3$): λ_{max} (log ε/dm^3 mol^{-1} cm^{-1}): 281 (4.5), 301 (4.4), 410 (4.2), 541 (4.5) nm.

Fluorescence ($CHCl_3$): λ_{ex} = 532 nm; λ_{em} = 575 nm.

XRD: Single crystals suitable for X-ray diffraction analysis were obtained by vapor diffusion of isooctane into its 1,2-dichloroethane solution. Crystallographic data and some refining details are summarized in the following table:

Chemical formula	$C_{64}H_{55}BN_6O_7$	
Formula weight	1030.99 g/mol	
Temperature	296(2) K	
Wavelength	0.71073 Å	
Crystal size	0.012 x 0.085 x 0.220 mm	
Crystal habit	Clear intense purple	
Crystal system	orthorhombic	
Space group	P 21 /c	
Unit cell dimensions	a = 11.4506(2) Å	α = 90°
	b = 21.5684(5) Å	β = 102°
	c = 22.2284(5) Å	γ = 90°
Volume	5354.66(3) $Å^3$	
Z	4	
Density (calculated)	1.279 g/cm^3	
Absorption coefficient	0.086 mm^{-1}	
F(000)	2936	

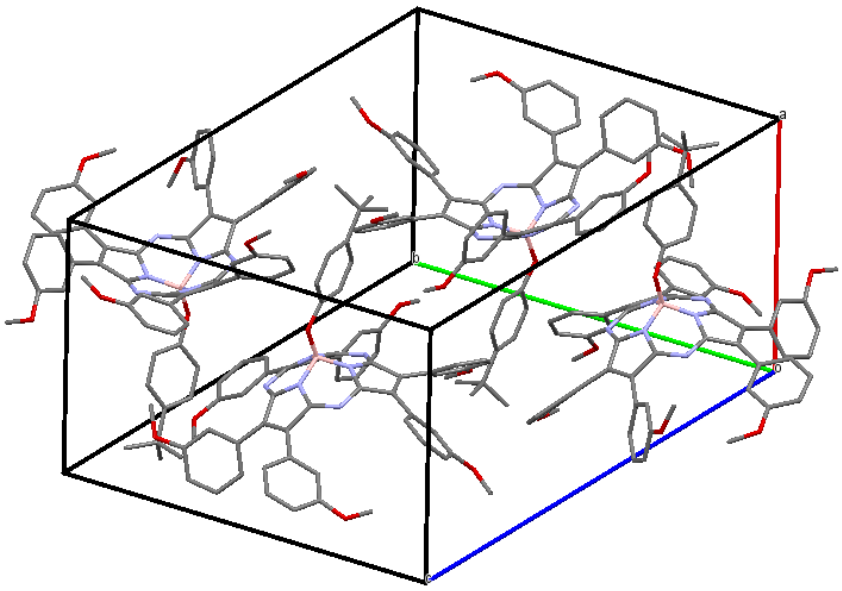

Figure 1.20. Unity cell and crystalline packing of SubPz **9**.

4-*tert*-Butylphenoxy[2,3,7,8,12,13-hexa(3'',4'',5''-trimethoxyphenyl) subporphyrazinato]boron(III) (10)

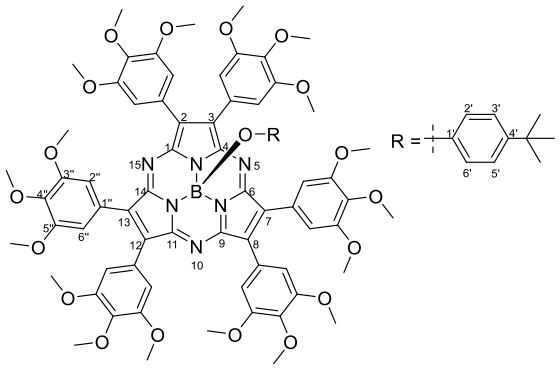

10

The residue was purified by silica gel column chromatography ($CHCl_3$/ethyl acetate 4:1). The product was obtained as a garnet solid (12 mg, 42%).

^{1}H NMR (400 MHz, $CDCl_3$): δ = 7.14 (s, 12H; $H^{2'', 6''}$), 6.89 (d, J = 8.5 Hz, 2H; $H^{3', 5'}$), 5.41 (d, J = 8.5 Hz, 2H; $H^{2', 6'}$), 3.91 (s, 18H; O-CH_3 $^{4''}$), 3.62 (s, 36H; O-$CH_3^{3'', 5''}$), 1.13 ppm (s, 9H; *t*-Bu).

^{13}C NMR (100.6 MHz, $CDCl_3$): δ = 156.9, 153.3, 150.7, 143.4, 138.7, 133.1, 127.0, 125.9, 117.3, 108.8, 61.0, 56.0, 33,8, 31.4 ppm.

MS (MALDI-TOF, DCTB): m/z = 1391.5 $[M + H]^+$; 1241.5 $[M - OPh^tBu]^+$.

FT-IR (film): ν = 3002, 2954, 2935, 2827, 1579, 1508, 1487, 1463, 1407, 1390, 1312, 1241, 1176, 1148, 1124, 1036, 1021, 1010, 872, 842, 753 cm^{-1}.

UV/Vis ($CHCl_3$): λ_{max} (log ε/dm^3 mol^{-1} cm^{-1}): 241 (4.7), 281 (4.7), 445 (4.5), 557 (4.6) nm.

Fluorescence ($CHCl_3$): λ_{ex} = 550 nm; λ_{em} = 668 nm.

XRD: Single crystals suitable for X-ray diffraction analysis were obtained by vapor diffusion of heptane into its 1,2-dichloroethane solution. Crystallographic data and some refining details are summarized in the following table:

Chemical formula	$C_{76}H_{79}BN_6O_{19}$	
Formula weight	1391.26 g/mol	
Temperature	296(2) K	
Wavelength	0.71073 Å	
Crystal size	0.010 x 0.090 x 0.240 mm	
Crystal habit	intense red-purple plate	
Crystal system	orthorhombic	
Space group	P 21 21 21	
Unit cell dimensions	a = 11.5995(3) Å	α = 90°
	b = 17.9668(4) Å	β = 90°
	c = 37.0913(8) Å	γ = 90°
Volume	7730.0(3) $Å^3$	
Z	4	
Density (calculated)	1.195 g/cm^3	
Absorption coefficient	0.086 mm^{-1}	
F(000)	2936	

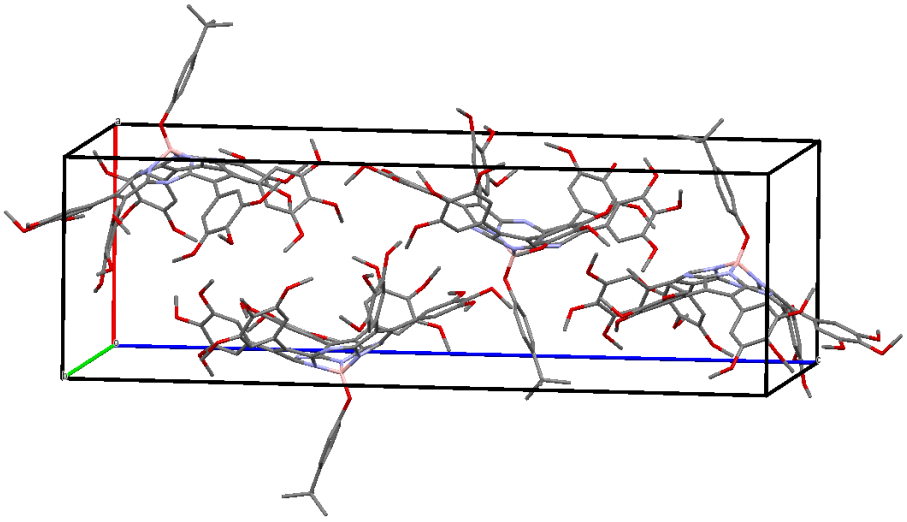

Figure 1.21. Unity cell and crystalline packing of SubPz **10**.

1.5.3 Synthesis of oligophenylene-SubPzs 11 – 13

4-*tert*-Butylphenoxy[2,3,7,8,12,13-hexa((1''*E*)-pentenyl)subporphyrazinato] boron(III) (11)

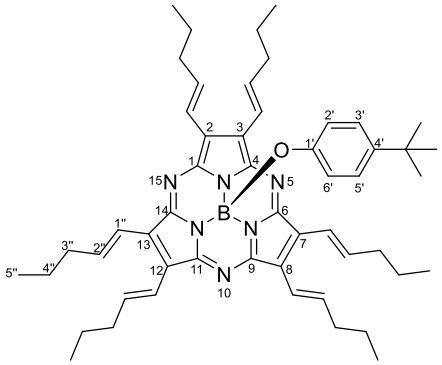

11

The residue was purified by silica gel column chromatography (hexane/ethyl acetate 25:1). The product was obtained as a red viscous solid (6.8 mg, 34%).

^{1}H NMR (400 MHz, $CDCl_3$): δ = 7.71 (dt, ^3J = 15.7, 7.2 Hz, 6H; $H^{2''}$), 6.81 (d, J = 15.7 Hz, 6H; $H^{1''}$), 6.79 (d, J = 8.6 Hz, 2H; $H^{3',5'}$), 5.27 (d, J = 8.6 Hz, 2H; $H^{2',6'}$), 2.41 (m, 12H; $CH_2^{3''}$), 1.66 (m, 12H; $CH_2^{4''}$), 1.11 (s, 9H; *t*-Bu), 1.05 ppm (t, J = 7.4 Hz, 18H; $CH_3^{5''}$).

^{13}C NMR (100.6 MHz, $CDCl_3$): δ = 155.5, 150.9, 140.4, 130.2, 129.3, 129.2, 125.5, 119.9, 117.4, 36.6, 31.4, 29.7, 22.6, 13.9 ppm.

MS (MALDI-TOF, DCTB): m/z = 802.6 $[M]^+$; 653.5 $[M - OPhtBu]^+$.

FT-IR (film): ν = 2956, 2922, 2853, 1718, 1636, 1508, 1457, 1258, 1178, 1032, 965, 800 cm^{-1}.

UV/Vis ($CHCl_3$): λ_{max} (log ε/dm3 mol-1 cm-1): 249 (4.7), 431 (4.5), 571 (4.5) nm.

Fluorescence ($CHCl_3$): λ_{ex} = 510 nm; λ_{em} = 604 nm.

4-*tert*-Butylphenoxy[2,3,7,8,12,13-hexa((1''*E*)-styryl)subporphyrazinato] boron(III) (12)

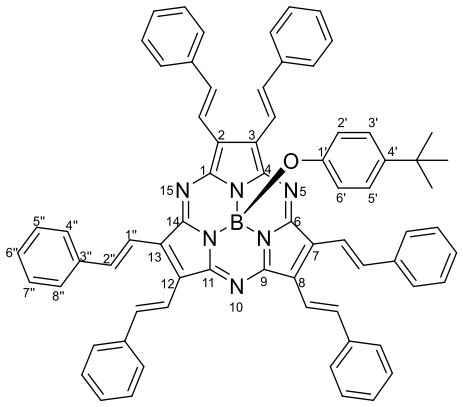

12

The reaction mixture was stirred at room temperature for 20 h under argon atmosphere. Then, the mixture was passed through a short silica gel column using THF as eluent. The solvent was removed and the residue was purified by silica gel column chromatography (hexane/DCM/Et_2O 6:3.5:0.5). The product was obtained as a dark-violet solid (12.4 mg, 62%).

^{1}H NMR (400 MHz, $CDCl_3$): δ = 8.86 (d, J = 16.1 Hz, 6H; $H^{2''}$), 7.74 (d, J = 7.6 Hz, 12H; $H^{4'',8''}$), 7.69 (d, J = 16.1 Hz, 6H; $H^{1''}$), 7.44 (t, J = 7.6 Hz, 12H; $H^{5'',7''}$), 7.36 (t, J = 6.9 Hz, 6H; $H^{6''}$), 6.90 (d, J = 8.6 Hz, 2H; $H^{3',5'}$), 5.48 (d, J = 8.6 Hz, 2H; $H^{2',6'}$), 1.15 ppm (s, 9H; *t*-Bu).

^{13}C NMR (100.6 MHz, $CDCl_3$): δ = 155.6, 150.7, 143.2, 137.5, 137.3, 130.3, 128.8, 127.3, 125.8, 117.8, 117.6, 33.9, 31.4 ppm.

MS (MALDI-TOF, DCTB): m/z = 1006.4 $[M]^+$; 857.4 $[M - OPhtBu]^+$.

FT-IR (film): ν = 3019, 2958, 2922, 2853, 1610, 1575, 1491, 1489, 1457, 1394, 1258, 1165, 1075, 1065, 962, 745, 688 cm^{-1}.

UV/Vis (CHCl3): λ_{max} (log $\varepsilon/dm^3\ mol^{-1}\ cm^{-1}$): 320 (4.9), 496 (4.7), 624 (4.5) nm.

Fluorescence (CHCl3): λ_{ex} = 570 nm; λ_{em} = 662 nm.

XRD: Single crystals suitable for X-ray diffraction analysis were obtained by vapor diffusion of isooctane into its 1,2-dichloroethane solution. Crystallographic data and some refining details are summarized in the following table:

Chemical formula	$C_{140}H_{110}B_2N_{12}O_2$	
Formula weight	2014.01 g/mol	
Temperature	296(2) K	
Wavelength	0.71073 Å	
Crystal size	0.190 x 0.250 x 0.560 mm	
Crystal habit	purple prismatic	
Crystal system	monoclinic	
Space group	C 1 2/c 1	
Unit cell dimensions	a = 25.0623(9) Å	α = 90°
	b = 25.2909(8) Å	β = 101.146(2)°
	c = 19.4705(7) Å	γ = 90°
Volume	12108.6(7) $Å^3$	
Z	4	
Density (calculated)	1.105 g/cm^3	
Absorption coefficient	0.066 mm^{-1}	
F(000)	4240	

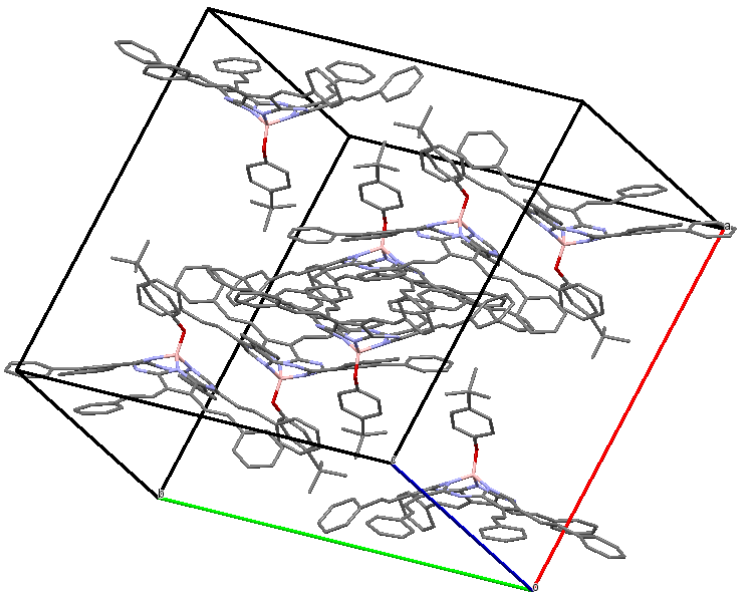

Figure 1.22. Unity cell and crystalline packing of SubPz **12**.

4-*tert*-Butylphenoxy[2,3,7,8,12,13-hexa((1'')*E*)-(*p*-phenyl)styryl) subporphyrazinato] boron(III) (13)

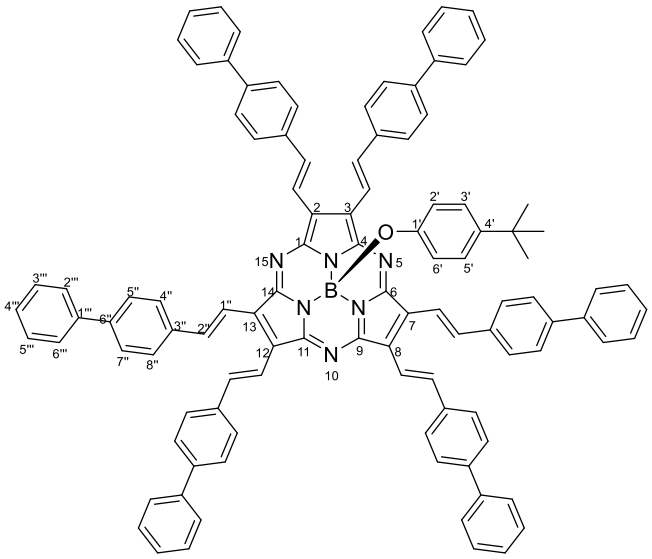

13

The residue was purified by silica gel column chromatography (hexane/DCM/Et_2O 6:3.5:0.5). The product was obtained as a dark-violet solid (23.2 mg, 80%).

^{1}H NMR (400 MHz, $CDCl_3$): δ = 8.88 (d, J = 16.1 Hz, 6H; $H^{2''}$), 7.78 (d, J = 8.0 Hz, 12H; $H^{4'',8''}$), 7.71 (d, J = 16.1 Hz, 6H; $H^{1''}$), 7.69–7.64 (m, 24H; $H^{5'',7'',2''',6'''}$), 7.44 (t, J = 7.4 Hz, 12H; $H^{3''',5'''}$), 7.35 (t, J = 7.3 Hz, 6H; $H^{4'''}$), 6.96 (d, J = 8.6 Hz, 2H; $H^{3',5'}$), 5.59 (d, J = 8.6 Hz, 2H; $H^{2',6'}$), 1.17 ppm (s, 9H; *t*-Bu).

^{13}C NMR (100.6 MHz, $CDCl_3$): δ = 155.7, 150.9, 143.2, 141.3, 140.5, 136.7, 130.3, 128.9, 127.8, 127.5, 127.4, 127.0, 125.9, 117.9, 117.5, 33.9, 31.4 ppm.

MS (MALDI-TOF, DCTB): m/z = 1463.6 $[M]^+$; 1313.5 $[M - OPhtBu]^+$.

FT-IR (film): ν = 3027, 2952, 2920, 2857, 1599, 1601, 1485, 1457, 1388, 1256, 1185, 1161, 962, 822, 759, 722, 695 cm^{-1}.

UV/Vis ($CHCl_3$): λ_{max} (log ε/$dm^3\ mol^{-1}cm^{-1}$): 282 (4.7), 341 (5.0), 517 (4.8), 619 (4.6) nm.

Fluorescence ($CHCl_3$): λ_{ex} = 590 nm; λ_{em} = 684 nm.

CHAPTER 2

Symmetrically Dodecafunctionalized Subnaphthalocyanines

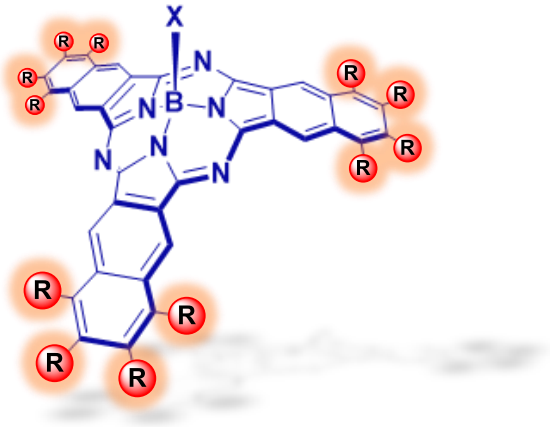

2.1 State of the art on Subnaphthalocyanines

As stated in the Introduction, **2,3-subnaphthalocyanines** are similar to SubPcs, but the former are composed of three benzo[f]isoindole subunits connected through nitrogen bridges and coordinated to a central boron atom. These compounds display extended conjugation that provides them with specific photophysical properties, including strong absorption in the red region and high fluorescence quantum yields (φ_F = 0.22). In addition, they show enhanced solubility related to the corresponding Pcs, as well as lower tendency to aggregate.[47c] 2,3-SubNcs are lower homologues of planar macrocycles **2,3-naphthalocyanines** (Ncs) (Figure 2.1), organic materials that are also promising for optical-limiting applications owing to their expanded ring structure and red-shifted transmission window.[80]

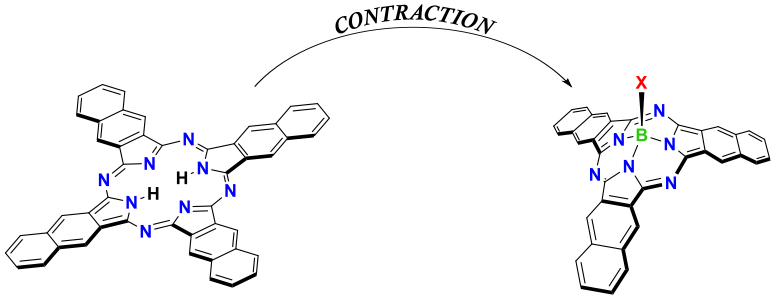

Figure 2.1. Chemical structure of 2,3-naphthalocyanine and 2,3-subnaphthalocyanine.

Just like SubPcs, SubNcs have been prepared by heating 2,3-dicyanonaphthalene with a boron templating agent (e.g. $PhBCl_2$, BBr_3, BCl_3) in an aromatic solvent. A

[80] a) M. Hanack, M. Lang, *Adv. Mater.* **1994**, *6*, 819; b) U. Drechsler, M. Hanack. In *Comprehensive Supramolecular Chemistry*; J. L. Atwood, J. E. D. Davies, D. D. Mac-Nicol, F. Vögtle, Eds.; Pergamon: Oxford, **1996**; Vol. 9, pp. 283; c) H. S. Nalwa, M. Hanack, G. Pawlowski, M. K. Engel, *Chem. Phys.* **1999**, *245*, 17; d) D. Dini, M. Barthel, M. Hanack, *Eur. J. Org. Chem.* **2001**, 3759; e) J. S. Shirk, R. G. S. Pong, S. R. Flom, H. Heckmann, M. Hanack, *J. Phys. Chem. A* **2000**, *104*, 1438; f) T. Schneider, H. Heckmann, M. Barthel, M. Hanack, *Eur. J. Org. Chem.* **2001**, 3055. g) M. S. Rodríguez-Morgade, T. Torres, Phthalocyanines and Related Compounds, *Science of Synthesis Knowledge Updates*, **2017**, *2*, pp.129-130.

relatively limited amount of work has been reported in the literature on the synthesis of SubNcs compared to SubPcs. The first report on the synthesis of a 2,3-SubNc was by Hanack and Rauschnabel in 1995 (Scheme 2.1, entry i), where they treated 2,3-dicyanonaphthalene and an alkylated 2,3-dicyanonaphthalene derivative with $PhBCl_2$ in boiling naphthalene to produce the respective SubNcs-(Ph), although only in analytical amounts.[46a,47a] In 1999, Kobayashi and co-workers reported the use of BBr_3 as the boron templating agent to synthesize an axially substituted bromo-SubNc in 34.6% yield (Scheme 2.1, entry ii).[29b] Hanack and co-workers reported hybrid structures prepared bycrossover cyclotrimerization reaction between 2,3-dicyanonaphthalene (A) and tetrafluorophthalonitrile (B), using BCl_3 as the boron template. This gave the two mixed A_2B and AB_2 cyclization products, in 20% yield, in addition to the symmetric A_3 and B_3 SubNPc and SubPc, respectively (Scheme 2.1, entry iii).[47b]

Later on (2000) Kennedy[47d] and our group[47c] reported a more effective methodology to prepare the more stable chloro-SubNc, in in 53% and 35%, respectively, using BCl_3 as the boron template and 2,3-dicyanonaphthalene as the precursor (Scheme 2.1, entry iv). In 2007, Giribabu and co-workers employed microwave irradiation to prepare a broad range of subphthalocyanine derivatives, in addition to *tert*-butylated SubNc-(Cl), which was obtained in 82% yield (Scheme 2.1, entry v).[81]

[81] L. Giribabu, C. V. Kumar, A. Surendar, V. G. Reddy, M. Chandrasekharam, P. Y. Reddy, *Synth. Commun*. **2007**, *37*, 4141–4147.

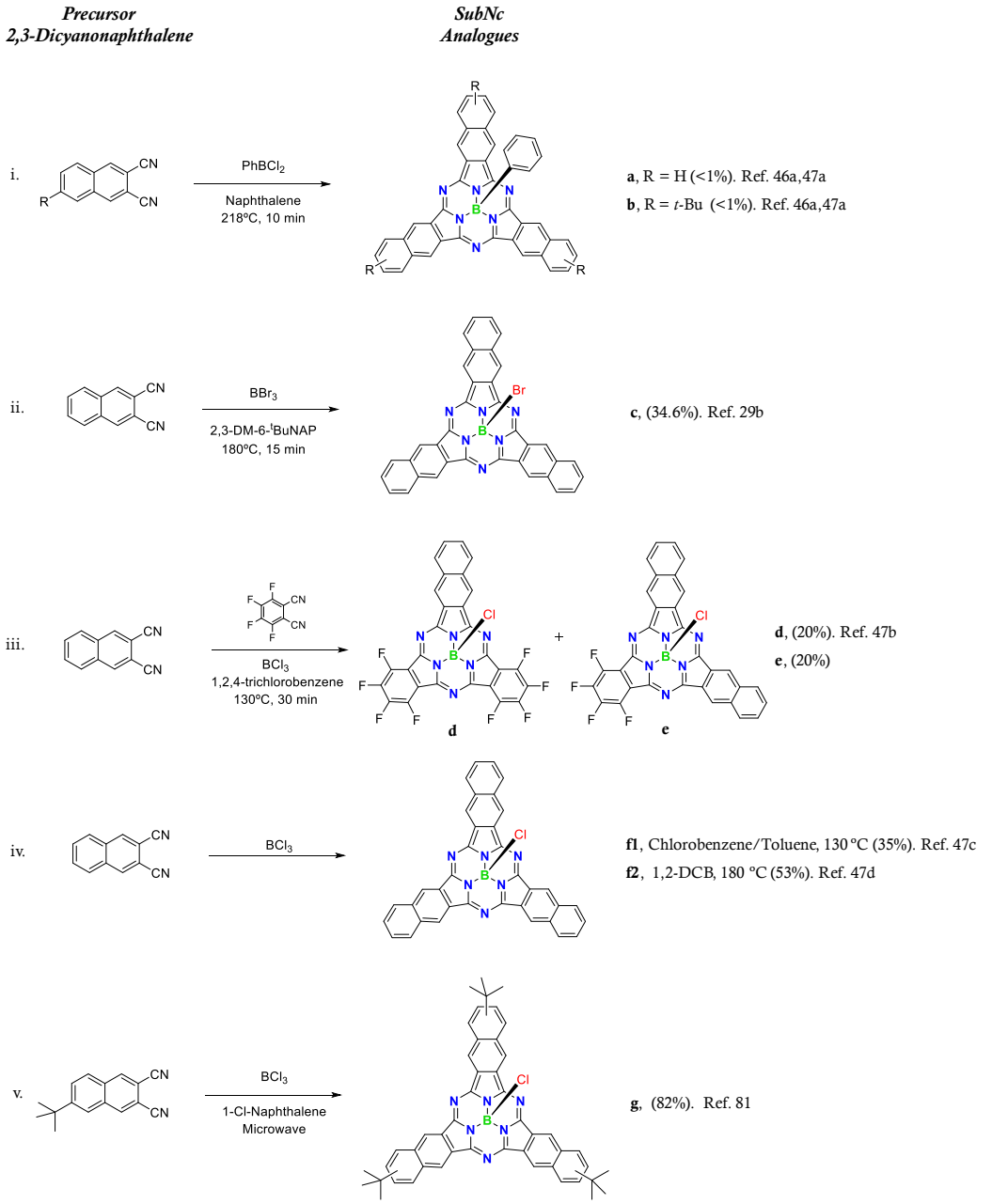

Scheme 2.1. Chronology of the first reported 2,3-SubNc syntheses through cyclotrimerization reactions.

More recently, Mizutani and co-workers reported the cyclotrimerization of fluorinated 2,3-naphthalenedicarbonitrile (Scheme 2.2, entry vi) by the slightly

modified Hanack's procedure[82], affording dodecafluorinated SubNc-(Cl) in a 44% yield,[47g] Following the same procedure, they have also prepared peripherally hexahalogenated SubNc-(Cl) derivatives, namely F_6-SubNc (26% yield),[47g] Cl_6-SubNc (22%),[83a] Br_6-SubNc (39%) [83b] and I_6-SubNc (73% yield), [83a] from their respective dihalogenated 2,3-dicyanonaphthalene derivatives, *via* multistep synthesis (Scheme 2.2, entry vii). The same authors treated the products with $AgBF_4$ in order to substitute the axial chloride with a fluoride, in a second stage. In addition, Mizutani and co-workers prepared peripherally chloroboron(III)- and fluoroboron(III)-hexaethynylsubnaphthalocyanine by Sonogashira coupling (Scheme 2.2, entry viii).

A comprehensive review of the above mentioned studies on the synthesis of 2,3-SubNc derivatives was carried out by Bender and co-workers in 2016. In this report the authors pointed to a generally poor characterization of these compounds is,[47h] and questioned the purity of all SubNcs-(Cl) derivatives synthesized by means of BCl_3 as the boron templating agent. In this respect, they provided a variety of experimental data supporting the idea that synthetic and commercially available samples of SubNc-(Cl) are actually a mixed alloyed chemical composition with random and significant amounts of chlorination at the bay positions of the SubNc-chromophore, that is, the middle benzene rings of the benzoisoindole subunits..

[82] a) G. Y. Yang, M. Hanack, Y. W. Lee, Y. Chen, M. –K. Y. Lee, D. Dini, *Chem. Eur. J.* **2003**, *9*, 2758–2762; b) G. Y. Yang, M. Hanack, Y. W. Lee, D. Dini, J. F. Pan, *Adv. Mater.* **2005**, *17*, 875–879.

[83] a) K. Yamamoto, A. Takagi, M. Hada, R. Taniwaki, T. Mizutani, Y. Kimura, Y. Takao, K. Moriwaki, F. Matsumoto, T. Ito, T. Iwai, K. Hida, T. Mizuno, T. Ohno, *Tetrahedron*, **2016**, *72*, 4918–4924; b) K. Shirai, A. Takagi, R. Taniwaki, M. Kurata, K. Kinugasa, K. Yamamoto, T. Mizutani, Y. Takao, K. Moriwaki, T. Ito, T. Iwai, F. Matsumoto, T. Ohno, *Tetrahedron*, **2018**, *74*, 4220–4225.

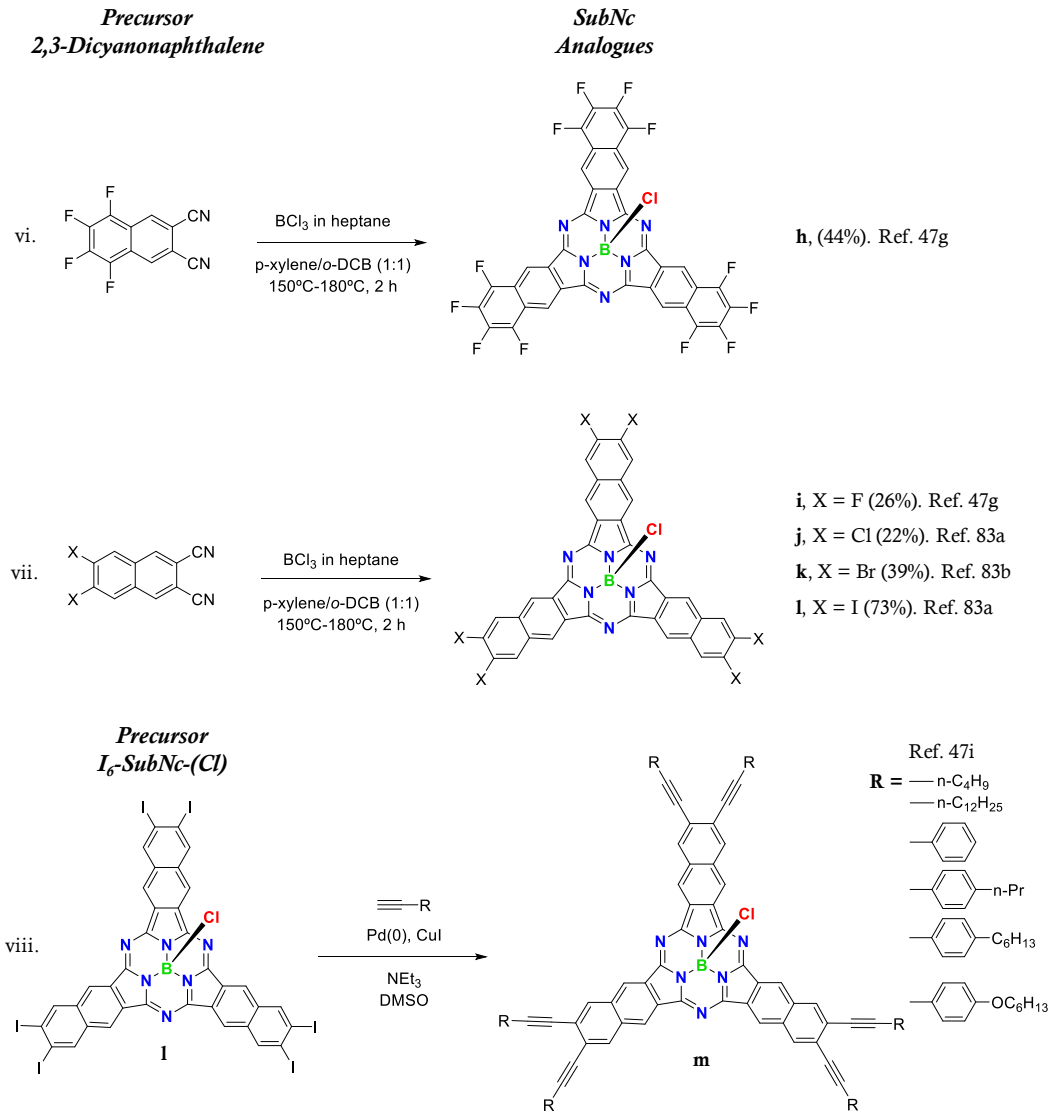

Scheme 2.2. Syntheses of peripherally halogenated SubNc derivatives and its functionalization.

Bender developed an alternative chemical process whereby samples with lower and higher amounts of chlorination at the bay position were obtained (Cl_n-SubNc-(Cl)). The positions and frequencies of the peripheral chlorine atoms were determined *via* single crystal X-ray crystallography of two different mixed alloyed compositions of Cl_n-SubNc-(Cl) samples, as well as XPS analysis of all Cl_n-SubNc-(Cl) samples (Figure 2.2).[47h]

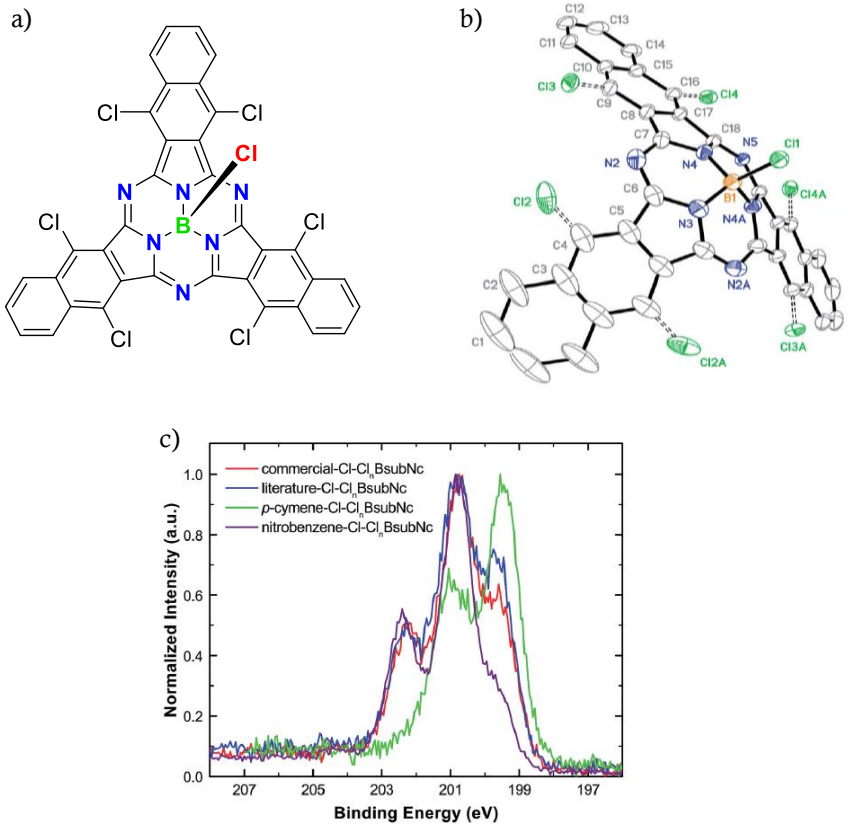

Figure 2.2. Mixed alloyed chemical composition of Cl_n-SubNc-(Cl): (a) Chemical structure of Cl_6-SubNc-(Cl) isolated; (b) ellipsoid plot (50% probability) showing the structure and atom numbering scheme of Cl_6-SubNc-(Cl) crystals; (c) overlay of the literature (blue), commercial (red), p-cymene (green), and nitrobenzene (purple) Cl_n-SubNc-(Cl) normalized Cl 2p core-level XPS spectra.[47h]

SubNc-(Cl) derivatives have become increasingly interesting as a photo- and electro-active materials in organic photovoltaics (OPVs), in part due to their red absorption with high molar extinction coefficients, Its inclusion in a planar heterojunction (PHJ) OPV cell resulted in a power conversion efficiency (PCE) of 8.4%, one of the highest values within PHJ OPVs.[56e] No other kind of SubNc derivatives have been explored for this application.

2.2 Specific Objectives

The aim of this chapter is the synthesis of peripherally dodecafunctionalized subnaphthalocyanine derivatives through cyclotrimerization reactions, in order to obtain a new series of chromophores with electron-withdrawing/-donating groups or π-conjugated moieties around the SubNc core. With this, we intended to alter the energies of the HOMO-LUMO orbitals and hence, the Q-band absorption/emission maxima, as well as the redox potentials (Scheme 2.3). Therefore, a part of the present chapter is devoted to develop a general strategy for preparing tetrasubstituted 2,3-naphthalenedicarbonitrile precursors, bearing functional groups of different nature, such as halogens, thioethers, sulfones, and aryl rings. All of these dinitriles were expected to provide different peripheral functionalization of the SubNcs.

Specific objectives for this chapter are the following:

- Preparation of tetrahalogenated 2,3-naphthalenedicarbonitrile precursors, i.e. tetrachloro-, tetrafluoro- and tetrabromo- compounds that could be used in cyclotrimerization reactions, as well as in substitution reactions to afford tetrasulfanylated, tetrasulfonylated, and tetraarylated naphthalenedicarbonitrile derivatives.
- Synthesis and characterization of dodecahalogenated SubNcs and functionalization of their axial positions with phenoxy group derivatives.
- Synthesis and characterization of dodecapentyl- sulfanylated and sulfonylated SubNcs and examination of their electronic –i.e. donor or acceptor – nature.
- Synthesis and characterization of π-extended dodecaarylated SubNcs and examination of their use as precursors of 3D-curved graphenic structures.

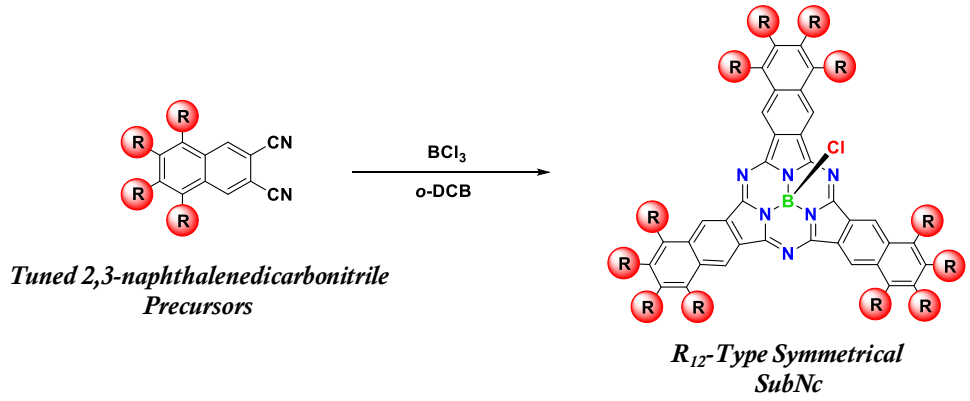

Scheme 2.3. General schematic representation of the synthesis of dodecafunctionalized SubNcs.

2.3 Results and Discussion

2.3.1 Synthesis of tetrasubstituted 2,3-naphthalenedicarbonitrile precursors

Synthetic procedures to prepare 2,3-naphthalenedicarbonitrile derivatives have not been developed enough, as in the case of the wide variety of procedures to obtain phthalonitrile derivatives, the well-known SubPc precursors. In this respect, 2,3-naphthalenedicarbonitriles and their derivatives are essential as starting materials of SubNcs.

The synthesis of tetrahalogenated precursors **21**, **22**, and **23** was carried out following the route described in Scheme 2.5 (see below). For this purpose, compounds **24a-c** were prepared, following reported procedures. Hence, tetrafluorinated derivative **24a** was obtained by reduction of commercially available tetrafluorodiethyl phthalate with $LiAlH_4$, to yield the 1,2-dihydroxymethylbenzene derivative **26**; the latter was treated with concentrated hydrobromic acid at reflux temperature, affording **24a** in 78% yield (Scheme 2.4a).[84]

Derivatives **24b** and **24c** were obtained in good yields by tetrachlorination and tetrabromination, of *o*-xylene using aluminum chloride and iron, respectively, as described in the methods developed by Kreher and Herd.[85] Perchlorination process was carried out with sulfuryl chloride as chlorine source, in the presence of disulfur dichloride and, on the other hand, elemental bromine was used in the perbromination reaction, affording **27** and **28**, respectively. In a second step, benzylic brominations were carried out with NBS in the presence of AIBN and light, in CCl_4 solutions, affording **24b** and **24c** (Scheme 2.4b,c).

[84] a) C. R. Swartz, S. R. Parkin, J. E. Bullock, J. E. Anthony, A. C. Mayer, G. G. Malliaras, *Org. Lett.* **2005**, *7*, 3163–3166; b) Z. Liang, Q. Tang, J. Liu, J. Li, F. Yan, Q. Miao, *Chem. Mater.* **2010**, *22*, 6438-6443.
[85] R. P. Kreher, K. J. Herd, *Chem. Ber.* **1988**, *121*, 1827–1832.

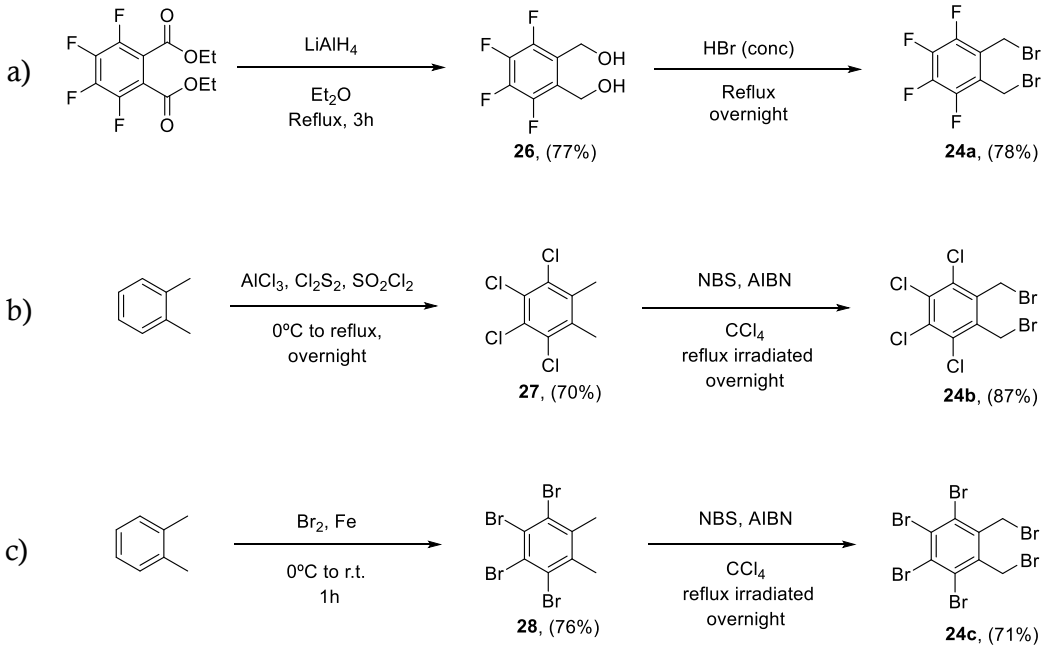

Scheme 2.4. Synthesis of 1,2-bis(bromomethyl)-3,4,5,6-tetrahalobenzene derivatives **24a**,**b**,**c**.

Next, tetrahalogenated 1,2-bis(bromomethyl)benzene derivatives **24a**,**b**,**c** were treated with fumaronitrile in the presence of sodium iodide in anhydrous DMF. In this process, treatment with NaI eliminates bromine to give an intermediate diene that is intercepted by fumaronitrile *via* Diels-Alder cycloaddition reaction, affording tetrahalogenated 2,3-tetrahydronaphthalenedicarbonitrile **25a**-**c** in good yields.[86] Aromatization reaction was carried out in a second step by treatment of **25a**-**c** with bromine and pyridine in *o*-DCB at 150ºC, leading to 2,3-naphthalenedicarbonitrle derivatives **21**-**23** in moderate yields.

[86] a) D. Dini, M. J. F. Calvete, M. Hanack, R. G. S. Pong, S. R. Flom, J. S. Shirk, *J. Phys. Chem. B* **2006**, *110*, 12230–12239. b) S. Kotha, S. Misra, V. Srinivas, *Eur. J. Org. Chem.* **2012**, 4052–4062.

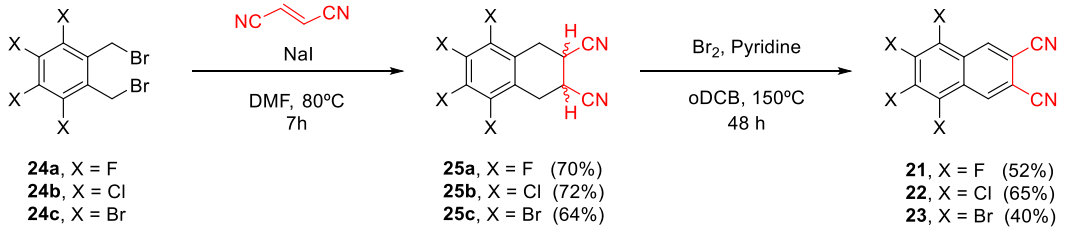

Scheme 2.5. Synthetic route of 5,6,7,8-tetrahalonaphthalene-2,3-dicarbonitrile derivatives **21**, **22**, and **23** in two steps (cycloaddition and aromatization reactions).

The synthesis of tetraalkylsulfanyl 2,3-naphthalenedicarbonitrile precursor **29** was performed in good yields (80%), by nucleophilic aromatic substitution reaction of tetrachlorinated compound **22** with 1-pentanethiol in the presence of trimethylamine, in anhydrous DMF (Scheme 2.6).[87]

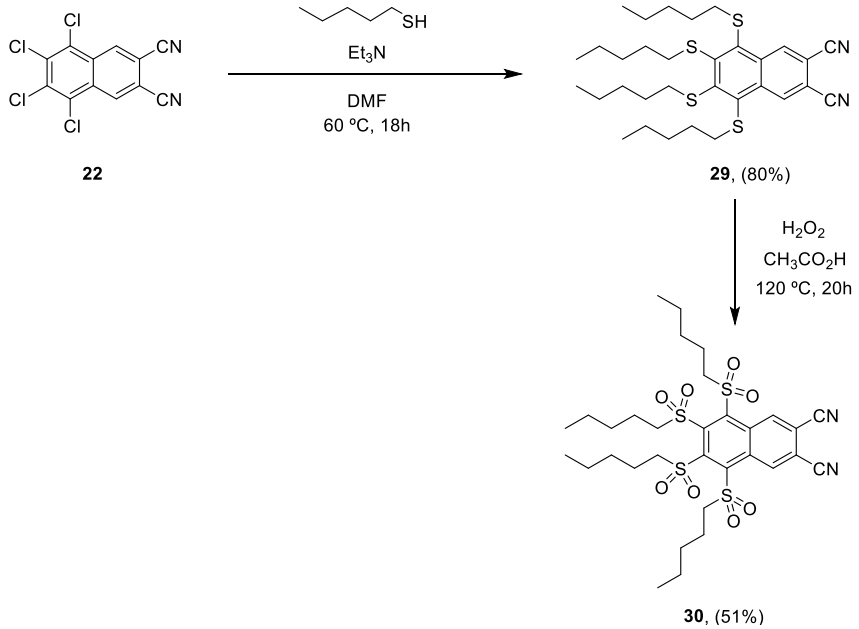

Scheme 2.6. Synthesis of tetrasulfanylated (**29**) and tetrasulfonylated (**30**) 2,3-naphthalenedicarbonitrile precursors.

[87] a) K. A. Volkov, G. V. Avramenko, V. M. Negrimovskii, E. A. Luk'yanets, *Russ. J. Gen. Chem.* **2007**, *77*, 1108–1116. b) E. M. Maya, C. García, E. M. García-Frutos, P. Vázquez, T Torres, *J. Org. Chem.* **2000,** *65,* 2733–2739; c) Y. Zhang, P. Ma, P. Zhu, X. Zhang, Y. Gao, D. Qi, Y. Bian, N. Kobayashi, J. Jiang, *J. Mater. Chem.* **2011**, *21*, 6515–6524.

The oxidation reaction of tetrasulfanylated **29** by treatment with excess hydrogen peroxide in refluxing acetic acid, gave the corresponding tetrasulfonylated derivative **30** in 51% yield (Scheme 2.6). This harsh oxidation condition ensures complete transformation of all *n*-pentylsulfanyl units into the *n*-pentylsulfone groups.

Tetrabromo 2,3-naphthalenedicarbonitrile **23** was used as the precursor for the synthesis of tetraarylated 2,3-naphthalenedicarbonitrile derivatives, through Suzuki-Miyaura cross-coupling reactions over the four bromo-substituents. Thus, tetrabromo derivative **23** was treated with phenylboronic- or 4-*tert*-butylphenylboronic acid, in the presence of a deaerated solution of $[Pd(PPh_3)_4]$ and Na_2CO_3, in a THF/Toluene/Water mixture, under argon, affording tetraarylated derivatives **31a**,**b** in good yields (Scheme 2.7).

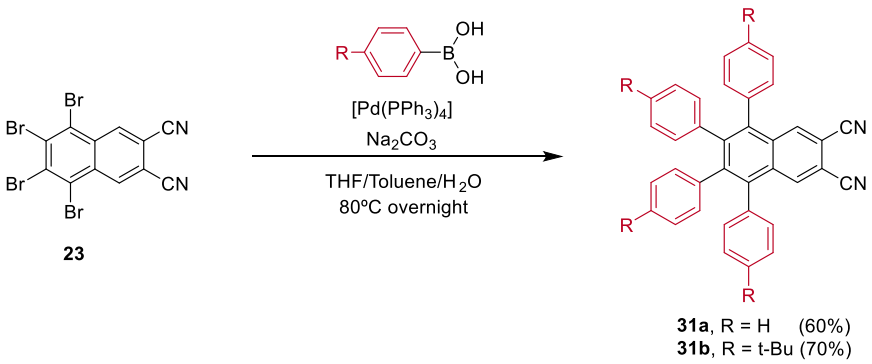

Scheme 2.7. Synthesis of tetraarylated 2,3-naphthalenedicarbonitrles **31a** and **31b**.

Compound **31b** was used as precursor of the naphthopentaphene derivative **32**, which was obtained in 64% yield, by oxidative cyclodehydrogenation reaction, using 2,3-dichloro-5,6-dicyano-*p*-benzoquinone (DQQ) as oxidizing agent, in dichlomethane, in the presence of trifluoromethanesulfonic acid (TfOH) (Scheme 2.8).[88]

[88] U. Hahn, E. Maisonhaute, J-F. Nierengarten, *Angew. Chem. Int. Ed.* **2018**, *57*, 10635–10639.

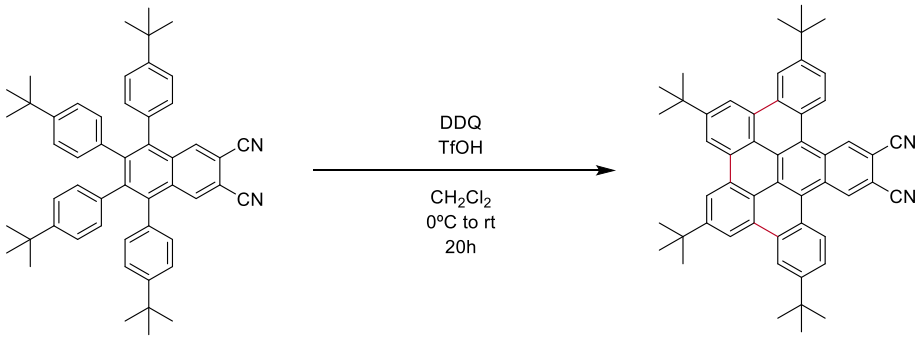

31b **32**, (64%)

Scheme 2.8. Synthesis of fused-ring 2,3-dicarbonitrile precursor **32**.

Single crystals of precursor **32** were obtained by slow diffusion of MeOH into a concentrated chloroform solution for three days. The X-ray diffraction analysis shows a π-extended, distorted non-planar conformation for the dinitrile **32** (Figure 2.3b).

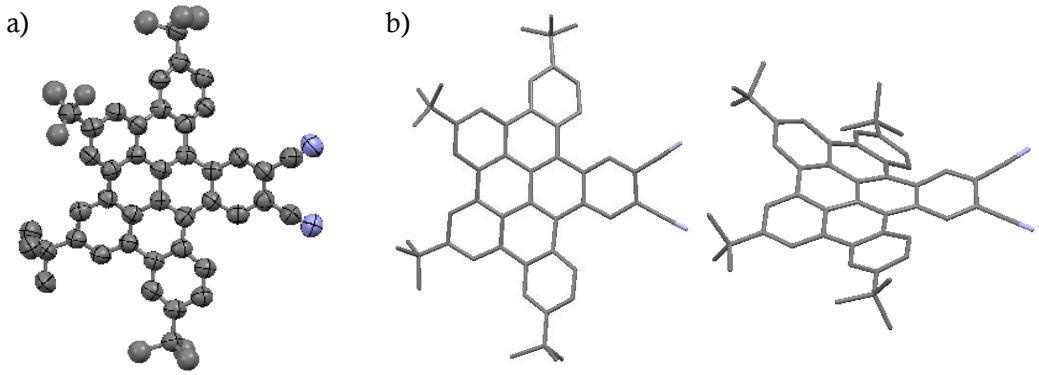

Figure 2.3. Molecular structure of **32**: (a) Thermal ellipsoids are scaled at 50% probability level, (b) structure displayed in stick (top and side view). Hydrogen atoms are omitted for clarity.

2.3.2 Synthesis of dodecafunctionalized subnaphthalocyanines

Chloro-substituted SubNcs bearing twelve halogen atoms at their periphery were synthesized by cyclotrimerization reaction of precursors **21**, **22** and **23**, using the general procedure consisting of treatment with boron trichloride (1 M in *p*-xylene) at reflux, for two hours (Scheme 2.9). Unlike the usual protocol for the synthesis of SubPzs and SubPcs, in this procedure the tetrahalogenated precursors should be dissolved in freshly distilled *o*-DCB, before treatment with BCl_3, to avoid the possible chlorination process at the bay position.

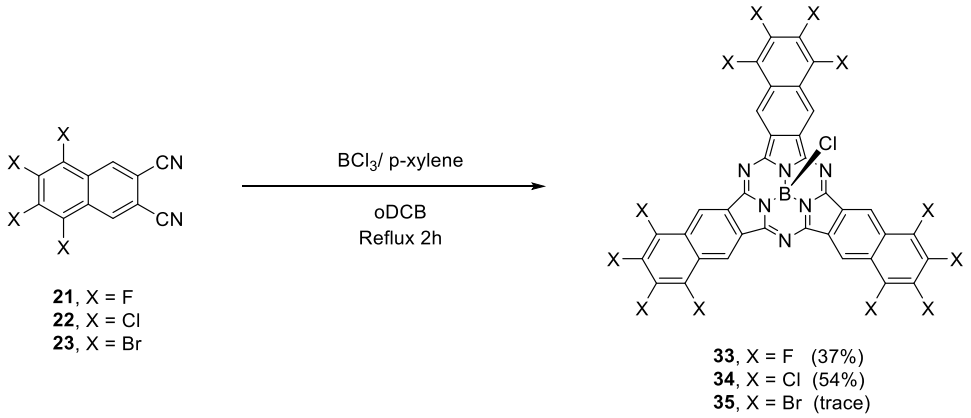

Scheme 2.9. General procedure for the synthesis of X_{12}-SubNc-(Cl) derivatives.

Dodecafluorinated and dodecachlorinated SubNcs **33** and **34** were obtained as dark blue solids (Figure 2.4a) in 37% and 54% respectively. However, only traces of dodecabrominated SubNc **35** were obtained, despite the several attempts of reactions at different temperatures. Purification of F_{12}-SubNc **33** by column chromatography (Figure 2.4b) and its characterization was straightforward, due to its excellent solubility and low tendency to aggregate in a wide variety of organic solvents. Contrasting, Cl_{12}-SubNc **34** and Br_{12}-SubNc **35** showed poor solubility in common organic solvents, this precluding purification by chromatographic techniques and difficulting the characterization for both compounds.

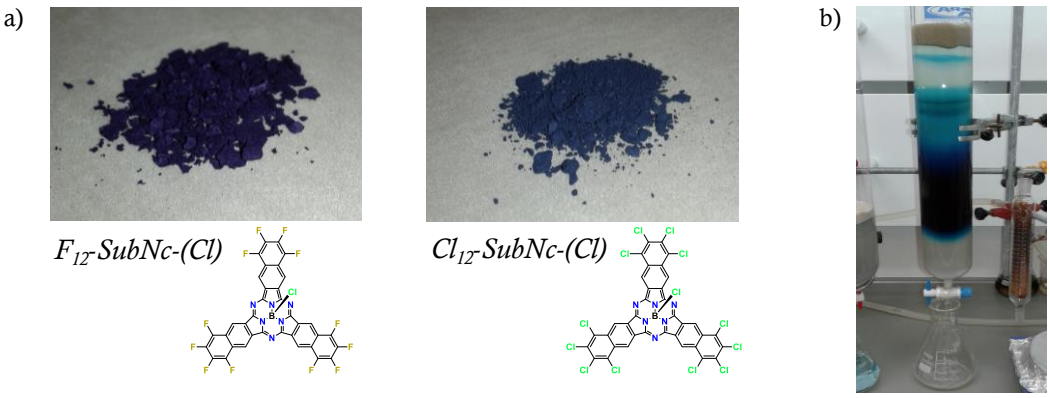

Figure 2.4. (a) Dark blue solids of SubNc **33** and **34** after their isolation. (b) Purification by chromatographic column on silica gel ($CHCl_3$/n-hexane 9:1) of SubNc **33**. The first descent dark blue fraction corresponds to **33**.

High-resolution MALDI-TOF mass spectrometry for SubNc **33** showed the molecular ion peak, detected at m/z = 795.0921 (calc. 795.0275) (Figure 2.5a), and MALDI-TOF mass spectrometry showed the isotopic distribution of molecular ion for SubNc **34** and **35**, at m/z = 987-1004 and 1517-1536, respectively (Figure 2.5b,c).

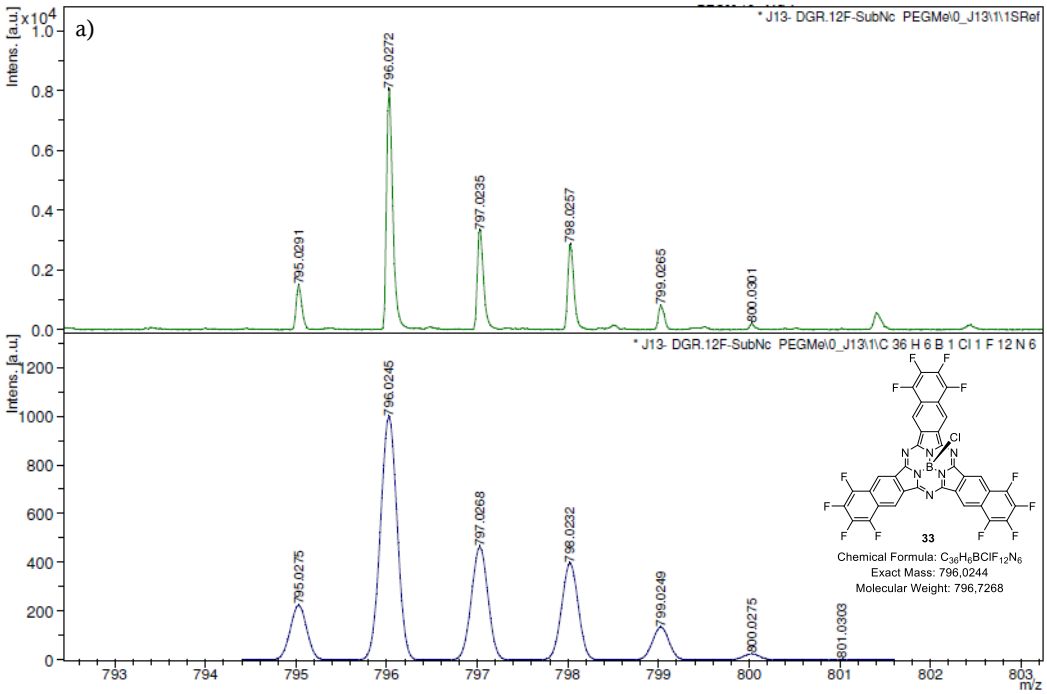

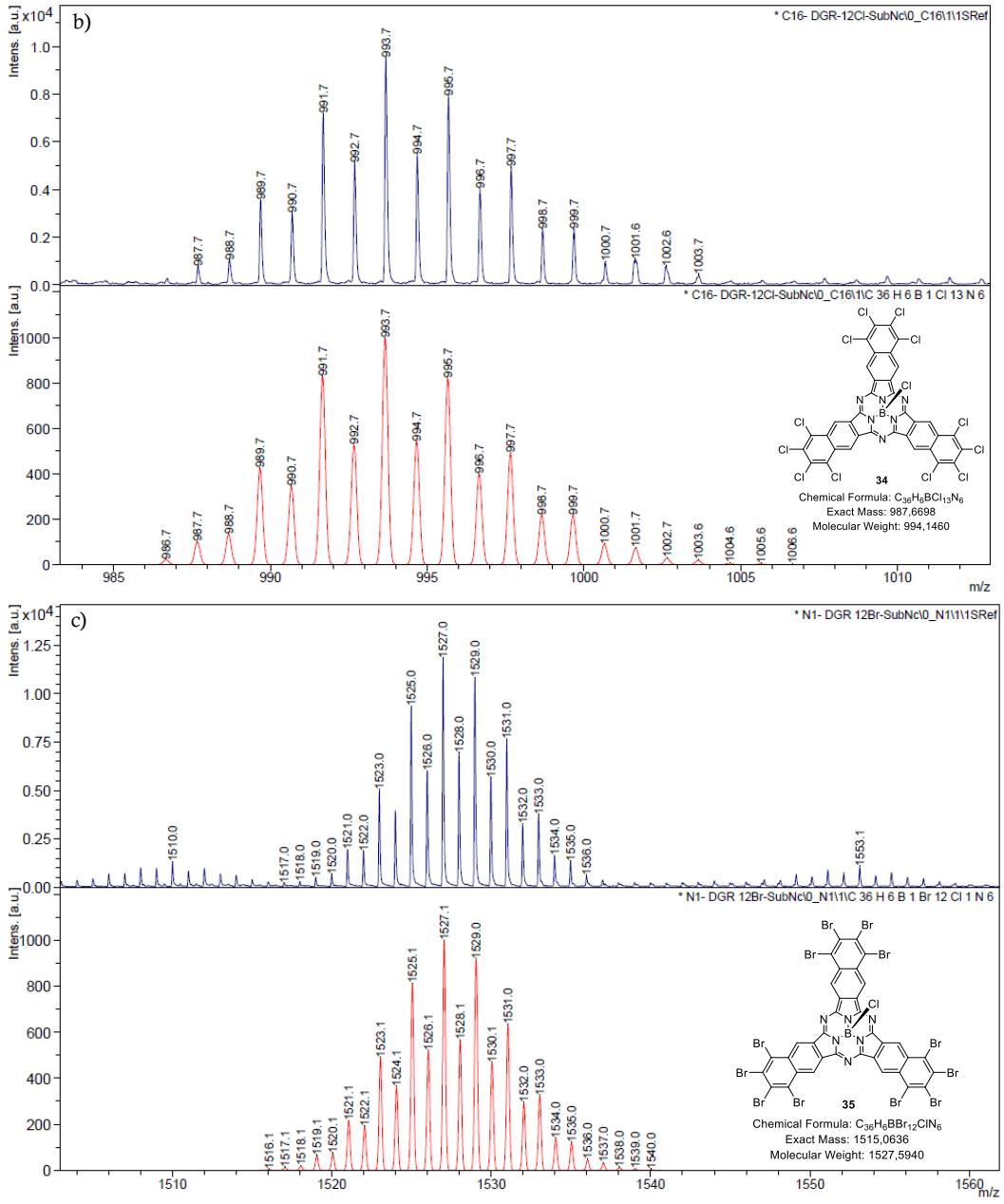

Figure 2.5. Isotopic distribution of the molecular ion peak in positive mode: (a) HRMS-MALDI-TOF of F_{12}-SubNc **33**, (b) and (c) MALDI-TOF of Cl_{12}-SubNc **34** and Br_{12}-SubNc **35**. Upper part-experimental, and lower part-predicted isotopic pattern.

A single crystal of F_{12}-SubNc **33**, suitable for X-ray diffraction analysis, was obtained by vapour diffusion of methanol into a solution of **33** in chloroform. The crystal structure revealed the cone –shape structure characteristic of the subporphyrinoid family,[16c] as well as its tendency to assemble with a columnar stacking organization (Figure 2.6).[89]

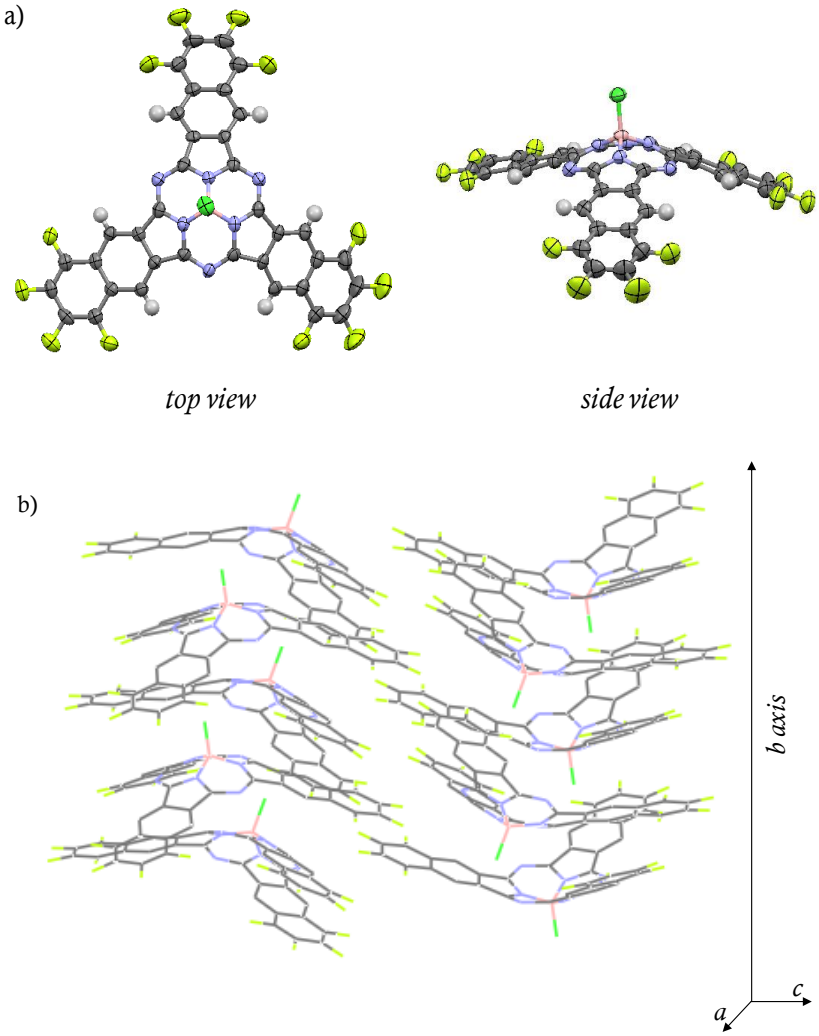

Figure 2.6. X-ray crystal structure of F_{12}-SubNc-(Cl) **33**: (a) Molecular structure showing thermal ellipsoids at the 50% probability level. (b) Columns packing along the *b* axis.

[89] CCDC number 1583669 for **33**.

The bulky *tert*-butylphenoxy group placed on the axial position excludes the formation of aggregates due to π-π interactions, thus providing better solubility in many organic solvents and better resolved ^{1}H-NMR and optical spectra than in the case of axially chloro-substituted SubNcs. Nevertheless, the axial substitution of the SubNc chloride ligand on **33** and **34** by *tert*-butylphenoxy through refluxing in toluene gave low reaction yields, remaining starting material in both cases. This result means that the B–Cl bond becomes stronger in the SubNc structure than the same bond in the SubPz and SubPc structures. Therefore, an alternative synthetic route was carried out to achieve the axial substitution (Scheme 2.10). The key-point of this method is the generation of an axial triflate-SubNc by axial chlorine exchange of SubNc **33** and **34** upon treatment with silver triflate and DIPEA, according to a well-established methodology developed in our research group.[24d] The *in-situ* formed intermediate readily enables the axial substitution reaction with *tert*-butylphenol or pentafluorophenol, in one-pot, two-step reaction.

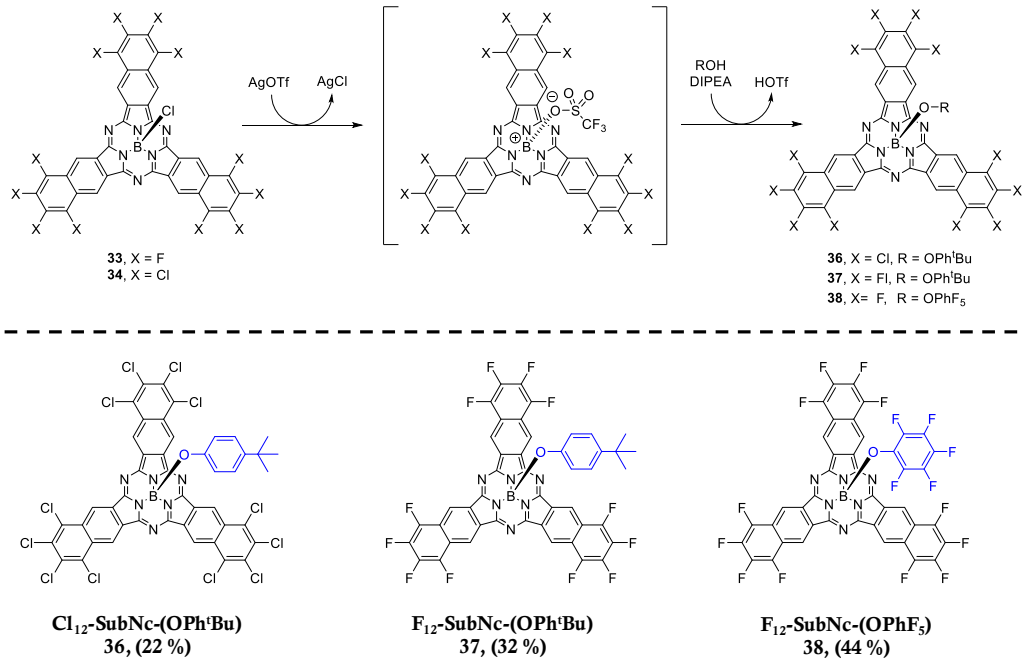

Scheme 2.10. General procedure for the axial substitution on SubNcs and synthesis of axially phenoxy-SubNc derivatives **36**, **37** and **38**.

Axial phenoxy-SubNc derivatives **36**, **37** and **38** were obtained in moderate yields by treatment of **33** and **34** with silver triflate overnight at 60ºC in freshly distilled toluene, followed by addition of the phenol derivative and DIPEA (Scheme2.10). ^{1}H-NMR spectra of SubNcs **36**, **37** and **38** in $CDCl_3$ show similar patterns: the signals corresponding to aromatic protons of the bay position appear at 9.80, 9.58 and 9.65 ppm respectively, while the *tert*-butylphenoxy group shows its signals with the usual chemical shift at $\delta \approx 6.8$ and 5.5 ppm (Figure 2.7).

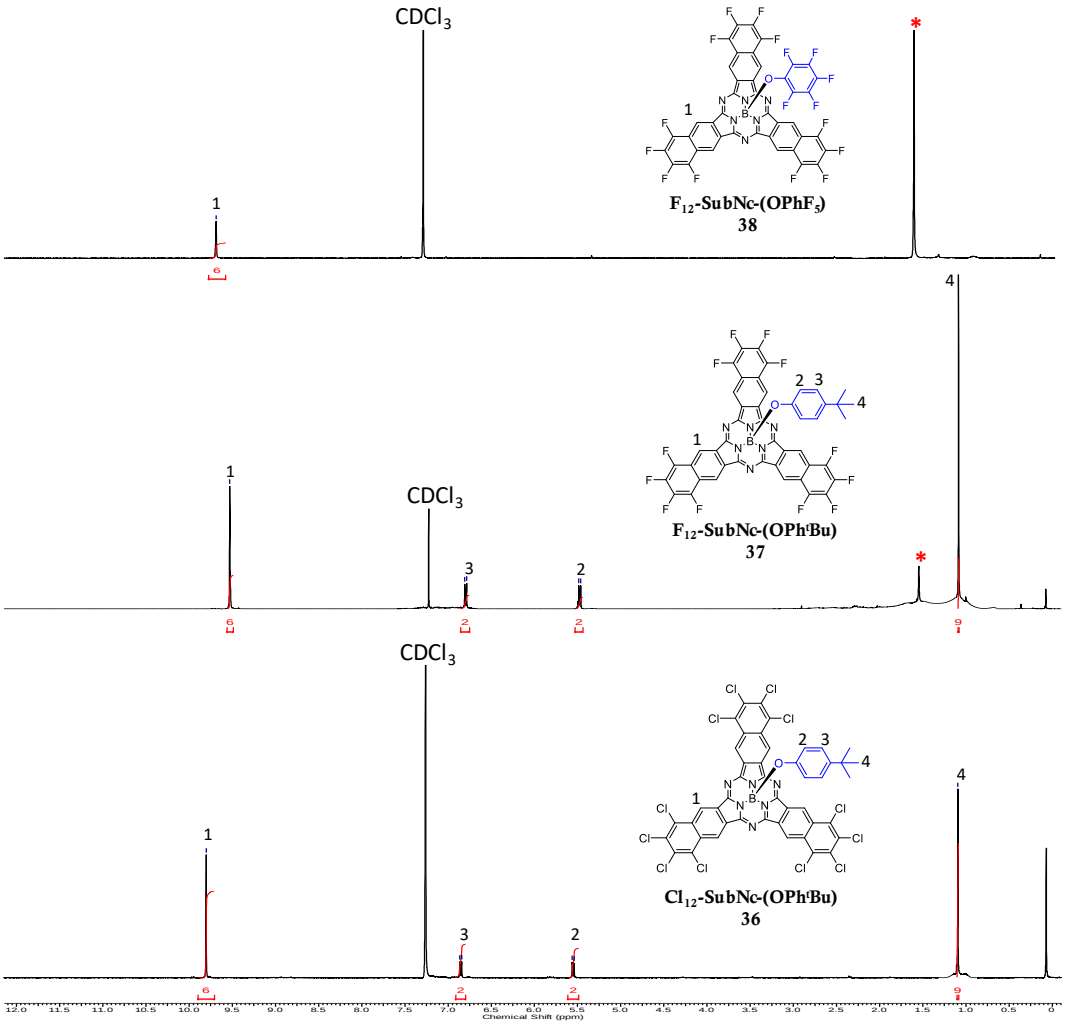

Figure 2.7. ^{1}H-NMR spectra in $CDCl_3$ at 25 °C of SubNcs **36**, **37** and **38**. Signals marked with * are due to residual solvents.

Axial chloro-dodecapentylsulfanylated and –and dodecapentylsulfonylated SubNcs **39** and **40** were prepared in moderate yields by cyclotrimerization reactions of the precursors **29** and **30**, respectively (Scheme 2.11). Initially, the synthesis of **39** was carried out employing the reaction conditions established in the general procedure (Scheme 2.9), but this afforded low yield (< 5%). Due to the low stability of **39** at high temperatures, different of reaction time and temperature conditions were tested. The best yield (25%) was encountered by the treatment of **29** with BCl_3 at 120ºC for 20 minutes. In contrast, **40** was prepared in 45% yield by the usual protocol.

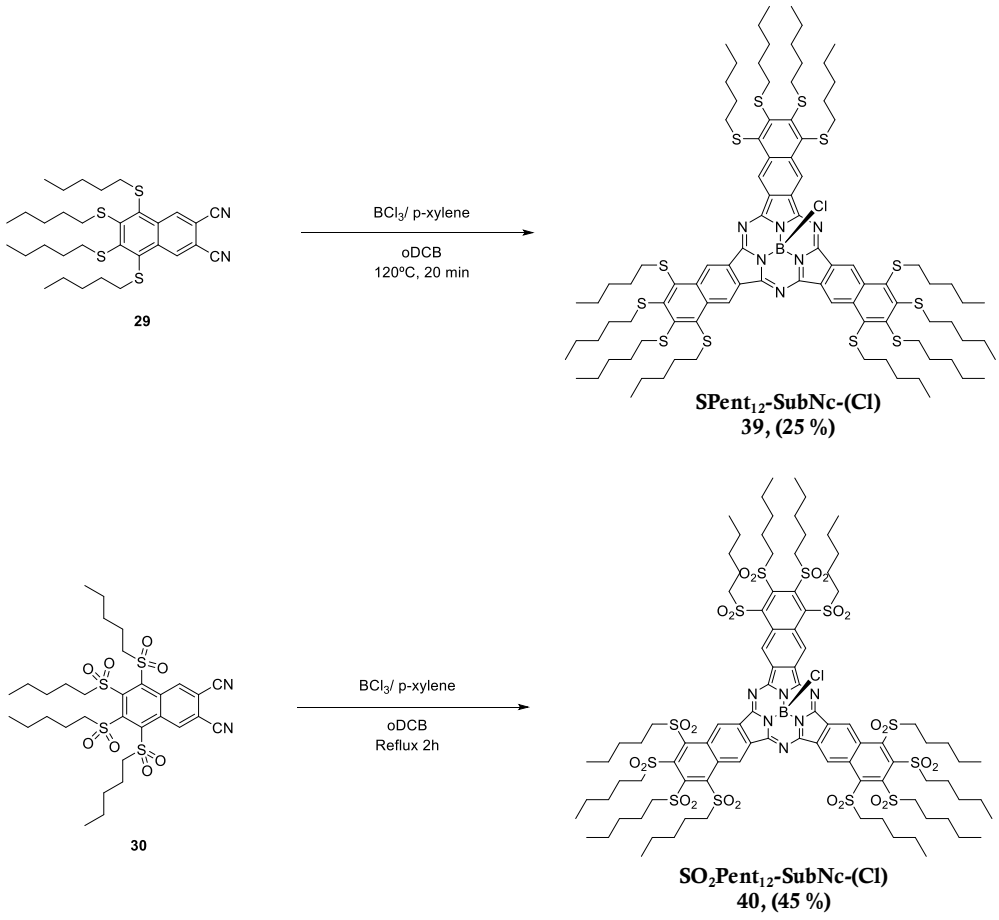

Scheme 2.11. Synthesis of axially chloro-dodecapentyl-sulfanylated **39** and –sulfonylated **40** SubNcs.

The twelve alkyl chains at the periphery, provide high solubility in a wide variety of organic solvents for both SubNcs **39** and **40**. Both compounds were found to be

unstable on silica gel or neutral alumina during the purification by column chromatography. Hence, the purification was carried out by size-exclusion chromatography using Bio-Beads™ S-X1 and toluene as eluent. SubNcs **39** and **40** were characterized by ^{1}H-NMR, ^{13}C-NMR spectroscopies and UV-Vis spectrophotometry as well as mass spectrometry.

Figure 2.8 shows the ^{1}H-NMR spectra of **39** and **40**. All the signals corresponding to **40** appear more downfield shifted than those of **39**, due to the presence and proximity of -SO_2- groups. Also, aromatic protons of the bay position split into two singlets at 10.79 and 10.89 ppm for **40**, contrasting with the singlet at 10.38 ppm for **39**.

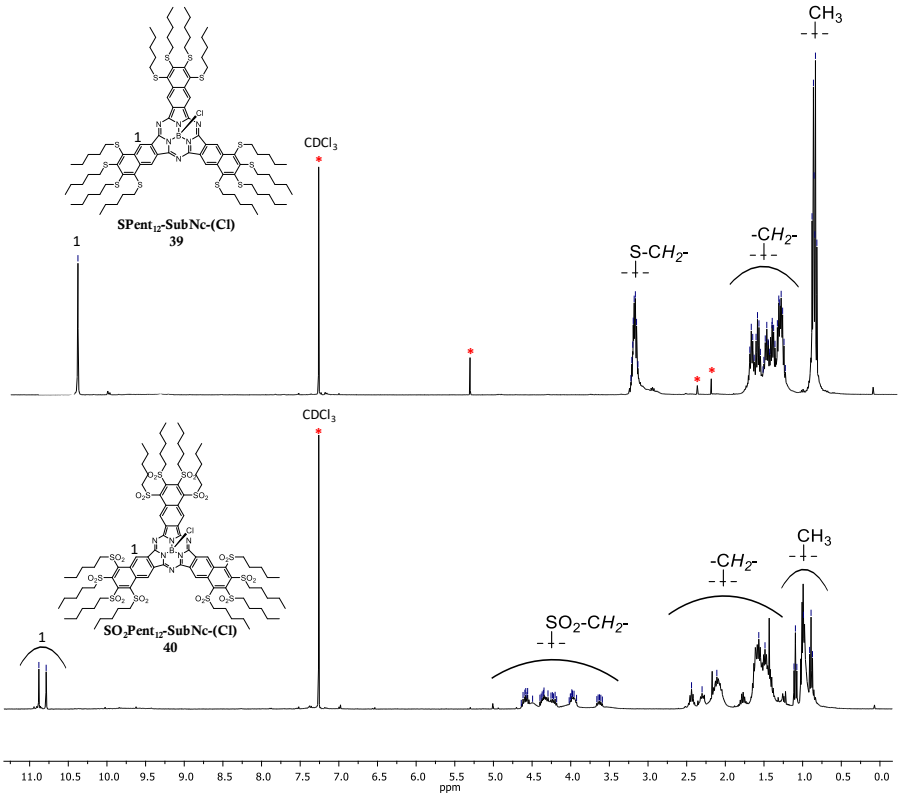

Figure 2.8. ^{1}H-NMR spectra in $CDCl_3$ at 25 °C of SubNcs **39** and **40**. Signals marked with * are due to residual solvents.

MALDI-TOF mass spectrometry showed the isotopic distribution of molecular ion for SubNcs **39** and **40**, at m/z = 1804-1814 and 2188-2198 respectively (Figure 2.9).

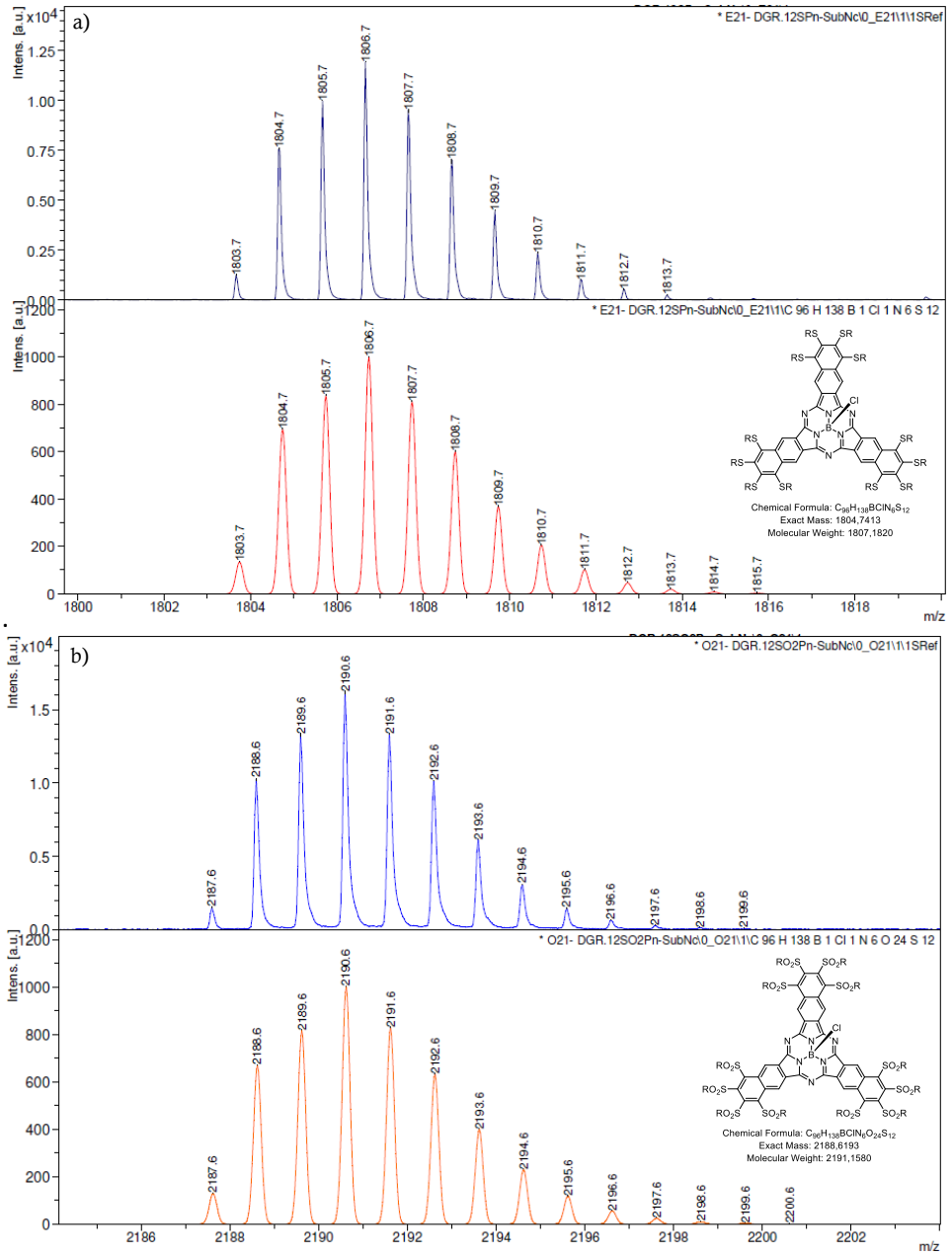

Figure 2.9. Isotopic distribution of the molecular ion peak in positive mode by MALDI-TOF of: (a) $SPent_{12}$-SubNc-(Cl) **39** and (b) SO_2Pent_{12}-SubNc-(Cl) **40**. Upper part-experimental, and lower part-predicted isotopic pattern.

The preparation of chloro-SubNcs **41a** and **41b** bearing twelve phenyl or *p-tert*-butylphenyl groups at their periphery, respectively, was attempted by direct cyclotrimerization of precursors **31a** and **31b** (Scheme 2.12). The efforts to isolate **41a**

were in vain due to the instability of this perphenylated SubNc, which restrained its purification and characterization. On the other hand, dodecaarylated SubNc **41b** was obtained in 8% yield, by doing the cyclotrimerization at 150ºC for 20 minutes. In this case, the *tert*-butyl groups that decorate the SubNc periphery must confer stability, besides high solubility in organic solvents, and help to reduce the self-aggregation tendency of this kind of compounds.

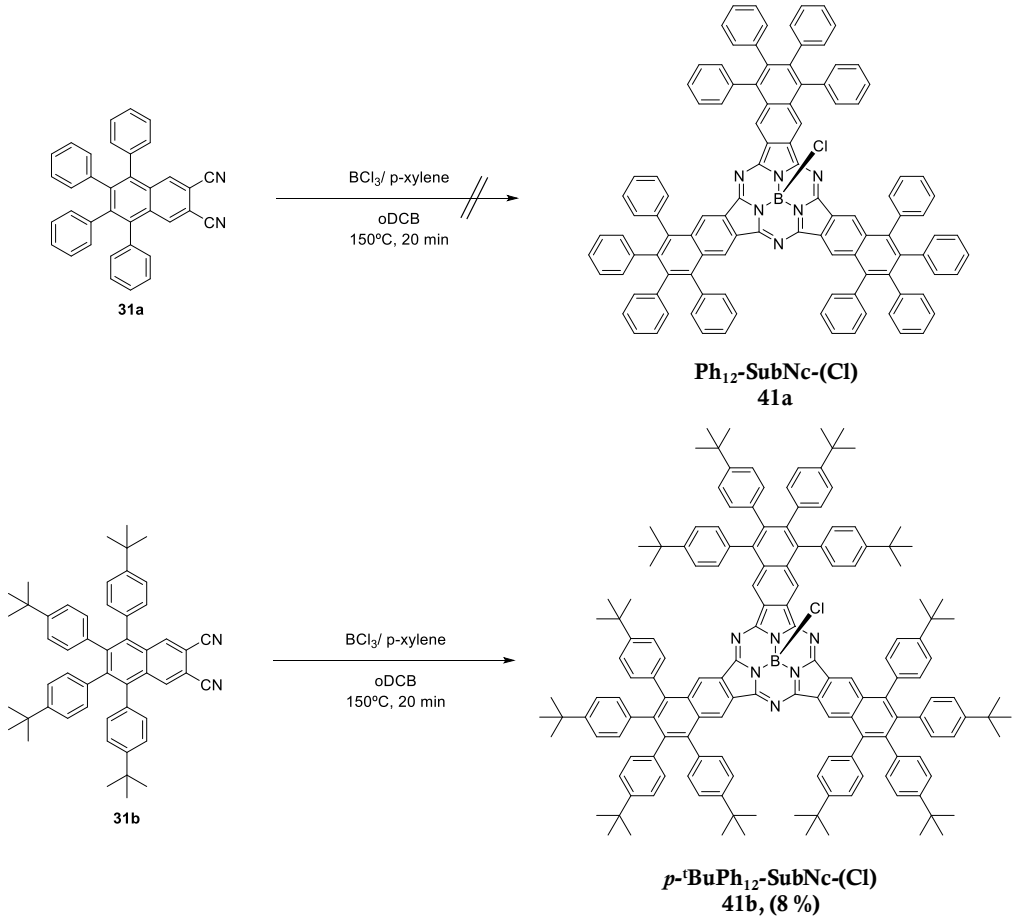

Scheme 2.12. Attempted synthesis of dodecaphenylated-SubNc **41a** and synthesis of dodecaarylated-SubNc **41b** by general procedure of cyclotrimerization.

As in the case of SubNcs **39** and **40**, perarylated SubNc **41b** was purified by size-exclusion chromatography using Bio-Beads^{TM} S-X1, and chloroform as the eluent, due to its low stability on contact with silica gel. ^{1}H-NMR spectrum of **31b** shows the presence of two AA'BB' systems corresponding to the *tert*-butylphenyl moieties, in addition to a singlet at 8.25 nm assigned to the benzene ring. (Figure 2.10). For **41b**,

the signals corresponding to the aromatic protons of the twelve *p-tert*-butylphenyl groups appear as a group of multiplets between 6.54 and 7.40 ppm. A group of signals between 9.3 and 9.6 ppm corresponds to the protons of the bay position. The manifold spliting of the aromatic resonances for **41b** suggests restriction of the rotation of peripheral aryl groups owing to steric constraints. This restriction produces non-equivalent aryl protons due to the macrocycle conical shape.

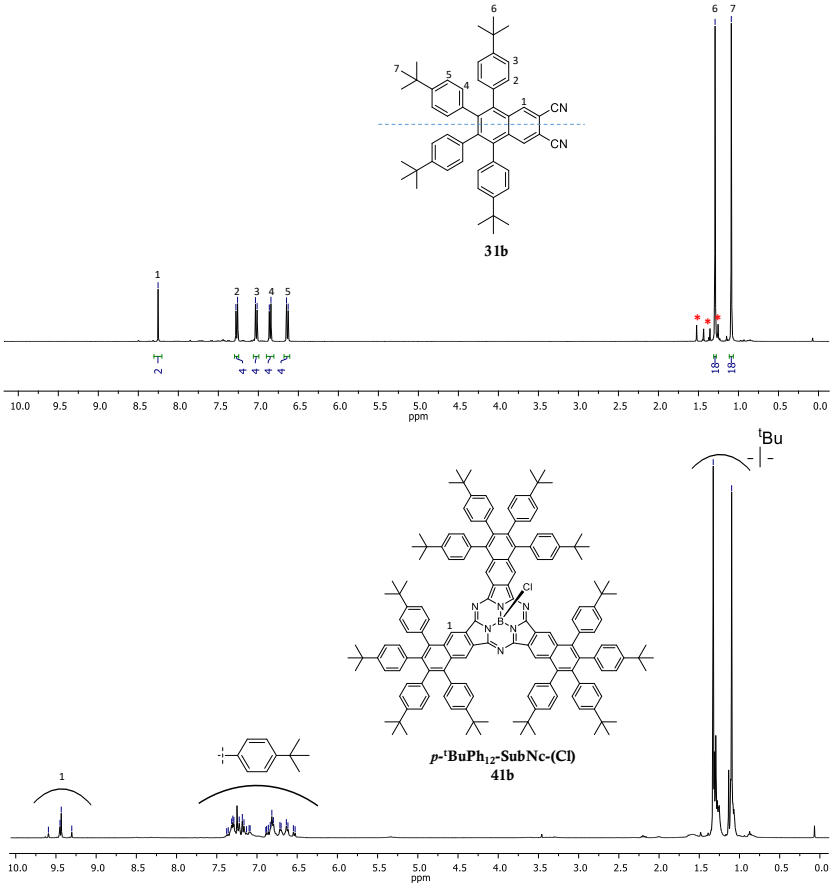

Figure 2.10. ^{1}H-NMR spectra in $CDCl_3$ at 25 ºC of precursor **31b** and SubNc **41b**. Signals marked with * are due to residual solvents.

MALDI-TOF mass spectrometry of **41b** showed a peak at *m/z* = 2160-2171 corresponding to a mixture of three ions, namely, $[M]^+$, $[M\text{-}2H]^+$, and $[M\text{-}4H]^+$, the last two arising from oxidative cyclodehydrogenation of **41b**. (Figure 2.11).

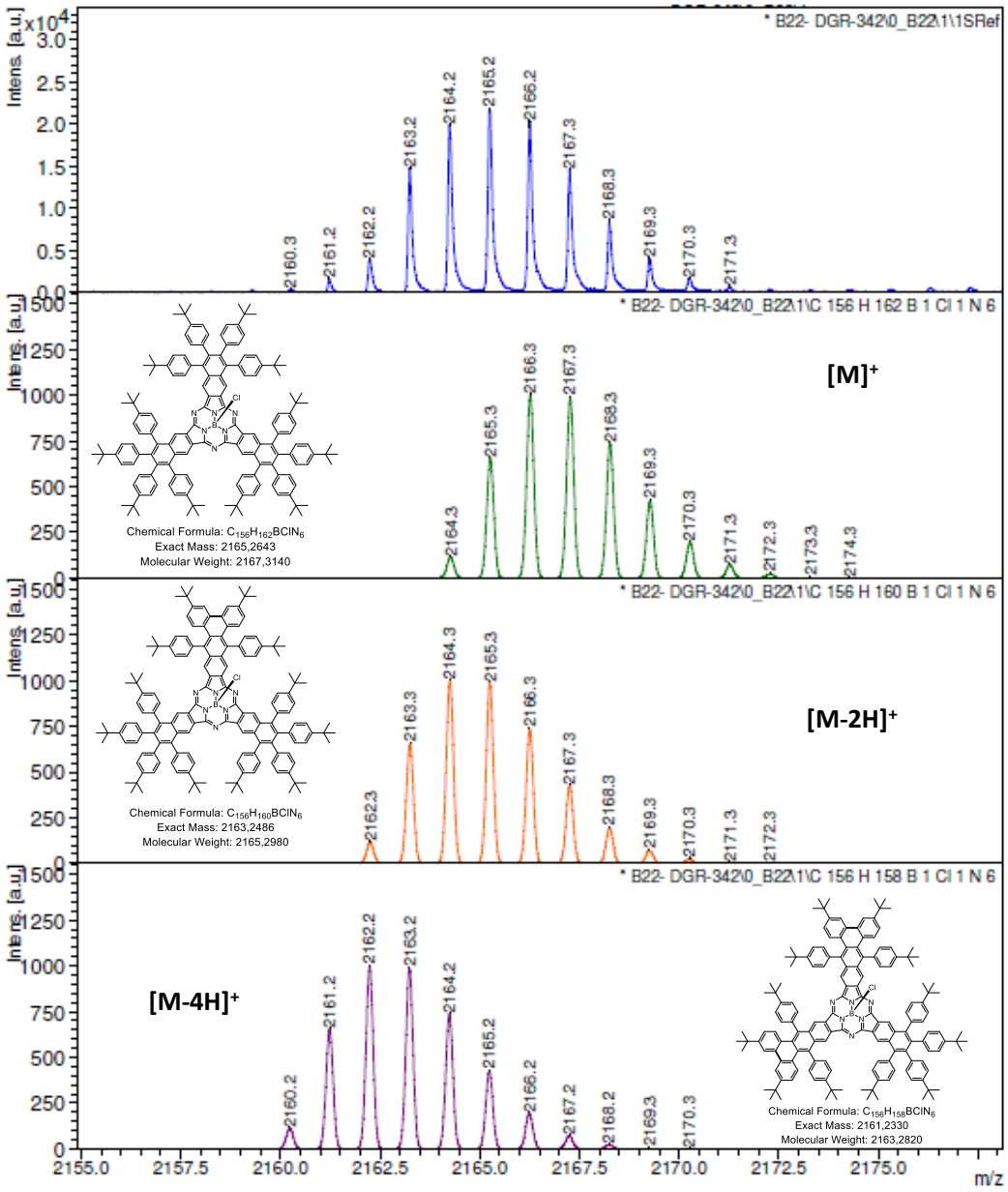

Figure 2.11. Detail of the by MALDI-TOF MS spectrum of **41b**. Theoretical isotopic distribution of $[M]^+$, $[M\text{-}2H]^+$, and $[M\text{-}4H]^+$.of..

The next goal was to prepare a fully conjugated SubNc system **42** by oxidative cyclodehydrogenation reactions of perarylated SubNc **41b** and by cyclotrimerization of precursor **32** (Scheme 2.13).

Carbon π-system materials owe their multitude of properties to a diversity of topologies such as, for example, closed surfaces, tubes, and sheets. Within the concept of sheet topology, conical and warped morphologies complement classical planar graphenic forms.[90] Curvature induces a shift in the orbital levels and HOMO-LUMO gap compared to a planar form. Sheet topological materials with mixed planar and curved regions open the possibility of controlling the electronic properties and frontier orbital profile/pattern.

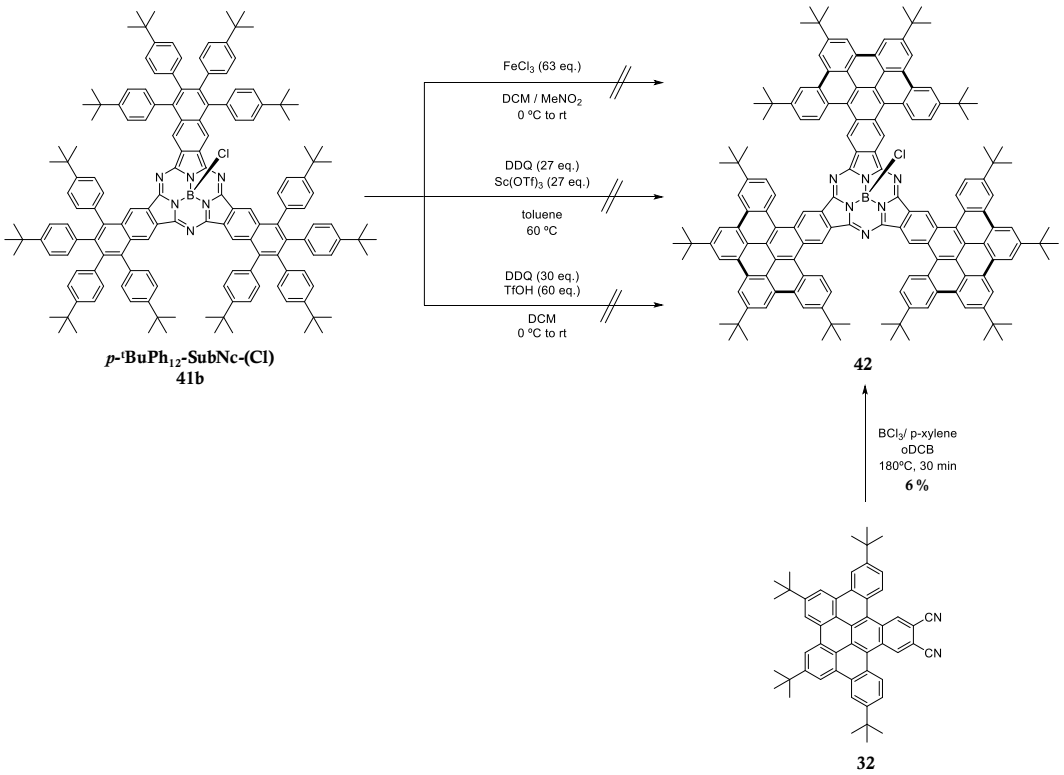

Scheme 2.13. Attempted synthesis of SubNc **42** by: oxidative cyclodehydrogenation reactions of **41b** and cyclotrimerization of precursor **32**.

[90] a) A. H. Castro-Neto, F. Guinea, N. M. R. Peres, K. S. Novoselov, A. K. Geim, *Rev. Mod. Phys*. **2009**, *81*, 109−162; b) V. Kapko, D. A. Drabold, M. F. Thorpe, *Phys. Status Solidi B* **2010**, *247*, 1197−1200.

Oxidative cyclodehydrogenation reactions of **41b** were essayed under different conditions reported in literature.[91] The first one consisted in treatment with $FeCl_3$ (63 equiv.) in DCM/nitromethane (115:1) at 0 ºC, and heating at room temperature for 1 hour. A second attempt was treatment with DDQ/$Sc(OTf)_3$ 1:1 (27 equiv.) in toluene at 60ºC.[91c] Finally, **41b** was treated with DDQ/TfOH (1:3) in DCM at 0 ºC.[88] All of these reaction conditions failed to give the desired fully π-conjugated SubNc **42**. For this reason, dinitrile **32** was subjected to the general conditions for the cyclotrimerization reaction, namely, treatment with BCl_3 at 180 ºC for 30 minutes. This afforded chloro-SubNc **42** in 6% yield, after purification by size-exclusion chromatography High-resolution MALDI-TOF mass spectrometry showed a peak corresponding to the molecular ion at m/z = 2146.1302 (calc. 2146.1265) (Figure 2.12), in addition to the expected isotopic pattern for **42** at m/z= 2146-2153.

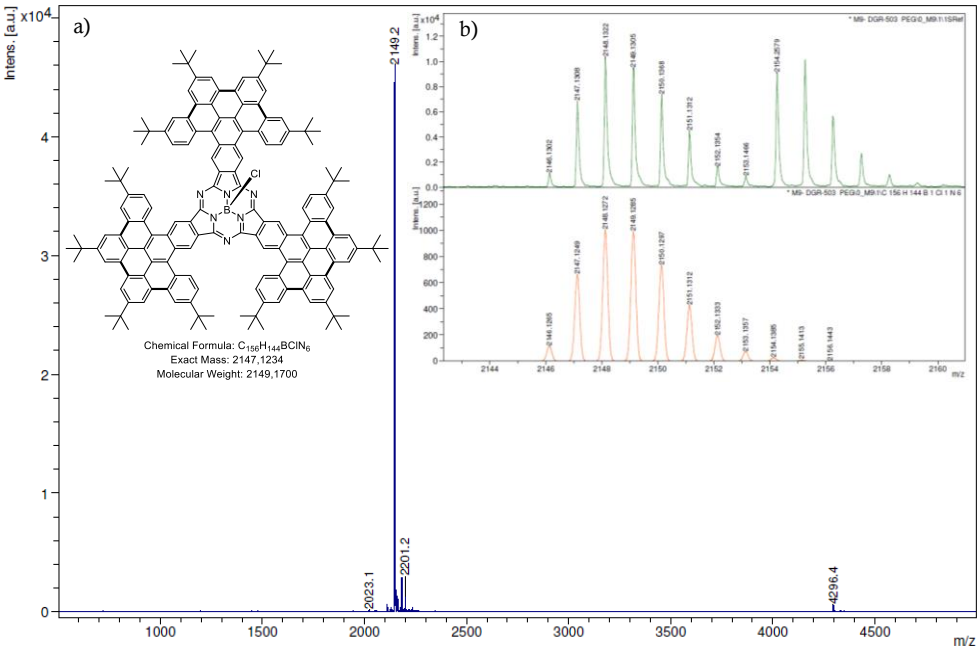

Figure 2.12. (a) MS (MALDI-TOF, DCTB) of **42**, (b) inset: HRMS of **42** and isotopic distribution of the molecular ion peak in positive mode; upper part-experimental, and lower part-predicted isotopic pattern.

[91] a) K. Kawasumi, Q. Zhang, Y. Segawa, L. T. Scott, K. Itami, *Nat. Chem.* **2013**, *5*, 739; b) D. Reger, P. Haines, F. W. Heinemann, D. M. Guldi, N. Ju, *Angew. Chem. Int. Ed.* **2018**, *57*, 5938–5942; c) N. Fukui, T. Kim, D. Kim, A. Osuka, *J. Am. Chem. Soc.* **2017**, *139*, 9075–9088.

The ^{1}H-NMR spectrum of **42** clearly shows the signals of aryl units fused in a π-conjugated system, which coalesce on going from **41b** to **42**. The aromatic protons of the bay position appear as a broad singlet at 10.53 ppm, more deshielded than for precursor **32**, which shows the corresponding singlet at 9.59 ppm (Figure 2.13). This effect arises from the larger diatropic ring current of the 14 π-electron macrocycle, related to that of the benzene ring.

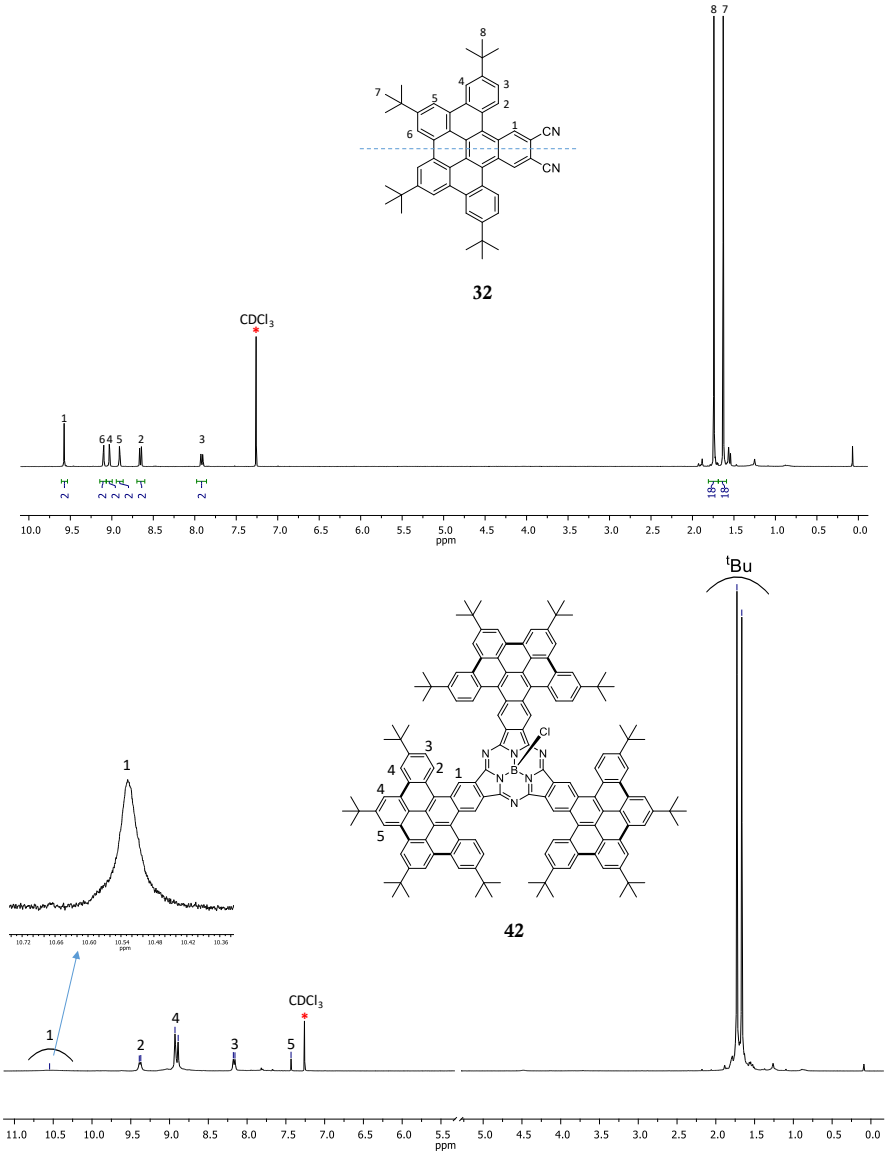

Figure 2.13. ^{1}H-NMR spectra in $CDCl_3$ at 25 °C of precursor **32** and SubNc **42**. Signals marked with * are due to residual solvents.

Although unfortunately it was not possible to obtain a single crystal suitable for X-ray diffraction analysis of SubNc **42**, its structure was calculated by optimized geometry MO-G PM3, using the Scigress software suite. Figure 2.14 shows the MM energy-minimized structure, in which the π-conjugated surface for each SubNc axes appears distorted. This distortion would be expected taking into account the X-ray crystal structure of precursor **32** (Figure 2.3).

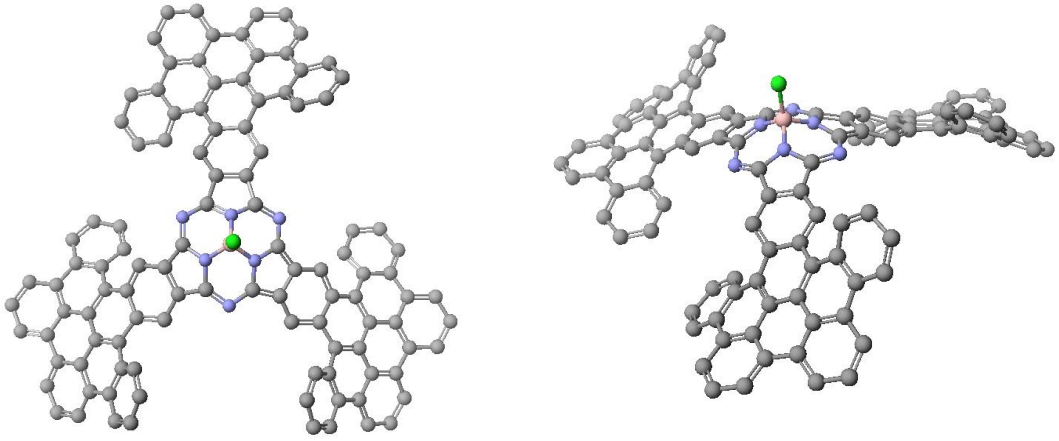

top view *side view*

Figure 2.14. Energy-minimized structure of axially-chloro SubNc **42**. *tert*-Butyl groups are omitted to simplify the optimized geometry.

2.3.3 Optical properties of dodecafunctionalized subnaphthalocyanines

Optical absorption and emission properties of dodecafunctionalized SubNc derivatives were studied using UV-Vis spectroscopy in toluene. Figure 2.15 shows the absorption spectra of axially chloro-dodecafluorinated and dodecachlorinated SubNcs **33** and **34**, and their axially phenoxy-substituted **36**, **37** and **38**. Apart from some differences in the shoulder like absorptions at *ca*. 550 and 600 nm, the absorption spectra have essentially similar shapes, including values of the molar absorption coefficient, as well as the positions of the main absorption bands.

Compounds bearing different axial substitution, on one side, **34** and **36**, and on the other side, **33**, **37** and **38**, exhibit very similar absorption profiles, indicating a small influence of the axial substituent on the absorption properties. More pronounced

fluctuations were observed upon peripheral functionalization. Here, the replacement of peripheral fluorine atoms by chlorine substituents – i.e. on going from **33** to **35**, or from **37** to **36** –produces an 11 nm redshift of the Q-bands.

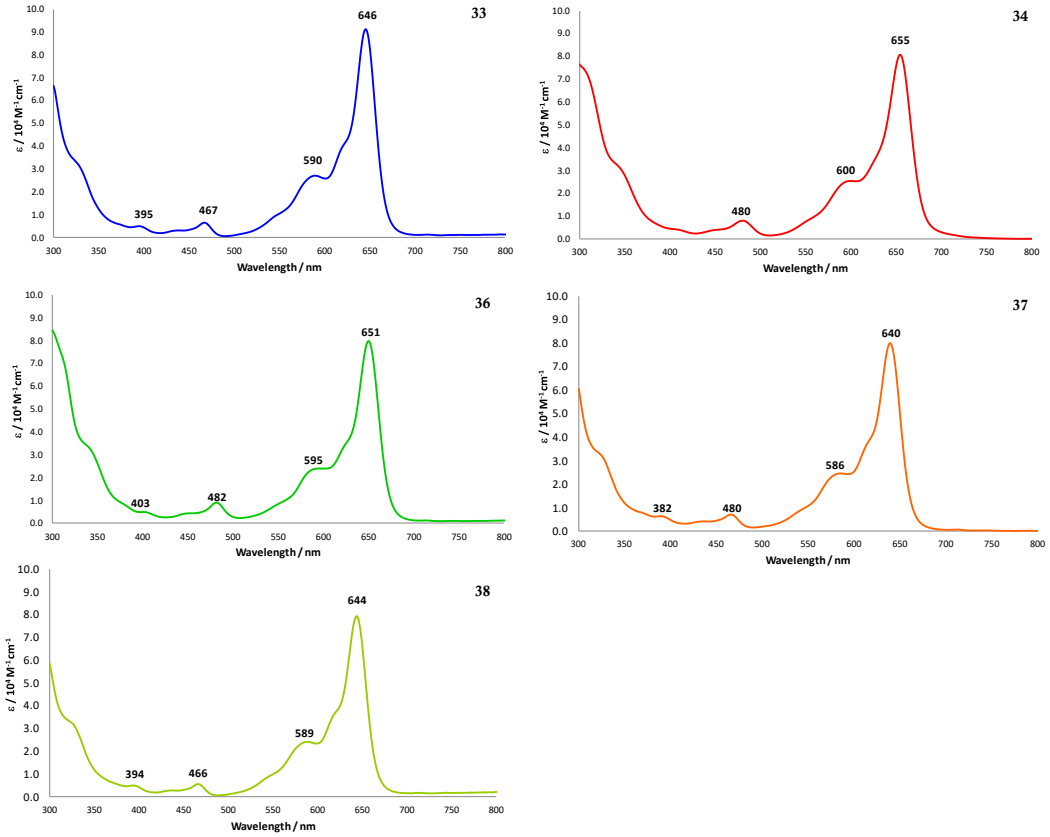

Figure. 2.15. UV/Vis absorption spectra of SubNcs **33**, **34**, **36**, **37**, and **38** in toluene.

Compared to unsubstituted 2,3-SubNc (maximum of Q-band is at 663 nm),[47c] the Q-band of F_{12}-SubNc-(Cl) **33** (646 nm) and Cl_{12}-SubNc-(Cl) **34** (655 nm) show a hypsochromic shift of 17 nm and 8 nm, respectively. The absorption spectra of SubPc molecules generally comprises two main broad bands in the Soret-band region,[15c] whereas these SubNc systems exhibit two additional small bands between the Soret and Q-band at 395 and 467 nm, in the case of **33**, which are associated with the presence of transitions to nearly degenerate excited states, due to the conjugate extension by incorporation of three fused benzene ring units.[29b] These bands are also influenced by peripheral and axial functionalization.

The molar absorption coefficients are in the order of 8-9 $\times 10^4$ $M^{-1}cm^{-1}$ for SubNcs **33**, **34** and **36-38**. The Lambert-Beer law is fulfilled in, at least, three orders of magnitude in concentration, confirming the lack of aggregates. This behaviour is different from that of planar, unsubstituted naphthalocyanines and phthalocyanines, which have a high tendency to form aggregates by π–π stacking. Regarding the emission spectra, all the SubNc are fluorescent and display intense mirror-imaged emission upon excitation on the Q-band. Stokes shifts values between 17 and 20 nm are observed. Figure 2.16 shows the normalized absorption and emission spectra of this first series.

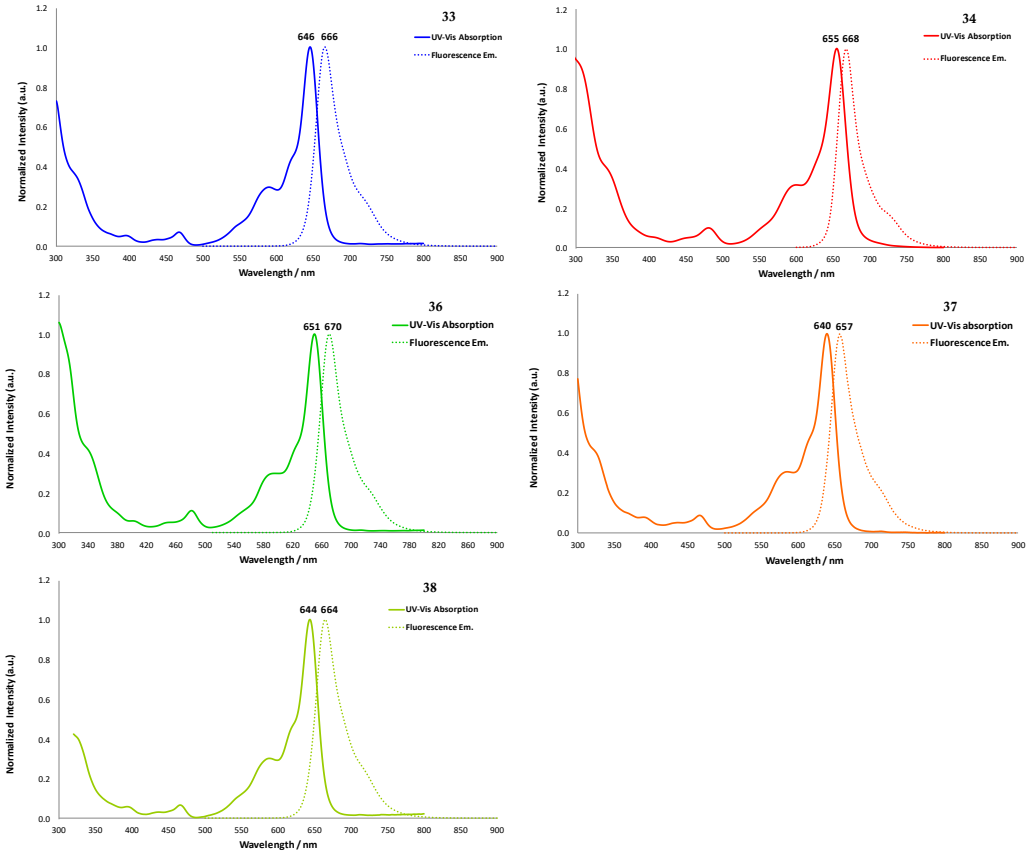

Figure 2.16. Normalized UV-Vis absorption (solid line) and fluorescence emission (dotted lined) spectra of SubNcs **33**, **34**, **36**, **37**, and **38** in toluene.

The fluorescence quantum yields were also measured using unsubstituted 2,3-SubNc (φ_F = 0.22) in toluene as standard,[47c] being around 0.21-0.24. The similitude of these values with those reported by Bender and co-workers suggest a same

photoelectronic behaviour of SubNcs.[47h] Notably, this first SubNc series exhibit a lower φ_F than hexachlorinated-SubPcs, suggesting shorter exciton lifetimes for SubNcs.[57e]

The absorption spectra of chloro-dodecapentylsulfanylated (**39**) and –sulfonylated (**40**) SubNcs exhibit bathocromically shifted Q-bands (20-30 nm) with respect to dodecahalogenated-SubNcs **33** and **34**. (Figure 2.17a). In spite of the differences between the π-donor character of the thiopentyl substituents and π-acceptor character from sulfonyl groups, both SubNcs display their Q-bands maxima at the same energy (*ca.* 676 nm) with similar molar absorption coefficients. More alteration is observed for the band corresponding to degenerate excited states, which appears at 533 nm for sulfonylated-SubNc **40**, and more intense compared to SubNc **39** and tetrahalogenated **3**3 – **38**. This electronic effect results in blue-violet colour in solution instead of the green one (Figure 2.17b). Similar results are observed in the case of hexasulfonylated-SubPc.[92]

Both SubNcs **39** and **40**, display fluorescence with significant Stokes shifts of 20 nm for **39** and 25 nm for **40**, while the fluorescence quantum yields are 0.18 and 0.30, respectively (Figure 2.17b).

[92] B. del Rey, U. Keller, T. Torres, G. Rojo, F. Agulló-López, S. Nonell, C. Martí, S. Brasselet, I. Ledoux, J. Zyss, *J. Am. Chem. Soc.* **1998**, *120,* 12808−12817.

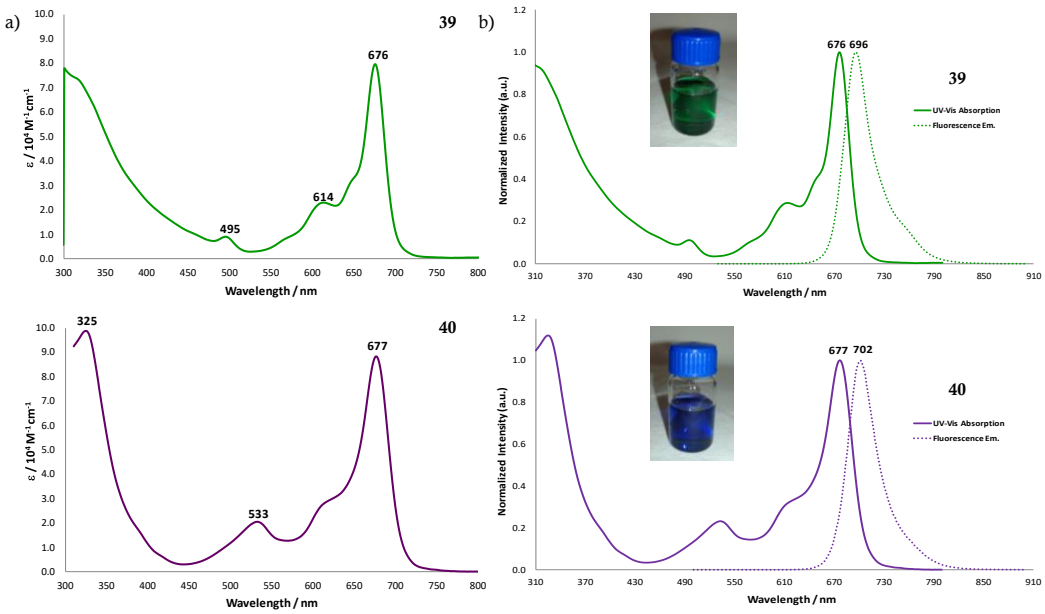

Figure 2.17. (a) UV/Vis absorption spectra and (b) normalized UV-Vis absorption (solid line), fluorescence emission (dotted lined) spectra, and SubNcs **39** and **40** in toluene solutions.

Figure 2.18 shows the absorption spectra of peripherally arylated SubNc **41b** and the π-extended **42**.SubNc **41b** shows a broad Q-band that spans from 500 to 740 nm, with maximum at 674 nm, similar to sulfanylated and sulfanylated **39** and **40**, and also similar molar absorption coefficient. (Figure 2.18a). Contrasting, π-extended macrocycle **42**, , exhibits a red-shifted Q-band at 715 nm (bathochromic shift of 41 nm with respect to SubNc **41b**) and with a more than twofold ε value of 20 $\times 10^4$ $M^{-1}cm^{-1}$. The Soret band appears at the same energy as in **41b**, at 305 nm. A new intense absorption appears at 398 nm. (Figure 2.18a).

Regarding the fluorescence emission, both arylated-SubNc **41b** and **42** are fluorescent and display intense mirror-imaged emission maxima at 688 and 738 with Stokes shifts values of 14 nm and 23 nm, respectively. Fluorescence quantum yields are of 0.22 for **41b** and significantly higher, 0.45, for **42** (Figure 2.18b). The optical absorption and emission properties of dodecafunctionalized SubNc series are summarized in Table 2.1.

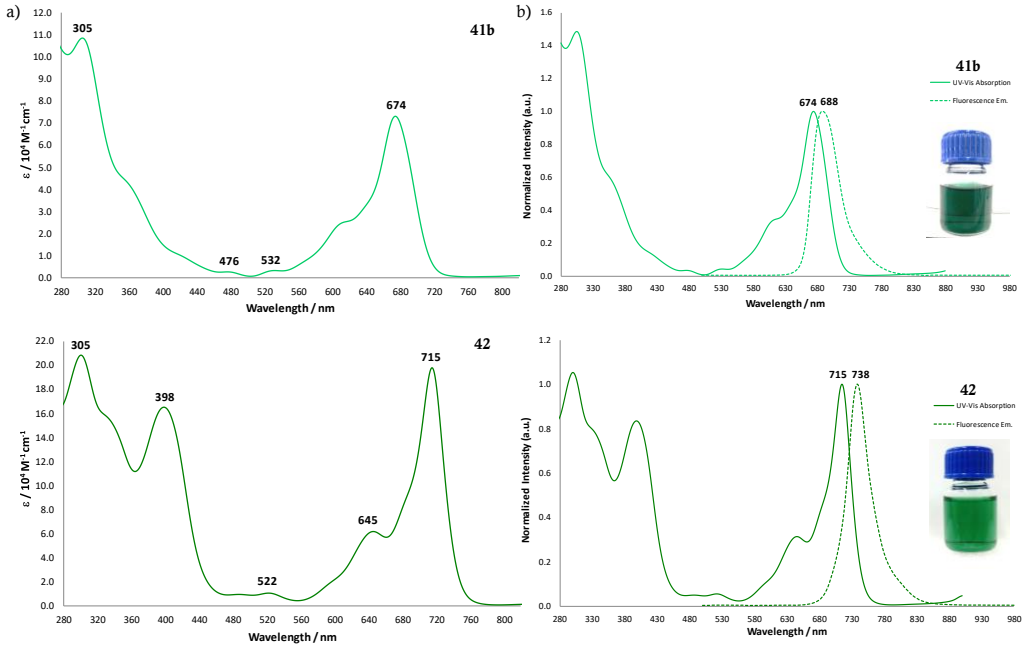

Figure 2.18. (a) UV/Vis absorption spectra and (b) normalized UV-Vis absorption (solid line), fluorescence emission (dotted lined) spectra, and SubNcs **41b** and **42** in toluene solutions.

SubNc	Absorption λ [nm] (ε[10^4 $M^{-1}cm^{-1}$])	Fluorescence λ_{em} [nm][a]	φ_F
33	395 (0.5), 467 (0.6), 590 (2.7), 646 (9.1)	666	0.21
34	480 (0.9), 600 (2.6), 655 (8.2)	668	0.25
36	403 (0.5), 482 (0.9), 595 (2.4), 651 (8.0)	670	0.24
37	382 (0.6), 466 (0.7), 586 (2.4), 640 (8.0)	657	0.22
38	394 (0.5), 466 (0.5), 589 (2.4), 644 (7.9)	664	0.21
39	495 (0.9), 614 (2.3), 676 (8.0)	696	0.18
40	324 (9.9), 533 (2.0), 677 (8.8)	702	0.30
41b	674 (7.3), 532 (0.3), 476 (0.3), 305 (10.8)	688	0.22
42	305 (20.4), 398 (16.5), 522 (1.1), 645 (6.2), 715 (19.8)	738	0.44

[a] Excited at the Q-band.

Table 2.1. Optical properties of SubNc **34** - **42** in toluene.

2.3.4 Electrochemical studies and energy levels of dodecafunctionalized SubNcs

Electrochemical experiments (cyclic voltammetry, squarewave voltammetry (SWV) and differential pulse voltammetry (DPV)) were conducted to investigate the influence of the peripheral functionalization on the redox properties of the SubNc series, as well as to determine the corresponding HOMO-LUMO energy values, in order to evaluate the acceptor or donor features for each of the SubNc derivatives. The measurements were carried out using a three-electrode cell in argon saturated THF solution containing 0.1 M $TBAPF_6$ supporting electrolyte. In these experiments, were used a glassy carbon working electrode, a Pt wire as counter electrode and $Ag/AgNO_3$ as reference electrode. Ferrocene was used as an internal standard, and all data are represented *vs* Fc/Fc^+ couple.

Figure 2.19 shows the cyclic voltammetry and square wave voltammetry of dodecahalogenated SubNcs **33**, **34**, **36-38**. For this SubNc series, the oxidation process displays only one quasi-reversible wave around 0.62 to 0.67 V. On the other hand, the first reduction potential is a reversible process in all cases. SubNc **33** shows three reduction potentials centred at –1.21, –1.76 and –2.16 V, with $\Delta E > 200$ mV between each reduction potentials, being the second potential an irreversible process. In the case of SubNc **34**, only one reduction process is observed at –1.15 V; due to its low solubility in THF and in other organic solvents used in CV measurements, detection of more negative reduction waves more difficult. Therefore, dodecachlorinated-SubNc **34** has more electron-acceptor character than dodecafluorinated-SubNc **33**. This can be easily understood on the basis of the lower M^+ character of chlorine, related to fluorine.

Regarding the axial aryloxy-substituted SubNcs **36-38**, they exhibit two reversible reduction potentials (Figure 2.19). The first reduction process appears at –1.26, –1.34 and –1.29 V for **36-38**, respectively. Here, the electron withdrawing character of the pentafluorophenoxy ligand, related to that of the *tert*-butylphenoxy ligand is evidenced by the 50 mV anodic shift in **38**, related to **37**.

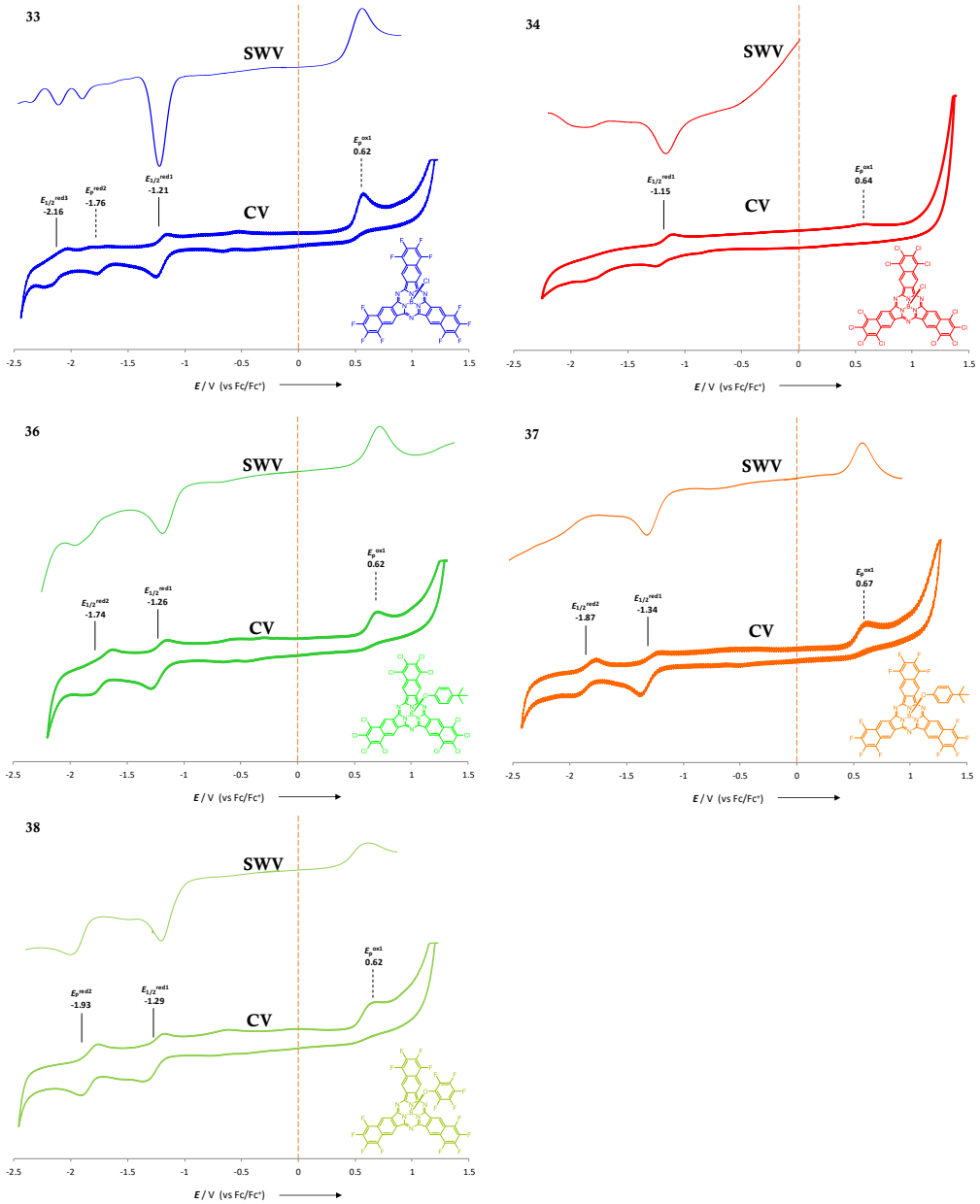

Figure 2.19. Cyclic voltammograms and SWV of SubNcs **33**, **34**, **36-38**. Solvent: THF; scan rate: 100 mVs^{-1}; working electrode: platinum; counter electrode: platinum wire; reference electrode: $Ag/AgNO_3$; electrolyte: Bu_4NPF_6.

The redox properties of dodecapentyl-sulfanylated SubNc **39** and –sulfonylated SubNc **40** are completely different. The cyclic voltammogram for SubNc **39** shows a reversible oxidation process at 0.40 V, and a second irreversible oxidation wave at 0.95 V, close to the window limit (Figure 2.20). The low potential of the first oxidation process could denote an effective electronic donation from the twelve thioether groups to the SubNc macrocycle. The first reduction potential for **39** displays a single irreversible wave at –1.40 V, and a second irreversible reduction process at –1.78 V. On the other hand, SubNc **40** shows complicated reduction processes in the range –1.0 - –2.3 V vs Fc/Fc^{+}, and undetected oxidation processes by CV and SWV measurements, probably due to multielectronic reductive events taking place at the sulfone substituents. The first reduction potential was only detectable in square wave voltammetry, at –1.11 V, followed by successive irreversible reductions the last one being at –2.13 V (Figure 2.20). These multiple reductive effects probably arise from the peripheral sulfone substituents of SubNc **40**.

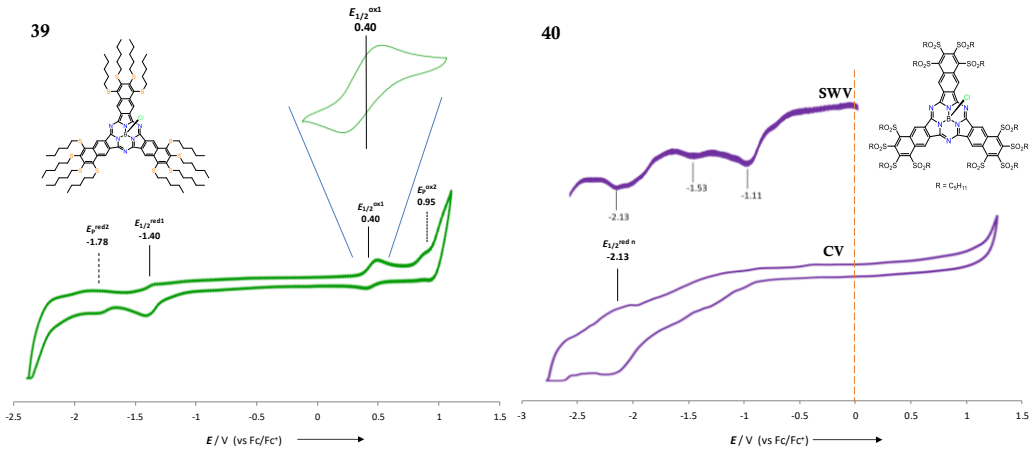

Figure 2.20. Cyclic voltammograms and SWV of SubNcs **39** and **40**. Solvent: THF; scan rate: 100 mVs^{-1}; working electrode: platinum; counter electrode: platinum wire; reference electrode: $Ag/AgNO_3$; electrolyte: Bu_4NPF_6.

The electrochemical properties of perarylated SubNcs **41b** and **42**, were also explored using cyclic voltammetry in THF. In the case of SubNc **41b**, three quasi-reversible reduction waves were detected at –1.43, –2.23 and –2.27 V versus Fc/Fc^+ couple. In addition, one well-defined quasi-reversible oxidation process is located at 0.42 V (Figure 2.21a). Regarding the redox processes of SubNc **42**, two reversible oxidation processes at 0.27 and 0.83 V were detected by CV, in addition to three quasi-reversible reduction waves at –1.42, –1.85 and –2.31 V (Figure 2.21b,cDifferential pulse voltammetry showed two additional oxidation processes at 0.59 and 1.11 V, and also one more reduction at –2.80 V. (Figure 2.22).

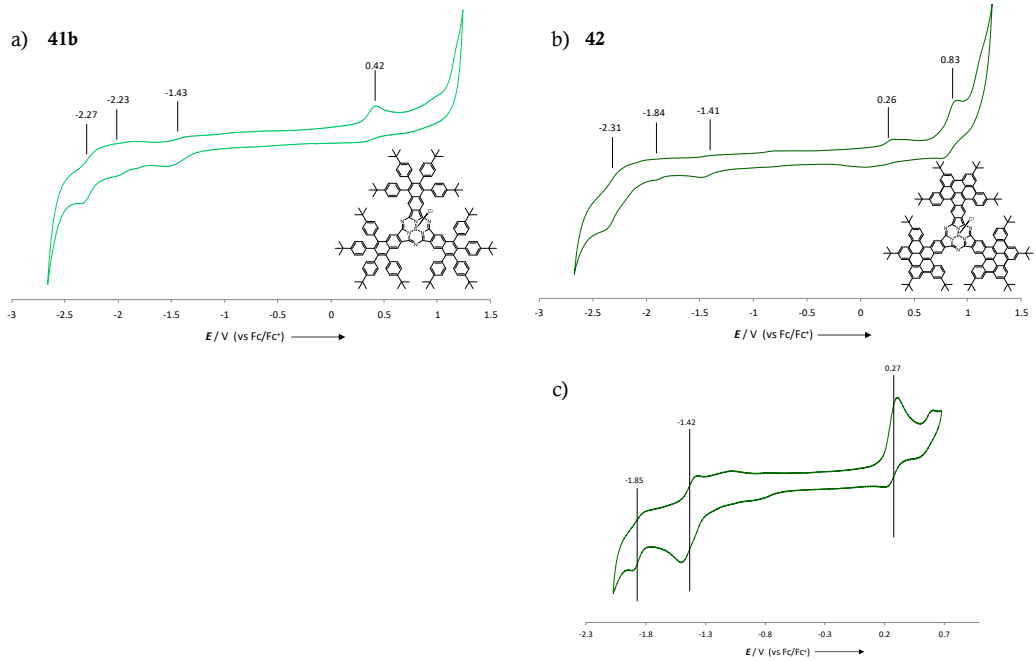

Figure 2.21. Cyclic voltammograms of (a) SubNc **41b**, (b) SubNc **42**, and (c) reduced window for **42**. Solvent: THF; scan rate: 100 mVs^{-1}; working electrode: platinum; counter electrode: platinum wire; reference electrode: $Ag/AgNO_3$; electrolyte: Bu_4NPF_6.

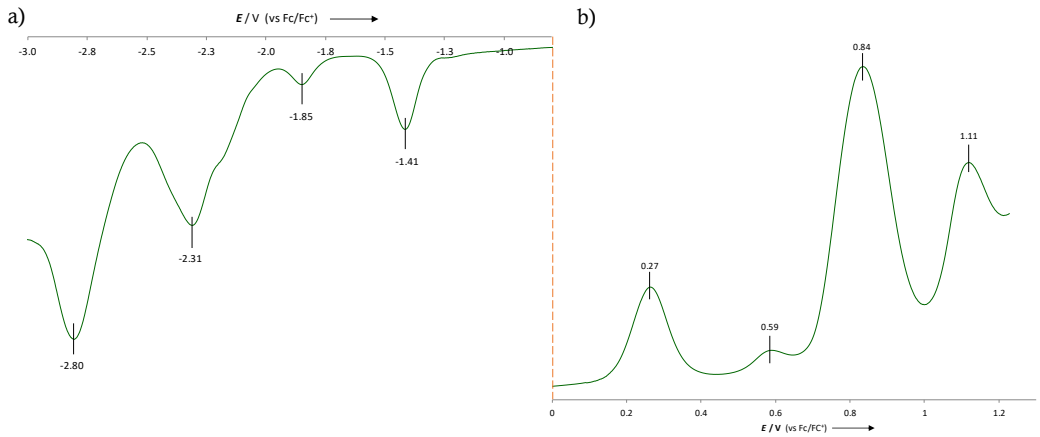

Figure 2.22. Differential pulse voltammogram of SubNc **42**: (a) anodic window and (b) cathodic window in THF.

In other words, π-extended SubNc **42** is 150 mV easier to oxidize than dodecaarylated SubNc **41b**, although they show similar tendency to accept one electron. All the electrochemical data are summarized in Table 2.2.

SubNc	E_{red4}	E_{red3}	E_{red2}	E_{red1}	E_{ox1}	E_{ox2}	E_{ox3}	E_{ox4}
33	-	–2.16	–1.76 [a]	–1.21	0.62 [a]	-	-	-
34	-	-	-	–1.15	0.64 [a]	-	-	-
36	-	-	–1.74	–1.26	0.62 [a]	-	-	-
37	-	-	–1.87	–1.34	0.67 [a]	-	-	-
38	-	-	–1.93	–1.29	0.62 [a]	-	-	-
39	-	-	–1.78 [a]	–1.40	0.40	0.95 [a,c]	-	-
40	-	-	–1.53 [b]	–1.11 [b]	-	-	-	-
41b	-	–2.27	–2.23 [a]	–1.43	0.42	-	-	-
42	–2.80 [b]	–2.31	–1.85	–1.42	0.27	0.59 [b]	0.83	1.11 [b]

[a] Irreversible process (potential corresponds to the peak potential).

[b] Taken from the SWV/DPV. [c] In the window limit.

Table 2.2. Electrochemical oxidation and reduction potentials (in V), **E** vs. Fc/Fc^+.

HOMO and LUMO energy levels of the dodecafunctionalized SubNc series were estimated from the reduction and oxidation potentials obtained by CV measurements, and by the optical band gap (E^g_{opt}) value, which was estimated from the offset

wavelength derived from the low energy absorption band, in the case of SubNc **40** (Table 2.3).

Among SubNc **33** – **40**, the most important alteration arises from peripheral sulfanylation, with compound **39** showing a notable destabilization of the HOMO level of *ca.* 20 eV. Perarylated SubNc **41b** shows similar energies for the frontier orbitals related to **39**. The enlarged π-conjugated system of **42** produces additional 15 eV destabilization of its HOMO energy.

SubNc	$HOMO_{exp}$	$LUMO_{exp}$[b]	$E^{g}_{H\text{-}L}$
33	–5.72	–3.89	1.83
34	–5.74	–3.95	1.79
36	–5.72	–3.84	1.88
37	–5.65	–3.76	1.89
38	–5.72	–3.81	1.91
39	–5.50	–3.70	1.80
40[a]	–5.79	–3.99	1.80
41b	–5.52	–3.67	1.85
42	–5.37	–3.68	1.69

[a] $E_{HOMO} = E_{LUMO} - E^{g}_{opt}$[74a] [b] Calculated using the expression $E_{LUMO} = -5.1 - E_{1/2}^{red1}$ (*vs.* Fc/Fc^{+}) (eV)[73]

Table 2.3. Experimental energy values in eV by CV measurements.

2.4 Summary and Conclusions

In this second chapter, the synthesis and characterization of new families of peripheral dodecafunctionalized SubNcs has been explored.

We have developed a synthetic strategy for tetrafluorinated, tetrachlorinated and tetrabrominated 2,3-naphthalenedicarbonitriles based in cycloaddition of and aromatization reactions. These halogenated precursors have been used in nucleophilic aromatic substitution reactions or palladium-catalyzed coupling reactions, to prepare sulfanylated, sulfonylated and arylated 2,3-naphthalenedicarbonitriles.

A chloro-SubNc series was obtained directly by cyclotrimerization reaction of the developed precursors. In a second step, the triflate-SubNc mediated axial functionalization was performed. The direct attachment of different chemical functions to SubNc periphery produces strong perturbation on the electronic and redox properties. Therefore, depending on the peripheral functionalization, SubNc can present an electron-accepting or -donor character.

We have also prepared an unprecedented π-extended dinitrile by oxidative dehydrogenation of hexaarylated 2,3-naphthalenedicarbonitrile. Cyclotrimerization reaction of this new precursor led to a π-extended macrocycle, made up of three naphthopentaphene subunits. The new chromophore shows a notable destabilization of its HOMO level, related to the corresponding dodecaarylated SubNc. This results in lower energy absorption (715 nm) and much higher reducing ability.

2.5 Experimental Section

2.5.1 Synthesis of tetrasubstituted 2,3-naphthalenedicarbonitrile precursors

1,2-Bis(hydroxymethyl)-3,4,5,6-tetrafluorobenzene (26)[85]

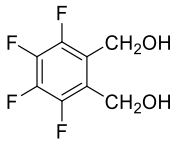

To a suspension of $LiAlH_4$ (1.10g, 29.0 mmol, 2 eq) in 20 mL of anhydrous diethyl ether stirred at 0 °C, a solution of diethyl 3,4,5,6-tetrafluorophthalate (4.26 g, 14.5 mmol, 1 eq) in 40 mL of anhydrous diethyl ether was added dropwise under argon atmosphere. The reaction mixture was refluxed for 3 hours and then cooled to 0 °C. A 4N solution of H_2SO_4 was added slowly to decompose the excess $LiAlH_4$. The mixture was extracted with diethyl ether and the combined organic layer was washed with brine, dried with anhydrous $MgSO_4$ and evaporated under reduced pressure, to give 1,2-bis(hydroxymethyl)-3,4,5,6-tetrafluorobenzene as a white powder (2.53 g, 77%).

^{1}H NMR (400 MHz, $CDCl_3$): δ = 4.83 (d, J = 4.5 Hz, 4 H; ArCH_2OH ×2), 2.97 ppm (t, J = 5.6 Hz, 2H; OH ×2).

^{13}C NMR (100.6 MHz, $CDCl_3$): δ = 148.5, 135.0, 125.5, 55.7 ppm.

1,2-Bis(bromomethyl)-3,4,5,6-tetrafluorobenzene (24a)[85]

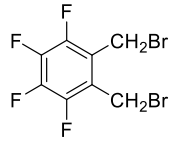

Tetrafluorobenzenedimethanol 26 (2.53 g, 12.0 mmol) was added to 92 mL concentrated hydrobromic acid. The reaction mixture was refluxed overnight, by which time all solid had disappeared, and an oil formed at the bottom of the flask. The mixture was diluted with water and extracted with diethyl ether. The combined

organic layer was washed with brine, dried with anhydrous $MgSO_4$ and evaporated under reduced pressure, giving **24a** as a yellow oil (3.80 g, 78%).

^{1}H NMR (400 MHz, $CDCl_3$): δ = 4.61 ppm (s, 4 H; ArCH_2Br ×2).

^{13}C NMR (100.6 MHz, $CDCl_3$): δ = 149.9, 137.0, 124.5, 23.3 ppm.

1,2,3,4-Tetrachloro-5,6-dimethylbenzene (27)[86]

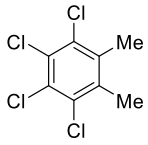

Sulfuryl chloride (210.0 mL, 2.6 mol, 5.5 eq) and sulfur monochloride (2.4 mL, 30.0 mmol, 0.055 eq) was added dropwise to a suspension of $AlCl_3$ (2.70 g, 20.0 mmol, 0.045 eq) in *o*-xylene (57.8 mL, 470.0 mmol, 1 eq). The mixture was stirred at room temperature and connected to a gas trap containing a solution of concentrated KOH. The reaction mixture was heated at 100 ºC overnight, then cooled to room temperature and poured into 500 mL ice-water. The suspension was filtered, washed with water and dried. The product was recrystallized from CCl_4 to give the desired compound **27** as a white solid (80.30 g, 70%).

^{1}H NMR (400 MHz, $CDCl_3$): δ = 2.42 ppm (s, 6 H; ArCH_3 ×2).

^{13}C NMR (100.6 MHz, $CDCl_3$): δ = 139.7, 131.6, 129.2, 12.7 ppm.

1,2,3,4-Tetrabromo-5,6-dimethylbenzene (28)[86]

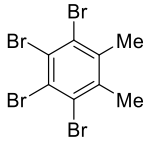

To a suspension of iron powder (1.23 g, 22.0 mmol, 0.2 eq) in bromine (48.0 mL, 940.0 mmol, 8.5 eq) stirred at 0ºC and connected to a gas trap containing a solution of concentrated KOH, *o*-xylene (14.0 mL, 110.0 mmol, 1 eq) was added dropwise. After, the reaction mixture was stirred for one hour at room temperature and then, the excess

of bromine was removed by gentle heating with an argon stream. The solid residue was filtered and washed with water, saturated $NaHCO_3$, 2N HCl and methanol. The product was recrystallized from toluene to give **28** as white needles (35.26 g, 76%).

^{1}H NMR (400 MHz, $CDCl_3$): δ = 2.55 ppm (s, 6 H; ArCH_3 ×2).

^{13}C NMR (100.6 MHz, $CDCl_3$): δ = 138.8, 123.4, 123.0, 18.2 ppm.

1,2-Bis(bromomethyl)-3,4,5,6-tetrachlorobenzene (24b)[86]

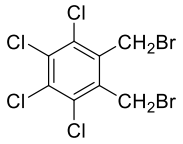

General procedure for the benzylic bromination: A mixture of tetrahalo-*o*-xylene (1 eq), *N*-Bromosuccinimide (2.5 eq) and AIBN (0.1 eq) in CCl_4 was refluxed overnight under argon atmosphere and irradiated by means of a halogen lamp of 300 W. After cooling to room temperature, succinimide was removed by filtration and the organic solvent was evaporated, to give a white solid, which was recrystallized from ethanol.

24b: Prepared according to the general procedure for the benzylic bromination; **27** (30.00 g, 123.0 mmol), *N*-Bromosuccinimide (54.80 g, 308.0 mmol) and AIBN (1.64 g, 10.0 mmol) in 500 mL of CCl_4. The product was obtained as a white solid (35.32 g, 87%).

^{1}H NMR (400 MHz, $CDCl_3$): δ = 4.77 ppm (s, 4 H; ArCH_2Br ×2).

^{13}C NMR (100.6 MHz, $CDCl_3$): δ = 140.0, 135.2, 129.6, 24.0 ppm.

1,2-Bis(bromomethyl)-3,4,5,6-tetrabromobenzene (24c)[86]

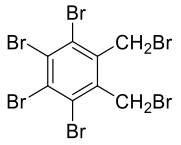

Prepared according to the general procedure for the benzylic bromination; **28** (22.98 g, 54.5 mmol), N-Bromosuccinimide (24.24 g, 136.2 mmol) and AIBN (715.0 mg, 4.4 mmol) in 500 mL of CCl_4. The product was obtained as a beige solid (27.60 g, 71%).

^{1}H NMR (400 MHz, $CDCl_3$): δ = 4.88 ppm (s, 4 H; ArC*H*$_2$Br ×2).

^{13}C NMR (100.6 MHz, $CDCl_3$): δ = 145.4, 126.6, 123.8, 24.9 ppm.

General procedure for the synthesis of precursors 21-23 by cycloaddition and aromatization reactions:

A mixture of 1,2-bis(bromomethyl)-3,4,5,6-tetrahalobenzene **24(a,b,c)** (1 mmol), fumaronitrile (2 mmol), and NaI (6.5 mmol) in dry *N,N*-dimethylformamide was heated at 80 ºC for 7 h under argon atmosphere and after, allowed to stand at room temperature overnight. The reaction mixture was poured into 0.5 L of a 40 % w/v solution of $NaHSO_3$ and the resulting suspension was filtered, washed with water, and air-dried. The product was recrystallized from a chloroform-THF mixture (5:1) or purified by column chromatography. Unaromatized Diels-Alder adduct **25(a,b,c)** (1 mmol) was dissolved in 1,2-dichlorobenzene and then, bromine (3 mmol) and pyridine (8 mmol) were added under argon atmosphere via syringe. The reaction mixture was stirred at 150 ºC for 18 h and then, cooled to room temperature and passed through a short pad of compressed celite. The celite pad was washed with several small portions of chloroform and finally, the filtrate was evaporated under reduced pressure. The residue was subjected to column chromatography on silica gel giving the respective pure target material.

5,6,7,8-Tetrafluoro-1,2,3,4-tetrahydronaphthalene-2,3-dicarbonitrile (25a)

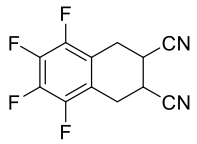

Prepared according to the general procedure; **24a** (2.14 g, 6.4 mmol), fumaronitrile (1.00 g, 12.8 mmol), and NaI (6.20 g, 41.3 mmol) in 22 mL of DMF. The product was purified by column chromatography (silica gel; $CHCl_3$/*n*-hexane, 8:2) yielding a white solid (1.35 g, 70%).

^{1}H NMR (400 MHz, $CDCl_3$): δ = 3.44 (m, 2H; C*H*CN), 3.33 (AB dd, J = 18.0, 4.4 Hz, 2H; ArCH_BHCH), 3.22 ppm (AB' dd, J = 19.6, 3.0 Hz, 2H; ArCHH_B'CH).

^{13}C NMR (100.6 MHz, $CDCl_3$): δ = 146.4, 135.6, 123.3, 119.2, 29.1, 22.9 ppm.

MS (EI-TOF, +): *m/z* (%) = 254.0 ($[M]^+$, 12), 227.0 ($[M - HCN]^+$, 19), 176.0 ([o-quinodimethane]$^+$, 100).

HRMS (EI-TOF, +): *m/z* calculated for $C_{12}H_6F_4N_2$ $[M]^+$ 254.0467; found 254.0469.

FT-IR (ATR), ν: 2936, 2924, 2248, 1723, 1517, 1483, 1307, 1118, 1060, 1033, 952, 924, 635 cm^{-1}

mp: 181 – 182 °C.

5,6,7,8-Tetrafluoronaphthalene-2,3-dicarbonitrile (21)

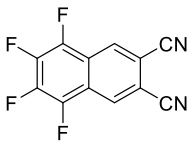

Prepared according to the general procedure; **25a** (1.20 g, 4.7 mmol) in 30 mL of 1,2-dichlorobenzene, bromine (0.7 mL, 14.1 mmol), and pyridine (3 mL, 37.6 mmol). The product was purified by column chromatography (silica gel; $CHCl_3$/*n*-hexane, 7:3) yielding white needles (0.61 g, 52%).

^{1}H NMR (400 MHz, $CDCl_3$): δ = 8.59 ppm (s, 2H; Ar-H).

^{13}C NMR (100.6 MHz, $CDCl_3$): δ = 143.4, 139.8, 127.2, 122.8, 115.8, 111.8 ppm.

MS (EI-TOF, +): *m/z* (%) = 250.0 ($[M]^+$, 100).

HRMS (EI-TOF, +): *m/z* calculated for $C_{12}H_2F_4N_2$ $[M]^+$ 250.0154; found 250.0142.

FT-IR (ATR), ν : 3106, 3029, 2235, 1833, 1660, 1609, 1510, 1469, 1441, 1353, 1131, 989, 921, 781, 670, 524, 449 cm^{-1}.

mp: 214 – 215 °C.

5,6,7,8-Tetrachloro-1,2,3,4-tetrahydronaphthalene-2,3-dicarbonitrile (25b)

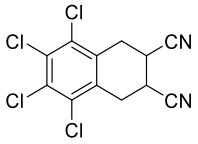

Prepared according to the general procedure; **24b** (10.00 g, 25.0 mmol), fumaronitrile (3.90 g, 50.0 mmol) and NaI (24.00 g, 161.3 mmol) in 80 mL of DMF. The product was purified by recrystallization from a (5:1) chloroform-THF mixture, yielding a white solid (5.78 g, 72%).

^{1}H NMR (400 MHz, $CDCl_3$): δ = 3.43 (m, 2H; C*H*CN), 3.38 (AB dd, *J* = 18.0, 4.4 Hz, 2H; ArCH_BHCH), 3.32 ppm (AB' dd, *J* = 19.6, 3.0 Hz, 2H; ArCH$H_{B'}$CH).

^{13}C NMR (100.6 MHz, $CDCl_3$): δ = 133.6, 131.7, 128.2, 119.2, 28.6, 23.6 ppm.

MS (EI-TOF, +): *m/z* (%) = 319.9 ($[M]^+$, 78), 292.9 ($[M - HCN]^+$, 39), 255.9 ($[M - HCN - Cl]^+$, 57), 241.9 ([o-quinodimethane]$^+$, 100).

HRMS (EI-TOF, +): *m/z* calculated for $C_{12}H_6Cl_4N_2$ $[M]^+$ 319.9303; found 319.9298.

FT-IR (ATR), *v*: 2245, 1481, 1380, 1238, 1105, 1003, 952, 924, 635 cm^{-1}.

mp: 255 – 256 °C.

5,6,7,8-Tetrachloronaphthalene-2,3-dicarbonitrile (22).

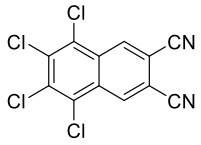

Prepared according to the general procedure; **25b** (5.78 g, 18.1 mmol) in 60 mL of 1,2-dichlorobenzene, bromine (2.8 mL, 54.2 mmol), and pyridine (11.7 mL, 145.0 mmol). The product was purified by column chromatography (silica gel; $CHCl_3$/*n*-hexane, 7:3) yielding a white solid (3.70 g, 65%).

^{1}H NMR (400 MHz, $CDCl_3$): δ = 8.81 ppm (s, 2H; Ar-H).

^{13}C NMR (100.6 MHz, $CDCl_3$): δ = 134.6, 130.1, 130.1, 129.5, 115.8, 114.5 ppm.

MS (EI-TOF, +): *m/z* (%) = 315.9 ($[M]^+$, 100).

HRMS (EI-TOF, +): *m/z* calculated for $C_{12}H_2Cl_4N_2$ $[M]^+$ 315.8997; found 315.9005.

FT-IR (ATR), *ν*: 3102, 3049, 2242, 1605, 1510, 1486, 1441, 1351, 1256, 989, 921, 781, 670, 524, 449 cm^{-1}.

mp: 270 – 271 °C.

5,6,7,8-Tetrabromo-1,2,3,4-tetrahydronaphthalene-2,3-dicarbonitrile (25c)

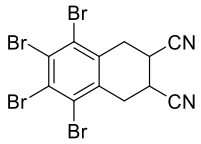

Prepared according to the general procedure; **24c** (5.86 g, 10.1 mmol), fumaronitrile (1.58 g, 20.2 mmol) and NaI (9.08 g, 60.6 mmol) in 60 mL of DMF. The product was obtained as a white solid after purification by column chromatographic (silica gel; $CHCl_3$/*n*-hexane, 8:2) yielding (3.22 g, 64%).

^{1}H NMR (400 MHz, $CDCl_3$): δ = 3.42 (m, 1 H; ArCH_BHCH), 3.37 (m, 2 H; C*H*CN ×2), 3.34 (d, *J* = 1.8 Hz, 1 H; ArC$H_{B'}$HCH), 3.29 (dd, *J* = 6.9, 1.9 Hz, 1 H; ArCH$H_{B'}$CH), 3.25 ppm (m, 1 H; ArCH$H_{B'}$CH).

^{13}C NMR (100.6 MHz, $CDCl_3$): δ = 132.7, 129.0, 128.0, 117.3, 29.7, 28.2 ppm.

MS (EI-TOF, +): *m/z* (%) = 497.7 ($[M]^+$, 100), 419.7 ([o-quinodimethane]$^+$, 44).

HRMS (EI-TOF, +): *m/z* calculated for $C_{12}H_6Br_4N_2$ $[M]^+$ 493.7264; found 493.7254.

FT-IR (ATR), *v*: 2245, 1481, 1380, 1238, 1105, 1003, 952, 924, 635 cm^{-1}.

mp: 260 – 262 °C.

5,6,7,8-Tetrabromonaphthalene-2,3-dicarbonitrile (23)

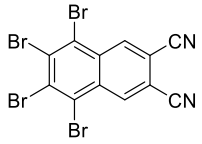

Prepared according to the general procedure; **25c** (3.22 g, 6.5 mmol), in 100 mL of 1,2-dichlorobenzene, bromine (0.7 mL, 13.6 mmol), and pyridine (4.2 mL, 51.8 mmol). The product was purified by column chromatography (silica gel; $CHCl_3$/ *n*-hexane, 8:2) yielding a white solid (1.28 g, 40%).

^{1}H NMR (400 MHz, $CDCl_3$): δ = 8.86 ppm (s, 2 H; Ar-H ×2).

^{13}C NMR (100.6 MHz, $CDCl_3$): δ = 136.1, 135.5, 134.1, 132.2, 130.6, 130.3, 116.5, 109.0 ppm.

MS (EI-TOF, +): *m/z* (%) = 493.7 ($[M]^+$, 100).

HRMS (EI-TOF, +): *m/z* calculated for $C_{12}H_2Cl_4N_2$ $[M]^+$ 493.6923; found 493.6931.

FT-IR (ATR), *v*: 3102, 3049, 2242, 1605, 1510, 1486, 1441, 1351, 1256, 989, 921, 781, 670, 524, 449 cm^{-1}.

mp: 274 – 277 °C.

5,6,7,8-Tetrakis(pentylthio)naphthalene-2,3-dicarbonitrile (29)

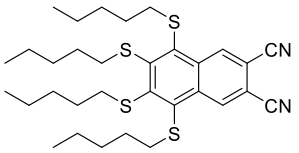

A 100 mL Schlenk tube held under argon atmosphere was charged with **22** (1.82 g, 5.8 mmol, 1 eq) and 50 mL of dry DMF and the solution stirred for 30 minutes. Then, 1-pentanethiol (4.3 mL, 34.8 mmol, 6 eq) and freshly distilled triethylamine (4.7 mL, 34.8 mmol, 6 eq) were added dropwise via syringe, and the resulting mixture was stirred at 60 ºC under argon atmosphere overnight. Once the reaction was completed (monitored by TLC), the solvent was removed under reduced pressure, and the crude material was chromatographed on silica gel (6:4 mixture of *n*-hexane/chloroform) giving pure compound **29** (2.71 g, 80%) as a dark yellow oil.

^{1}H NMR (400 MHz, $CDCl_3$): δ = 9.26 (s, 2H; Ar-H), 3.11 (t, J = 7.2 Hz, 4H; SCH_2Bu), 2.92 (t, J = 7.2 Hz, 2H; SCH_2Bu), 1.50 (m, 8H; 4SCH$_2$CH_2), 1.39 – 1.21 (m, 16H; 8CH_2), 0.84 (t, J = 7.2 Hz, 6H; 2CH_3), 0.83 ppm (t, J = 7.2 Hz, 6H; 2CH_3).

^{13}C NMR (100.6 MHz, $CDCl_3$): δ = 151.2, 140.2, 135.7, 135.5, 115.9, 110.9, 38.2, 37.7, 30.9, 29.2, 22.1, 13.8 ppm.

MS (MALDI-TOF, DCTB, +): m/z (%) = 586.3 ([M]$^+$, 100).

HRMS (MALDI-TOF, +): m/z calculated for $C_{32}H_{46}N_2S_4$ [M]$^+$ 586.2538; found 586.2535.

FT-IR (ATR), ν: 2955, 2925, 2856, 2233, 1523, 1492, 1463, 1378, 1252, 1133, 1105, 917, 729, 523 cm^{-1}.

5,6,7,8-Tetrakis(pentylsulfonyl)naphthalene-2,3-dicarbonitrile (30)

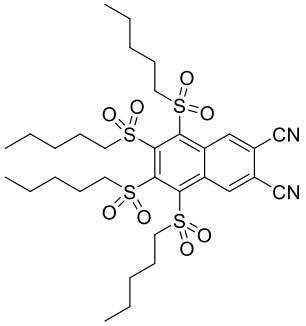

A two-neck flask (500 mL) connected to a condenser and held under argon atmosphere was charged with ***29*** (2.00 g, 3.4 mmol) and 300 mL of glacial acetic acid and the solution was stirred for 10 minutes at room temperature, and then, heated at 90 °C. Hydrogen peroxide 33% w/v (190 mL) was added in 4 mL portions in the course of 4 hours and the resulting reaction mixture was heated at 120 °C for 4 hours. The white turbid mixture was stirred at 80 °C overnight and then, cooled to room temperature. The white precipitate was collected by filtration and washed several times with water. The white solid was chromatographed on silica gel (2:8 mixture of *n*-hexane/chloroform) giving pure compound **5** (1.23 g, 51%) as a white solid.

^{1}H NMR (400 MHz, $CDCl_3$): δ = 9.67 (s, 2H; Ar-H), 4.50 – 4.43 (m, 2H; SO_2CH_2Bu), 4.30 – 4.22 (m, 2H; SO_2CH_2Bu), 4.07 – 4.00 (m, 2H; SO_2CH_2Bu), 3.46 – 3.39 (m, 2H; SO_2CH_2Bu), 2.24 –1.98 (m, 8H; $4SO_2CH_2CH_2$), 1.61 – 1.40 (m, 16H; $8CH_2$), 0.98 (t, J = 7.2 Hz, 6H; $2CH_3$), 0.97 ppm (t, J = 7.2 Hz, 6H; $2CH_3$).

^{13}C NMR (100.6 MHz, $CDCl_3$): δ = 156.3, 147.1, 134.1, 132.7, 115.4, 114.3, 62.9, 57.7, 30.4, 23.4, 22.1, 20.7, 13.7 ppm.

MS (MALDI-TOF, DCTB + NaI, +): *m/z* (%) = 737.3 ($[M]^+$, 100).

HRMS (MALDI-TOF, NaI,+): *m/z* calculated for $C_{32}H_{46}N_2NaO_8S_4$ $[M]^+$ 737.2053; found 737.2029.

FT-IR (ATR), *ν*: 2957, 2930, 2871, 2238, 1459, 1407, 1335, 1312, 1287, 1223, 1144, 1104, 898, 771, 630, 616, 508 cm^{-1}.

mp: 268 – 269 °C.

5,6,7,8-Tetraphenylnaphthalene-2,3-dicarbonitrile (31a)

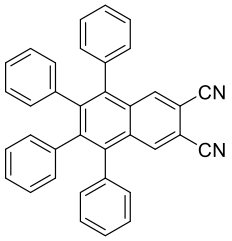

General procedure for the tetra Suzuki-Miyaura cross-coupling reactions: A Schlenk tube equipped with a magnetic stir bar under argon atmosphere was charged with a mixture of tetrabromo **23** (1 mmol), appropriate boronic acid (8 mmol), and Na_2CO_3 (10 mmol) in a (1:1:1) mixture of water/THF/toluene. The resulting mixture was degassed with argon for 20 min. [$Pd(PPh_3)_4$] (10 mol-%) was added and the mixture was heated at 80º overnight. The reaction was monitored by TLC) and when concluded, the reaction mixture was diluted with water and extracted with AcOEt. The combined organic layers were washed with water and brine, and dried with Na_2SO_4. The solvent was evaporated and the residue was loaded onto a silica gel column. Elution with mixtures of hexanes/EtOAc gave the desired cross-coupling product.

31a; Prepared according to the general procedure; **23** (350.0 mg, 0.72 mmol), phenylboronic acid (700.0 mg, 5.7 mmol), Na_2CO_3 (763.0 mg, 7.2 mmol), and [$Pd(PPh_3)_4$] (83.0 mg, 0.072 mmol) in 30 mL of water/THF/toluene (1:1:1). The product was purified by column chromatography using a 6:4 mixture of hexanes/$CHCl_3$. The product was obtained as a white solid (172.0 mg, 60%).

^{1}H NMR (400 MHz, $CDCl_3$): δ = 8.14 (s, 2H; Ar-H), 7.31 (m, 6H; Ph-H), 7.15 (m, 4H; Ph-H), 6.90 (m, 6H; Ph-H) 6.81 ppm (m, 4H; Ph-H).

^{13}C NMR (100.6 MHz, $CDCl_3$): δ = 144.0, 139.6, 138.8, 136.9, 135.2, 132.3, 130.8, 130.6, 129.2, 127.7, 127.0, 126.2, 116.2, 109.6 ppm.

MS (MALDI-TOF, DCTB, +): *m/z* (%) = 482.2 ([M]$^+$, 100).

HRMS (MALDI-TOF, +): *m/z* calculated for $C_{36}H_{22}N_2$ [M]$^+$ 482.1783; found 482.1778

FT-IR (ATR), *ν*: 3058, 3024, 2924, 2226, 1807, 1598, 1575, 1555, 1493, 1412, 1374, 1223, 1028, 908, 757, 696, 525, 491 cm^{-1}.

5,6,7,8-Tetra(4-*tert*-butylphenyl)naphthalene-2,3-dicarbonitrile (31b)

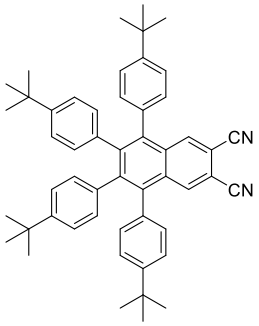

Prepared according to the general procedure; **23** (320.0 mg, 0.65 mmol), 4-*tert*-butylphenylboronic acid (926.0 mg, 5.2 mmol), Na_2CO_3 (690.0 mg, 6.5 mmol), and $[Pd(PPh_3)_4]$ (75.0 mg, 0.065 mmol) in 42 mL of water/THF/toluene (1:1:1). The product was purified by column chromatography using a 6:4 mixture of hexanes/$CHCl_3$,and obtained as a white solid (487.0 mg, 70%).

^{1}H NMR (400 MHz, $CDCl_3$): δ = 8.26 (s, 2H; Ar-H), 7.28 (d, J = 8 Hz, 4H; Ph-H), 7.03 (d, J = 8 Hz, 4H; Ph-H), 6.85 (d, J = 8 Hz, 4H; Ph-H), 6.64 (d, J = 8 Hz, 4H; Ph-H), 1.30 (s, 18H; *t*-Bu), 1.10 ppm (s, 18H; *t*-Bu).

^{13}C NMR (100.6 MHz, $CDCl_3$): δ = 150.3, 148.7, 144.6, 139.6, 136.1, 135.5, 134.1, 132.2, 130.6, 130.3, 124.8, 123.4, 116.5, 109.0, 34.5, 34.1, 31.2, 31.1 ppm.

MS (MALDI-TOF, DCTB + NaI, +): *m/z* (%) = 729.5 ($[M]^+$, 100).

HRMS (MALDI-TOF, +): *m/z* calculated for (+Na) $C_{52}H_{54}N_2Na$ $[M]^+$ 729.4179; found 729.4210, *m/z* calculated for $C_{52}H_{54}N_2$ $[M]^+$ 706.4282; found 706.4290

FT-IR (ATR), *ν*: 2961, 2904, 2868, 2233, 1612, 1509, 1462, 1394, 1363, 1269, 1117, 1019, 913, 833, 569 cm^{-1}.

3,6,9,12-Tetra-*tert*-butyldibenzo[fg,ij]naphtho[1,2,3,4-rst]pentaphene-16,17-dicarbonitrile (32)

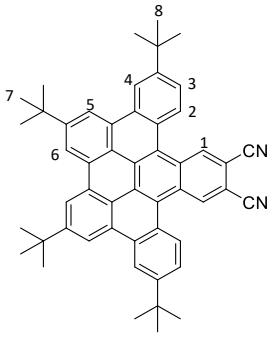

In a round-bottomed Schlenk flask a solution of **31b** (100.0 mg, 0.14 mmol) in 50 mL of dry dichloromethane was deoxygenated by bubbling argon for 10 min. The solution was cooled to 0 °C and DDQ (321.0 mg, 1.41 mmol) was added under argon atmosphere. After bubbling argon for 5 min more, triflic acid (0.4 mL, 4.2 mmol) was added. The reaction mixture was warmed up to room temperature and stirred overnight protected from light. After completion,the reaction was quenched with a saturated aqueous solution of $NaHCO_3$. The organic layer was separated, washed with brine, dried over anhydrous $MgSO_4$ and filtered. The organic solvent was removed under reduced pressure and the residue was purified by column chromatography (SiO_2, $CHCl_3$/Hexanes 1:1), yielding **32** as a yellow solid (63.1 mg, 64%).

^{1}H NMR (400 MHz, $CDCl_3$): δ = 9.59 (s, 2H; Ar-H^1), 9.10 (s, 2H; Ar-H^6), 9.03 (s, 2H; Ar-H^4), 8.91 (s, 2H; Ar-H^5), 8.65 (d, J = 8 Hz, 2H; Ar-H^2), 7.92 (dd, J_1 = 8, J_2 = 4 Hz, 2H; Ar-H^3), 1.74 (s, 18H; *t*-Bu-H^8), 1.63 ppm (s, 18H; *t*-Bu-H^7).

^{13}C NMR (100.6 MHz, $CDCl_3$): δ = 151.1, 136.2, 131.5, 130.8, 130.3, 129.1, 128.3, 126.2, 125.8, 124.4, 124.2, 121.7, 119.8, 119.6, 119.1, 116.8, 108.8, 35.8, 35.4, 31.8, 31.5 ppm.

MS (MALDI-TOF, DCTB, +): *m/z* (%) = 700.4 ([M]$^+$, 100).

HRMS (MALDI-TOF, +): *m/z* calculated for $C_{52}H_{48}N_2$ [M]$^+$ 700.3812; found 700.3814.

FT-IR (ATR), *ν*: 2955, 2906, 2868, 2227, 1607, 1515, 1478, 1464, 1393, 1368, 1249, 1260, 872, 841, 622, 526 cm^{-1}.

XRD: Single crystals suitable for X-ray diffraction analysis were obtained by vapor diffusion of methanol into a chloroform solution. Crystallographic data and some refining details are summarized in the following table:

Chemical formula	$C_{52}H_{48}N_2$	
Formula weight	700.97 g/mol	
Temperature	200(2) K	
Wavelength	0.71073 Å	
Crystal size	0.038 x 0.040 x 0.341 mm	
Crystal habit	Clear intense yellow prismatic	
Crystal system	monoclinic	
Space group	C 1 2/c 1	
Unit cell dimensions	a = 29.134(3) Å	α = 90°
	b = 19.126(4) Å	β = 108.4(3)°
	c = 34.663(5) Å	γ = 90°
Volume	18326.(4) $Å^3$	
Z	16	

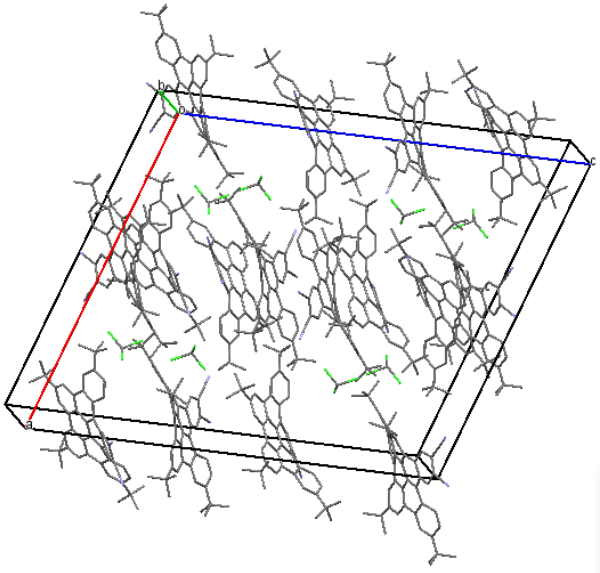

Figure 2.23. Unity cell and crystalline packing of **32**.

2.5.2 Synthesis of dodecafunctionalized subnaphthalocyanines

General procedure for the synthesis of axially chloro-substituted SubNcs:

An oven-dried, two-neck, round-bottom flask connected to a condenser and held under argon atmosphere, was charged with a naphthalene-2,3-dicarbonitrile precursor (1 mmol),dissolved in freshly distilled 1,2-dichlorobenzene and heated at 80 °C. BCl_3 (1 M in *p*-xylene, 2 mmol) was added *via* syringe under argon atmosphere, and the reaction mixture was refluxed for 2 hours. Once the reaction was completed (monitored by TLC), the solvent was removed under reduced pressure and the residue was chromatographed on silica gel or Bio-Beads™ S-X1 (200-400 mesh). The pure fraction of target material was triturated with methanol for 40 minutes, filtered, washed with a hexane-methanol mixture, and air-dried, to afford the desired product.

2,3,4,5,11,12,13,14,20,21,22,23-Dodecafluorosubnaphthalocyanato boron(III) chloride (33)

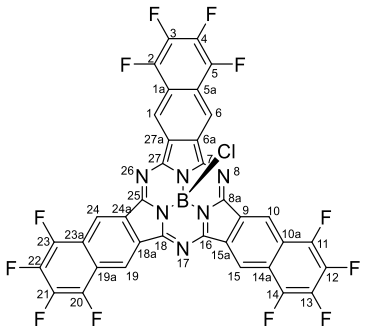

Prepared according to the general procedure; **21** (350.0 mg, 1.4 mmol), BCl_3 1 M/*p*-xylene (2.8 mL, 2.8 mmol) in 5 mL of 1,2-dichlorobenzene. Once the reaction was completed, the solvent was removed under reduced pressure, and the crude material was passed through a short silica gel column using a 4:1 mixture of toluene/THF as eluent. The solvent was removed and the residue was purified by column chromatography (silica gel; $CHCl_3$/*n*-hexane, 9:1) yielding a dark blue solid (136.8 mg, 37%).

^{1}H NMR (400 MHz, $CDCl_3$): δ = 9.67 ppm (s, 6H; Ar-H$^{1, 6, 10, 15, 19, 24}$).

MS (MALDI-TOF, DCTB, +): *m/z* (%) = 796.1 ($[M]^+$, 100), 778.1 ($[M]^+$– Cl + OH, 30).

HRMS (MALDI-TOF, +): *m/z* calculated for $C_{36}H_6BClF_{12}N_6$ $[M]^+$ 796.0245; found 796.0272.

FT-IR (ATR), *ν*: 1673, 1595, 1494, 1364, 1214, 1176, 1044, 989, 948, 880, 792, 706 cm^{-1}.

UV/Vis (toluene): λ_{max} (log ε/dm^3 mol^{-1} cm^{-1}) = 646 (5.0), 590 (4.7), 467 (3.7) nm.

Fluorescence (toluene): λ_{ex} = 640 nm; λ_{max} = 666 nm.

mp: > 400 °C

XRD: Single crystals suitable for X-ray diffraction analysis were obtained by vapor diffusion of methanol into its chloroform solution. Crystallographic data and some refining details are summarized in the following table:

Chemical formula	$C_{36}H_6BClF_{12}N_2$	
Formula weight	796.73 g/mol	
Temperature	296(2) K	
Wavelength	0.71073 Å	
Crystal size	0.010 x 0.020 x 0.180 mm	
Crystal habit	Dark purple needle	
Crystal system	monoclinic	
Space group	P 1 21/n 1	
Unit cell dimensions	a = 15.2360(16) Å	α = 90°
	b = 7.5104(8) Å	β = 98.470(5)°
	c = 26.630(3) Å	γ = 90°
Volume	3014.0(6) $Å^3$	
Z	4	

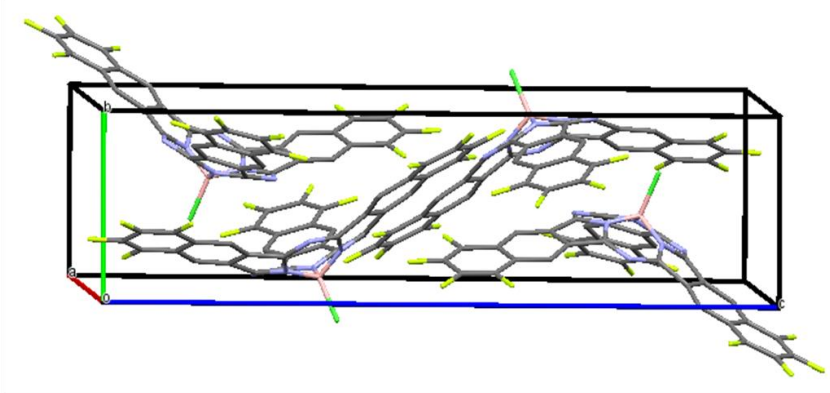

Figure 2.23. Unity cell and crystalline packing of **33**.

2,3,4,5,11,12,13,14,20,21,22,23-Dodecafluorosubnaphthalocyanato boron(III) chloride (34)

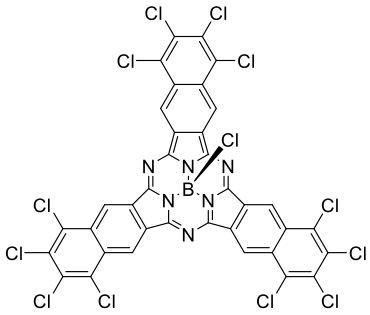

Prepared according to the general procedure; **34** (500.0 mg, 1.6 mmol), BCl_3 1 M/*p*-xylene (3.2 mL, 3.2 mmol) in 10 mL of 1,2-dichlorobenzene. Once the reaction was completed, the solvent was removed under reduced pressure, and the residue was loaded on a short pad of compressed celite. The celite pad was washed with several portions of methanol, cold chloroform, and cold toluene. Then, the product was solubilized by washing the pad several times with hot toluene. The filtrate was evaporated under reduced pressure and the product was obtained as a dark blue solid (284.0 mg, 54%). This compound is insoluble in common organic solvents.

MS (MALDI-TOF, DCTB, +): *m/z* (%) = 993.7 ($[M]^+$, 100).

FT-IR (ATR), *ν*: 2953, 2925, 2855, 1555, 1467, 1349, 1300, 1266, 1232, 1190, 1143, 1106, 1070, 1000, 804, 776, 741, 706 cm^{-1}.

UV/Vis (toluene): λ_{max} (log ε/dm^3 mol^{-1} cm^{-1}) = 655 (4.9), 600 (sh), 480 (3.8) nm.

Fluorescence (toluene): λ_{ex} = 650 nm; λ_{max} = 668 nm.

mp: > 400 °C

2,3,4,5,11,12,13,14,20,21,22,23-Dodeca(pentylthio)subnaphthalocyanato boron(III) chloride (39)

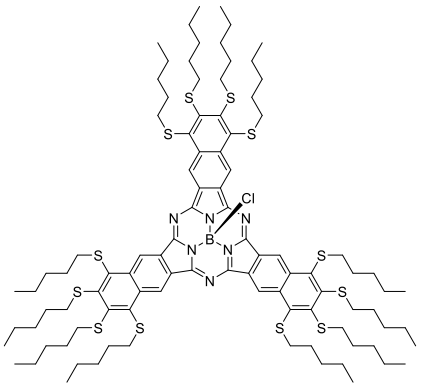

Prepared according to the general procedure; **29** (149.0 mg, 0.5 mmol), BCl_3/1 M in *p*-xylene (0.8 mL, 0.8 mmol) in 3 mL of 1,2-dichlorobenzene at 120 °C for 20 min. The solvent was removed under reduced pressure, and the residue was passed through a pad of compressed celite using 9:1 mixture of *n*-hexane/ethyl acetate. Then, the solvent was removed and the residue was purified by column chromatography on Bio-Beads^{TM} S-X1 (200-400 mesh) using chloroform as the eluent, to give the target material as a dark green, viscous solid (38.0 mg, 25%).

^{1}H NMR (400 MHz, $CDCl_3$): δ = 10.38 (s, 6H; Ar-H$^{1, 6, 10, 15, 19, 24}$), 3.21–3.12 (m, 24H; 12×SCH_2Bu), 1.57–1.24 (m, 72H; CH_2), 0.86–0.80 ppm (m, 12H; CH_3).

^{13}C NMR (100.6 MHz, $CDCl_3$): δ = 149.3, 146.9, 141.8, 135.5, 129.4, 123.1, 38.7, 38.1, 31.1, 31.0, 30.9, 29.5, 29.3, 22.3, 22.2, 13.9 ppm.

MS (MALDI-TOF, DCTB, +): *m/z* (%) = 1806.7 ([M]$^+$, 100).

HRMS (MALDI-TOF, +): *m/z* calculated for $C_{36}H_6BClF_{12}N_6$ [M]$^+$ 796.0245; found 796.0272.

FT-IR (ATR), *ν*: 2955, 2924, 2855, 1731, 1636, 1498, 1337, 1217, 1177, 1108, 799, 723, 701, 466 cm^{-1}.

UV/Vis (toluene): λ_{max} (log ε/dm^3 mol^{-1} cm^{-1}) = 676 (4.9), 614 (4.4), 495 (4.0) nm.

Fluorescence (toluene): λ_{ex} = 675 nm; λ_{max} = 696 nm.

2,3,4,5,11,12,13,14,20,21,22,23-Dodeca(pentylsulfonyl)subnaphthalocyanato boron(III) chloride (40)

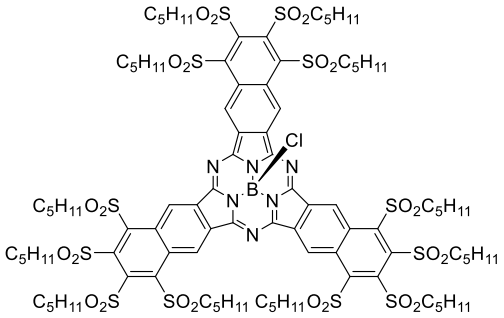

Prepared according to the general procedure; **30** (350.0 mg, 0.5 mmol), BCl_3/1 M in *p*-xylene (1.0 mL,1.0 mmol) in 5 mL of 1,2-dichlorobenzene. Once the reaction is completed, the solvent was removed under reduced pressure, and the crude material was passed through a pad of compressed celite using 9:1 mixture of *n*-hexane/ethyl acetate. Then, the solvent was evaporated and the residue was purified by column chromatography on Bio-Beads^{TM} S-X1 (200-400 mesh) using toluene as the eluent. The dark violet fraction was passed again through a pad of compressed celite using toluene. The product was triturated with methanol for 40 minutes, filtered and washed with a hexane-methanol mixture, to give the target material as a dark violet solid (165.0 mg, 45%).

^{1}H NMR (400 MHz, $CDCl_3$): δ = 10.89 (s, 3H; Ar-H$^{1, 6, 10, 15, 19, 24}$), 10.79 (s, 3H; Ar-H$^{1, 6, 10, 15, 19, 24}$), 4.64 – 4.19 (m, 16H; 8×SO_2CH_2Bu), 4.01 – 3.93 (m, 4H; 2×SO_2CH_2Bu), 3.66 – 3.59 (m, 4H; 2×SO_2CH_2Bu), 2.48 – 2.04 (m, 24H; 12×CH_2), 1.87 – 1.37 (m, 48H; 24×CH_2), 1.10 (t, J = 7.6 Hz, 9H; 3×CH_3), 1.03 – 0.97 (m, 18H; 6×CH_3) 0.90 ppm (t, J = 7.2 Hz, 9H; 3×CH_3).

^{13}C NMR (100.6 MHz, $CDCl_3$): δ = 152.8, 152.2, 149.7, 149.5, 148.1, 131.7, 131.6, 130.9, 123.0, 122.8, 63.0, 62.8, 57.5, 57.4, 30.7, 30.5, 30.3, 23.5, 22.3, 22.0, 20.9, 20.8, 13.8, 13.6 ppm;

MS (MALDI-TOF, DCTB, +): *m/z* (%) = 2190.6 ($[M]^+$, 100).

HRMS (MALDI-TOF, +): *m/z* calculated for $C_{96}H_{138}BClN_6O_{24}S_{12}$ $[M]^+$ 2190.6202; found 2190.6105.

FT-IR (ATR), *ν*: 2957, 2931, 2872, 1465, 1316, 1146, 1092 (S=O), 705, 619 cm^{-1}.

UV/Vis (toluene): λ_{max} (log ε/dm^3 mol^{-1} cm^{-1}) = 677 (5.0), 533 (4.3), 324 (5.0) nm.

Fluorescence (toluene): λ_{ex} = 670 nm; λ_{max} = 702 nm.

mp: 240 – 242 °C (decomposition).

2,3,4,5,11,12,13,14,20,21,22,23-Dodeca(4-*tert*-butylphenyl)subnaphthalocyanato boron(III) chloride (41b)

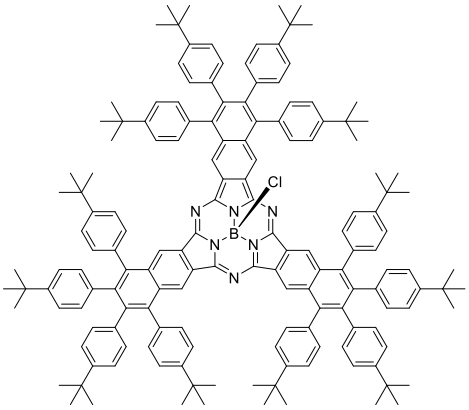

Prepared according to the general procedure; **31b** (332.0 mg, 0.5 mmol), BCl_3/1 M in *p*-xylene (1.0 mL, 1.0 mmol) in 5 mL of 1,2-dichlorobenzene at 120 °C for 30 min. The solvent was removed under reduced pressure, and the residue was passed through a pad of compressed celite using *n*-hexane. Then, the solvent was evaporated and the residue was purified by column chromatography on Bio-Beads™ S-X1 (200-400 mesh) using chloroform as the eluent, to give the target material as a dark green solid (29.0 mg, 8%).

^{1}H NMR (400 MHz, $CDCl_3$): δ = 9.61 – 9.32 (m, 6H; Ar-$H^{1, 6, 10, 15, 19, 24}$), 7.39 – 7.10 (m, 24H; Ar), 6.90 – 6.64 (m, 24H; Ar), 1.34 (s, 54H; *t*-Bu), 1.11 ppm (s, 54H; *t*-Bu).

^{13}C NMR (100.6 MHz, $CDCl_3$): δ = 149.4, 147.7, 147.2, 141.8, 140.2, 137.6, 136.1, 132.1, 131.5, 131.2, 130.7, 130.5, 128.7, 124.7, 124.3, 123.1, 123.0, 122.2, 34.5, 34.1, 31.6, 31.4, 31.2 ppm;

MS (MALDI-TOF, DCTB, +): *m/z* (%) = 2165.3 ($[M]^+$, 100).

FT-IR (ATR), ν: 2958, 2924, 2855, 1732, 1641, 1462, 1361, 1268, 1116, 1018, 833, 569 cm^{-1}.

UV/Vis (toluene): λ_{max} (log ε/dm^3 mol^{-1} cm^{-1}) = 674 (4.9), 532 (3.5), 476 (3.5), 305 (5.0) nm.

Fluorescence (toluene): λ_{ex} = 670 nm; λ_{max} = 688 nm.

π-conjugated SubNc 42

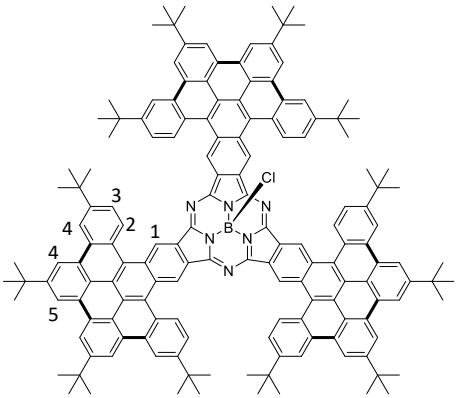

Prepared according to the general procedure; **32** (150.0 mg, 0.21 mmol), BCl_3/1 M in *p*-xylene (0.4 mL, 0.4 mmol) in 4 mL of 1,2-dichlorobenzene at 180 °C for 30 min. The solvent was removed under reduced pressure, and the residue was passed through a pad of silica gel using chloroform. Then, the solvent was evaporated and the residue was purified by column chromatography on Bio-Beads™ S-X1 (200-400 mesh) using chloroform as the eluent and protected from light, to give the target material as a green solid (9.0 mg, 6%).

^{1}H NMR (400 MHz, $CDCl_3$): δ = 10.53 (br s, 6H; Ar-H^1), 9.37 (d, *J* = 8.0 Hz, 6H; H^2), 8.92 (s, 6H; H^4), 8.88 (s, 6H; H^4), 8.15 (d, *J* = 8.0 Hz, 6H; H^3), 8.09 (s, 6H; H^5), 1.72 (s, 54H; *t*-Bu), 1.65 ppm (s, 54H; *t*-Bu).

^{13}C NMR (100.6 MHz, $CDCl_3$): δ= 165.4, 150.8, 149.8, 133.7, 130.5, 130.1, 129.7, 127.7, 125.7, 122.6, 119.6, 118.9, 118.5, 35.6, 35.3, 31.8, 31.4, 29.7, 29.4 ppm.

MS (MALDI-TOF, DCTB, +): *m/z* (%) = 2149.2 ($[M]^+$, 100).

HRMS (MALDI-TOF, +): *m/z* calculated for $C15_6H_{144}BClN_6$ $[M]^+$ 2148.1272; found 2148.1322.

FT-IR (ATR), *ν*: 2960, 2907, 2867, 1731, 1607, 1477, 1366, 1286, 1175, 1064, 935, 793, 704, 438 cm^{-1}.

UV/Vis (toluene): λ_{max} (log ε/dm^3 mol^{-1} cm^{-1}) = 715 (5.3), 645 (4.5), 522 (4.5), 398 (4.7), 305(5.3) nm.

Fluorescence (toluene): λ_{ex} = 700 nm; λ_{max} = 738 nm.

General procedure for the synthesis of axially phenoxy-substituted SubNcs:

A Schlenk tube of 50 mL held under argon atmosphere was charged with the corresponding X_{12}-SubNc-(Cl) (1 mmol)and silver trifluoromethanesulfonate (1.25 mmol), and dissolved in freshly distilled toluene. The reaction mixture was stirred at 60 ºC under argon atmosphere overnight. Once the X_{12}-SubNc-(Triflate) is generated, 4-*tert*-butylphenol (3 eq) and DIPEA (1.25 eq) were added in one portion, and the mixture was stirred at 80 ºC until the reaction was complete (monitored by TLC). The solvent was removed under reduced pressure, and the residue was purified by column chromatography on silica gel. The pure fraction was triturated with methanol for 40 minutes, filtered, washed with a *n*-hexane-methanol mixture, and air-dried to afford the desired product.

4-*tert*-Butylphenoxy[2,3,4,5,11,12,13,14,20,21,22,23-dodecachlorosubnaphthalocyanato] boron(III) (36)

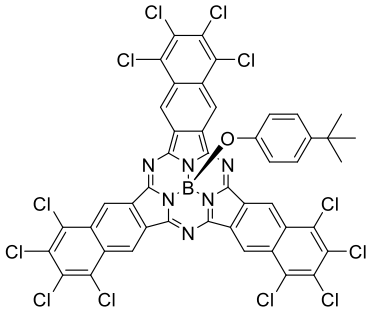

Prepared according to the general procedure; **34** (75.0 mg, 0.08 mmol), AgOTf (25.7 mg, 0.1 mmol) in 20 mL of toluene for 24 hours. 4-*tert*-Butylphenol (36.0 mg, 0.24 mmol) and DIPEA (12.9 mg, 0.10 mmol), 24 hours. The solvent was evaporated under reduced pressure and the product was purified by column chromatography (silica gel; 8:2 mixture of toluene/*n*-hexane,) yielding a blue solid (46.1 mg, 52%).

^{1}H NMR (400 MHz, $CDCl_3$): δ = 9.80 (s, 6H; Ar-$H^{1, 6, 10, 15, 19, 24}$), 6.85 (d, J = 8.8 Hz, 2H; $H^{b, b'}$), 5.55 (d, J = 8.8 Hz, 2H; $H^{a, a'}$), 1.09 ppm (s, 9H; *t*-Bu).

MS (MALDI-TOF, DCTB, +): *m/z* (%) = 1107.8 ($[M]^+$, 100).

HRMS (MALDI-TOF, +): *m/z* calculated for $C_{46}H_{19}BCl_{12}N_6O$ $[M]^+$ 1107.7899; found 1107.7890

FT-IR (ATR), *ν*: 2923, 2852, 1673, 1597, 1495 S*, 1365, 1276, 1261, 1171, 1045, 989, 973, 894, 880, 764, 750, 707, 517, 491, 439 cm^{-1}

UV/Vis (toluene): λ_{max} (log ε) = 651 (4.9), 595 (sh), 482 (3.9) nm.

Fluorescence (toluene): λ_{ex} = 650 nm; λ_{max} = 670 nm.

mp: > 400 °C.

4-*tert*-Butylphenoxy[2,3,4,5,11,12,13,14,20,21,22,23-dodecachlorosubnaphthalocyanato] boron(III) (37)

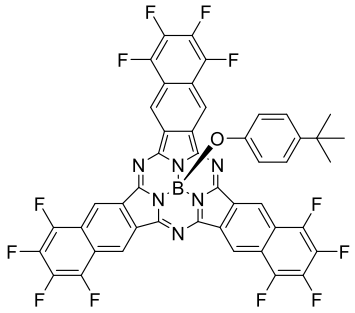

Prepared according to the general procedure; **33** (30.0 mg, 0.04 mmol), AgOTf (12.8 mg, 0.05 mmol) in 5 mL of toluene for 18 hours. 4-*tert*-Butylphenol (31.0 mg, 0.12 mmol) and DIPEA (6.5 mg, 0.05 mmol) for 18 hours. The solvent was evaporated under reduced pressure and the product was purified by column chromatography (silica gel; 6:4 mixture of $CHCl_3$/*n*-hexane,) yielding a blue solid (24.0 mg, 65%).

^{1}H NMR (400 MHz, $CDCl_3$): δ = 9.58 (s, 6H; Ar-$H^{1, 6, 10, 15, 19, 24}$), 6.82 (d, J = 8.8 Hz, 2H; $H^{b, b'}$), 5.50 (d, J = 8.8 Hz, 2H; $H^{a, a'}$), 1.09 ppm (s, 9H; *t*-Bu).

^{13}C NMR (100.6 MHz, $CDCl_3$): δ = 150.2, 149.5, 144.6, 141.9, 140.0, 137.4, 129.5, 126.0, 120.1, 120.0, 119.9, 117.9, 115.2, 33.9, 31.3 ppm.

MS (MALDI-TOF, DCTB, +): *m/z* (%) = 910.2 ($[M]^+$, 100), 761.1 ($[M]^+$–axial ligand, 15).

HRMS (MALDI-TOF, +): *m/z* calculated for $C_{46}H_{19}BF_{12}N_6O$ $[M]^+$ 910.1524; found 910.1536.

FT-IR (ATR), *ν*: 3101, 2956, 2925, 2855, 1673, 1597, 1496, 1364, 1240, 1171, 988, 879, 833, 706, 635, 530 cm^{-1}

UV/Vis (toluene): λ_{max} (log ε) = 640 (4.9), 586 (sh), 467 (3.8) nm.

Fluorescence (toluene): λ_{ex} = 640 nm; λ_{max} = 657 nm.

mp: > 400 °C

Pentafluorophenoxy[2,3,4,5,11,12,13,14,20,21,22,23-dodecachlorosubnaphthalocyanato] boron(III) (38)

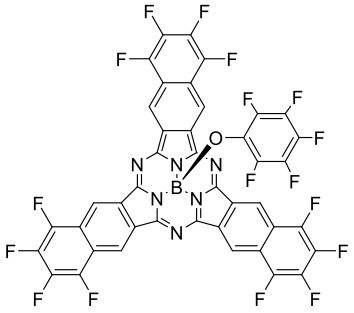

Prepared according to the general procedure; **33** (83.0 mg, 0.1 mmol), AgOTf (54 mg, 0.21 mmol) in 5 mL of toluene for 18 hours. Pentafluorophenol (31.0 mg, 0.12 mmol) and DIPEA (16.2 mg, 0.05 mmol) for 18 hours. The solvent was evaporated under reduced pressure and the product was purified by column chromatography (silica gel; 6:4 mixture of $CHCl_3$/*n*-hexane) yielding a blue solid (42.0 mg, 44%).

^{1}H NMR (400 MHz, $CDCl_3$): δ = 9.65 ppm (s, 6H; Ar-H$^{1, 6, 10, 15, 19, 24}$).

MS (MALDI-TOF, DCTB, +): *m/z* (%) = 944.1 ($[M]^+$, 100), 761.1 ($[M]^+$–axial ligand, 20).

HRMS (MALDI-TOF, +): *m/z* calculated for $C_{46}H_6BF_{17}N_6O$ $[M]^+$ 944.0426; found 944.0415.

FT-IR (ATR), *ν*: 2923, 2851, 1673, 1597, 1406, 1365, 1275, 1171, 1045, 989, 893, 880, 764, 750, 707, 516 cm^{-1}

UV/Vis (toluene): λ_{max} (log ε) = 644 (4.9), 589 (sh), 466 (3.8), 394 (3.7) nm.

Fluorescence (toluene): λ_{ex} = 640 nm; λ_{max} = 664 nm.

mp: > 400 °C.

CHAPTER 3

Applications of Subnaphthalocyanines and Subporphyrazines in Photovoltaic Devices

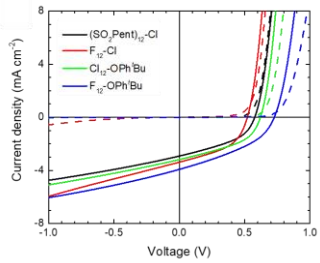

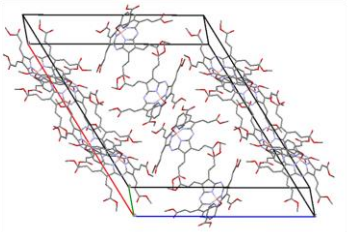

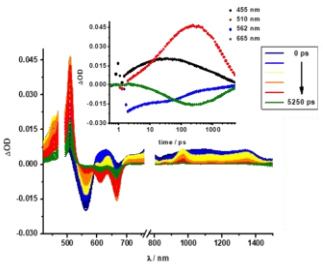

3.1 Solar Energy and Photovoltaic Devices

Sunlight is the most abundant renewable energy source and underpins life on our planet. Nature has developed complex photosynthetic processes to harvest this light for the generation of chemical energy.[93] While chemical energy supports the natural world, electrical energy is a more easily transmittable form in human societies. As a matter of fact, solar energy alone possesses the potential of becoming the successor of fossil fuels, which will cover the world's current energetic needs.[94] Sunlight strikes the Earth's surface every hour with enough energy to supply world consumption per annum. This is by far the biggest source of energy available to us, and a great candidate for a transition to a more sustainable production of energy. Consequently, harvesting sunlight for the generation of electrical energy is highly desirable, and great developments in the conversion efficiency of photovoltaic (PV) cells have been made over the last 50 years. A desire for low-cost, low toxicity, large-area, thin-film technologies has led to organic photovoltaic cells showing promise to satisfy all of these properties.[95]

The development of new materials and technologies based on photovoltaic devices for solar energy conversion involves many areas of chemistry and physics, including design and synthesis of materials, experimental and theoretical characterization of materials and processes, as well as device construction and characterization. PV technology exhibits a series of remarkable merits such as the following:

1. Possibility to be scaled from the KW to the GW scale without affecting efficiency and economic performance.

[93] a) N. S. Lewis, D. G. Nocera, *Proc. Natl. Acad. Sci.* **2006**, *103*, 15729−15735; b) A. J. Nozik, J. Miller, *Chem. Rev.* **2010**, *110*, 6443−6445; c) M. F. Hohmann-Marriott, R. E. Blankenship, *Annu. Rev. Plant Biol.* **2011**, *62*, 515−548; d) G. D. Scholes, G. R. Fleming, A. Olaya-Castro, R. van Grondelle, *Nat. Chem.* **2011**, *3*, 763−774.

[94] Q. Schiermeier, J. Tollefson, T. Scully, A. Witze, O. Morton, *Nature* **2008**, *454*, 816–823.

[95] C. J. Brabec, *Sol. Energy Mater. Sol. Cells* **2004**, *83*, 273−292.

2. An up-front investment followed by decades of electricity produced by a 100% guaranteed free primary source.

3. No moving parts, implying negligible wear and very low maintenance cost.

4. Installation possible on existing platforms (e.g., roofs) with no land consumption.

5. Decentralization of the electricity production system, as needed to enhance energy security.

6. Possibility of providing electricity to communities in off grid rural or isolated areas, improving the quality of life in underdeveloped regions.[96]

Solar energy can be transformed into electricity either thermodynamically or electronically. In the first method, the solar thermal energy is usually focused in the design of optical collectors to generate electricity by heating a fluid to drive a turbine connected to an electrical generator. The second method, converts directly the solar energy into electricity by opto-electronic devices, called solar cells. Light shining on the solar cell produces both a current and a voltage to generate electric power. This process requires firstly, a material in which the absorption of light raises an electron to a higher energy state, and secondly, the movement of this higher energy electron from the solar cell into an external circuit. The electron then dissipates its energy in the external circuit and returns to the solar cell. A variety of materials and processes can potentially satisfy the requirements for photovoltaic energy conversion, but in practice, nearly all photovoltaic energy conversion uses semiconductor materials in the form of a p-n junction.[97]

The efficient production of electricity by means of solar cells is nowadays available and PV is one of the fastest growing, renewable energy technology.

[96] N. Armaroli, V. Balzani, *Chem. Eur. J.* **2016**, *22*, 32–57.

[97] a) C. Richter, D. Lincot, C. A. Gueymard, *Solar Energy*; Solar Energy; Springer New York, **2012**; b) B. Norton, *Harnessing Solar Heat*; Lecture Notes in Energy; Springer Netherlands, **2016**.

3.1.1 Inorganic solar cells

Over 90% of today's commercial solar cells are still based on the same material and basic concepts developed at the Bell Laboratories in the early 1950s:[98] light-induced charge separation at a p–n junction between two slices (wafers) of doped silicon in either single-crystal, or polycrystalline form (sc-Si and poly-Si, respectively). Both mono- and polycrystalline solar cells are known as 1st generation solar cells. Their maximum efficiencies, 25.0% and 20.4%, respectively, are close to the Shockley–Queisser theoretical limit, i.e., 33% (Figure 3.1).[99] Nevertheless, this type of solar cells presents an important drawback: their elevated production cost. This is mainly due to the high and prolonged temperatures required to achieve large and ultrapure silicon single crystals, which has promoted the search for alternative, cheaper materials to use in photovoltaics.

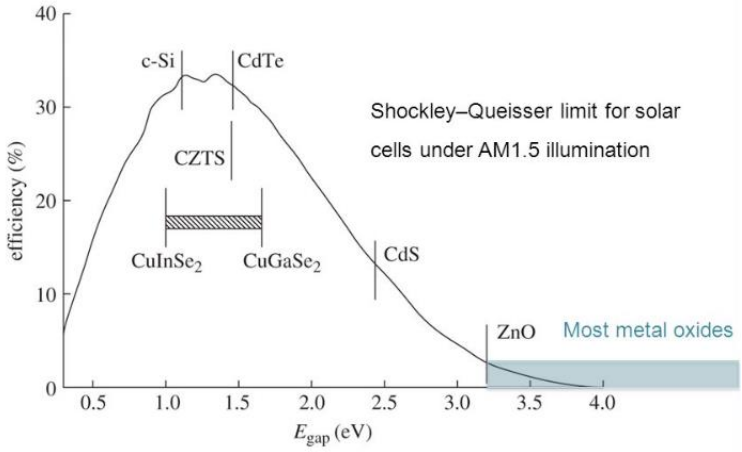

Figure 3.1. Maximum theoretical efficiency (Shockley–Queisser limit) for solar cells.[99a]

In the early 60s, the 2nd generation of PV cells appeared: *thin film inorganic solar cells*, based primarily on chemical vapour deposited amorphous silicon (a-Si, maximum efficiency of 13.4%), as well as polycrystalline indium or cadmium telluride (InSe or

[98] D. M. Chapin, C. S. Fuller, G.L. A. Pearson, *J. Appl. Phys.* **1954**, *25*, 676–677.
[99] a) W. Shockley, H. J. Queisser, *J. Appl. Phys*. **1961**, *32*, 510; b) C. A. Nelson, N. R. Monahan, X. –Y. Zhu, *Energy Environ. Sci.* **2013**, *6*, 3508–3519.

CdTe, maximum efficiency of 21.5%) or copper gallium indium selenide ($CuInGaSe_2$, known as CIGS with maximum efficiency of 21.7%).[100] The main downsides of this second generation are the employment of hazardous toxic materials in the devices and the resource scarcity of the materials needed. These gave rise to the third generation of photovoltaic cells, based on environmentally friendly materials that allow inexpensive solvent-based fabrication techniques. Leading examples are low-cost, thin-film solar cells based on novel concepts, like hot carrier solar cells, multiple exciton generation, tandem, or multijunction solar cells.[101] The third generation has the aim of reducing production costs, as well as exceeding the Shockley and Queisser efficiency limit.[102,99b]

3.1.2 Organic photovoltaics (OPV)

All-organic photovoltaics, as well as *hybrid solar cells*, are considered also as a type of 3rd generation devices, and have the merits of low cost, stability, simple fabrication and flexibility.[103] By means of these cells, the Shockley-Queisser limit, as defined for 1st generation solar cells, is expected to be surpassed.

In the late 50s and 60s, semiconducting properties were discovered for many important biological molecules, like carotenes and chlorophylls, and many other common dyes, such as methylene blue, porphyrins and related synthetic analogues, such as phthalocyanines. These dyes were among the first organic materials exhibiting the photovoltaic effect. As early as 1958, Kearns et al. reported the photovoltaic effect of a cell based on a single layer of magnesium(II) phthalocyanine, which had a photovoltage of 200 mV.[104] From then on, organic materials have gained broader interest and several new concepts associated to the configuration of the device have

[100] a) H.W. Schock, *Appl. Surf. Sci*. **1996**, *92*, 606; b) L. M. Peter, *Phil. Trans. R. Soc. A* **2011**, *369*, 1840.
[101] M. A. Green, in *Third Generation Photovoltaics*, Springer-Verlag, Berlin, **2003**.
[102] a) M. A. Green, *Prog. Photovoltaics* **2001**, *9*, 123.
[103] a) F. G. Brunetti, R. Kumar, F. Wudl, *J. Mater. Chem*. **2010**, *20*, 2934; b) J. L. Delgado, P.-A. Bouit, S. Filippone, M. A. Herranz, N. Martin, *Chem. Comm*. **2010**, *46*, 4853; c) J. Yan, B. R. Saunders, *RSC Adv*. **2014**, *4*, 43286; d) K. A. Mazzio, C. K. Luscombe, *Chem. Soc. Rev*. **2015**, *44*, 78; e) M.-E. Ragoussi, T. Torres, *Chem. Commun***. 2015**, *51*, 3957.
[104] D. Kearns, M. Calvin, *J. Chem. Phys.* **1958**, *29*, 950–951.

been presented. A milestone came in 1986 when Tang used a two component, donor/acceptor active layer (planar bilayer heterojunction, PHJ, or p-n solar cell, Figure 3.2a).[105] This structural modification benefits from the facile formation of the charge carriers (electrons and holes) by electron transfer from the photoexcited donor to the acceptor component. Also, the separated charge transport layers ensure connectivity with the correct electrode and give the separated charge carriers only a small chance to recombine with their counterparts. The drawback of this methodology is that only excitons (i.e., electron-hole pairs formed by light excitation) formed very close to the interface between donor and acceptor layers are able to dissociate. To overcome this structural problem, the concept of bulk-heterojunction (BHJ, Figure 3.2b) was introduced by Yu *et al.*,[106] in which a blend of a donor and an acceptor with a bicontinual phase separation is formed.[107] The advantage of this type of cell is the large interpenetrated area, which results in a dramatic increase of the contact area, enhancing a more efficient charge separation.

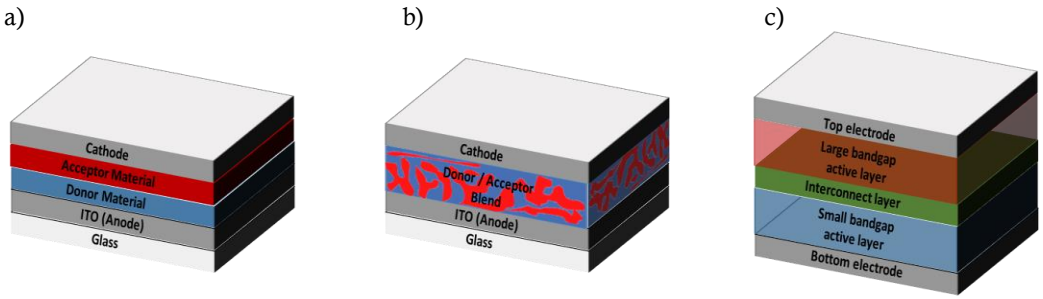

Figure 3.2. Schematic representation of (a) PHJ solar cell, (b) BHJ solar cell, and (c) tandem solar cell.

Ultimately, another type of architectures called tandem solar cells (Figure 3.2c), have gained much attention. They consist in a combination of two or more single junction cells (one on top of the other) that absorb in different wavelength ranges. Their advantage is that a combination of absorbing molecules can allow for a large spectral

[105] a) C. W. Tang, *Appl. Phys. Lett*. **1986**, *48*, 183; b) C. W. Tang, *US* Patent, 4, 164, 431, **1979**.
[106] G. Yu, J. Gao, J. C. Hummelen, F. Wudl, A. J. Heeger, *Science* **1995**, *270*, 1789.
[107] a) M. Hiramoto, H. Fujiwara, M. Yokoyama, *Appl. Phys. Lett*. **1991**, *58*, 1062; b) J. J. M. Halls, C. A. Walsh, N. C. Greenham, E. A. Marseglia, R. H. Friend, S. C. Moratti, A. B. Holmes, *Nature* **1995**, *376*, 498.

coverage with efficient absorption, which would be difficult to obtain with a single heterojunction.[108]

From a different point of view, another classification of the organic solar cells based on the active material can be established: *polymer-based photovoltaic cells*, also known as plastic solar cells,[109] which are constituted by conjugated polymers; and *small molecule-based photovoltaic devices*, in which discrete chromophores form the active layer.[110] Regarding efficiencies, while polymeric tandem solar cells have reached a conversion efficiency of 12%,[111] it is worth noting that the record in multi-junction architectures is held by Heliatek,[112] who reported a tandem, oligomer-based device with a certified power conversion efficiency of 13.2%. The best conversion efficiency for a single junction device has been achieved by Toshiba Corporation, reaching a 11.2% value.[113]

---

[108] a) J. Y. Kim, K. Lee, N. E. Coates, D. Moses, T.-Q. Nguyen, M. Dante, A. J. Heeger, *Science* **2007**, *317*, 222; b) A. Hadipour, B. de Boer, P. W. M. Blom, *Adv. Funct. Mater*. **2008**, *18*, 169; c) T. Ameri, G. Dennler, C. Lungenschmied, C. J. Brabec, *Energy Environ. Sci*. **2009**, *2*, 347; d) M. Riede, C. Uhrich, J. Widmer, R. Timmreck, D. Wynands, G. Schwartz, W.-M. Gnehr, D. Hildebrandt, A. Weiss, J. Hwang, S. Sundarraj, P. Erk, M. Pfeiffer, K. Leo, *Adv. Funct. Mater.* **2011**, *21*, 3019; f) S. Sista, Z. Hong, L.-M. Chen, Y. Yang, *Energy Environ. Sci*. **2011**, *4*, 1606; g) T. Ameri, N. Li, C. J. Brabec, *Energy Environ. Sci*. **2013**, *6*, 2390; h) J. You, L. Dou, Z. Hong, G. Li, Y. Yang, *Prog. Polym. Sci*. **2013**, *38*, 1909; i) O. Adebanjo, B. Vaagensmith, Q. Qiao, *J. Mater. Chem. A* **2014**, *2*, 10331.

[109] a) C. J. Brabec, N. S. Saricifti, J. C. Hummelen, *Adv. Funct. Mat*. **2001**, *11*, 15; b) J. Peet, M. L. Senatore, A. J. Heeger, G. C. Bazan, *Adv. Mater*. **2009**, *21*, 1521; c) C. J. Brabec, S. Gowrisanker, J. J. M. Halls, D. Laird, S. Jia, S. P. Williams, *Adv. Mater*. **2010**, *22*, 3839; d) J. Peet, A. J. Heeger, G. C. Bazan, *Acc. Chem. Res*. **2009**, *42*, 1700; e) D. Gendron, M. Leclerc, *Energy Environ. Sci*. **2011**, *4*, 1225; f) L. Lu, T. Zheng, Q. Wu, A. M. Schneider, D. Zhao, L. Yu, *Chem. Rev.* **2015**, *115*, 12666.

[110] a) A. Mishra, P. Bauerle, *Angew. Chem. Int. Ed.* **2012**, *51*, 2020; b) Y. Lin, Y. Li, X. Zhan, *Chem. Soc. Rev.* **2012**, *41*, 4245.

[111] S. Li, L. Ye, W. Zhao, S. Zhang, S. Mukherjee, H. Ade, J. Hou, *Adv. Mater.* **2016**, *28*, 9423–9429.

[112] Heliatek. Heliatek sets new Organic Photovoltaic world record efficiency of 13.2% http://www.heliatek.com/en/press/press-releases/details/heliatek-sets-new-organic-photovoltaic-world-record-efficiency-of-13-2.

[113] a) S. Mori, H. Oh-oka, H. Nakao, T. Gotanda, Y Nakano, H. Jung, A. Iida, R. Hayase, N. Shida, M. Saito, *et al. MRS Proc. 1737*; b) M. A. Green, Y. Hishikawa, E. D. Dunlop, D. H. Levi, J. Hohl-Ebinger, A. W. Ho-Baillie, *Prog. Photovoltaics Res. Appl.* **2018**, *26*, 3–12.

3.1.3 Dye-Sensitized Solar Cells (DSSCs)

Apart from the fully organic solar cells, combinations of organic-inorganic materials have been of great relevance in recent years. In this sense, the development of DSSCs in the 90s opened up new horizons in the area of photovoltaics, and entered dynamically the race for cost-efficient devices functioning at the molecular and nanoscale levels.[114] The seminal paper by O'Regan and Grätzel in 1991[115] introduced a pioneering architecture, an n-type DSSC, in which an organic light-absorbing dye is anchored to a mesoporous inorganic n-type semiconductor film (this semiconductor operates as photoanode) and filled in with a redox-active electrolyte. This type of DSSCs has shown a good potential and, in the future, it could turn out to be a good alternative to the standard silicon photovoltaics,[116] thanks to the already obtained efficiencies. Currently the PCEs have grown from 7% in the seminal report,[115] using ruthenium complexes as the dye, to the current 13.0% employing porphyrins as sensitizers, which leave out the need for rare and costly, ruthenium-based sensitizers as a requirement for high efficiencies.[117] Alternatively, p-type DSSCs (an active photocathode) have been also explored but they have not exhibited yet energy conversion values as high as conventional DSSCs. This has been ascribed to drawbacks associated with the electrolytes and the p-type semiconductors,[118] and to date, there is just one example of "comparable" efficiency, i.e., 2.51%.[119] Other important point is

[114] a) A. Hagfeldt, G. Boschloo, L. Sun, L. Kloo, H. Pettersson, *Chem. Rev*. **2010**, *110*, 6595; b) M. K. Nazeeruddin, E. Baranoff, M. Grätzel, *Solar Energy* **2011**, *85*, 1172; c) J. Albero, P. Atienzar, A. Corma, H. García, *Chem. Rec*. **2015**, *15*, 803.

[115] B. O'Regan, M. Grätzel, *Nature* **1991**, *353*, 737.

[116] H. S. Jung, J.-K. Lee, *J. Phys. Chem. Lett*. **2013**, *4*, 1682.

[117] S. Mathew, A. Yella, P. Gao, R. Humphry-Baker, B. F. E. Curchod, N. Ashari-Astani, I. Tavernelli, U. Rothlisberger, M. K. Nazeeruddin, M. Grätzel, *Nat. Chem*. **2014**, *6*, 242.

[118] F. Odobel, Y. Pellegrin, E. A. Gibson, A. Hagfeldt, A. L. Smeigh, L. Hammarström, *Coord. Chem. Rev.* **2012**, *256*, 2414–2423.

[119] I. R. Perera, T. Daeneke, S. Makuta, Z. Yu, Y. Tachibana, A. Mishra, P. Bauerle, C. A. Ohlin, U. Bach, L. Spiccia, *Angew. Chem. Int. Ed*. **2015**, *54*, 3758.

the growing tendency nowadays to develop all-solid state devices versus the liquid-based DSSCs, which represents a step forward into the future commercialization.[120]

The working principle of a n-type DSSC is depicted in Figure 3.3. A sensitizing dye is chemically anchored to a nanocrystalline semiconductor,[121] such as TiO_2, ZnO or SnO_2, deposited onto an adequate conducting glass substrate. The semiconducting material is mesoporous, in order to produce a high surface area for dye coverage, thus increasing the light harvesting capabilities of the cell. After photoexcitation, the organic dye is able to inject electrons from its LUMO into the conduction band (CB) of the semiconductor. Electrons pass through the nanocrystalline structure and arrive at the conductive substrate; after that, the circuit is closed in the counter electrode, where an electrolyte (usually I^-/I_3^- or cobalt complexes)[122] is reduced and regenerates the chromophore (Figure 3.3).

The solar-to-electric power conversion efficiencies of DSSCs depend on a delicate balance of the kinetics for injection, dye regeneration and recombination reactions.[123] In fact, in addition to the basic processes, other unwanted and competitive processes can take place in the cell, such as the recombination of injected electrons in the CB of TiO_2 with the oxidized form of the dye, or with the electrolyte (the so called "dark current"). Furthermore, the chromophore can return to its ground state by a non-radiative relaxation (Figure 3.4).

[120] a) P. Docampo, S. Guldin, T. Leijtens, N. K. Noel, U. Steiner, H. J. Snaith, *Adv. Mater.* **2014**, *26*, 4013–4030; b) A. Fakharuddin, R. Jose, T. M. Brown, F. Fabregat-Santiago, J. A. Bisquert, *Energy Environ. Sci.* **2014**, *7*, 3952–3981.

[121] a) R. Jose, V. Thavasi, S. Ramakrishna, *J. Am. Ceram. Soc.* **2009**, *92*, 289; b) N. Sharifi, F. Tajabadi, N. Taghavinia, *ChemPhysChem* **2014**, *15*, 3902; c) M. Urbani, M. Grätzel, M. K. Nazeeruddin, T. Torres, *Chem. Rev*. **2014**, *114*, 12330.

[122] J. Wu, Z. Lan, J. Lin, M. Huang, Y. Huang, L. Fan, G. Luo, *Chem. Rev*. **2015**, *115*, 2136.

[123] S. A. Haque, E. Palomares, B. M. Cho, A. N. M. Green, N. Hirata, D. R. Klug, J. R. Durrant, *J. Am. Chem. Soc.* **2005**, *127*, 3456.

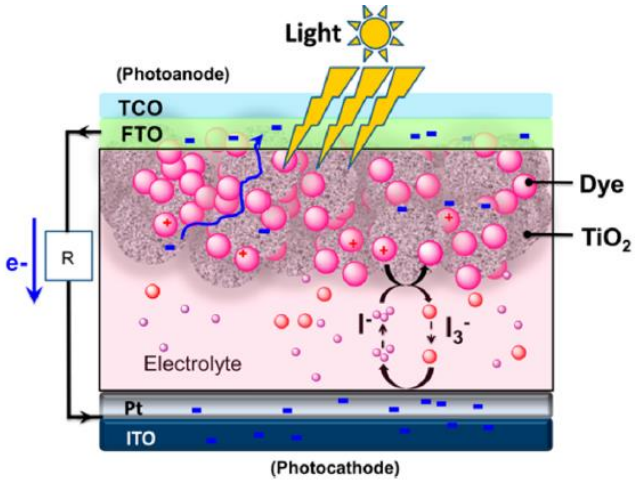

Figure 3.3. Schematic illustration of a typical n-type DSSC.[121c]

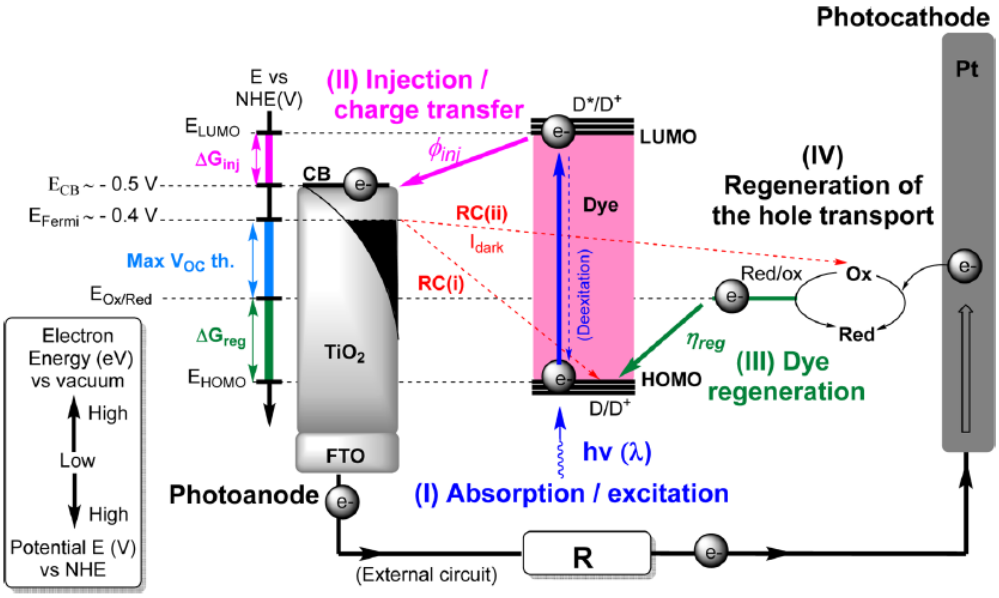

Figure 3.4. Schematic energetic diagram of an operative and conventional (n-type) TiO_2-DSSC using a redox couple in the electrolyte. [121c]

This plethora of photophysical processes are dependent on the three main components of the cell: the light-absorber dye, the nanocrystalline semiconductor, and the redox couple in the electrolyte. For a device to be successful, all three components

require fine-tuning.[124] In terms of the dye in particular, until ten years ago, the best performance had been achieved by polypyridyl complexes of ruthenium(II) as the molecular sensitizer, with overall PCEs of 11.5% being reached.[125] In view of the economic, as well as environmental high cost, , nd the insufficient light-harvesting properties of the above mentioned Ru(II) photosensitizers (their absorption spectra are rather broad but the NIR absorption is restricted and the molar extinction coefficients are low), much research has focused on the use of organic sensitizers,[126] and particularly of porphyrins.[127]

3.1.4 Hybrid solar cells

Organic–inorganic hybrid solar cells combine organic and inorganic particles, with the intent of incorporating the advantages associated with both material groups, *i.e.* the excellent transport properties of inorganic materials plus the high absorption coefficients and low cost processability of organic compounds, among others.[128] Within hybrid solar cells, quantum dot[129] and, specially, perovskite solar cells (PSC) deserve a special mention. [130] The latter stand out as promising candidates to contribute

[124] a) B. E. Hardin, H. J. Snaith and M. D. McGehee, *Nat. Photonics* **2012**, *6*, 162; b) V. Sugathan, E. John, K. Sudhakar, *Renew. Sust. Energ. Rev.* **2015**, *52*, 54.

[125] a) C.-Y. Chen, M. Wang, J.-Y. Li, N. Pootrakulchote, L. Alibabaei, C. Ngoc-le, J.-D. Decoppet, J.-H. Tsai, C. Grätzel, C.-G. Wu, et al. *ACS Nano* **2009**, *3*, 3103–3109; b)J.-F. Yin, M. Velayudham, D. Bhattacharya, H.-C. Lin, K.-L. Lu, *Coord. Chem. Rev.* **2012**, *256*, 3008–3035.

[126] a) J. N. Clifford, M. Planells, E. Palomares, *J. Mater. Chem.* **2012**, *22*, 24195–24201; b) R. K. Kanaparthi, J. Kandhadi, L. Giribabu, *Tetrahedron* **2012**, *68*, 8383–8393.

[127] a) L.-L. Li,E. W.-G. Diau, *Chem. Soc. Rev.* **2013**, *42*, 291–304; b) H. Imahori, T. Umeyama, S. Ito, *Acc. Chem. Res.* **2009**, *42*, 1809–1818.

[128] M. Wright, A. Uddin, *Sol. Energ. Mat. Sol. Cells* **2012**, *107*, 87.

[129] a) M. A. Halim, *Nanomaterials* **2013**, *3*, 22; b) M. R. Kim, D. Ma, *J. Phys. Chem. Lett*. **2015**, *6*, 85.

[130] a) H. J. Snaith, *J. Phys. Chem. Lett*. **2013**, *4*, 3623; b) M. A. Loi, J. C. Hummelen, *Nat. Mater*. **2013**, *12*, 1087; c) S. Kazim, M. K. Nazeeruddin, M. Grätzel, S. Ahmad, *Angew. Chem. Int. Ed*. **2014**, *53*, 2812; d) M. He, D. Zheng, M. Wang, C. Lin, Z. Lin, *J. Mater. Chem. A* **2014**, *2*, 5994; e) P. Gao, M. Grätzel, M. K. Nazeeruddin, *Energy Environ. Sci*. **2014**, *7*, 2448; f) M. A. Green, A. Ho- Baillie, H. J. Snaith, *Nature Photon*. **2014**, *8*, 506; g) H.-S. Kim, S. H. Im, N.-G. Park,

to a large scale solar energy production, owing to their high efficiency (already over 20%) and compatibility with scalable processes. Perovskites have the general formula of ABX_3 (Figure 3.5a), where A and B are monovalent and divalent ions, respectively, and X is O, C, N or a halogen.

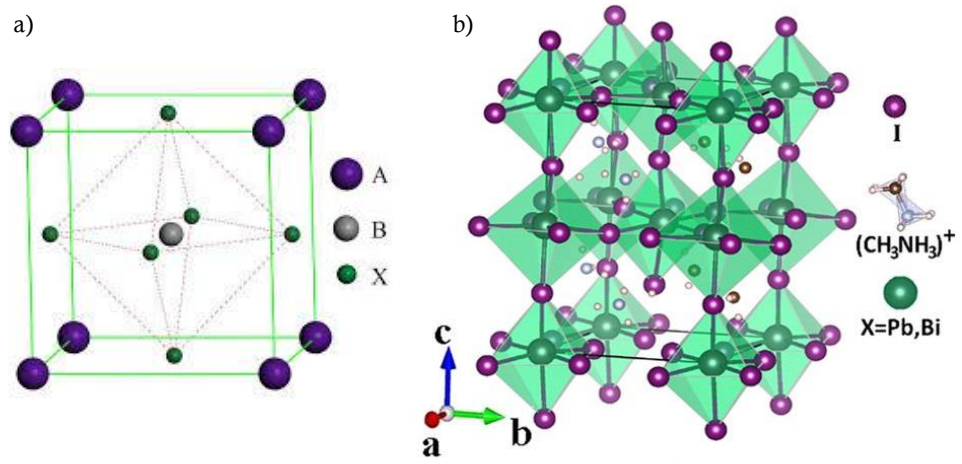

Figure 3.5. (a) ABX_3 crystal structure of perovskites and (b) Lattice structure schematic of organometal halide perovskites materials $CH_3NH_3XI_3$ (X = Pb, Bi),(tetragonal phase).

At present, the record certified efficiency for a perovskite cell is 22.1%,[131] a truly impressive value if one considers that these devices were non-existent ten years ago. The by far dominant material in the PV perovskite field remains $CH_3NH_3PbI_3$ (Figure 3.5b), the best performer described in the seminal paper of Miyasaka and co-workers.[132] Unfortunately, this is a material with significant problems.[133] Its solubility makes it excellent for facile device fabrication, but, on the other hand, the device needs to be rigorously kept away from moisture, substantially enhancing sealing requirements. Moreover, its perfect crystallinity can be lost at temperatures typically experienced inside solar panels under intensive irradiation and, upon dissolution, it generates PbI_2, a carcinogen banned in many countries. It has been recently demonstrated that

J. Phys. Chem. C **2014**, *118*, 5615; h) G. Giorgi, K. Yamashita, *J. Mater. Chem. A* **2015**, *3*, 8981; i) W.-J. Yin, J.-H. Yang, J. Kang, Y. Yan, S.-H. Wei, *J. Mater. Chem. A* **2015**, *3*, 8926.

[131] W. S. Yang, B.-W. Park, E. H. Jung, N. J. Jeon, Y. C. Kim, D. U. Lee, S. S. Shin, J. Seo, E. K. Kim, J. H. Noh, et al. *Science* **2017**, *356*, 1376–1379.

[132] A. Kojima, K. Teshima, Y. Shirai, T. Miyasaka, *J. Am. Chem. Soc.* **2009**, *131*, 6050.

[133] M. Grätzel, *Nat Mater* **2014**, *13*, 838–842.

environmental contamination would not be disastrous even in the case of catastrophic failure of perovskite modules and exposition to rain.[134] However, the stability issues should be overcome, and robustness under any circumstances must be strictly guaranteed for market distribution. The routes attempted to overcome the $CH_3NH_3PbI_3$ impasse have been recently reviewed.[135] The most obvious one, namely, replacing Pb with less toxic Sn, has been relatively disappointing, as tin tends to oxidize and the perovskite tends to lose crystallinity over time.[135]

3.1.5 Characteristic parameters of solar cells

The properties of photovoltaic devices can be characterized by plotting the measured current density output *J* of the cell versus the voltage output *V* of the cell (*J-V* graph, Figure 3.6). In the dark, this *J-V* curve passes through the origin, since at that moment no current is flowing through the device and no potential is present. By exposing the photovoltaic device to light, the *J-V* curve shifts downwards. The most important characteristic parameters of photovoltaic devices can be found on this *J-V* curve:

- **Open-circuit voltage** (V_{OC}): It is the maximum possible voltage across a photovoltaic device. This is the voltage across the cell, under sunlight, when no current is flowing through the device. It is mainly defined by the difference in voltage between the Fermi level of the semiconductor and the reduction potential of the electrolyte redox pair.

- **Short-circuit current** (I_{SC}): It is the current that flows through an illuminated solar cell when there is no external resistance *i.e.* when the electrodes are simply connected or short-circuited. I_{SC} is the maximum current that a photovoltaic device is able to produce. Under an external load, the current will always be less than I_{SC}. The short-circuit current depends on a number of

[134] B. Hailegnaw, S. Kirmayer, E. Edri, G. Hodes, D. Cahen, *J. Phys.Chem. Lett.* **2015**, *6*, 1543–1547.
[135] P. P. Boix, S. Agarwala, T. M. Koh, N. Mathews, S. G. Mhaisalkar, *J. Phys. Chem. Lett.* **2015**, *6*, 898–907.

factors, such as the area of the solar cell. To remove the dependence of the solar cell area, it is more common to list the short-circuit current density (J_{SC} in mA/cm^2), rather than the short circuit current (I_{SC} in mA).

- **Maximum power point** (M_{pp}): It is the point (V_m, J_m) on the *J-V* curve at which the maximum power is produced. Power is the product of current I and voltage *V*. This is represented in Figure 3.6 as the area of the rectangle formed between a point on the *J-V* curve and the axes *J* and *V*. The maximum power point is that point on the I-V curve at which the area of the resulting rectangle, *J* x *V*, is largest.

- **Fill Factor** (FF): It is the ratio of its actual maximum power output to its theoretical power output, if current and voltage would be at their maxima, J_{SC} and V_{OC}, respectively. This is a very important property used to measure photovoltaic device performance. It is a measure of the 'squareness' of the *J-V* curve. FF can be written down as follows (Equation 3.1):

$$FF = \frac{J_m \times V_m}{J_{sc} \times V_{oc}} \tag{3.1}$$

- **Power Conversion Efficiency** (PCE or η): It is the ratio of power output (P_{out}), to power input (P_{in}). PCE measures the amount of power produced by a photovoltaic device relative to the power available in the incident solar radiation. P_{in} is the sum over all wavelengths, which usually has a value of 100 mW/cm^2 when solar simulators are used. This is the most general way to define the efficiency of a photovoltaic device. PCE can be written down as follows (Equation 3.2):

$$PCE\ (\eta) = \frac{P_{out}}{P_{in}} = \frac{J_m \times V_m}{P_{in}} = \frac{J_{sc} \times V_{oc} \times FF}{P_{in}} \tag{3.2}$$

PCE is one of the most important parameters to characterize solar cell performances. In order to compare results from various devices, regardless of the design and active material, photovoltaic cells are all subjected to the same standard test conditions.

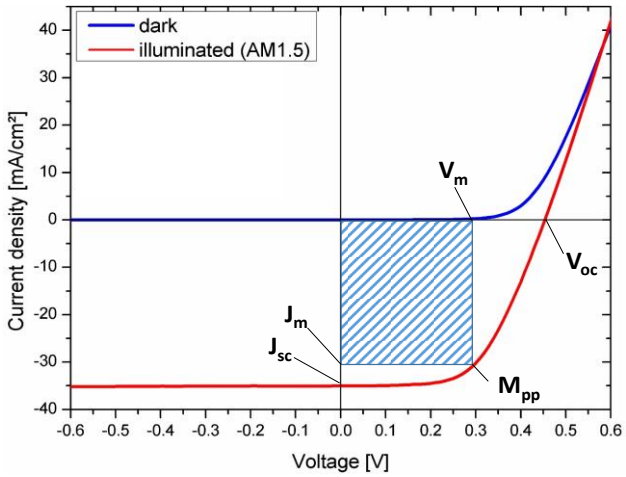

Figure 3.6. Typical *J-V* curve for any type of solar cell in the dark and under illumination (the most important photovoltaic parameters are indicated).

To determine their PCE, the cells are typically illuminated at a constant density of roughly 100 mW/cm2, which is defined as the standard "1 Sun" value, with a spectrum consistent to an air-mass global value of 1.5 (*AM 1.5G*), at a temperature of 25 °C. Air mass describes the spectrum of radiation and can be defined as the amount of atmosphere though which sunlight has to travel to reach the Earth's surface. This is abbreviated as *AMx*, in which *x* is the inverse of the cosine of the zenith angle of the sun θ. The above mentioned *AM 1.5G* conditions correspond to the spectrum and irradiance of sunlight incident when $\theta = 48.2°$; solar cells intended for space use are measured under *AM0* conditions (Figure 3.7).

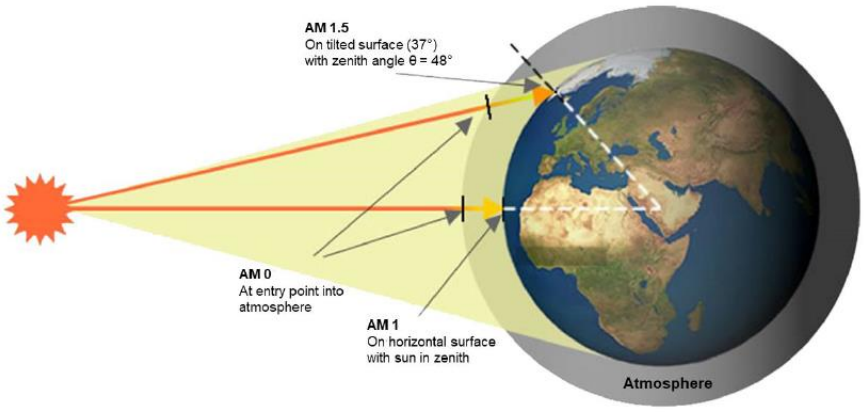

Figure 3.7. The air-mass value AM 0 equates to insulation at sea level with the Sun at its zenith. AM 1.0 represents sunlight with the Sun at zenith above the Earth's atmosphere. AM 1.5 is the same, but with the Sun at an oblique angle of 48.2°, which simulates a longer optical path through the Earth's atmosphere.

- **External Quantum Efficiency** (EQE): Also known as Incident Photon to Current Efficiency (IPCE), is another important parameter for solar cell characterization. It is calculated by the number of electrons extracted in an external circuit divided by the number of incident photons at a certain wavelength under short-circuit condition. EQE can be written down as follows (Equation 3.3):

$$EQE\ (\lambda) = \frac{number\ of\ electrons}{number\ of\ incident\ photons} = \frac{J_{sc}\ (\lambda)/e}{P_{in}(\lambda)/(\frac{hc}{\lambda})} = \frac{J_{sc}\ (\lambda)\times hc}{P_{in}(\lambda)\times e\lambda} \quad (3.3)$$

Where λ is the wavelength, e is the elementary charge, h is the Planck constant, and c is the speed of light in vacuum.

3.1.6 Fundaments of electron transfer

Nature has solved many engineering problems such as self-healing abilities, environmental exposure tolerance and resistance, hydrophobicity, self-assembly, and specially harnessing solar energy. In fact, the photosynthetic system found in nature is the photoactive device par excellence that has served as inspiration to many scientists.

Photosynthesis[136] is the process employed by plants, algae and cyanobacteria to convert the radiant energy from the sun into chemical energy to fuel the activities of these organisms. The success of this conversion relies upon the efficient absorption and conversion of sunlight. Much effort has been devoted to the understanding of the mechanism of light conversion in the photosynthetic system, with the aim of designing artificial ensembles that can behave similarly in human's profit.

The main players in the photosynthetic process are chlorophylls and carotenoids with characteristic absorption features. While the latter play mainly a photoprotective role, chlorophylls are involved in light harvesting and charge separation processes.[136] Photosynthetic systems present two basic components: an antenna complex for light harvesting, and a reaction center for charge separation The first step in photosynthesis is light absorption by the antenna complex. Photoinduced energy transfer is a process of great importance in the light harvesting complex. Energy transfer is a photophysical process where the excitation of a chromophore is transferred to a radiation-less relaxation. Spectral overlap between the emission of the donor and the absorption of the acceptor is required for energy transfer to occur. The aim of this event in the photosynthetic system is to progressively direct the energy from sunlight to the reaction centre and trigger the charge separation process.

In the case of photosynthesis, energy transfer takes place through the dipolar coupling mechanism described by Theodore Förster in 1914. Förster resonance energy transfer (FRET) takes place when non-radiative excitation transfer occurs between two molecular entities separated by distances that exceed the sum of their Van der Waals radii.[137] This energy exchange happens *via* the electromagnetic field associated to the electron in the LUMO of the donor, which causes a perturbation on the electrons in the HOMO of the acceptor. The effectiveness of the energy transfer depends on the distance between the chromophores and the relative orientation of the chromophores.

[136] B. Alberts, A. Johnson, J. Lewis, D. Morgan, M. Raff, K. Roberts, P. Walter, *Molecular Biology of the Cell*; 500 Tips; Garland Science, **2014**.
[137] V. Helms, *Principles of Computational Cell Biology*; Wiley, **2008**.

In this regard, organization of the chromophores is very important for an efficient photosynthetic process. A common feature of photosynthetic systems is a ring-like organization of the antenna (Figure 3.8) complex around the reaction center. Such degree of organization of the photosynthetic pigments, addressed to ensure formation of efficient antennas and reaction centers, is based on supramolecular interactions involving not only the pigments but also proteins and protein dimers.

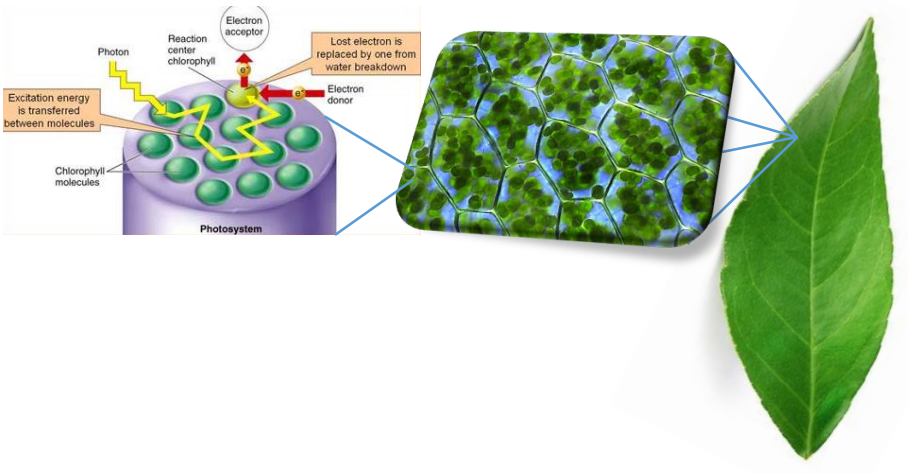

Figure 3.8. Schematic representation of photosystem.

Eventually, conversion of sunlight energy into chemical energy takes place through a cascade of unidirectional electron transfer reactions that ultimately lead to the synthesis of carbohydrates. The success of this process relies on the effectiveness of these electron transfers and the lack of recombination reactions that would interrupt the process and cause a waste of the absorbed energy. In terms of charge separation, the characteristics of the individual electron acceptors and electron donors are decisive to determine the overall efficiency.

In summary, in natural photosynthetic systems, cascades of energy– and electron–transfer reactions are triggered either directly by photoexcitation or indirectly by energy transfer from light–harvesting antenna systems. Therefore, designing, synthesizing, and probing efficient energy capacitors and chromophores featuring unique panchromatic absorptive, redox, and electrical properties is of a crucial

importance for the preparation of artificial photosynthetic models. Considering the structural complexity presented by the natural photosynthetic systems, much of the scientific effort has been devoted towards the preparation and study of structurally simpler systems, with the aim of reproducing some of the fundamental steps occurring in natural photosynthesis, one of the most important being the photoinduced charge separation.[138]

3.1.7 Photoinduced electron transfer (PET) in artificial systems

In their most simple version, artificial photosystems are constituted by an electron donor unit (D) connected to an electron acceptor moiety (A) through a linker (L). This linker can connect both units either by covalent or supramolecular interactions (Figure 3.9).

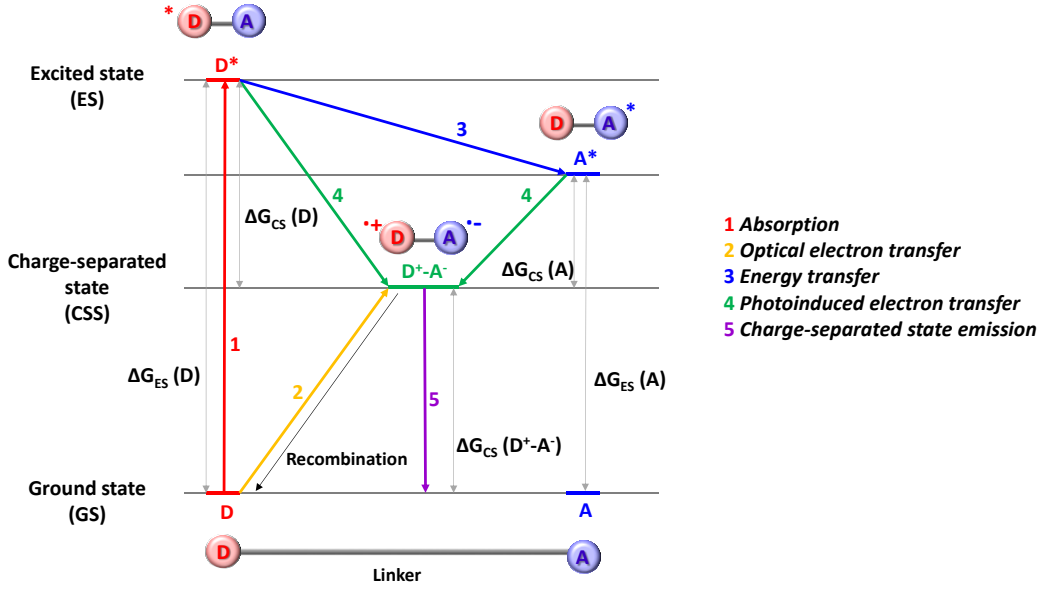

Figure 3.9. Representation of the photoinduced electron transfer between a donor and an acceptor connected through a linker.

[138] a) M. N. Paddon-Row, Covalently Linked Systems Based on Organic Components. In *Electron Transfer in Chemistry*; Wiley-VCH Verlag GmbH, **2008**; pp 178–271; b) D. Gust, *Nature* **1997**, *386*, 21–22; c) M. A. Fox, *Photochem. Photobiol.* **1990**, *52*, 617–627.

Photoinduced electron transfer (PET) is a process by which an excited electron is transferred from a donor to an acceptor, and in can take place in two different ways.[139] If the electron donor is photoexcited, an electron will be promoted from its HOMO to its LUMO and then, it will be transferred to the energetically lower-lying LUMO of the electron acceptor (Figure 3.10a). On the other hand, if the electron acceptor is the part of the molecule being photoexcited, a hole will appear in its HOMO, which is filled with an electron originating from the higher-lying HOMO of the electron donor (Figure 3.10b). Both possibilities lead to the formation of an ion-pair or charged separated state (CSS) which will subsequently recombine to the electronic ground state.

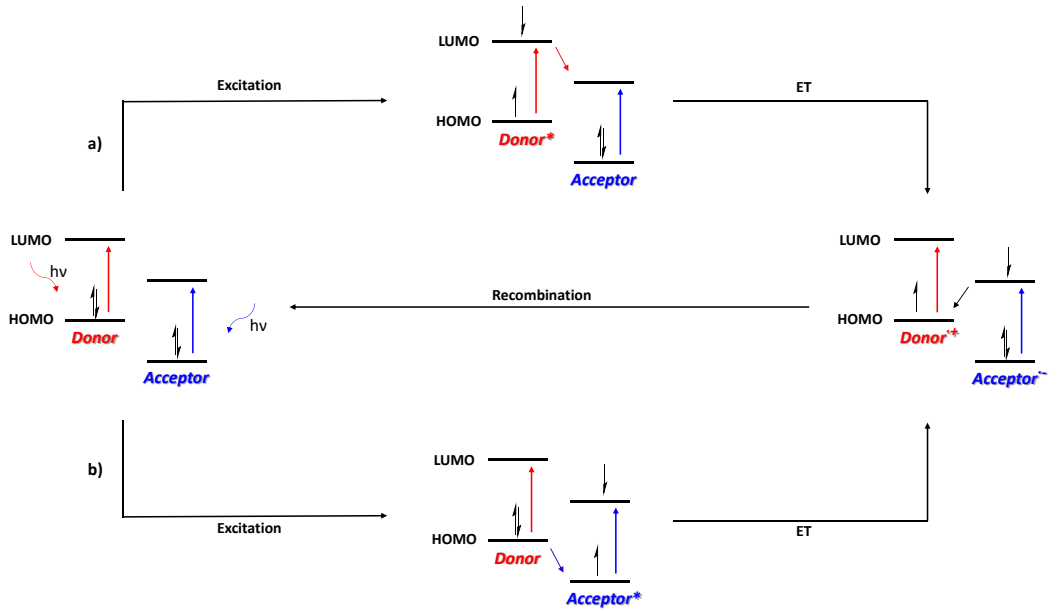

Figure. 3.10. Possible pathways for PET reactions: a) photoexcitation of the donor; b) photoexcitation of the acceptor.

Within this context, the molecular or supramolecular systems must fulfil several requirements regarding PET:

[139] a) *Photoinduced Electron Transfer*, (Eds. M. A. Fox, M. Chanon), Elsevier, Amsterdam, **1988**; b) S. Speiser, *Chem. Rev.* **1996**, *96*, 1953; c) *Electron Tranfer in Chemistry* Vol I-IV (Ed. V. Balzani), Wiley-VCH, Weinheim, **2001**; d) U. E. Steiner, in *Photodynamic Therapy - From Theory to Application*,(Ed. M. H. Abdel-Kader), Springer, **2014**, Chapter 2, p 25.

- High extinction coefficients in the visible range of the spectrum.
- The charge separation processes quantum yield must be close to 1, so there are no losses of the excitation energy.
- The energetic level of the CSS must be high and close to the energy level of the initial excited state, to minimize de energy loss.
- Recombination kinetics must be as slow as possible so the CSS lifetime is as high as possible.

3.1.8 Singlet fission

Singlet fission is a process in which an organic chromophore in an excited singlet state shares its excitation energy with a neighboring ground-state chromophore and both are converted into triplet excited states (Figure 3.11).[140] The two chromophores can be of the same kind ("homofission") or of different kinds ("heterofission"). In principle, the sharing of excitation energy could be more extensive, resulting in the formation of more than two triplet states.

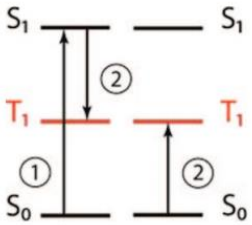

Figure 3.11. Singlet fission: (1) The chromophore on the left undergoes an initial excitation to S_1. (2) The excited chromophore shares its energy with the chromophore on the right, creating a T_1 state on each.

Singlet fission is spin-allowed in the sense that the two resulting triplet excitations produced from an excited singlet are born coupled into a pure singlet state. Singlet fission can therefore be viewed as a special case of internal conversion (radiationless

[140] a) C. E. Swenberg, N. E. Geacintov, *Org. Mol. Photophysics* **1973**, 18, 489; b) M. Pope, C. E. Swenberg, Electronic Processes in Organic Crystals and Polymers, 2nd ed.; Oxford University Press: Oxford, U.K., **1999**; pp 134-191; c) M. C. Beard, J. C. Johnson, J. M. Luther, A. J. Nozik, *Philos. Trans. R. Soc. London Ser. A* **2015**, *373*, 20140412.

transition between two electronic states of equal multiplicity).[141] Like many other internal conversion processes, it can be very fast, particularly in molecular crystals. There, when it is isoergic or slightly exoergic and the coupling is favorable, the transformation occurs on a ps or even sub-ps time scale, competing with vibrational relaxation and easily outcompeting prompt fluorescence. Only excimer formation and separation into positive and negative charge carriers appear to have the potential to be even faster under favorable circumstances.

In the absence of any interaction between the two triplets, the singlet ^{1}(TT), triplet ^{3}(TT), and quintet ^{5}(TT) states that result from the nine substates originating in the three sublevels of each triplet would have the same energy. In reality, there will be some interaction and the ^{1}(TT), ^{3}(TT), and ^{5}(TT) states will not be exactly degenerate. As long as they are at least approximately degenerate, they will be mixed significantly by small spin-dependent terms in the Hamiltonian, familiar from electron paramagnetic resonance spectroscopy (EPR). In organic molecules that do not contain heavy atoms, these terms are primarily the spin dipole-dipole interaction, responsible for the EPR zero-field splitting, and the Zeeman interaction if an outside magnetic field is present. Hyperfine interaction with nuclear magnetic moments, responsible for the fine structure in EPR spectra, is also present but is weaker. In molecular crystals, where triplet excitons are mobile, its effect averages to zero if exciton hopping is fast on the EPR time scale. Spin-orbit coupling is present as well, but in molecules without heavy atoms it is weak and is normally negligible relative to the spin dipole-dipole and Zeeman interactions.

There is an interesting difference between intersystem crossing induced by singlet fission, primarily as a result of the existence of spin dipole-dipole interaction, and the much more common intersystem crossing induced by spin-orbit coupling. Unlike the spin-orbit coupling operator, which connects singlets only with triplets, the spin dipole-dipole interaction is a tensor operator of rank two, and it has nonvanishing matrix elements between singlets and triplets, as well as between singlets and quintets.

[141] a) M. B. Smith, J. Michl, *Chem. Rev.* **2010**, *110*, 6891–6936; b) M. B. Smith, J. Michl, *Annu. Rev. Phys. Chem.* **2013**, *64*, 361–386.

Therefore, singlet fission has the potential for converting singlets into both triplets and quintets efficiently, thus expanding the Jablonski diagram as shown in red in Figure 3.12. Excited quintet states of organic chromophores with a closed-shell ground state have never been observed to our knowledge. In the singlet fission literature they are usually dismissed as too high in energy, but this need not be always justified

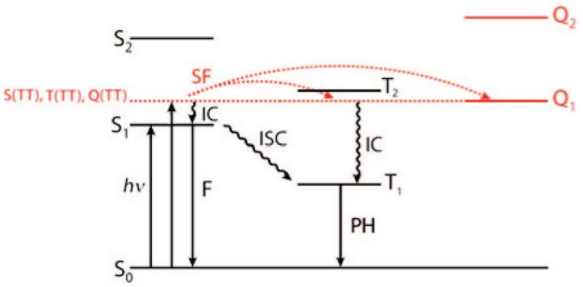

Figure 3.12. Expanded Jablonski diagram with the singlet fission (SF) process shown in red. F, fluorescence; IC, internal conversion; ISC, intersystem crossing; PH, phosphorescence

The case for using singlet fission in a solar cell is based on a quantitative analysis[142] that showed that the ShockleyQueisser limit[99] of about 1/3 for the efficiency of an ideal single-stage photovoltaic cell would increase to nearly 1/2 in a cell whose sensitizer is capable of quantitative singlet fission, provided that the two triplets resulting from the absorption of a single photon of sufficient energy are sufficiently independent of each other to produce charge carriers separately and quantitatively (Figure 3.13a). The ideal efficiency of such a singlet fission cell is shown schematically as a function of the S_0-T_1 band gap in Figure 3.13b, assuming a 200% yield of charge carrier pairs per photon. The optimal location of the S_0-S_1 absorption edge is ~2 eV, with the triplet energy at ~1 eV, but minor deviations from these values would have little effect. In the derivation of the optimum efficiency value close to 1/2, it was assumed that the layer doped with singlet-fission capable sensitizer absorbing at 2 eV and above would be immediately followed by a layer of an ordinary sensitizer capable of absorbing photons

[142] M. C. Hanna, A. J. Nozik, *J. Appl. Phys.* **2006**, *100*, 074510/1; b) A. Kunzmann, M. Gruber, R. Casillas, J. Zirzlmeier, M. Stanzel, W. Peukert, R. R. Tykwinski, D. M. Guldi, *Angew. Chem. Int. Ed.* **2018**, 57, 10742–10747.

of energies between 1 and 2 eV and generating a single electron and hole per photon. It is then arguable whether the assembly can still be called a single junction cell, but because no current matching is necessary, even if it is viewed as a double junction cell, it would be one of a particularly simple kind.

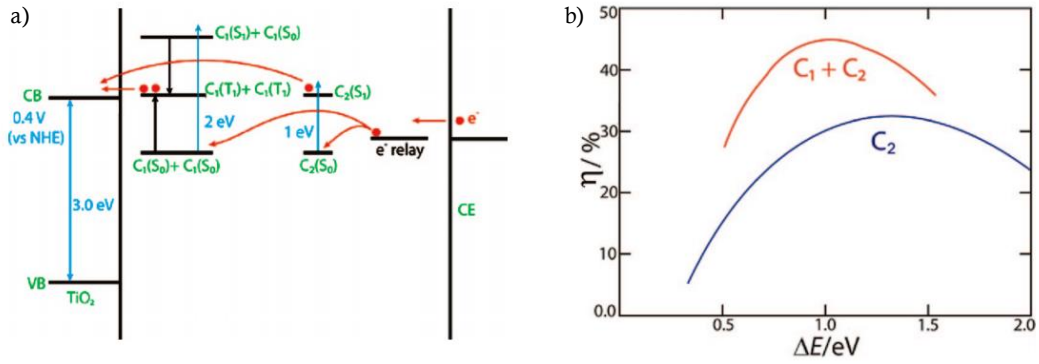

Figure 3.13. (a) DSSC that uses a singlet fission sensitizer (C_1) in conjunction with a conventional sensitizer (C_2). The C_1 sensitizer comprises the top layer of the cell and absorbs light above 2 eV. The C_2 sensitizer absorbs the remaining light between 1 – 2 eV. CB, conduction band; VB, valence band; CE, counterelectrode; NHE, normal hydrogen electrode. (b) Schematic sketch of theoretical efficiency as a function of the S_0-T_1 band gap for a singlet fission solar cell defined in (a) (red) and a conventional DCCS (blue).

3.2 Specific Objectives

In this chapter, we aimed at exploring and evaluating unreported applications of SubPzs and SubNcs as active molecular materials in photovoltaic devices, as well as at optimizing the photophysical response.

1- In the first part of this chapter, SubNcs bearing various peripheral and axial substituents with electron acceptor features will be evaluated in solution-processed bulk-heterojunction polymer solar cells. The resulting solar cells should exhibit modest photovoltaic performance with contributions from both the polymer donor and SubNc acceptor to the photocurrent. Also in this part we aimed at preparing electron-acceptor SubPzs based in the studies carried out in chapter 1. In this respect, functionalization with electron-accepting ester moieties, connected through vinylidene linkers should provide SubPzs with considerable electron-accepting character, and absorption features in the yellow-orange region.

The fabrication of the BHJ devices and the measurements of their performance will be carried out in the laboratory of Prof. Rene Janssen in the Eindhoven University of Technology.

Specific objectives of this section are the following:

- Assessment of the photovoltaic performances in bulk-heterojunction polymer solar cells using SubNcs **33**, **36**, **37**, and **40** as electron-acceptor active agents.

- Synthesis, characterization and electrochemical studies of peripheral hexavinylester-substituted SubPzs bearing different axial substituents.

2- The aim of the second part of this chapter is the synthesis of a first generation of photosensitizers based on SubPz derivatives for their application in n-type dye sensitized solar cells (DSSCs). These new ligands will have a common structure consisting of a SubPz functionalized with five peripheral aryl functions with donor substituents, and one anchoring group based in a carboxylic acid unit. The effect of the

diverse peripheral substitution of SubPzs, as well as the anchoring motif in the performance of the SubPzs in DSSCs, will be studied.

The photovoltaic studies using these dyes as photosensitizers will be performed at Global GET-Future Laboratory and Department of Advanced Materials Chemistry in Korea University within the group of Prof. Hwan Kyu Kim.

Specific objectives of this second section are the following:

- Synthesis and characterization of a series of A_2B SubPzs, in which the A units are pyrrole rings substituted at the two β-positions with aryl groups and the B subunit is a pyrrole ring containing an aryl group at one β-carbon and a carboxylic acid function at the other one. This anchoring group will be linked to the macrocycle through a *p*-phenylethynyl linker, either directly, or as the 2-carboxy-2-cyanovinyl anchoring motif (Scheme 3.1).[143]

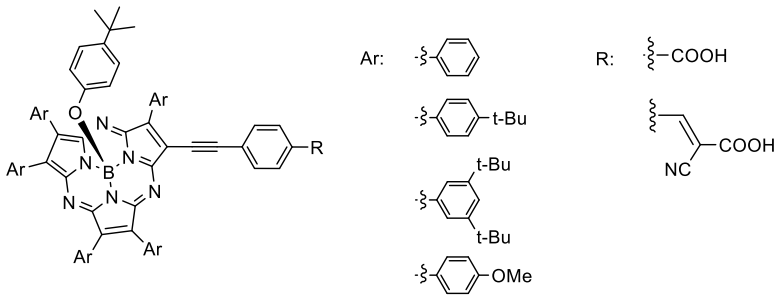

Scheme 3.1. Photosensitizer based on SubPzs

- Assessment of the photovoltaic performances in n-type TiO_2-DSSCs.

3- The goal of the third part of this chapter is to build a SubPz-pentacene system able to synergistically undergo singlet fission. To this end, a singlet excited-state-donating SubPz, should transfer the energy via FRET to the SF performing pentacene, which should double the number of excitons that are formed. For the system to undergo FRET, the SubPz dye should display absorptions in a window that enable the sole excitation of this chromophore, as well as an emission band matching the optical

[143] G. Copley, D. Hwang, D. Kim, A. Osuka, *Angew. Chem. Int. Ed.* **2016**, *55*, 10287 –10291

absorption of the Pn chromophore. Peripheral trimethoxyphenyl substitution produces a chromophore with absorption bands at 445 and 557 nm, where the pentacene shows none or marginal absorption, and an emission band at 668 nm, matching the pentacene largest absorption band (see chapter 1). In order to maintain the absorption and fluorescence profiles of the SubPz, the pentacene dimer should be attached to the axial position of the SubPz.[15c] Transient absorption spectroscopy will be carried out in the laboratories of Prof. Dirk M. Guldi (Friedrich-Alexander Univertität Erlangen-Nürnberg).

Specific objectives of this third section are the following:

- Synthesis and characterization of a SubPz-Pnc_2 triad, in which the two chromophores are connected through the SubPz axial position. This array can be prepared by esterification reaction of a suitable SubPz endowed with an axial hydroquinone moiety[61] and a pentacene dimer containing a carboxylic acid function (Schema 3.2).[142b]

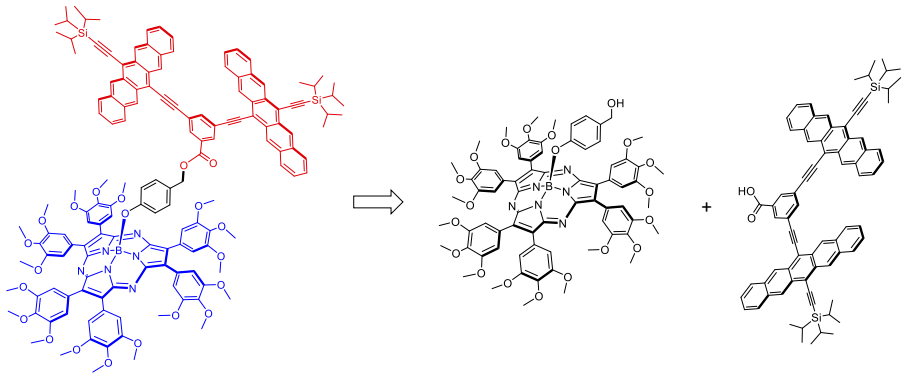

Scheme 3.2. Retrosynthesis of SubPz-Pnc_2 triad.

- Photophysical characterization of the ground and excited states and singlet fission measurement of the triad system.

3.3 Results and Discussion

3.3.1 Photovoltaic studies of SubNc as electron acceptors in bulk-heterojunction polymer solar cells

The incorporation of SubNcs **33**, **36**, **37**, and **40** as electron-acceptors in BHJ polymer solar cells has been performed in the group of Prof. René Janssen in Eindhoven University of Technology (The Netherlands), following protocols well established in the group.

The motivation for the design of these molecules starts from Cl_6-SubPc-(Cl), which was a successful reported SubPc-based acceptor.[57e] The related Cl_{12}-SubNc-(Cl) **34** hasperipheral and axial substituents of the same nature, but the number of peripheral electron-withdrawing chlorine atoms is larger. Nevertheless, the solubility of SubNc **34** in organic solvents is extremely poor. Hence studies were performed only with SubNcs **33**, **36**, **37**, and **40**. The optical absorption spectra and the relevant frontier orbital energy levels of the SubNcs **33**, **36**, **37**, and **40** in films are collected in Figure 3.14.

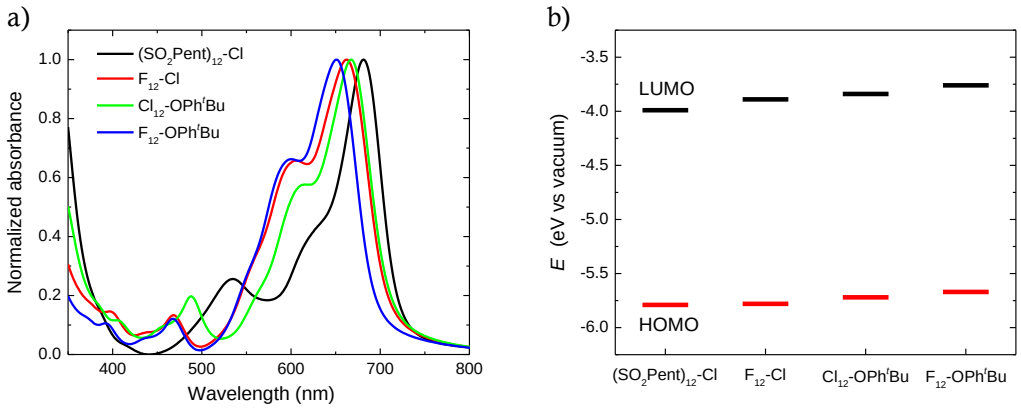

Figure 3.14. (a) Optical absorption spectra and (b) energy levels of their films for SubNc series: ($(SO_2Pent)_{12}$-Cl, **40**), (F_{12}-Cl, **33**), (Cl_{12}-OPh^{t}Bu, **36**) and (F_{12}-OPh^{t}Bu, **37**).

The photovoltaic properties of the SubNc acceptors were evaluated in solar cells in combination with PTB7-Th as a low band gap donor polymer in an ITO/ZnO/PTB7-

Th:SubNc-X/MoO_x/Ag device structure under simulated air mass 1.5 global (AM1.5G) illumination (100 mW cm^{-2}). Integration of the external quantum efficiency (EQE) with the AM1.5G spectrum was used to accurately determine the short-circuit current density and calculate the PCE of the solar cells. The current density–voltage (*J*–*V*) curves and EQE spectra of the optimized devices are shown in Figure 3.15 and Table 3.1 summarizes the photovoltaic parameters. Results from different fabricating conditions are presented in Table 3.2. The highest PCE of 1.09% was found for SubNc **37**, along with a short-circuit current density (J_{sc}) of 3.9 mA cm^{-2}, an open-circuit voltage (V_{oc}) of 0.73 V, and a fill factor (FF) of 0.38. The V_{oc} provided by SubNc **37** is only slightly less than for PTB7-Th: fullerene devices (about 0.8 V), but the V_{oc} of the other SubNcs with PTB7-Th as donor is lower, consistent with their deeper LUMO levels.[144]

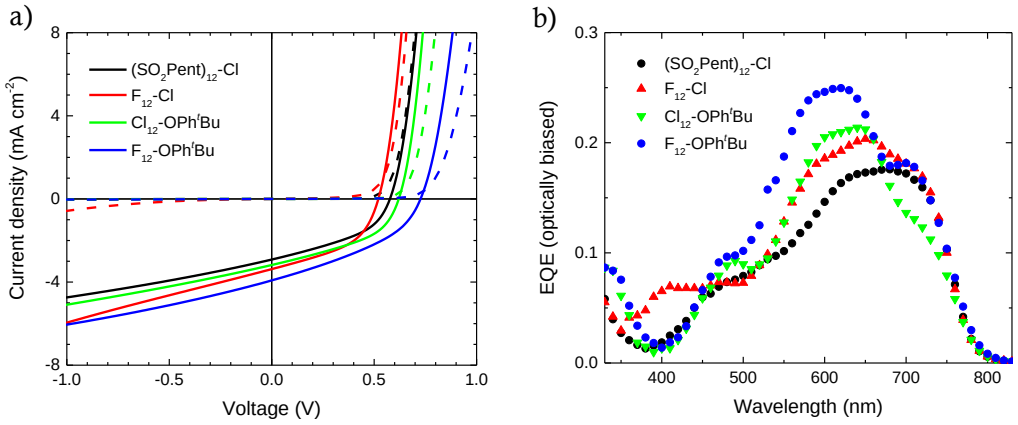

Figure 3.15. (a) *J*–*V* curves of the PTB7-Th:SubNc solar cells in dark (dashed lines) and under illumination (solid lines); (b) corresponding EQE spectra.

[144] M. C. Scharber, D. Mühlbacher, M. Koppe, P. Denk, C. Waldauf, A. J. Heeger and C. J. Brabec, *Adv. Mater.*, 2006, **18**, 789-794.

SubNc	J_{sc}[a] (mA cm^{-2})	V_{oc} (V)	FF	P_{max} (mW cm^{-2})	J_{sc} (EQE)[b] (mA cm^{-2})	**PCE[c] (%)**
40	3.94 (3.92±0.02)	0.58 (0.57±0.01)	0.42 (0.42±0.02)	0.96 (0.93±0.04)	2.9	**0.71**
33	3.86 (3.81±0.05)	0.52 (0.50±0.02)	0.46 (0.43±0.03)	0.93 (0.83±0.09)	3.4	**0.82**
36	3.69 (3.72±0.07)	0.62 (0.62±0.01)	0.44 (0.42±0.03)	1.00 (0.96±0.06)	3.2	**0.86**
37	4.74 (4.59±0.08)	0.73 (0.73±0.01)	0.38 (0.39±0.01)	1.32 (1.28±0.03)	3.9	**1.09**

[a] Acquired directly from *J–V* measurements under AM1.5G illumination (100 mW cm^{-2}).
[b] Determined by integrating the EQE with the AM1.5G solar spectrum.
[c] Calculated by using J_{sc} (EQE).

Table 3.1. Solar cell characteristics and charge carrier mobilities of PTB7-Th:SubNc devices.

As shown in Figure 3.15b, both the polymer donor and the SubNc acceptor contribute to the photocurrent in each case. Except for SubNc **40** whose absorption spectra has substantial overlap with the donor polymer PTB7-Th, all other SubNcs exhibit a EQE maximum located at about 540 nm and EQE shoulder located at about 710 nm, which originate from the SubNcs and PTB7-Th, respectively. Nevertheless, all these SubNcs afforded relative low overall EQEs of ≤ 0.25 and thereby low J_{sc} values of < 4 mA cm^{-2}. Another common limitation of these solar cells is their low FF (≤ 0.46), which is much lower than that of high-performing solar cells based on fullerene acceptors and A-D-A acceptors. As a result, all these devices show relative low PCE values. A low FF may result from space-charge limited photocurrent, when the mobilities for holes and electrons are largely unbalanced. We thus focused on understanding the reason for the low Jsc and FF of the devices based on these SubNcs acceptors.

SubNc	D:A	Solvent	Annealing	J_{sc} (mA cm^{-2})	V_{oc} (V)	FF	P_{max}[a] (mW cm^{-2})	**PCE[b] (%)**
$(SO_2Pent)_{12}$-Cl **40**	3:1	CB	No	2.35	0.548	0.412	0.53	
	2:1	CB	No	2.89	0.555	0.422	0.68	
	1.5:1	CB	No	3.33	0.556	0.428	0.79	
	1:1	CB	No	3.50	0.559	0.429	0.84	**0.70**
	1:1	**CB**	**90 °C, 5 min**	**3.94**	**0.577**	**0.423**	**0.96**	**0.71**
	1:1	CB (2% CN)	90 °C, 5 min	3.13	0.569	0.419	0.75	
	1:1	CB (2% DIO)	90 °C, 5 min	2.00	0.582	0.403	0.47	
	1:1.5	CB	No	3.01	0.541	0.428	0.70	
	1:2	CB	No	3.13	0.563	0.434	0.77	
F_{12}-Cl **33**	1:1	CB	No	2.70	0.511	0.453	0.63	**0.54**
	1:1	CB	90 °C, 5 min	2.84	0.481	0.400	0.55	
	1:1	CB (2% CN)	No	1.89	0.259	0.329	0.16	
	1:1	CB (2% CN)	90 °C, 5 min	2.28	0.168	0.319	0.12	
	1:1.5	**CB**	**No**	**3.86**	**0.521**	**0.463**	**0.93**	**0.82**
	1:1.5	CB (2% DIO)	No	2.70	0.635	0.439	0.75	
Cl_{12}-OPh^{t}Bu **36**	1:1	CB	No	2.59	0.765	0.405	0.80	
	1:1	CB	90 °C, 5 min	2.71	0.812	0.456	1.01	
	1:1	CB (2% CN)	No	3.28	0.566	0.441	0.82	
	1:1	**CB (2% CN)**	**90 °C, 5 min**	**3.69**	**0.620**	**0.438**	**1.00**	**0.86**
	1:1.5	CB (2% CN)	90 °C, 5 min	2.85	0.599	0.430	0.73	
F_{12}-OPh^{t}Bu **37**	1:1	CB	No	4.54	0.715	0.399	1.30	
	1:1	**CB**	**90 °C, 5 min**	**4.74**	**0.726**	**0.384**	**1.32**	**1.09**
	1:1	CB (2% CN)	No	1.44	0.708	0.386	0.39	
	1:1	CB (2% CN)	90 °C, 5 min	1.44	0.571	0.326	0.27	
	1:1.5	CB	90 °C, 5 min	4.66	0.675	0.382	1.20	

[a] Acquired directly from *J–V* measurements under AM1.5G illumination (100 mW cm^{-2}).
[b] Acquired by using the integration of EQE with the AM1.5G spectrum as the J_{sc}.

Table 3.2. Performance parameters of the PTB7-Th:SubNc solar cells in device structure of ITO/ZnO (40 nm)/PTB7-Th:SubNc /MoO_x (10 nm)/Ag (100 nm) under different conditions.

The transport and recombination of charge carriers in the blend films of PTB7-Th:SubNc were investigated. Hole mobilities (μ_h) and electron mobilities (μ_e) (Table 3.3) were estimated from single-carrier PTB7-Th:SubNc devices by fitting the *J–V* data (Figure 3.16) to a space-charge-limited current model, resulting in a $\mu_h \approx 10^{-4}$ and a μ_e

≈ 10^{-6} cm^2 V^{-1} s^{-1} for all four acceptors. Bearing in mind that both the μ_h and μ_e of PTB7-Th:fullerene blends are usually ≈ 10^{-3} cm^2 V^{-1} s^{-1}, the greatly reduced electron transport capability of the PTB7-Th:SubNc films is likely causing the low J_{sc} and low FF.

SubNc	μ_h (cm^2 V^{-1} s^{-1})	μ_e (cm^2 V^{-1} s^{-1})	μ_h/μ_e
$(SO_2Pent)_{12}$-Cl, **40**	5.7× 10^{-4}	3.1× 10^{-6}	184
F_{12}-Cl, **33**	2.4× 10^{-4}	0.9× 10^{-6}	267
Cl_{12}-OPh^{t}Bu, **36**	4.8× 10^{-4}	2.5× 10^{-6}	192
F_{12}-OPh^{t}Bu, **37**	5.3× 10^{-4}	1.4× 10^{-6}	379

Table 3.3. Charge carrier mobilities of the PTB7-Th:SubNc blends measured from single-carrier devices using SCLC method.

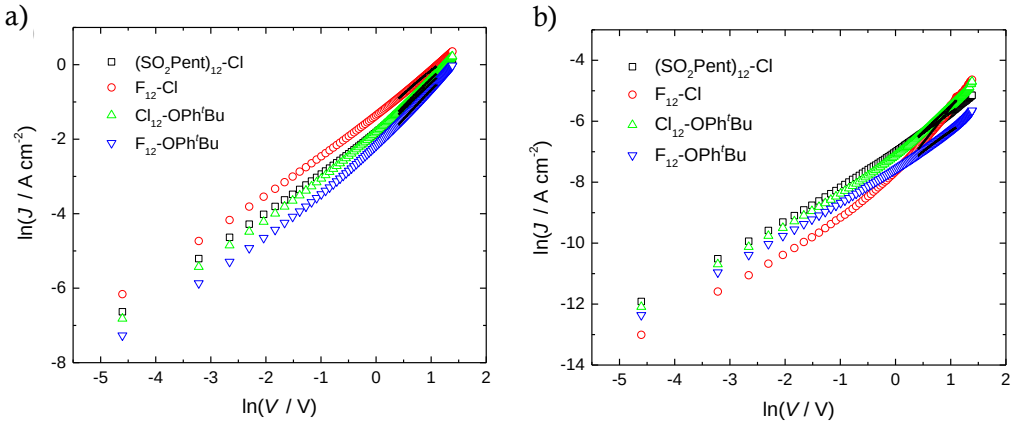

Figure 3.16. Current density versus voltage characteristics plotted in the format of ln$J$ ~ ln$V$ of (a) ITO/MoO_x (40 nm)/ PTB7-Th:SubNc/ MoO_x (40 nm)/Ag (100 nm) hole-only devices, and (b) ITO/ZnO (40 nm)/ PTB7-Th:SubNc/LiF (1 nm)/Al (100 nm) electron-only devices.

Moreover, the transport of hole and electron in these films is highly imbalanced as suggested by the high μ_h/μ_e value of >100 for all SubNc-based acceptors. The build-up of space charge due to the imbalanced hole/electron transport further increased the possibility of bimolecular charge recombination, an important factor resulting in photocurrent loss and poor FF. The strong bimolecular recombination is further

evidenced by the large difference between the EQE measured with light bias (EQE_{bias}) and without light bias (EQE_{nobias}) (Figure. 3.17).

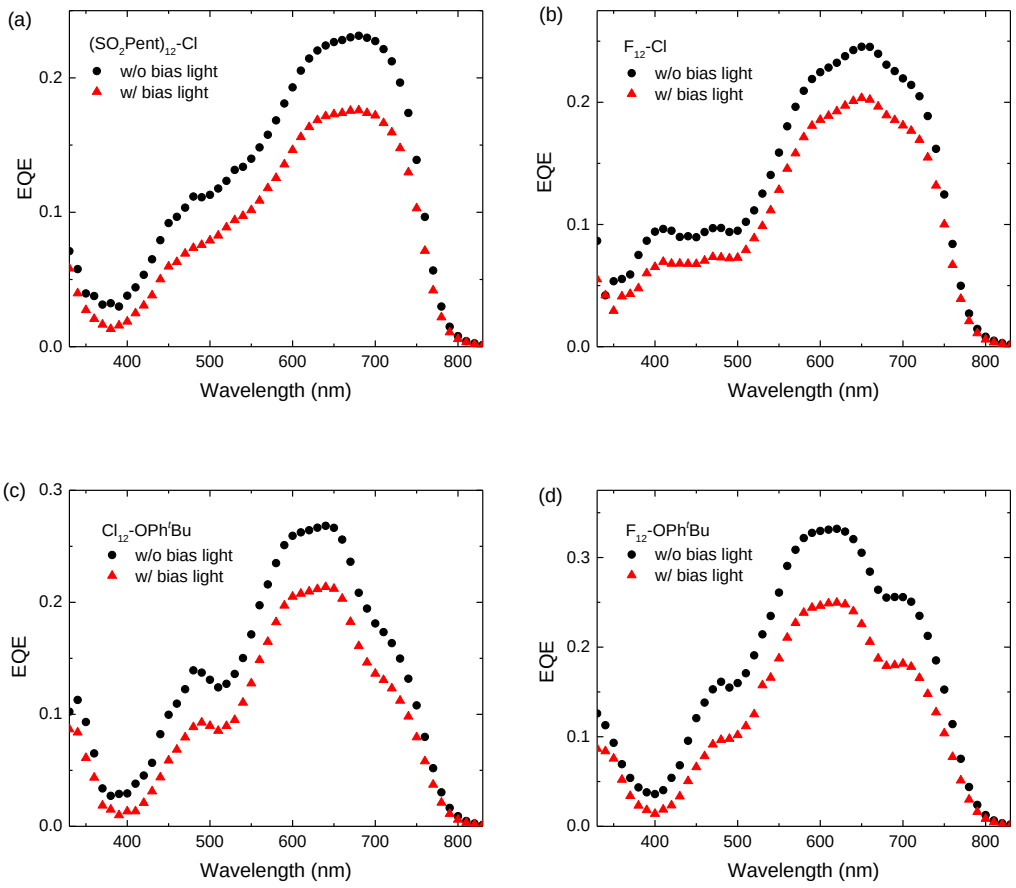

Figure 3.17. EQE spectra measured with and without light bias of the ITO/ZnO (40 nm)/PTB7-Th:SubNc-X/MoO_x (10 nm)/Ag (100 nm) solar cells: (a) **40** $(SO_2Pent)_{12}$-Cl, (b) **33** F_{12}-Cl, (c) **36** Cl_{12}-OPh^tBu, and (d) **37** F_{12}-OPh^tBu.

The average values for $\rho = EQE_{bias}/EQE_{nobias}$ (Figure 3.18) can be used to evaluate the bimolecular recombination efficiency via $\eta_{BR} = 1 - \rho$.[145] Clearly, the low ρ values indicate substantial bimolecular recombination. State-of-the-art PSCs often show a ρ value approaching unity. The ρ values of these PTB7-Th:SubNc solar cells are all lower

[145] L. J. A. Koster, M. Kemerink, M. M. Wienk, K. Maturová, R. A. J. Janssen, *Adv. Mater.* **2011**, *23*, 1670-1674.

than 0.85, suggesting significant bimolecular recombination losses, even at short-circuit. The extensive bimolecular recombination in the maximum power point and at short-circuit is also evidenced by the steady increase of current density of illuminated solar cells under reverse bias (Figure 3.15a) where the enhanced electric field promotes transport of the slowest carriers. The fact that the dark current does not increase to the same extent under reverse bias excludes the possibility that the increased current density under illumination is due to a low shunt resistance. Such behaviour is often found in bulk-heterojunction blends with an intimately mixed morphology and one slow carrier.[146]

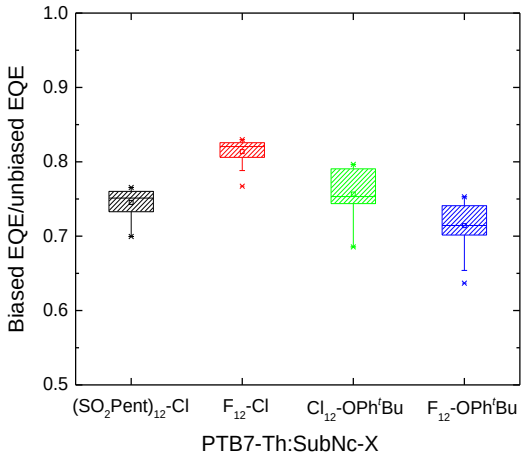

Figure 3.18. Average EQE_{bias}/EQE_{nobias} values of PTB7-Th:SubNc solar cells.

The morphology of PTB7-Th:SubNc blend films was studied by transmission electron microscopy (TEM). In TEM, all PTB7-Th:SubNc blends exhibit rather homogeneous films without noteworthy phase separation (Figure 3.19). In such intimately mixed blends, charge separation is impeded because of the lack of pure domains. It is well recognized that pure domains promote charge dissociation from the donor/acceptor interface, while impure domain often results in serious geminate recombination.[147] Moreover, charge transport is blocked in such intimately mixed

[146] D. Bartesaghi, M. Turbiez, L. J. A. Koster, *Org. Electron.* **2014**, *15*, 3191-3202.
[147] D. Veldman, O. Ipek, S. C. J. Meskers, J. Sweelssen, M. M. Koetse, S. C. Veenstra, J. M. Kroon, S. S. v. Bavel, J. Loos, R. A. J. Janssen, *J. Am. Chem. Soc.* **2008**, *130*, 7721-7735.

blends due to lack of continuous pathways for the transport of the photogenerated charge carriers, causing accumulation of space charge and recombination losses. Collectively, the low charge mobility, imbalanced hole/electron transport, and the suboptimal BHJ morphology are factors that contribute to recombination losses and that limit the J_{sc} and FF of PTB7-Th:SubNc solar cells.

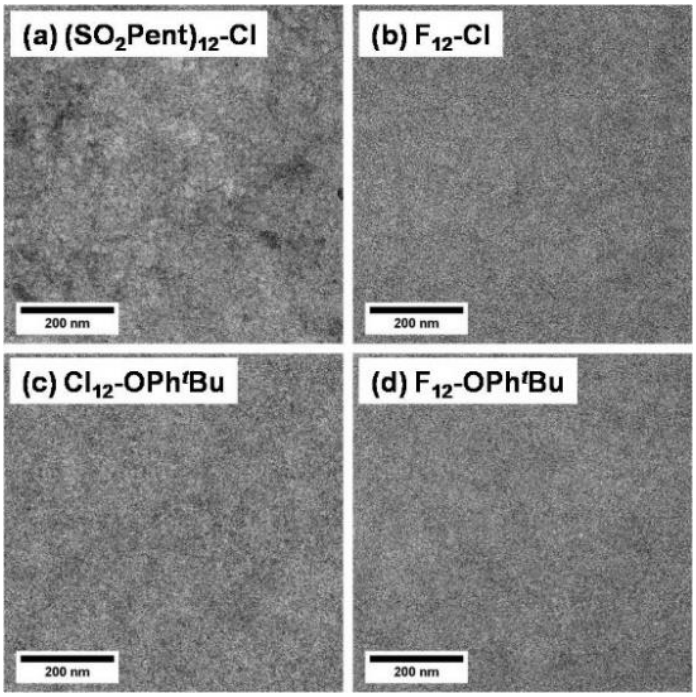

Figure 3.19. Bright-field TEM images of the PTB7-Th:SubNc blend films deposited with the same methods as those for PSC fabrication. Scale bar: 200 nm.

Notably, the highest PCE of SubNcs is much lower than that of the previously reported acceptor Cl_6-SubPc-(Cl) (1.09% versus 4.0 %).[57e] This can be rationalized considering the following aspects. First, Cl_6-SubPc-(Cl) has a small chlorine atom at the axial position, whereas SubNc **37**, which provided the best solar cells, has a bulky *t*-BuC_6H_4-O- group in this position. The small axial chlorine atom favors the formation of head-to-tail columnar stacks and thus prompts charge transport, whereas the bulky *t*-BuC_6H_4-O- group precludes this behavior and thus deteriorates charge transport.[57e] Second, the shorter exciton lifetimes of SubNcs compared to Cl_6-SubPc-(Cl), as suggested by the lower fluorescence quantum yields, is limiting the fraction of excitons

that reach the donor/acceptor interface, in which the exciton dissociates, reducing the EQEs of the SubNcs-based solar cells. Third, the SubNcs show redshifted absorption spectra with respect to SubPcs, which have a considerable spectral overlap between SubNcs and the polymer donor PTB7-Th.

3.3.2 Hexavinylester-SubPzs as new electron-acceptor molecules

Several studies in the Chapter 1 have demonstrated that the linkage of chromophores or redox/active units to the periphery of SubPzs through vinylene linkers can greatly influence the macrocycle electronic properties, as well as adjust its HOMO/LUMO energies. On this behalf, we decided to provide electron strong accepting nature to SubPzs by incorporating six methylester groups via ethene linkers. Three hexavinylester-SubPzs differently substituted at their axial positions, namely, with *p-tert*-butylphenoxy, phenoxy and fluorine groups, were designed and synthesized, in order to evaluate their optical and electrochemical properties (Figure 3.20).

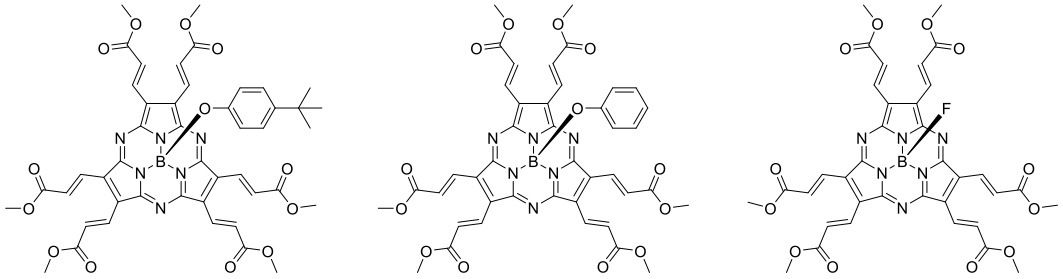

43 **44** **45**

Figure 3.20. Chemical structures of hexavinylester-SubPz **43**-**45** series.

3.3.2.1 Synthesis

The synthetic route devised for the SubPz derivatives **43**, **44** and **45** was the palladium-catalyzed, copper(I) thiophene-2-carboxylate (CuTC)-mediated coupling reactions on hexasulfanyl-SubPzs with vinilmethylester-boronic acid **46**, under the conditions described in Chapter 1 (Scheme 3.2). The synthesis of [(1*E*)-3-Methoxy-3-oxoprop-1-en-1-yl]boronic acid **46** was carried out following a reported procedure, that consists in the hydroboration reaction of methylpropiolate in excellent yields (Scheme 3.1).[148]

[148]a) F. Berrée, A. Debache, Y. Marsac, B. Collet, P. Girard-Le Bleiza, B. Carboni, *Tetrahedron* **2006**, *62,* 4027; b) M. V. Chelliah et al., *J. Med. Chem.* **2007**, *50,* 5147.

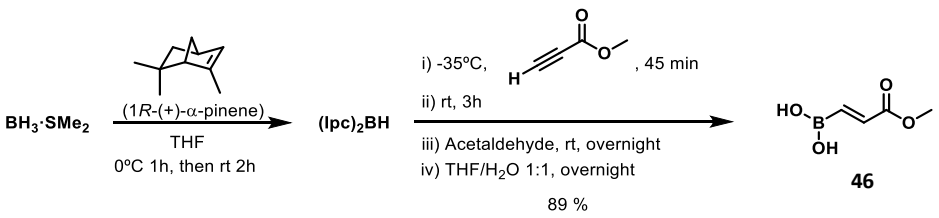

Scheme 3.1. Synthesis of boronic acid **46**.

p-tert-Butylphenoxy-substituted SubPz **43** was directly prepared from hexasulfanyl-SubPz precursor **2b**, and purified by column chromatography on silica gel, affording **43** in 35% yield as blue-green solid. SubPz **44** was obtained in 38% yield, using the corresponding phenoxy-substituted hexasulfanyl-SubPz **47**. The synthesis of SubPz **45** was carried out by treating SubPz **44** with excess $BF_3 \cdot OEt_2$ in toluene overnight at 80 ºC,[16c] affording **45** in 60% yield as a blue crystalline solid.

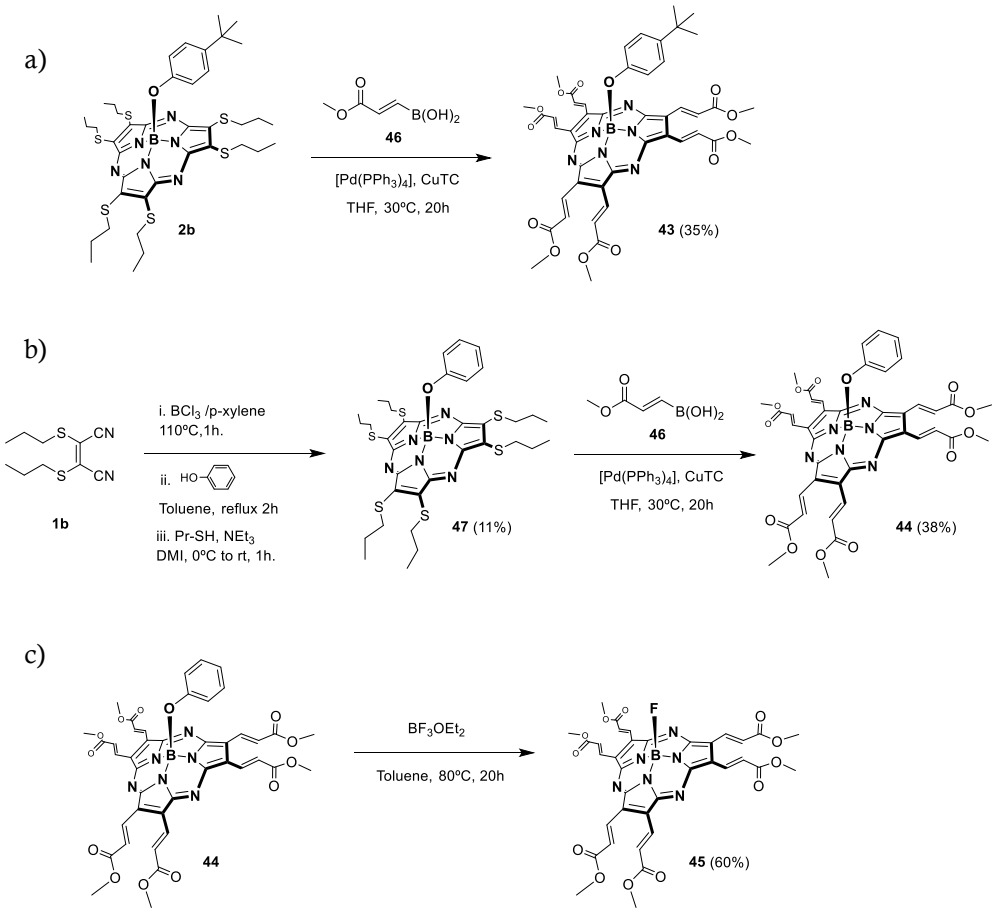

Scheme 3.2. Synthetic routes of hexavinylester-SubPz: (a) **43**, (b) **44** and (c) **45**.

A monocrystal of SubPz **44** was obtained by slow vapour diffusion of heptane into a solution of the SubPz in 1,2-dichloroethane, and the molecular structure was determined by X-Ray diffraction analysis. Figure 3.21 shows the *trans* configuration of the six vinylene moieties and the conical shape of the SubPz.

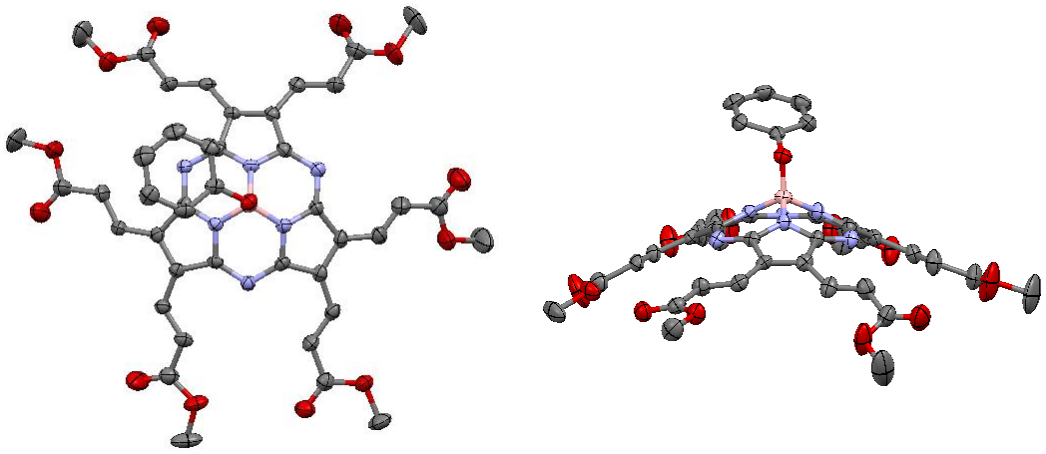

top view *side view*

Figure 3.21. Molecular structure showing thermal ellipsoids at the 50% probability level of SubPz **44**. Hydrogen atoms are omitted for clarity.

Figure 3.22 shows the ^{1}H-NMR spectra of SubPzs **43**-**45**. The signals corresponding to the six methyl groups of the ester functionsappear as a singlet at δ =3.95 ppm. The signals assigned to the vinyl protons are strongly downfield shifted owing to the SubPz diatropicity appearing as two doublets at δ = 8.00 and 8.14 ppm, with J ~16 Hz, that denote *trans*-stereochemistry, already anticipated by X-Ray diffraction analysis. Finally, the signals corresponding to the aromatic protons of the axial ligand for SubPzs **43** and **44** are found as two doublets at 5.3 and 6.8 ppm for **43**, and a doublet and two multiplets at 5.41, 6.73and 6.86 ppm for **44**.

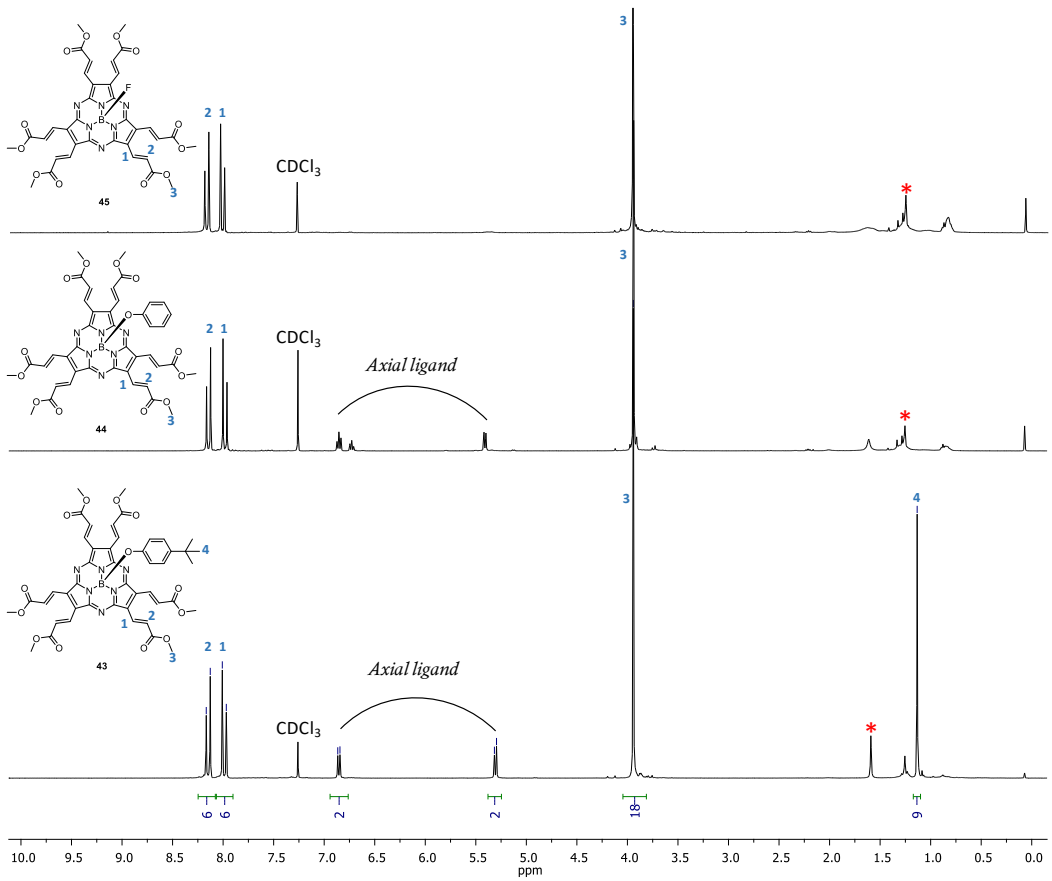

Figure 3.22. ^{1}H-NMR spectra in $CDCl_3$ at 25 °C of hexavinylester-SubPzs (**43-45**). Signals marked with * are due to residual solvents.

3.3.2.2 Optical properties

The optical absorption spectra of SubPzs **43-45** are shown in Figure 3.23. These spectra are similar and present a Q-band at 600 nm, that is, 100 nm red shifted related to that of hexapropyl SubPz **14**, but the Soret band remains at 280 nm. A CT band is found at 426 nm, denoting electronic delocalization over the vinylester moieties, but with lower absorption coefficients than for hexavinylene-SubPzs **11-13** owing to the electron-withdrawing character of the ester function.[48]

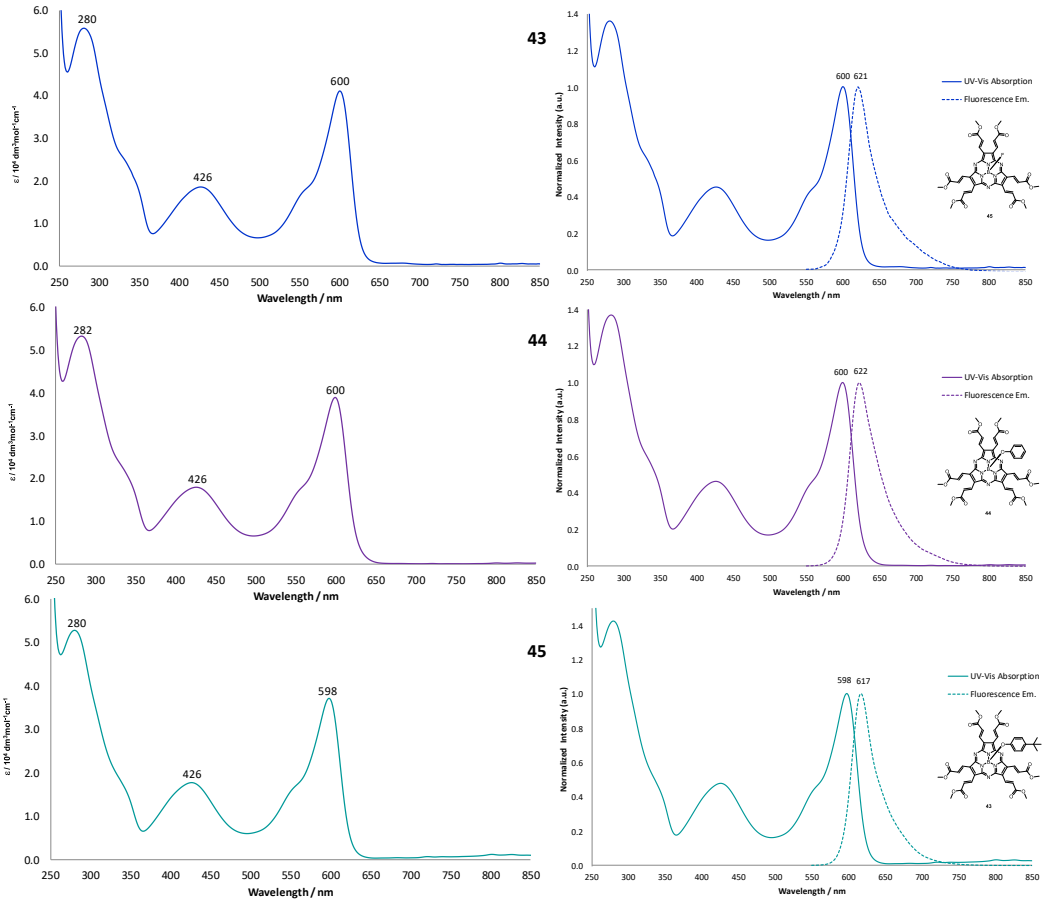

Figure 3.23. UV/Vis absorption spectra and normalized UV-Vis absorption (solid line)/fluorescence emission (dotted lined) spectra of SubPzs **43**-**45** in $CHCl_3$.

Regarding the emission spectra of SubPzs **43**-**45**, all of them consist in mirror images of the lowest energy absorption, with λ_{em} = 621, 622 and 617 nm, respectively, and corresponding stokes shifts of around 20 nm. Figure 3.23 displays the normalized absorption and emission spectra. Fluorescence quantum yields were measured using quinine (φ_F = 0.544) in water as standard, and the integrated area of fluorescence intensities (Figure 3.24)[149] afforded φ_F = 0.4%, 4.0% and 30% for **43**-**45**, respectively. The low influence of the axial substituents in the SubPz absorption profiles indicates low influence of these substituents in the SubPz ground state. Conversely, the different

[149] K. Rurack, M. Spieles, *Analytical Chemistry*, **2011**, *83*, 1232–1242.

values of the fluorescence quantum yields suggest their more important influence in the SubPz excited states.

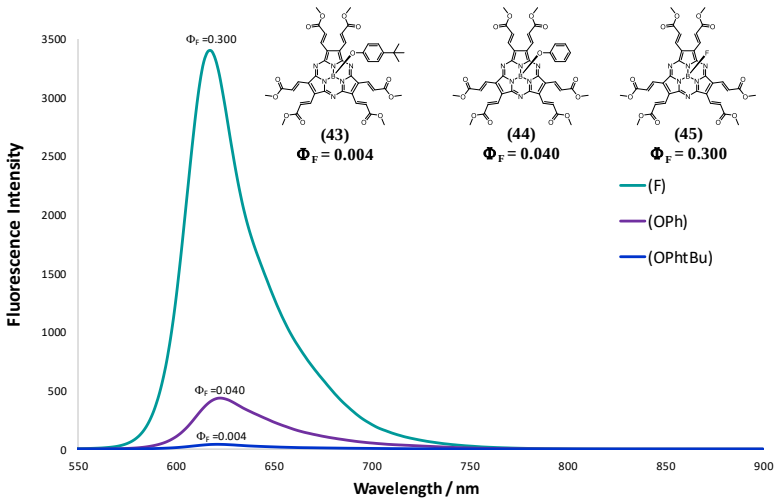

Figure 3.24. Fluorescence emission spectra of SubPzs **43-45** in $CHCl_3$

3.3.2.3 Electrochemical studies and energy levels

The electrochemical properties of SubPzs **43-45** have been investigated by cyclic voltammetry and square wave voltammetry in dry DCM, with a glassy carbon electrode as working electrode and using ferrocene as an external reference, with scan rate at 50 mVs^{-1}.

Similarly to hexavinylene SubPzs **12** and **13**, **43-45** show four strong reversible reduction potentials between –0.5 V and –1.70 V. No oxidation process was detected in CV and SWV for any of the three SubPzs (Figure 3.25).

The first reduction takes place at –0.75, –0.76 and –0.73 V for SubPzs **43-45**, respectively. Therefore, the ester-substituted **43-45** are 420 mV easier to reduce than SubPzs **12** and **13**, as a result of the good electronic communication between the terminal, electron accepting ester moieties and the SubPz. Compound **43** is also 330 mV easier to reduce than the corresponding hexaaryl derivative *para*-substituted with six ester functions.[48] Clearly, the vinylene linker serves to efficiently transmit the redox features of the ester function to the SubPz macrocycle. The four reversible reduction

waves are distributed between 0.2 and 0.3 V. All the electrochemical data are summarized in Table 3.4.

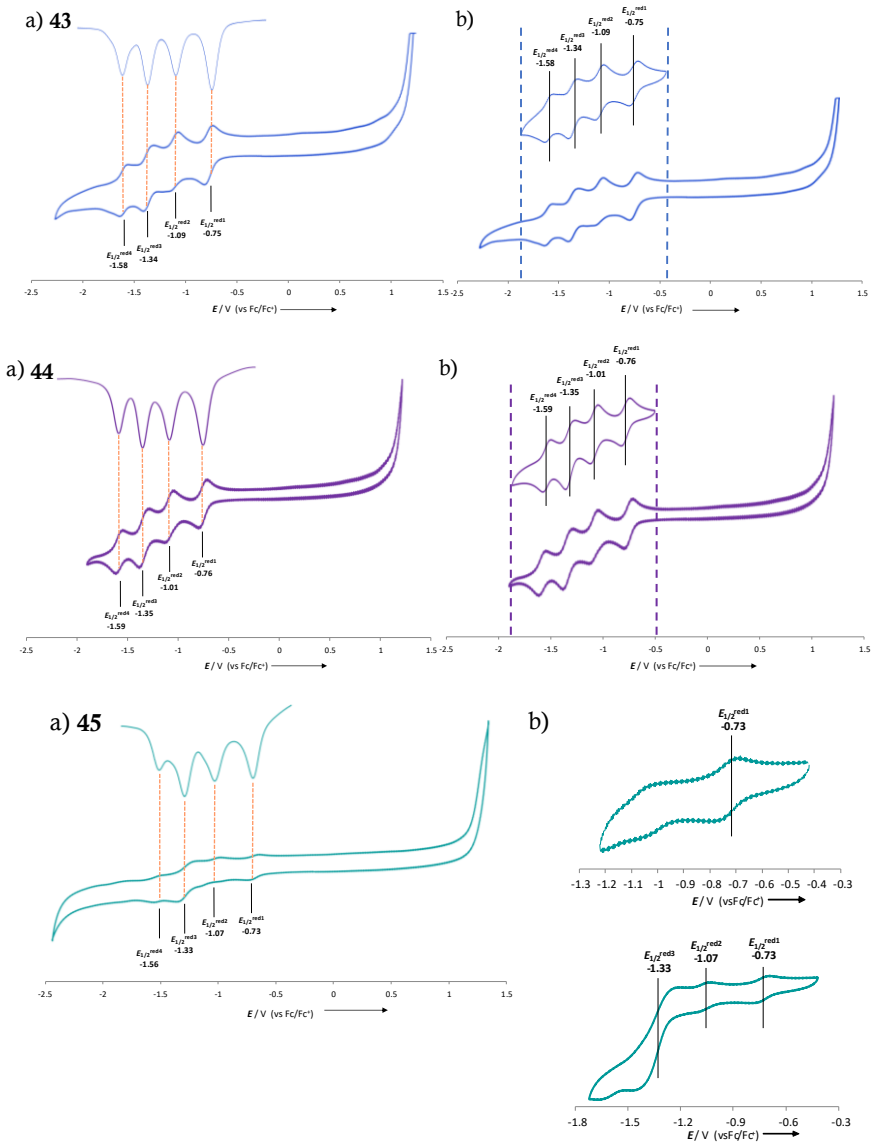

Figure 3.25. (a) Cyclic voltammograms and SWV of **43**-**45**; (b) Scan CV in the reduction window. Solvent: CH_2Cl_2 ; scan rate: 50 mVs^{-1}; working electrode: platinum; counter electrode: platinum wire; reference electrode: $Ag/AgNO_3$; electrolyte: Bu_4NPF_6.

SubPz	E_{red1}	E_{red2}	E_{red3}	E_{red4}
43	**–0.75**	–1.09	–1.34	–1.58
44	**–0.76**	–1.01	–1.35	–1.59
45	**–0.73**	–1.07	–1.33	–1.56

Table 3.4. Electrochemical reduction potentials (in V) for SubPzs **43**-**45** , **E** vs. Fc/Fc^{+}.

LUMO energies were estimated applying the reported approximation[74] (directly from the first reduction values derived from CV data). And HOMO energies were obtained from LUMO values and optical band gap E^{g}_{opt} values, which were estimated from the offset wavelength derived from the low energy absorption band.[75] Experimental values place the HOMO level of SubPz **43** at –6.38 eV and the LUMO at –4.35 eV. The values are very similar to those found for SubPz **44** and **45**. Figure 3.26 shows the schematic representation of the HOMO/LUMO energy values of the series compared with SubPz **12** and the electron-acceptor fullerene derivative PCBM.[150]

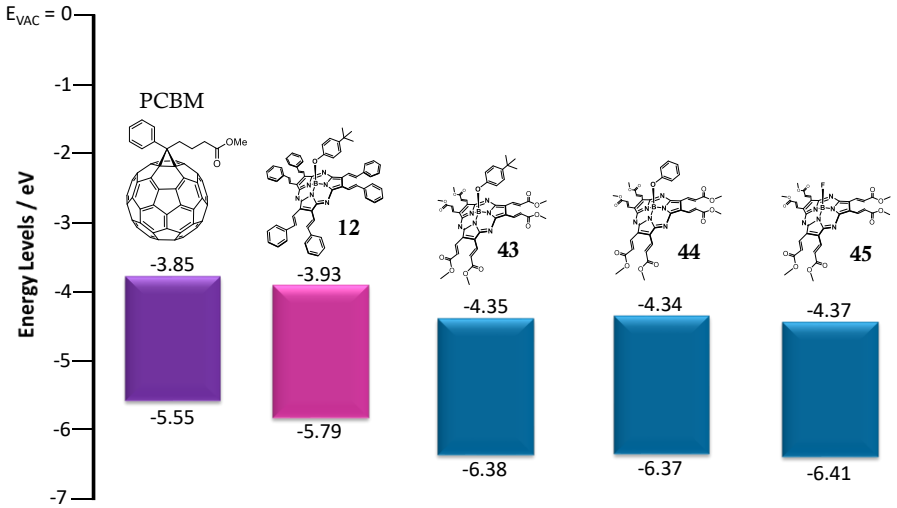

Figure 3.26. Representation of the HOMO and LUMO levels of PCBM and hexavinylated SubPz series **12**, **43-45**.

[150] T. Kim, J.-H. Kim, T. E. Kang, C. Lee, H. Kang, M. Shin, C. Wang, B. Ma, U. Jeong, T.-S. Kim, B. J. Kim, *Nat. Commun.* **2015**, *6*, 8547.

3.3.3 Subporphyrazine based molecular sensitizers for DSSCs

The work presented in this section is focused on the design, synthesis and application in DSSCs of novel sensitizers based on SubPzs, where a spaced carboxylic acid group is anchored to the periphery of a SubPz taking advantage of the unsymmetrical functionalization of the monochlorinated pentasulfanyl-SubPz **3b**. In addition, the macrocycles are functionalized with five peripheral aryl functions with electron-donor features, which can also reduce the aggregation phenomena owing to their steric bulk (SubPz **48**-**52**, Figure 3.27). Our inspiration emanates from previous works on the application of subporphyrinoid-based sensitizers in DSSCs. In particular, subphthalocyanines bearing a carboxylic acid either at the peripheral or axial positions have been reported as photosensitizers for DSSCs.[151] On the other hand, subporphyrin-based molecular sensitizers have proven their potential in this field. Specifically, a SubPs *meso*-substituted with two sterically demanding 3,5-di-*tert*-butylphenyl rings, and a cyanoacrylic acid anchoring group attached through a *meso*-ethynylphenyl spacer, achieved a power conversion efficiency of 10.1% (Figure 3.28).[143]

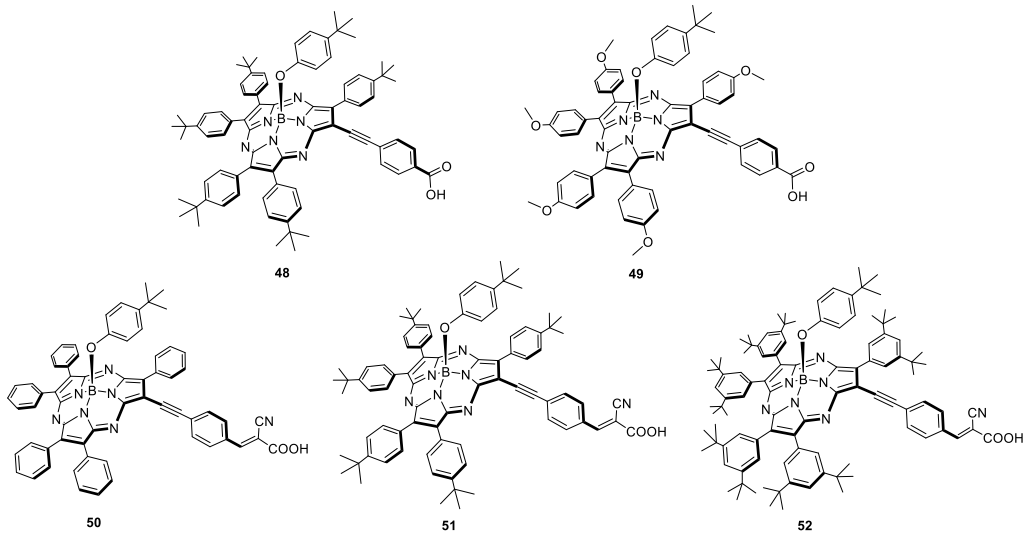

Figure 3.27. Chemical structure of SubPzs **48**-**52**.

[151] a) M. Ince, A. Medina, J.-H. Yum, A. Yella, C. G. Claessens, M. V. Martínez-Díaz, M. Grätzel, M. K. Nazeeruddin, T. Torres, *Chem. Eur. J.* **2014**, *20*, 2016–2021; b) M. Urbani, F. A. Sarı, M. Grätzel, M. Nazeeruddin, T. Torres, M. Ince, *Chem. Asian J.* **2016**, *11*, 1223–1231.

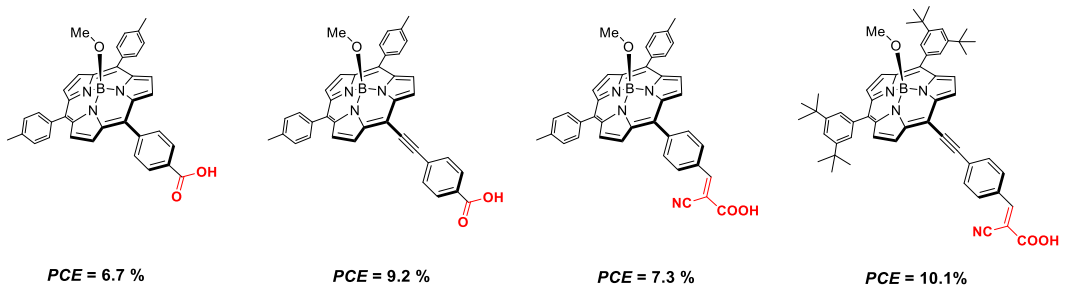

Figure 3.28. First generation SubP sensitizers for use in DSSCs.[143]

Compound **53** (Scheme 3.3) constitutes a common synthetic intermediate for the preparation of SubPzs **48**-**52**. This compound was prepared by Sonogashira coupling reaction on the inseparable mixture of sulfanylated-SubPz **2b** and **3b** (see Scheme 1.6 on page 51) with 4-ethynylbenzaldehyde. Fortunately, the Sonogashira product was easily separated from hexasulfanyl-SubPz **2b**, which remains unchanged under this reaction conditions. SubPz **53** was obtained in good yield (58%), taking into account the 1:1 ratio of **2b** and **3b.**

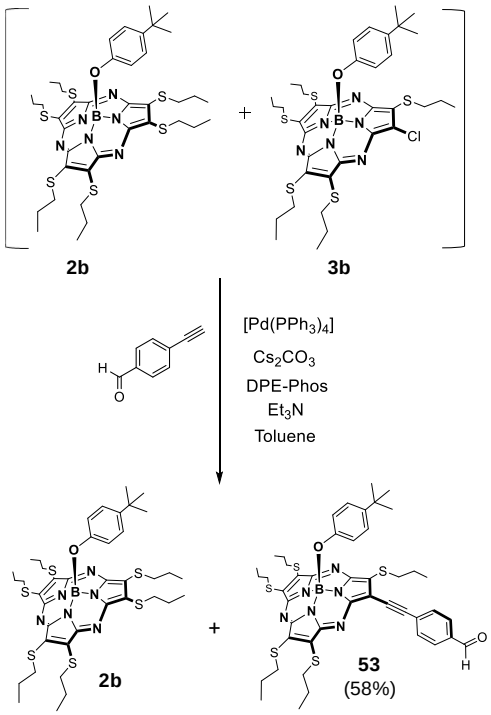

Scheme 3.3. Synthesis of SubPzs **48** by Sonogashira coupling reaction of SubPz **3b**.

Next CuTC-mediated Liebeskind and Srogl cross-coupling reactions of SubPz **53** with a variety of arylene-boronic acids at 60 ºC afforded the pentaarylated-SubPzs **54**–**57**, with yields of isolated products ranging from 15% to 40% (Scheme 3.4). In The role of the aryl moieties is to provide stability to the SubPz structure, as well as optimize the absorption, fluorescence and electrochemical properties.

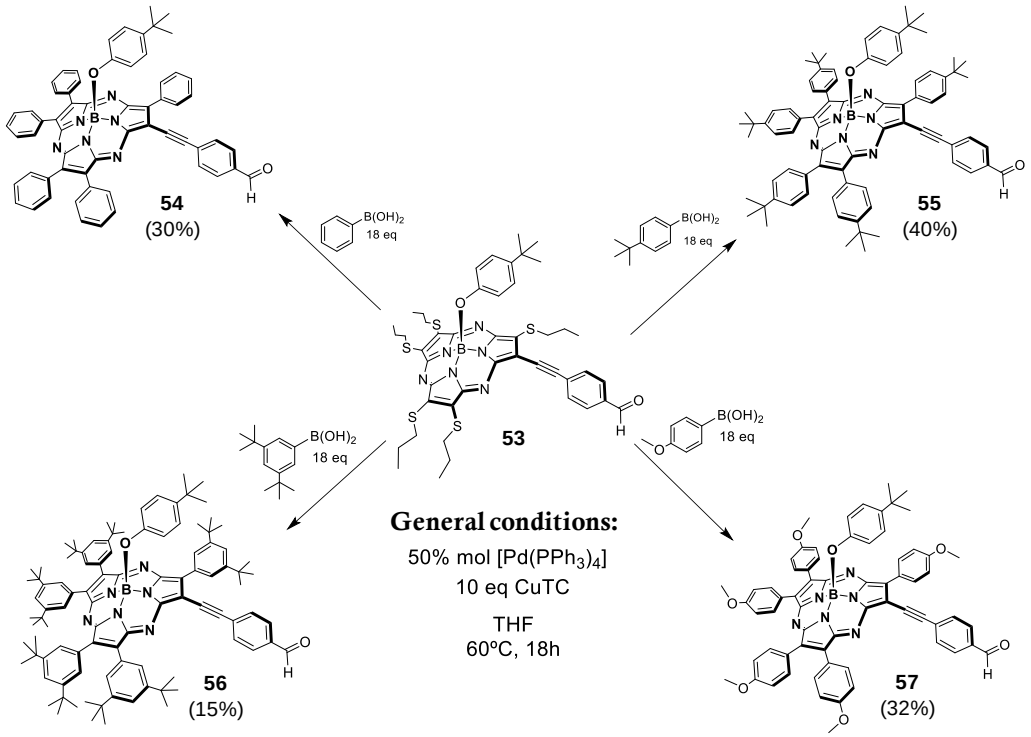

Scheme 3.4. General procedure for the synthesis of arylated-SubPzs **54**-**57**.

Figure 3.29 shows the ^{1}H-NMR spectra of SubPzs **53**-**57**. All of them display the signal corresponding to the proton of the aldehyde at around 10.1 ppm. The axial *tert*-butylphenoxy substituent appears as two doublets at 5.3-5.4 ppm and 6.8-6.9 ppm, and a singlet around 1.11-1.15 ppm. In addition, the signals assigned to the phenyl ring adjacent to the ethynyl spacer of SubPzs **54**-**57**, are found at 8.3-8.8 ppm, strongly downfield shifted. Contrasting, the signals of the other phenyl rings appear at 7.2-7.9 ppm for **54**-**56** and at 6.9-7.1 ppm for the 4-methoxy-substituted SubPz **57**.

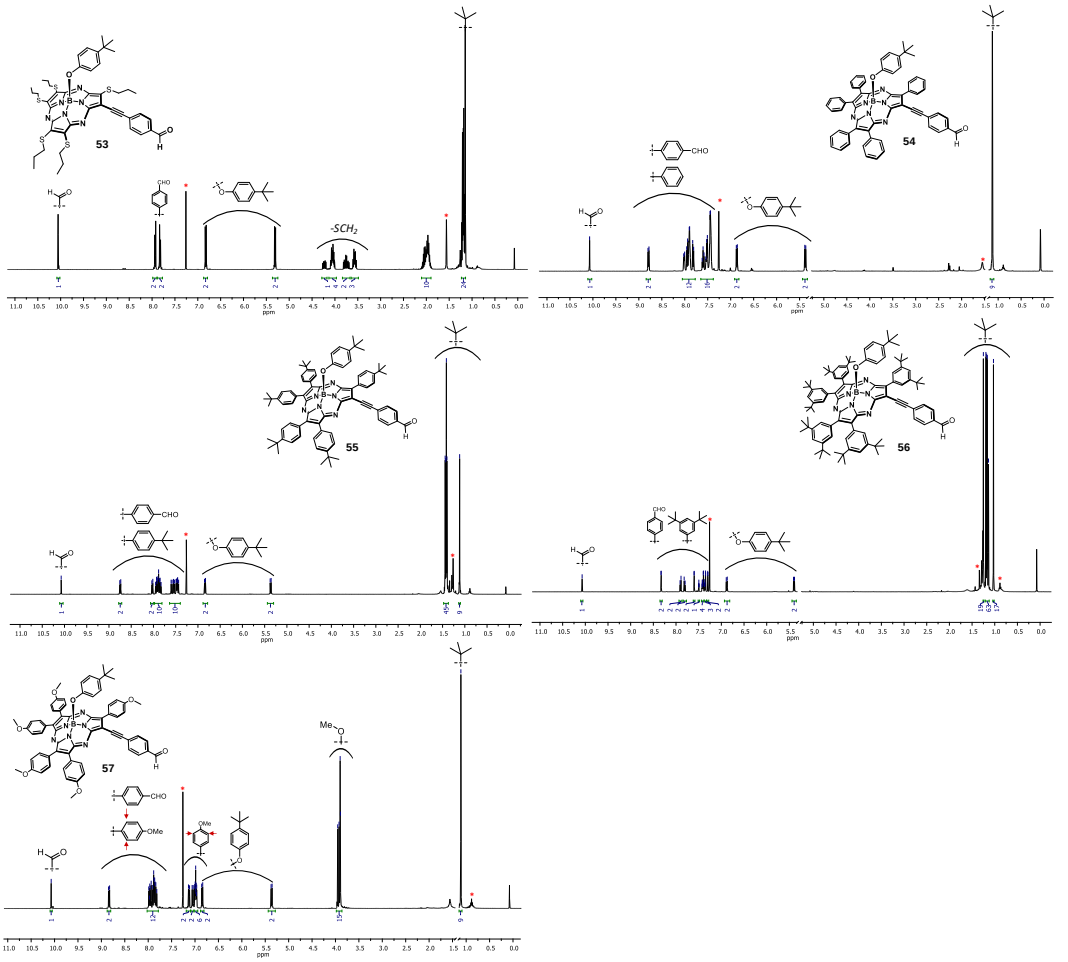

Figure 3.29. ^{1}H-NMR spectra in $CDCl_3$ at 25 °C of SubPzs **53**-**57**.

The preparation of sensitizers **48** and **49** was carried out by oxidation of the formyl group of ***55*** and **57** to carboxylic acid, through treatment with six equivalents of sodium chlorite ($NaClO_2$), as oxidative reagent and six equivalents of sulfamic acid, as hypochlorite scavenger, in acetone at 0 °C. Here, the reaction time was found crucial to achieve high yields of the carboxylated product. Thus, two hours were necessary to oxidize SubPz **48** in 70% yield, while SubPz **49** was oxidized in 68% yield only in 30 minutes. (Scheme 3.5).

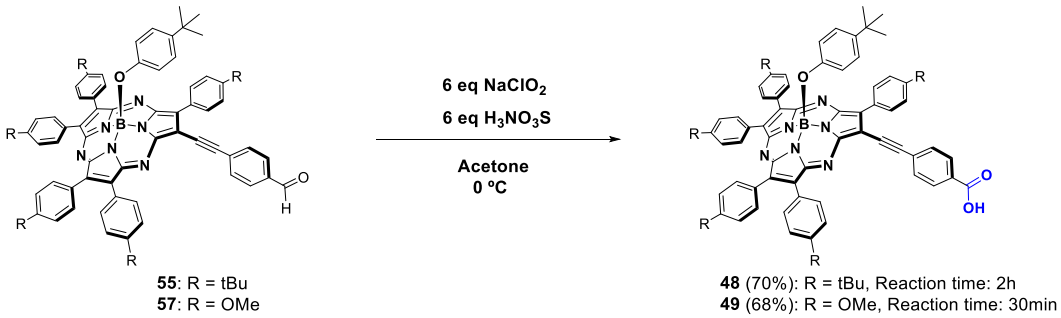

Scheme 3.5. Synthesis of SubPzs **48** and **49** by oxidation of **55** and **57**.

Compounds **50**-**52** were prepared through a classical Knoevenagel condensation of **54**-**56**. The reaction was carried out using excess of cyanoacetic acid and ammonium acetate catalyst, in toluene, at 80 °C, for 25 h, to furnish SubPzs **50**-**52** in good yields (Scheme 3.6). It is worth mentioning that the cyanoacrylic acid anchoring group had been proved as an optimal anchoring unit, since it provides efficient electron transfer to the TiO_2 in the device.[114a,121c]

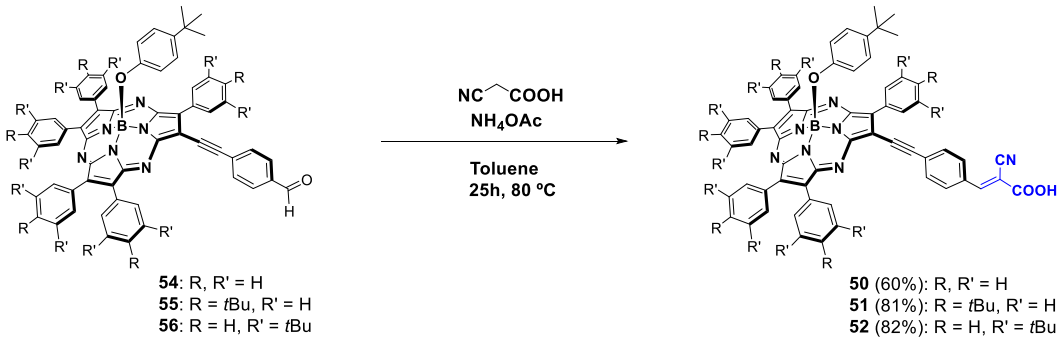

Scheme 3.6. Synthesis of SubPzs **50**, **51** and **52**.

All SubPz dyes were purified by column chromatography on silica gel, using a (4 : 4 :1.5 : 0.5) mixture of *n*-hexane/DCM/AcOEt/MeOH as eluent. The structures of SubPzs **48**-**52** were unequivocally confirmed by MALDI-TOF or APCI mass spectrometry, UV-Vis, FT-IR, and NMR techniques.

Figure 3.30 displays the UV-Vis absorption spectra of SubPzs **48**-**52** in $CHCl_3$. All compounds exhibit panchromatic absorption in the range of 270-600 nm, with the

typical Soret, CT and Q- absorption bands of peripherally arylated-SubPzs, with molar absorption coefficients of the Q-bands around 4.5×10^4 $cm^{-1}\cdot M^{-1}$ and 6.0×10^4 $cm^{-1}\cdot M^{-1}$.

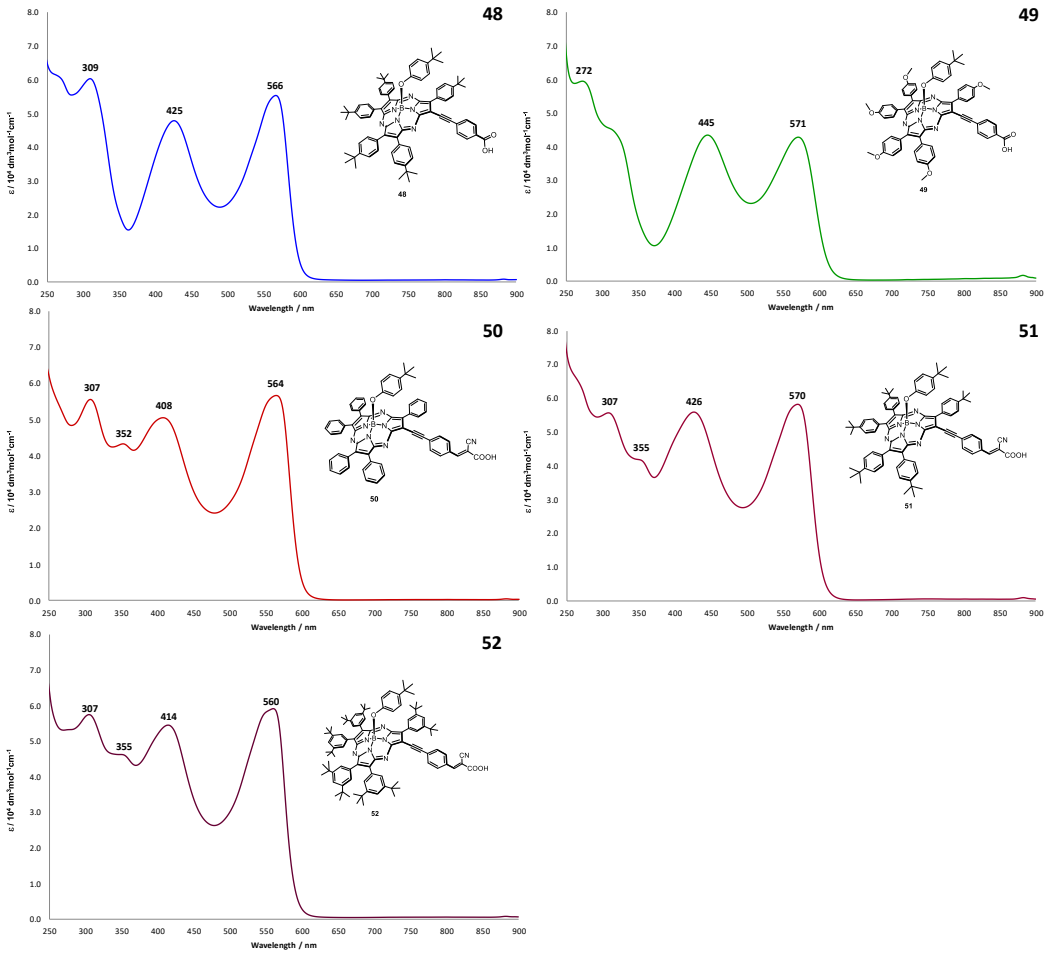

Figure 3.30. Absorption spectra of SubPzs **48**-**52** in $CHCl_3$.

SubPzs **48** and **49**, bearing a carboxyphenylethynyl anchoring unit, display their Q-band at 566 nm and 571 nm, respectively, in addition to CT bands at 425 nm and 445 nm, respectively, being slightly more red-shifted for SubPz **49**. On the other hand, the conjugation of SubPzs **50**-**52** with a cyanoacrylic acid anchoring group enhances the panchromatic absorption.

Regarding the fluorescence spectra (Figure 3.31), the emission band of SubPzs **48**-**52** upon excitation at 500 nm (for **49** and **51**) or 520 nm (for **48**, **50** and **52**), mirror-

images the Q-band. The Stokes shift are in the 39-43 nm range for SubPzs **48** and **51-52**, and 52 nm for SubPz **49**. With these data, the zero-zero excitation energy $E_{0\text{-}0}$ was obtained from the intersection between the normalized absorption and emission spectra.

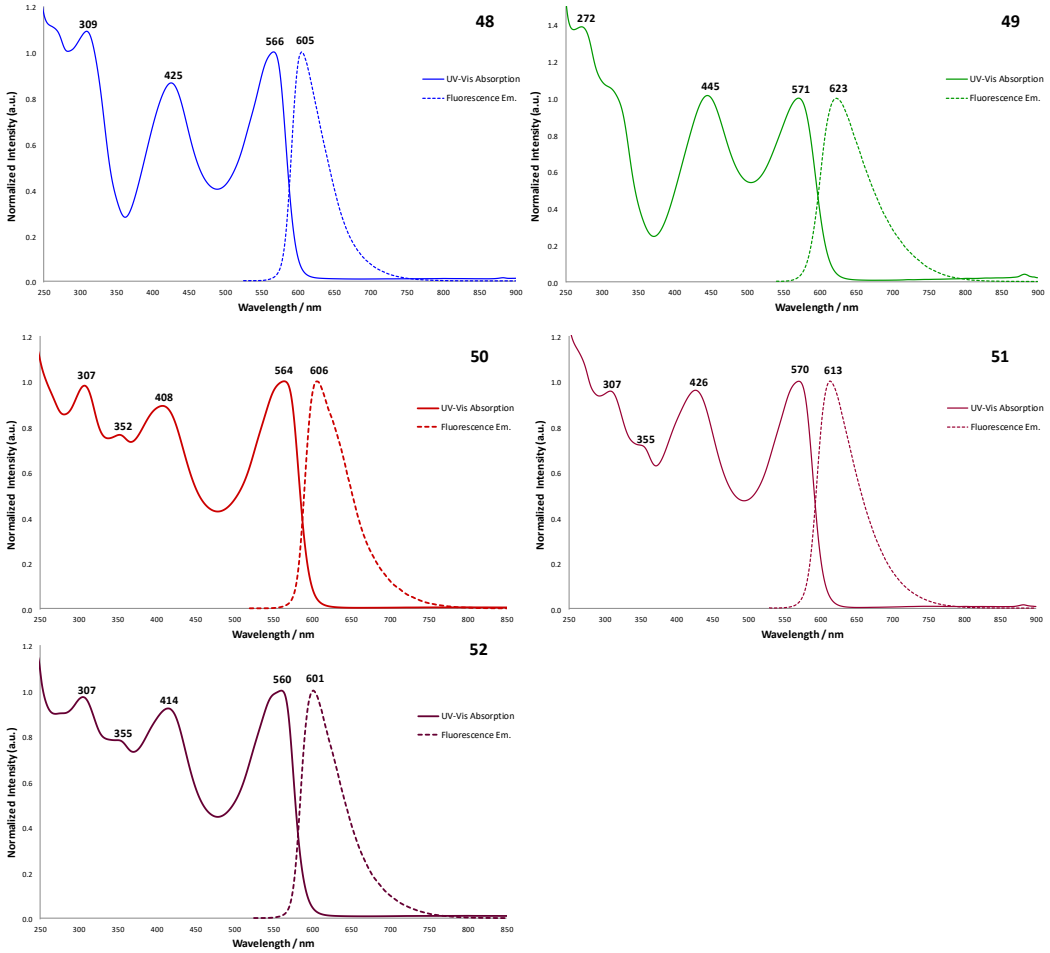

Figure 3.31. Normalized UV/Vis absorption and fluorescence emission spectra of SubPzs **48-52** in $CHCl_3$

Electrochemical characterization of SubPzs **48-52** was performed by cyclic voltammetry in 0.1M tetrabutylammonium phosphate ($TBAPF_6$) CH_2Cl_2 solutions, using ferrocene as internal reference (Figure 3.32). All of them display in CV an irreversible wave for the first oxidation, with values in the 0.92–1.06 V range versus Fc/Fc^+. For the reduction, three or four waves could be observed, the first one being

reversible or quasi-reversible, at around –1.16 V (for **50**) and –1.31 V (for **52**). Due to the presence of multiple reduction waves, oxidation (E_{Ox1}) and reduction potentials were determined by square-wave voltammetry (Figure 3.32). The respective first oxidation/reduction potentials, together with the HOMO/LUMO values vs the normal hydrogen electrode (NHE), are summarized in Table 3.5. HOMO and LUMO levels were estimated from peak potentials by setting the oxidative and reductive peak potentials of Fc/Fc^+ vs NHE to 0.642 V.[74,152]

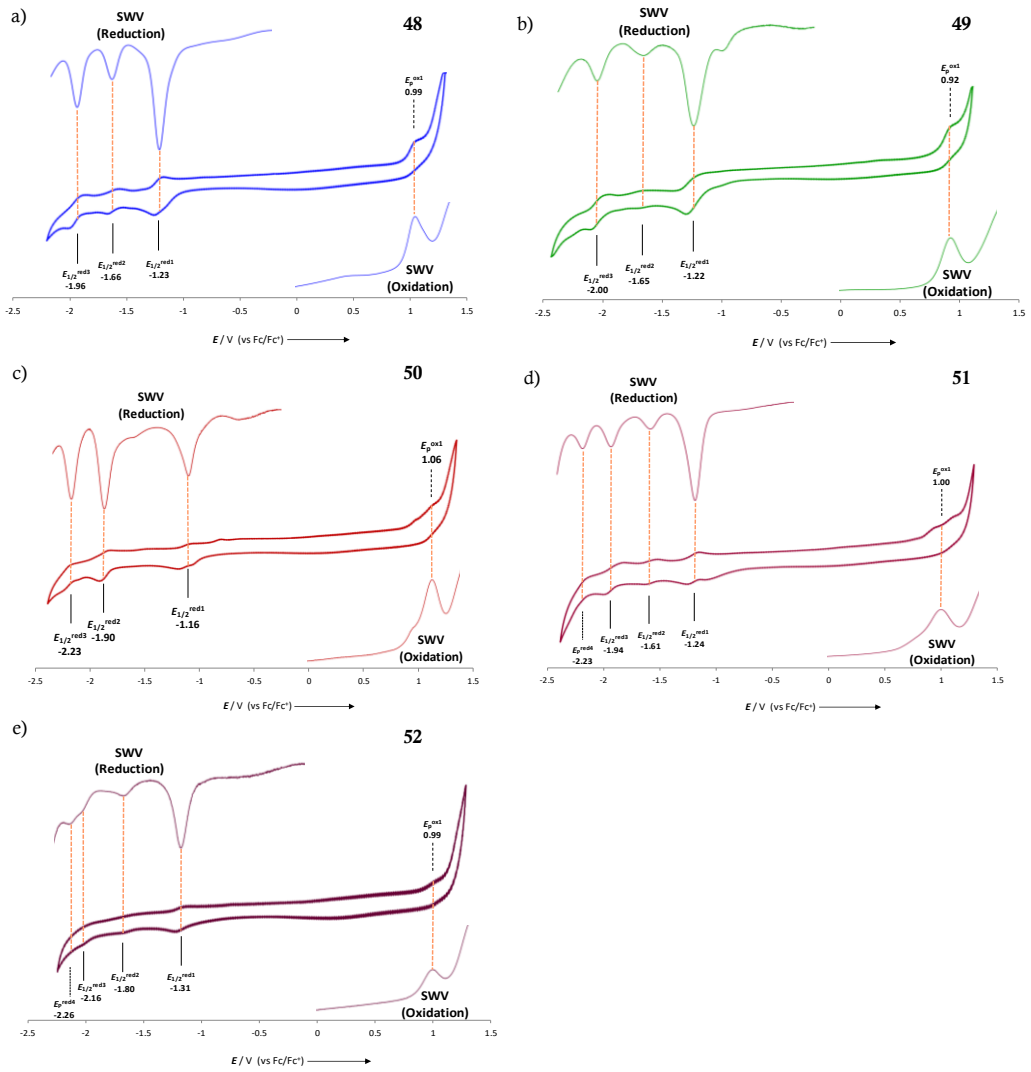

Figure 3.32. Cyclic voltammograms and SWV of SubPzs **48**-**52**.

[152] N. G. Connelly, W. E. Geiger, *Chem. Rev.* **1996**, *96*, 877–910.

Notably, the electrochemical HOMO–LUMO bandgap is consistent with the optical ($E_{0\text{-}0}$) bandgap obtained from the intersection between the absorption and emission spectra (Table 3.5). Figure 3.33 shows an energy-level diagram for the SubPz dyes **48**-**52**, comparing their HOMO–LUMO levels with the standard potential for the CB of TiO_2 *vs.* NHE (E_{CB} = *–0.5 V*), and for the $Co(bpy)_3^{2+/3+}$ redox couple mediator *vs.* NHE (*E = 0.59 V*).[153] The driving forces for electron injection from the SubPz singlet excited state to the CB of TiO_2 (ΔG_{inj}) and for the regeneration of the SubPz radical cation by the $Co(bpy)_3^{2+/3+}$ redox couple (ΔG_{reg}) in a conventional DSSC have been determined (Table 3.5). The oxidation potentials of all SubPzs are by far more positive than that of the $Co(bpy)_3^{2+/3+}$ redox couple of the electrolyte ensuring a very large driving force for dye regeneration (ΔG_{reg}) in the operative DSSCs. Thus, we would expect a high dye-regeneration efficiency for all dyes. The LUMO energy-levels of all SubPzs are more negative than the TiO_2 conduction band, hence making the electron injection of the excited dye in the TiO_2-CB thermodynamically feasible. However, the low-lying LUMO levels of these sensitizers result in relatively small driving forces for electron injection (ΔG_{inj} = –0.02 - –0.17 eV), which certainly constitute the main issue for this class of sensitizers, limiting their electron-injection efficiency and hence their J_{SC} in DSSC.

[153] M. Wang, C. Grätzel, S. M. Zakeeruddin, M. Grätzel, *Energy Environ. Sci.* **2012**, *5*, 9394.

SubPz	E^{red1}/ V (vs Fc/Fc$^+$)	E^{ox1}/ V (vs Fc/Fc$^+$)	E^{red1}/ V (vs NHE)	E^{ox1}/ V (vs NHE)	$E_{0\text{-}0}$ /eV	$E_{0\text{-}0}^*$ /eV	ΔG_{inj} /eV	ΔG_{reg} /eV
48	**-1.23**	**0.99**	**-0.59**	**1.63**	**2.11**	**2.22**	**-0.09**	**-1.04**
49	**-1.22**	**0.92**	**-0.58**	**1.56**	**2.08**	**2.14**	**-0.08**	**-0.97**
50	**-1.16**	**1.06**	**-0.52**	**1.70**	**2.11**	**2.22**	**-0.02**	**-1.11**
51	**-1.24**	**1.00**	**-0.60**	**1.64**	**2.09**	**2.24**	**-0.10**	**-1.05**
52	**-1.31**	**0.99**	**-0.67**	**1.63**	**2.13**	**2.30**	**-0.17**	**-1.04**

zero-zero excitation energy:
E_{0-0} was determined from the intersection of absorption and emission spectra in $CHCl_3$
E_{0-0}^* Electrochemical HOMO-LUMO bandgap

Table 3.5. Electrochemical data by CV and SWV, HOMO/LUMO levels, zero-zero excitation energy ($E_{0\text{-}0}$), and driving forces for electron injection and regeneration for SubPzs **48**-**52**.

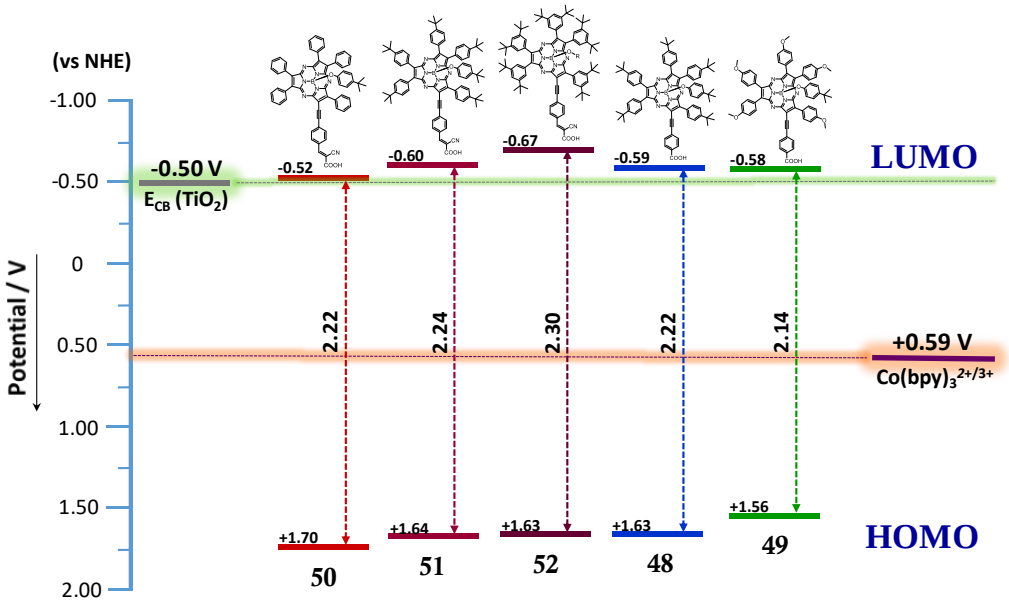

Figure 3.33. Schematic energy-levels diagram of SubPzs **48**-**52**.

To gain insight into the geometrical and electronic structures of the new dyes, density functional theory (DFT) calculations were performed on the five SubPz sensitizers **48**–**52**, using the GAUSSIAN 09 package and applying B3LYP exchange-

correlation functional and 6-31G basis set for the geometry optimization, followed by 6-311g (d,p) for the calculation of the energy levels. Figure 3.34 shows the electronic distribution and the energy levels of frontier orbitals obtained both by computational studies and from the electrochemical data. The trends of calculated energies are consistent by theoretical and experimental methods, although in all cases the values obtained by the former are higher in energy than those arising from the latter. All dyes show some extent of orbital partitioning. As predicted in chapter 1 for peripherally arylated SubPzs, **48**-**52** display the HOMOs mainly localized on the SubPz macrocycle, with only partial electronic distribution on the aryl rings, according to each substitution pattern, and marginal or no electronic delocalization over the anchoring moiety. Consistent with its substitution pattern, **49** shows the HOMO also delocalized over the methoxyphenyl units. The LUMOs of the series, however, are delocalized both on the SubPz macrocycle and over the anchoring group. The latter is an important factor, because it governs the efficiency of the electron injection of the excited dye into the TiO_2.

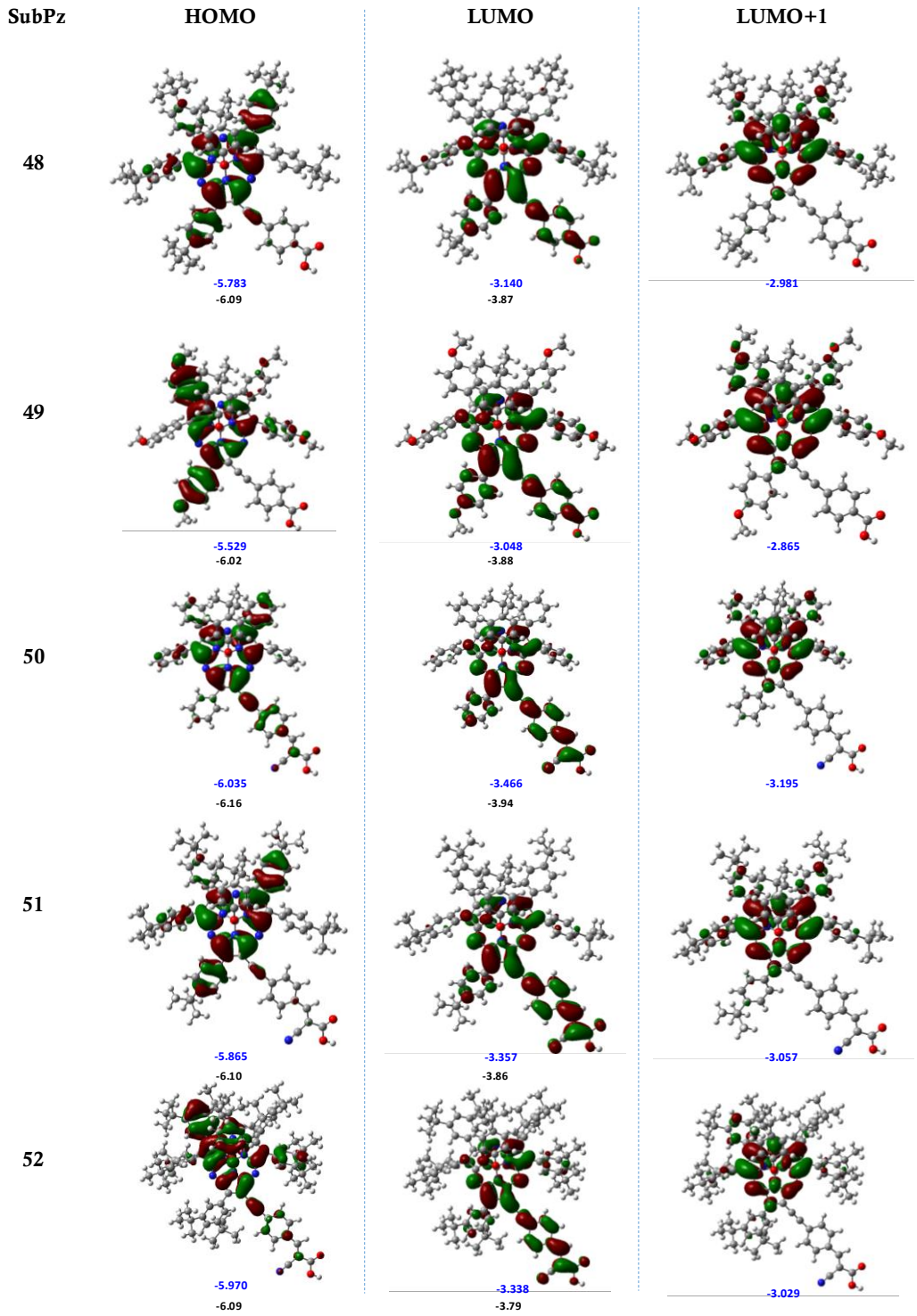

Figure 3.34. DFT predicted frontier orbitals for SubPzs **48**-**52**. Values in black are obtained from electrochemical data.

3.3.3.1 Photovoltaic performances in TiO_2-DSSC

The study of the performance of the prepared dyes was carried out in the laboratory of Prof. Hwan Kyu Kim at Global GET-Future Laboratory and Department of Advanced Materials Chemistry in Korea University.

The five sensitizers **48**-**52** were tested in DSSCs on [9+4] mm thick TiO_2-films, which consist of a 3.5 mm thick active layer and an additional 3.5 mm thick scattering layer. For the preparation of the devices, the TiO_2 photoanodes were immerged in a 0.2 mM solution of SubPz in (EtOH/THF = 4:2) with 0.8 mM CDCA for 1 h. Table 3.6 summarizes the dye-loading densities and photovoltaic data obtained for the SubPz-based DSSC devices. The optical absorption spectra of SubPzs **48**-**52** on TiO_2 film and after desorption experiments are collected in Figure 3.35.

Dye	Electrolyte	Adsorption amount (10^{-8} mol cm^{-2})	J_{SC} (mA cm^{-2})	V_{OC} (V)	FF (%)	**PCE[a] (%)**
50[b]		4.08	0.01	0.001	44.6	**0.01**
51[b]		2.81	0.01	0.432	73.2	**0.01**
52[b]	$Co(bpy)_3^{2+/3+}$	3.10	0.01	0.431	74.2	**0.01**
48[b]		3.46	0.01	0.430	73.3	**0.01**
49[b]		4.07	0.01	0.418	73.6	**0.01**
50[b]		-	0.01	0.001	44.6	**0.01**
51[b]		-	0.01	0.423	68.2	**0.01**
52[b]	I^-/I_3^-	-	0.01	0.431	70.5	**0.01**
48[b]		-	0.01	0.430	71.3	**0.01**
49[b]		-	0.01	0.418	69.6	**0.01**

[a]Irradiated light: AM 1.5G (100 mWcm^{-2}); cell area tested with a metal mask: 0.141 cm^2.
Cobalt electrolyte: 0.22 M $[Co^{II}(bpy)_3](TFSI)_2$, 0.05 M $[Co^{III}(bpy)_3](TFSI)_3$, 0.1 M LiTFSI and 0.8 M TBP in CH_3CN.
Iodine electrolyte: 0.6 M DMPII, 0.5 M TBP, 0.05 M I_2 and 0.1 M LiI in CH_3CN.
[b]Dipping condition: 0.2 mM dye solution (EtOH/THF = 4:2) with 0.8 mM CDCA for 1 h.

Table 3.6. Photovoltaic performances of the DSSCs based on SubPzs **48**-**52** under one-sun illumination (AM 1.5G).

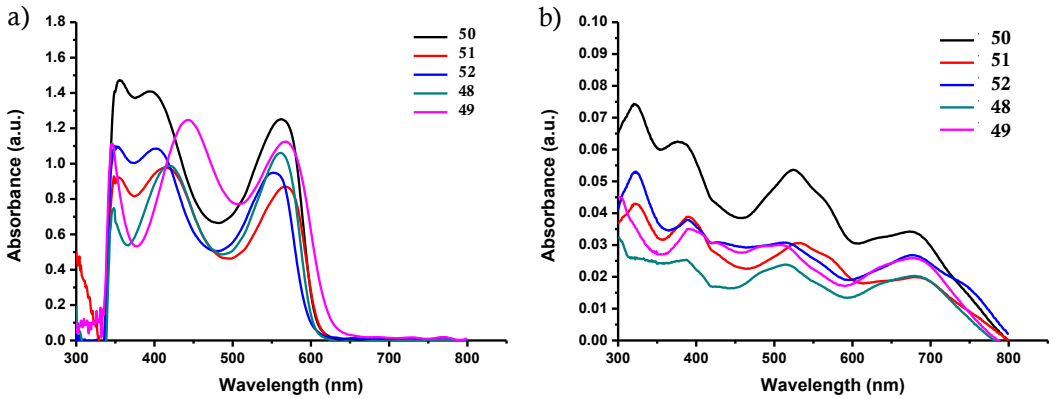

Figure 3.35. (a) UV-Vis spectra of SubPz-series on TiO_2 film and (b) UV-Vis spectra in 0.1 M NaOH solution (THF/EtOH/H_2O (v/v =1:1:1)) after desorption experiments.

Unfortunately, the photovoltaic parameters were lower than expected, even using I^-/I_3 as electrolyte. The LUMO energy levels of **48**-**52**, which are close to the Fermi Level of TiO_2 could be responsible for inefficient charge injection from the sensitizers to TiO_2, resulting in the low photovoltaic efficiencies observed. Figure 3.36 shows the *J-V* curves of DSSC devices based on SubPzs **48**-**52** with the $Co(bpy)_3^{2+/3+}$ redox electrolyte.

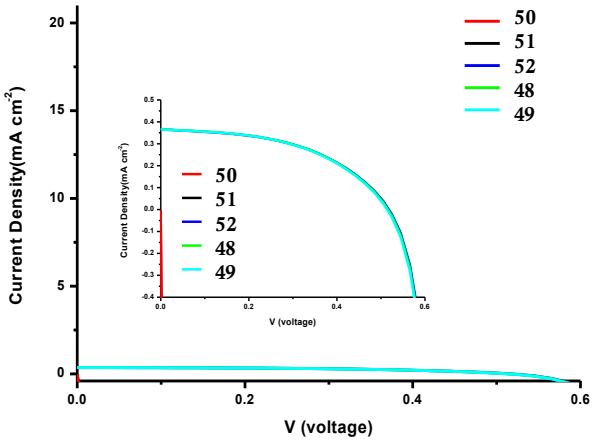

Figure 3.36. *J-V* curves of DSSCs based on SubPzs **48**-**50**. Irradiated light: AM 1.5G (100 $mWcm^{-2}$).

In order to enhance electron injection from the dye to TiO_2 photoanodes, doping of niobium into TiO_2 lattice was carried out, as a commonly adopted method of tailoring

properties of the CB position and trap/defect level distribution in nano-TiO_2.[154] Nb-doped TiO_2 photoanode was used in this case as a favourable electron-transfer mediator in DSSC devices based on SubPz **48**-**50**. Table 3.7 summarizes the photovoltaic performances with a dipping time of 4 hours based on a 5.0 mol% Nd-doped TiO_2, using I^-/I_3 electrolyte.

Dye	Electrolyte	J_{SC} (mA cm^{-2})	V_{OC} (V)	FF (%)	**PCE[a] (%)**
50[b]		1.20	0.377	81.8	**0.37**
51[b]		2.02	0.414	70.1	**0.59**
52[b]	I^-/I_3	1.12	0.423	80.0	**0.38**
48[b]		1.10	0.406	79.3	**0.36**
49[b]		2.38	0.424	66.7	**0.67**

[a]Irradiated light: AM 1.5G (100 $mWcm^{-2}$); cell area tested with a metal mask: 0.3 $cm^{2.}$
The Nb-doped (5%) TiO_2 layer was composed of an 8 μm thick transparent layer and a 3.5 μm thick scattering layer. Iodine electrolyte: 0.05 M I_2, 0.5 M LiI and 0.5 M NaI in CH_3CN.
[b]Dipping condition: 0.2 mM dye solution (EtOH/THF = 4:2) for 4 h

Table 3.7. Photovoltaic performances of the DSSCs based on SubPz **48**-**50** with a Nd-doped TiO_2.

In this case, a better response of the photocurrent was found, as a result of a decrease in the TiO_2-CB levels when it is doped with 5 mol% in niobium. This makes possible a more efficient electron injection from the excited SubPz dyes into TiO_2. Although the J_{sc} values and overall PCE are still low, SubPz **49** represents the best case, showing an efficiency of 0.67%. Figure 3.37 shows the new *J-V* curves of DSSC devices made with SubPzs **48**-**50**, Nd-doped TiO_2, and with the I^-/I_3 electrolyte.The incident photon-to-current efficiency (IPCE) indicates a value of almost 14% at the maximum of the Q-band for SubPz **49**.

[154] a) M. R. Hoffman, S. T. Martin, W. Choi, D. W. Bahneman, *Chem. Rev.*, **1995**, *95*, 69; b) A. V. Emeline, Y. Furubayashi, X. T. Zhang, M. Jin, T. Murakami, A. Fujishima, *J. Phys. Chem. B*, **2005**, *109*, 24441; c) S. G. Kim, M. J. Ju, I. T. Choi, W. S. Choi, H. Choi, J.–B. Baekb, H. K. Kim, *RSC Adv.*, **2013**, *3*, 16380–16386.

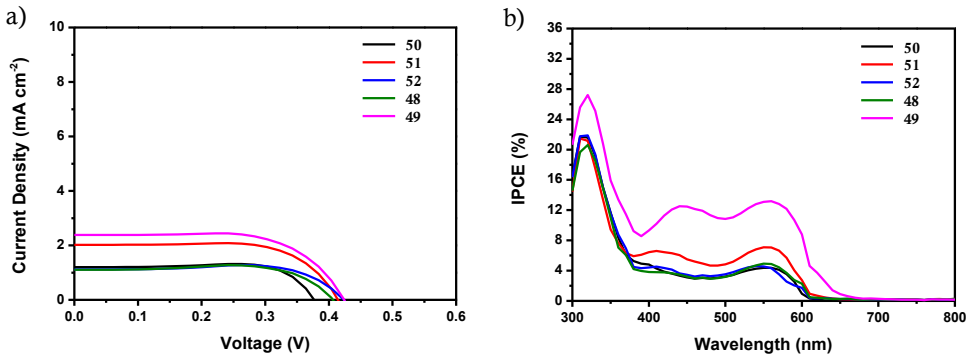

Figure 3.37. (a) *J-V* curves of DSSCs based on SubPzs **48**-**50** with a Nd-doped TiO_2. (b) *IPCE* spectra of the DSSC devices.

3.3.4 Activating Intramolecular Singlet Fission on SubPz-Pnc$_2$ Conjugate

In this part, a SubPz-Pnc$_2$ triad **58**, where the two chromophores are connected through the SubPz axial position, was synthesized (Scheme 3.7). The synthesis of axially formyl-SubPz **61** was carried out by the general procedure described for hexasulfanyl-SubPz in the chapter 1, affording **61** in a 12% yield. The next step of peripheral hexaarylation by the general procedure for Liebeskind-Srogl cross-coupling of SubPz **61** have achieved the incorporation of trimethoxyphenyl moieties to afford **62** in a 36% yield. Finally the array of SubPz-Pnc$_2$ triad **58** was prepared by esterification reaction of a suitable SubPz **59**, after reduction with $NaBH_4$ of **62**, endowed with an axial hydroquinone moiety and a pentacene dimer (Pnc$_2$) **60**, containing a carboxylic acid function.[142b]

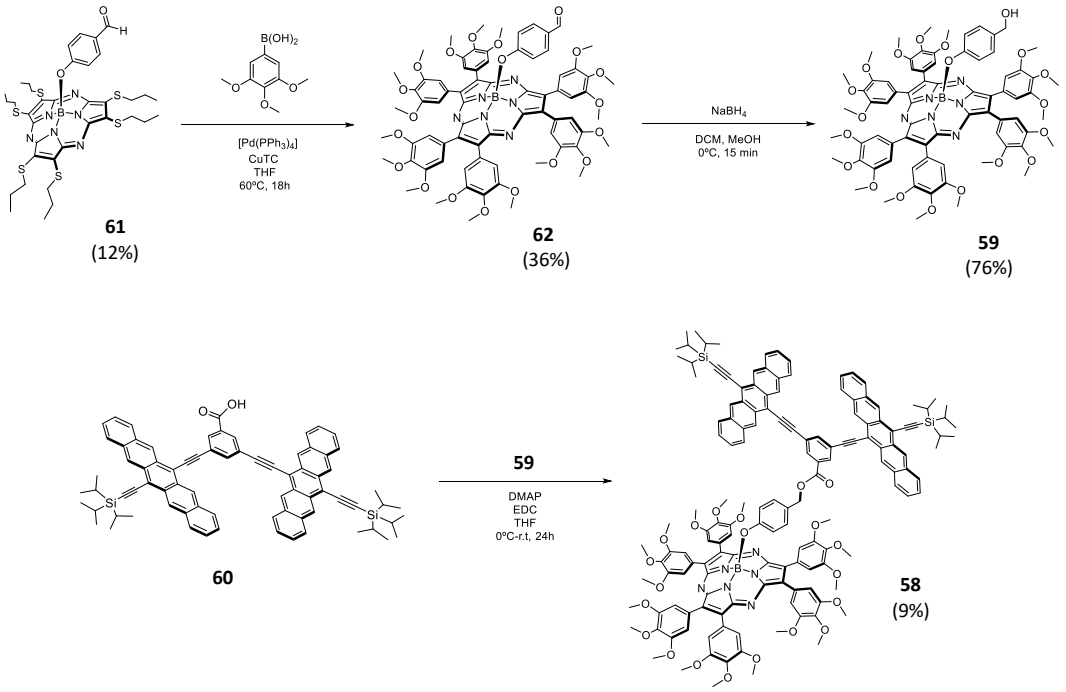

Scheme 3.7. Synthetic route for SubPz-Pnc$_2$ triad **58**.

3.3.4.1 Steady-State Spectroscopy

Absorption

The absorption spectra of the SubPzOH **59** reference compound in toluene and in benzonitrile shows a Q-band at 562 and 560.5 nm, respectively (Figure 3.38). Turning to PnCOOH **60**, it shows short-wavelength absorptions in the region of 300–500 nm and long-wavelength absorptions in the region of 500–750 nm, both in toluene and in benzonitrile. The absorption spectra of SubPz-Pnc_2 **58** is the linear superimposition of the individual components, indicating only marginal, if any, ground-state interactions between the Pnc_2 and the SubPz. In particular, the SubPz Q-band feature evolve at 562.5, both in toluene and in benzonitrile, and the long-wavelength maximum of the **60** absorption is centered around 662 nm and 666.5, respectively, in toluene and in benzonitrile.

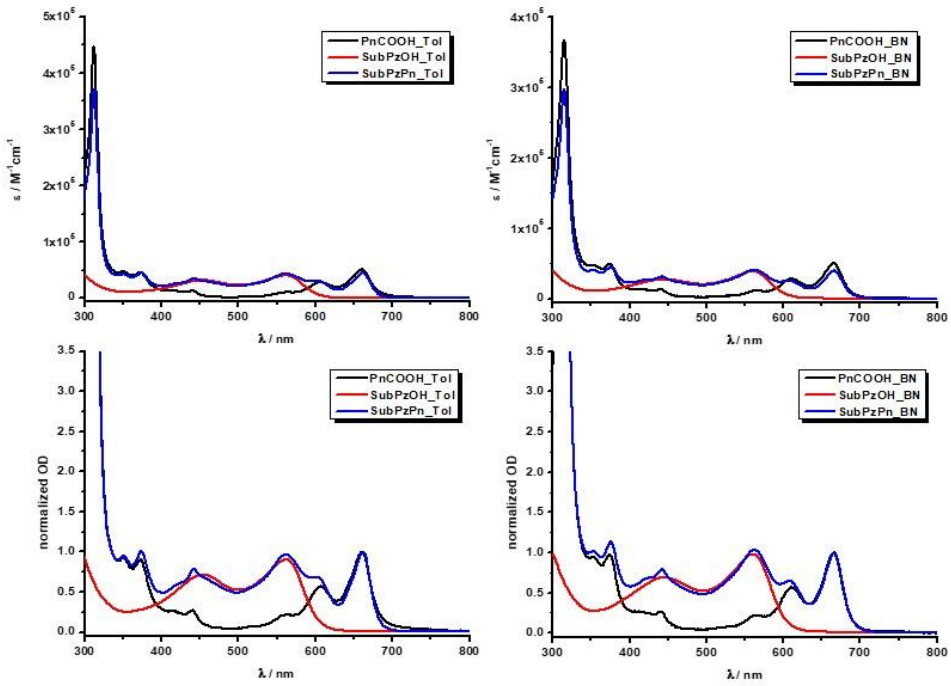

Figure 3.38. Absorption spectra of **60**, **59** and **58** in toluene and in benzonitrile.

Fluorescence

Excitation at the Q-band region of **59** leads in toluene to a weak fluorescence with a maximum at 671 nm and rather low fluorescence quantum yields of 0.018 (Figure 3.39). The fluorescence lifetimes of **59** is 954 ps. Upon changing the solvent to benzonitrile, the fluorescence maximum is bathochromically shifted to 688.5 nm and the fluorescence quantum yield decreases to 0.002. The fluorescence lifetimes of **59** in benzonitrile is 598 ps.

Concerning **60**, photoexcitation at the long-wavelength absorptions results in a fluorescence maximum at 666 nm in toluene (673 nm in benzonitrile) and fluorescence quantum yield of 0.016, with fluorescence lifetimes lower than 200 ps.

Due to the fact that the fluorescence maxima of the SubPz precursor and the Pnc_2 precursor are similar both in toluene and in benzonitrile, it is not possible to detect the SubPz centered fluorescence upon excitation of **58** at the Q-band region of the SubPz, as the SubPz fluorescence maximum is located under the Pn c_2 centered emission in the hybrid system. For this reason, it is not possible to determine if the SubPz centered fluorescence is quenched in the **58** conjugate respect to the reference compound **59**. Indeed, in this case the steady-state fluorescence measurements do not give any information about a possible energy transfer process occurring from the SubPz to the Pnc_2.[155]

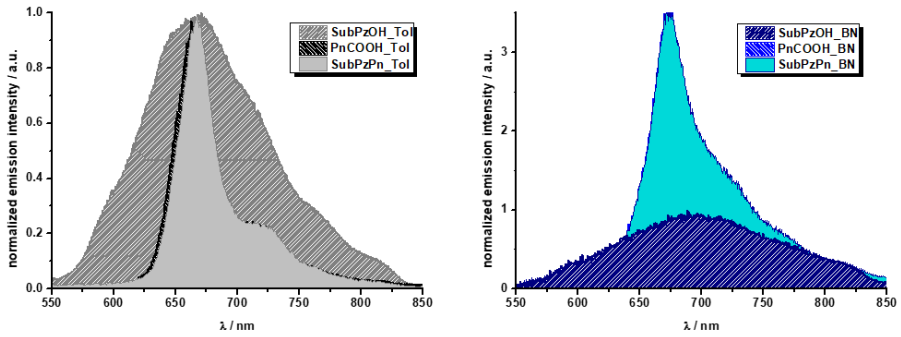

Figure 3.39. Fluorescence spectra of **60**, **59** and **58** in toluene and in benzonitrile.

[155] G. Lavarda, J. Zirzlmeier, M. Gruber, P. R. Rami, R. R. Tykwinski, T. Torres, D. M. Guldi, *Angew. Chem. Int. Ed.* **2018**, *57*, 16291–16295.

A summary of the photophysical properties in toluene and benzonitrile of the investigated compound is given in Table 3.8.

Compound	λ_{abs} / nm		λ_{em} / nm		Φ_F	τ_F / ps
	SubPz	Pn	SubPz	Pn	SubPz[a]	SubPz[a]
PnCOOH_Tol	-	660	-	666	0.016[b]	<200[b,c]
SubPzOH_Tol	562	-	671	-	0.018	954
SubPzPn_Tol	562.5	662	-[d]	667	0.021[d]	<200[c,d]
PnCOOH_BN	-	665.5	-	673	0.016[b]	<200[b,c]
SubPzOH_BN	560.5	-	688.5	-	0.002	598
SubPzPn_BN	562.5	666.5	-[d]	674	0.003[d]	<200[c,d]

Table 3.8: Photophysical properties of **60**, **59** and **58** in toluene and in benzonitrile. [a] values refer to the Pz centered fluorescence if not stated otherwise. [b] value refers to the Pn centered fluorescence. [c] lifetime is below the resolution limit of the time-correlated single photon counting (TCSPC) setup. [d] SubPz centered fluorescence is not detectable / under the Pn centered emission in the hybrid system.

3.3.4.2 Femtosecond / Nanosecond Transient Absorption Spectroscopy

Femtosecond (fsTA) and nanosecond (nsTA) transient absorption experiments with reference compound **59** and **58** have been performed with 480 nm photoexcitation. On the other hand, fsTA and nsTA experiments with **60** have been performed with 633 nm photoexcitation.

In **59**, the typical singlet excited state features are discernable in fsTA and nsTA experiments right after the conclusion of the photoexcitation in toluene (Figures 3.40 and 3.41). These are characterized by transient ground-state bleaching (GSB) at 460 and 562 nm and maxima at 620, 880 and 1060 nm. The singlet excited state $^1(S_1)$ then evolves to afford the corresponding triplet excited states $^3(T_1)$, which features maxima at 510 and 610 nm. The lifetime of the singlet excited state from global analyses is 955 ps. In the nsTA experiments, the triplet excited state is then replaced at longer timescale by the ground state (lifetime of the triplet excited state: 80.06 μs).

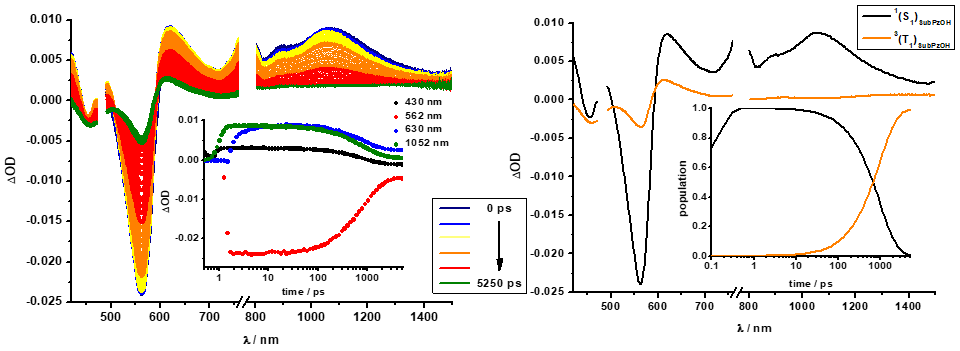

Figure 3.40. Left: Differential absorption spectra (visible) obtained upon fsTA experiments (480 nm) of **59** in toluene with several time delays between 0 and 5250 ps at room temperature. Right: Evolution-associated spectra of the transient absorption data of **59**. The inset depicts the relative populations of $^1(S_1)$ and $^3(T_1)$.

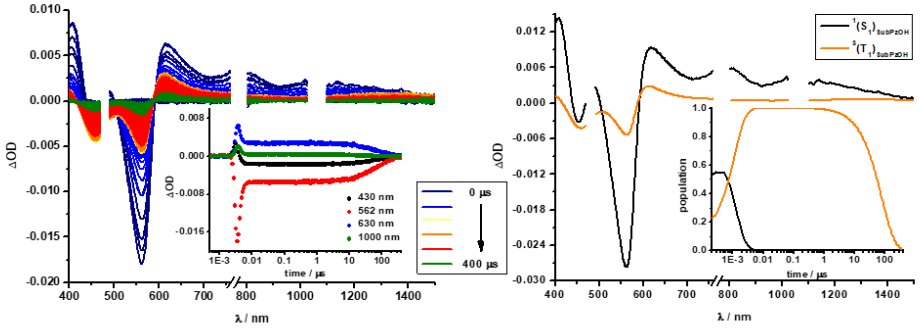

Figure 3.41. Left: Differential absorption spectra (visible) obtained upon nsTA experiments (480 nm) of SubPzOH in toluene with several time delays between 0 and 400 μs at room temperature. Right: Evolution-associated spectra of the transient absorption data of SubPzOH. The inset depicts the relative populations of $^1(S_1)$ and $^3(T_1)$.

The deactivation pathway for **59** in benzonitrile is identical to that observed in toluene, except for the singlet and triplet excited states lifetimes (532 ps and 111.30 μs, respectively) (Figures 3.42 and 3.43).

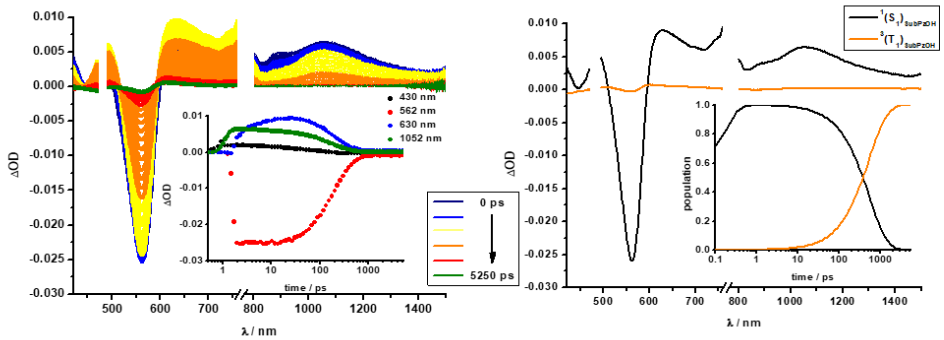

Figure 3.42. Left: Differential absorption spectra (visible) obtained upon fsTA experiments (480 nm) of **59** in benzonitrile with several time delays between 0 and 5250 ps at room temperature. Right: Evolution-associated spectra of the transient absorption data of **59**. The inset depicts the relative populations of $^1(S_1)$ and $^3(T_1)$.

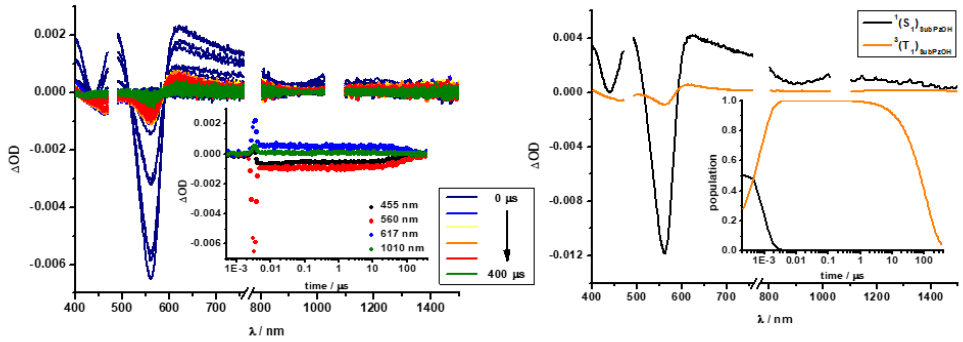

Figure 3.43. Left: Differential absorption spectra (visible) obtained upon nsTA experiments (480 nm) of **59** in benzonitrile with several time delays between 0 and 400 μs at room temperature. Right: Evolution-associated spectra of the transient absorption data of **59**. The inset depicts the relative populations of $^1(S_1)$ and $^3(T_1)$.

For **60**, photoexcitation in toluene is followed by the formation of the singlet excited state $^1(S_1S_0)$, which features in toluene, GSB in the 550–750 nm region, as well as characteristic maxima at 451 and 508 nm in the visible region and at 1386 nm in the NIR (Figure 3.44), with a singlet excited state lifetime of 7.86 ps. Singlet fission then leads to the biphasic formation of $^1(T_1T_1)$, characterized by maxima at 473 and 506 nm. Intramolecular triplet–triplet annihilation of $^1(T_1T_1)$ concludes the deactivation cascade to repopulate the electronic ground state on a timescale of 3.25 ns.

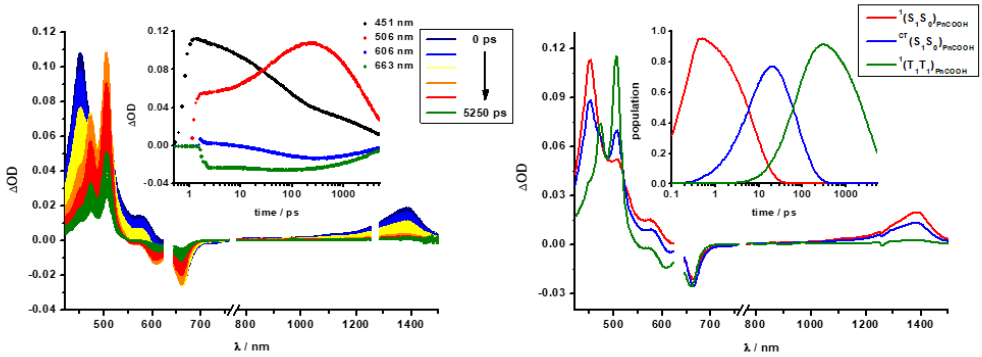

Figure 3.44. Left: Differential absorption spectra (visible) obtained upon fsTA experiments (633 nm) of **60** in toluene with several time delays between 0 and 5250 ps at room temperature. Right: Evolution-associated spectra of the transient absorption data of **60**. The inset depicts the relative populations of $^{1}(S_1S_0)$, $^{CT}(S_1S_0)$ and $^{1}(T_1T_1)$.

In benzonitrile, once excited PnCOOH **60** follows the same decay pathway, with a singlet excited state lifetime of 14.52 and a timescale of 3.24 ns for repopulation of the electronic ground state (Figure 3.45).

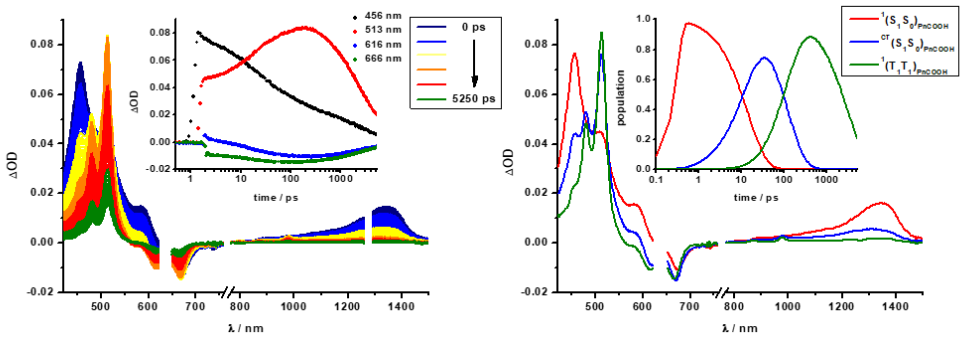

Figure 3.45. Left: Differential absorption spectra (visible) obtained upon fsTA experiments (633 nm) of **60** in benzonitrile with several time delays between 0 and 5250 ps at room temperature. Right: Evolution-associated spectra of the transient absorption data of **60**. The inset depicts the relative populations of $^{1}(S_1S_0)$, $^{CT}(S_1S_0)$ and $^{1}(T_1T_1)$.

For SubPz-Pnc$_2$ **58**, the features of the SubPz $^{1}(S_1)$ are observable after the photoexcitation in toluene (Figure 3.46). In stark contrast to **59**, the singlet excited state of the SubPz evolves to the $^{1}(S_1S_0)$ of the pentacene dimer. This evidence indicates that FRET is taking place. The deactivation cascade after the formation of the singlet

excited state of the Pnc moiety is the same observed for **60**, that is to say formation of $^1(T_1T_1)$ and triplet–triplet annihilation to repopulate the electronic ground state.

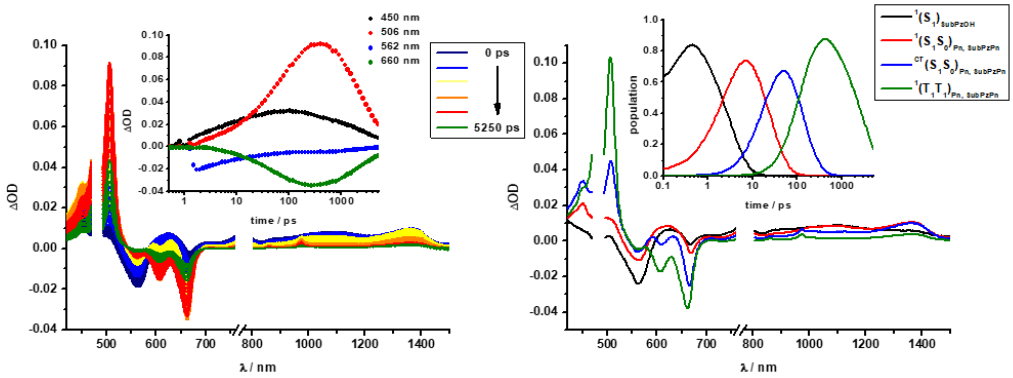

Figure 3.46. Left: Differential absorption spectra (visible) obtained upon fsTA experiments (480 nm) of **58** in toluene with several time delays between 0 and 5250 ps at room temperature. Right: Evolution-associated spectra of the transient absorption data of **58**. The inset depicts the relative populations of $^1(S_1)$, $^1(S_1S_0)$, $^{CT}(S_1S_0)$ and $^1(T_1T_1)$.

The same deactivation processes occur when **58** is photoexcited in benzonitrile (Figure 3.47). From the global fitting, the two lifetimes for the population of the $^1(T_1T_1)$ state are respectively 22.55 and 1150.1vps in toluene as well as 24.44 and 116.09 ps in benzonitrile. Once formed, the multiexcitonic state undergoes triplet–triplet annihilation to populate the ground state, with a lifetime of 2.88 and 2.44 ns in toluene and benzonitrile, respectively.

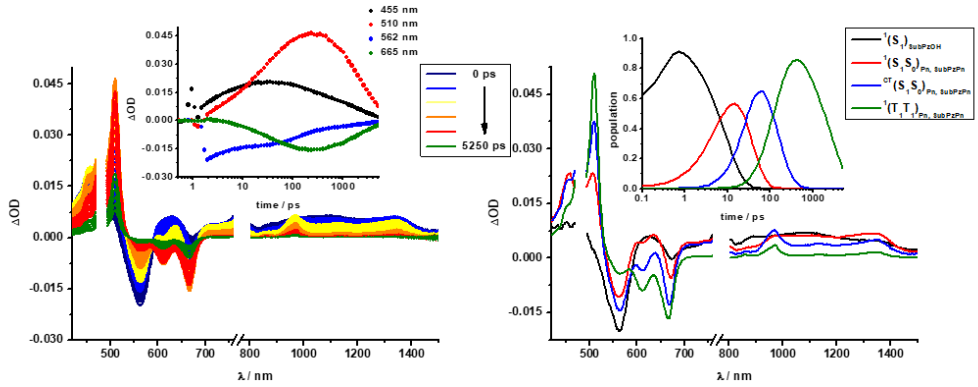

Figure 3.47. Left: Differential absorption spectra (visible) obtained upon fsTA experiments (480 nm) of **58** in benzonitrile with several time delays between 0 and 5250 ps at room temperature. Right: Evolution-associated spectra of the transient absorption data of **58**. The inset depicts the relative populations of $^1(S_1)$, $^1(S_1S_0)$, $^{CT}(S_1S_0)$ and $^1(T_1T_1)$.

A summary of the lifetimes for all involved states and the respective quantum yields of $^1(T_1T_1)$ state, in toluene is provided in Tables 3.9.

	fsTA					nsTA	
Compound	$^1(S_1)_{SubPz}$	$^1(S_1S_0)_{Pn}$	$^{CT}(S_1S_0)_{Pn}$	$^1(T_1T_1)_{Pn}$	**TQY[a,b]**	$^1(S_1)_{SubPz}$	$^3(T_1)_{SubPz}$
SubPzOH	955 ps					975 ps	80.06 µs
PnCOOH	-	7.86 ps	75.57 ps	3.25 ns	135%	-	-
SubPzPn	3.37 ps	22.55 ps	115.01 ps	2.88 ns	152%	n.r.[c]	-

[a] determined via following the intensification of the transient bleaching of the Pn moiety and comparing the relative intensification of the evolution-associated for the $^{CT}(S_1S_0)_{Pn}$ and the $^1(T_1T_1)_{Pn}$ state, respectively. [b] an error margin in the range of ±20% may be considered when determining the TQYs. [c] n.r. = not resolvable. Lifetimes are either too long to be resolved with fsTA or too short to be resolved with nsTA.

Table 3.9: Summary of kinetic data of the investigated compounds from fsTA and nsTA in toluene.

About the efficiency of the energy transfer, for SubPz-Pnc_2 **58** a FRET rate constant of $2.95 \cdot 10^{11}$ s^{-1} in toluene and $1.14 \cdot 10^{11}$ s^{-1} in benzonitrile can be calculated. This difference could stem from the lower spectra overlap between SubPz fluorescence and Pnc_2 absorption in the latter solvent.

In general, even if in this system we see again a fast energy transfer from the porphyrinoid to the pentacene dimer moiety followed by singlet fission, the overall performance is worse compared to the previously studied SubPc-Pnc_2 system.[153] This is due, on one hand, to the overall low fluorescence quantum yield of subporphyrazine and, on the other hand, to the fact that the emission maximum of the SubPz is quite far in the red and overlaps with the edge of the pentacene-absorption. Anyway, energy-transfer is still taking place, as the subporphyrazine emission is quite broad and makes the overall spectral overlap of subporphyrazine emission and pentacene absorption sufficient enough.

3.4 Summary and Conclusions

In this third chapter, the synthesis and characterization of novel active molecular materials based on SubPzs and SubNcs, and the studies of their applications in photovoltaic devices and of photophysical response have been evaluated.

In the first part, SubNcs **33**, **36**, **37** and **40** bearing different peripheral and axial substituents have been utilized as electron acceptors in bulk-heterojunction polymer solar cells for the first time. Due to their acceptor character and optical properties, their blends with PTB7-Th, a narrow band gap conjugated polymer, exhibit photovoltaic performance with contributions from both the polymer donor and the SubNc acceptor to the photocurrent. Moreover, the morphology of PTB7-Th:SubNc blend films was studied by transmission electron microscopy, and all blends exhibit rather homogeneous films without noteworthy phase separation. Nevertheless, the PCE values of the SubNc-based solar cells are only 0.71 %, 0.82 %, 0.86 % and 1.09 % for SubNc **40**, **33**, **36** and **37** respectively. The main limitations of these SubNc-based solar cells is their low short-circuit current density and fill factor, which is a combined result of low charge mobility, imbalanced hole/electron transport, and a suboptimal BHJ morphology contributing to recombination losses. Therefore, the future research involving SubNcs as electron-acceptor agents should focus on improving electron mobility, and controlling morphology of the blends to avoid geminate recombination and reduce bimolecular recombination losses.

Additionally, the preparation and structural characterization of a new series of three peripheral hexavinylester-substituted SubPzs as electron-acceptor molecules have been reported. The synthesis of these derivatives was carried out by our synthetic strategy in coupling of hexasulfanyl-SubPzs bearing different axial substituents with vinilmethylester-boronic acid. The peripheral electron-accepting ester moieties connected through *trans*-vinylidene linkers projects a coplanar configuration with the SubPz core, which has been confirmed by ^{1}H-NMR and X-ray crystallography studies. The absorption features for this series are identical, reflecting a marked Q-band over the yellow-orange region and a less intense CT band in comparison with the

hexavinylene-SubPzs family reported in the chapter 1, on the other hand, the influence of the axial ligands are noticed in the SubPz excited states due to different values of the fluorescence quantum yields. Cyclic and square-wave voltammetry of this series showed the most remarkable feature, whereby undergoes four reversible reduction processes between –0.5 V and –1.70 V against couple Fc/Fc^+, demonstrating their electron-accepting ability as possible active candidates for BHJ solar cells.

In the second part of this chapter, we have designed and synthesized a battery of five SubPz derivatives with push-pull substitution pattern as photosensitizers for application in n-type DSSCs. These dyes possess one ethynylphenyl-spaced carboxylic or cyanoacrylic acid group and five aryl functions with electron-donor features at the peripheral position. We have studied the electronic and redox properties of these novel photosensitizers and estimated the HOMO and LUMO energy levels based in experimental data and DFT calculations, which showed a low-lying LUMO energy levels for all five dyes, resulting in a small driving forces for electron injection towards the TiO_2 conduction band. Measurements of the performance of the dyes revealed efficiencies practically null in all cases. Nevertheless, optimization of the parameter of the cell such as the dipping conditions and the doping of 5 mol% niobium into TiO_2 lattice improved the response of the photocurrent, as a result of decrease in the TiO_2-CB levels, showing a raised efficiency of 0.67 % for SubPz endowed with five peripheral *p*-methoxyphenyl groups.

In the last part of this chapter, we have successfully synthesized and characterized a triad molecular system bearing a peripheral trimethoxyphenyl-SubPz and connected through axial position with a bis-pentacene unit (SubPz-Pnc_2). The synthesis of this assembly was carried out by an esterification reaction of peripheral trimethoxyphenylated-SubPz endowed with an axial hydroquinone moiety and a pentacene dimer containing a carboxylic acid group. The photophysical characterization for this molecular system has been evaluated by transient absorption spectroscopy using two different solvents, in which the SubPz-Pnc_2 system display a panchromatic absorption spectrum. The SubPz moiety produces a chromophore with

absorption bands at 445 and 557 nm, where the pentacene shows none or marginal absorption, and an emission band at 668 nm, matching the pentacene largest absorption band. For this triad was calculated a FRET rate constant of $2.95 \cdot 10^{11}$ s^{-1} in toluene and $1.14 \cdot 10^{11}$ s^{-1} in benzonitrile as a result of a lower spectra overlap between SubPz fluorescence and Pnc_2 absorption. Notwithstanding the effects as the low fluorescence quantum yield of SubPz and its redshifted emission maximum that overlaps with the edge of the Pnc_2 absorption, a fast energy-transfer take place followed by a singlet fission process.

3.5 Experimental Section

Specific Methods

Cyclic Voltammetry (CV), Square Wave Voltammetry (SWV): Electrochemical measurements were performed on an Autolab PGStat 30 equipment using a three electrode configuration system. The measurements were carried out using freshly distilled $CHCl_2$ solutions containing 0.1 M tetrabutylammonium hexafluorophosphate ($TBAPF_6$) and a concentration of approximately 10^{-4} M of the corresponding compound. A glassy carbon electrode (3 mm diameter) was used as the working electrode, and a platinum wire and an $Ag/AgNO_3$ (in CH_3CN) electrode were employed as the counter and the reference electrodes, respectively. Ferrocene (Fc) was used as an internal reference and all the potentials were given relative to the Fc/Fc^+ couple. Scan rate was 100 mV s^{-1} unless otherwise specified.

Theoretical calculation: DFT calculations have been performed using the Gaussian 09 Revision B.01 package. The ground state geometries have been optimized using the popular B3LYP exchange-correlation functional with the 6-31G(d,p) level. All optimized geometries have been confirmed by computation of the harmonic vibrational frequencies at the same level of theory (B3LYP/6-31G(d)/LANL2DZ). The vertical electronic transitions have been computed using the wB97xD functional with the 6-31G(d) basis set for all atoms, the first 15 excited singlet states have been calculated for the SubPzs.

Femtosecond and nanosecond transient absorption spectroscopy: Pump probe experiments were performed in Friederich-Alexander University in Erlangen, with an amplified Ti:Sapphire CPA-2110 fs laser system (Clark MXR: output 775 nm, 1 kHz, 150 fs pulse width) using transient absorption pump/probe detection systems (Helios and Eos, Ultrafast Systems). The 530 and 656 nm excitation wavelengths were generated with a noncolinear optical parametric amplifier (NOPA, Clark MXR). Fluorescence lifetimes were determined by the time correlated single photon counting

technique using a FluoroLog3 emission spectrometer (Horiba JobinYvon) equipped with an R3809U-58 MCP (Hamamatsu) and a 405LH laser diode (Horiba JobinYvon) exciting at 403 nm (675 ps fwhm) as well as a 650L laser diode (Horiba JobinYvon) exciting at 647 nm (<200 ps fwhm).

3.5.1 Device fabrication and photovoltaic characterization

3.5.1.1 Photovoltaic studies of SubNc as electron acceptors in bulk-heterojunction polymer solar cells

Transmission electron microscopy (TEM) was performed on a Tecnai G^2 Sphera transmission electron microscope (FEI) operated at 200 kV.

Charge carrier mobility was acquired through the single-carrier devices with a configuration of ITO/MoO_x (10 nm)/PTB7-Th:SubNc-X/MoO_x (10 nm)/Al (100 nm) for hole-only devices and ITO/ZnO (40 nm)/PTB7-Th:SubNc-X/LiF (1 nm)/Al (100 nm) for electron-only devices. The dark current densities of PTB7-Th:SubNc-X blends were measured by applying a voltage between 0 and 4 V using a computer-controlled Keithley 2400 source meter in N_2 atmosphere. These data were analysed according to the Mott-Gurney laws that includes a Poole-Frenkel-type dependence of mobility on the electric field, given by $J = \frac{9}{8}\varepsilon_r \varepsilon_0 \mu_0 \frac{V^2}{d^3} \exp(0.89\gamma\sqrt{\frac{V}{d}})$, where ε_0 is the permittivity of free space, ε_r is the dielectric constant of the polymer which is assumed to be 3 for the conjugated polymers, μ_0 is the zero-field mobility, V is the voltage drop across the device, d is the film thickness of active layer, and γ is a parameter that describes the strength of the field-dependence effect. The applied voltage is used without correcting from series resistance or built-in voltage, which offers the best fitting of the experimental data following the protocol reported in literature. The electron mobilities are extracted with the fit parameters at an electric field (E) of 2×10^5 V cm^{-1} by the Murgatroyd equation $\mu = \mu_0 \exp(\gamma\sqrt{E})$.

Fabrication and characterization of BHJ solar cells

Photovoltaic devices were made with an inverted architecture (glass/ITO/ZnO (40nm)/ PTB7-Th:SubNc-X/MoO_x (10 nm)/Ag (100 nm). Patterned ITO substrates (14 Ω per square) (Naranjo Substrates) were cleaned by sonication in acetone, detergent, deionized water, and isopropanol, followed by UV-ozone treatment. ZnO layers were deposited by spin coating a zinc acetate dehydrate (100 mg) precursor solution (28.3 μL ethanolamine in 0.937 mL 2-methoxyethanol) at 4000 rpm for 60 seconds, followed by annealing at 180 °C for 10–15 min in air, giving layers of 40 nm. The PTB7-Th:SubNc-X photoactive layers were deposited by spin coating in air from the solutions containing PTB7-Th and corresponding SubNc-X at room temperature. We adopted the optimal active layer thickness of about 75 nm. Unless indicated otherwise, thermal annealing were performed in glovebox at indicated temperature for 5 min. MoO_x (10 nm) and Ag (100 nm) were deposited by vacuum evaporation at ~3 × 10^{-7} mbar as the back electrode. The active area of the cells was 0.09 or 0.16 cm^2, which provided similar results. Current density–voltage ($J-V$) curves were measured under simulated solar light (100 mW cm^{-2}) from a tungsten–halogen lamp filtered by a Hoya LB100 daylight using a Keithley 2400 source meter. No mismatch correction was done. All measurements were conducted in nitrogen-filled glove box. The accurate short-circuit current density (J_{sc}) was determined from the external quantum efficiency (EQE) by convolution with the AM1.5G solar spectrum. EQE measurements were performed in a homebuilt set-up, with the devices kept in a nitrogen filled box with a quartz window and illuminated through an aperture of 2 mm. Mechanically modulated (Stanford Research, SR 540) monochromatic (Oriel, Cornerstone 130) light from a 50 W tungsten halogen lamp (Osram 64610) was used as probe light, in combination with continuous bias light from a solid state laser (B&W Tek Inc. 532 nm, 30 mW). The intensity of the bias laser light was adjusted using a variable-neutral density filter. The response was recorded as the voltage over a 50 Ω resistance, using a lock-in amplifier (Stanford Research Systems SR 830). For all devices, the measurements were carried out under representative illumination intensity (AM1.5G equivalent, provided by the 532 nm laser).

3.5.1.2 Photovoltaic studies of SubPzs in DSSC's

DSSC fabrications

FTO glass plates (Pilkington TEC Glass-TEC 8, Solar 2.3 mm thickness) were cleaned in a mucasol liquid cleaner (Aldrich) in an ultrasonic bath for 30 min, then rinsed with deionized water and ethanol. The FTO glass plates were immersed in 40 mM $TiCl_4$ (aqueous) at 70 °C for 30 min, then washed with deionized water and ethanol. A transparent nanocrystalline layer on the FTO glass plate was prepared by repeated screen printing with TiO_2 paste (Dyesol, 18NR-T) or 5% (mol) Nb-doped TiO_2 paste and then dried at 120 °C. The TiO_2 electrodes were gradually heated under an air flow at 325 °C for 5 min, at 375 °C for 5 min, at 450 °C for 15 min, and at 500 °C for 15 min. A paste for the scattering layer containing 400 nm anatase particles (CCIC, PST-400C) was deposited by screen printing and then dried for 1 h at 25 °C. The TiO_2 electrodes were gradually heated under an air flow at 325 °C for 5 min, at 375 °C for 5 min, at 450 °C for 15 min and at 500 °C for 15 min. The resulting layer was composed of a 4.0 μm thick transparent layer and a 3.5 μm thick scattering layer. The thickness of the transparent layer was measured using an Alpha-step 250 surface profilometer (Tencor Instruments, San Jose, CA). The TiO_2 electrodes were again treated with $TiCl_4$ at 70 °C for 30 min and sintered at 500 °C for 30 min. The TiO_2 electrodes were immersed in the dye solution (0.2 mM in THF/EtOH=1:2 containing 20 mm CDCA or without CDCA) and kept at room temperature for 3 h or 4h or 12 h. The FTO plate (Pilkington TEC Glass-TEC 8, solar 2.3 μm thickness) used as the counter electrode was cleaned in an ultrasonic bath in H_2O, acetone and 0.1 M HCl aqueous. The counter electrodes were prepared by coating with a drop of H_2PtCl_6 solution (2 mg of Pt in 1 mL of ethanol) on an FTO plate and heated at 400 °C for 15 min. The dye adsorbed on the TiO_2 electrode and the Pt-counter electrode were assembled into a sealed sandwich-type cell by heating at 80 °C with a hot-melt film (25 μm thick Surlyn) as a spacer between the electrodes. A drop of the electrolyte solution was placed on a drilled hole in the counter electrode of the assembled cell and driven into the cell through vacuum backfilling. Finally, the hole was sealed using additional Surlyn and cover glass (0.1 μm thick).

Photoelectrochemical measurements of DSSC

Photoelectrochemical data were measured using a 1000 W xenon light source (Oriel, 91193) that was focused to provide 100 mW cm^{-2}, the equivalent of one sun at AM 1.5 G at the surface of the test cell. The light intensity was adjusted with a Si solar cell that was double-checked with an NREL-calibrated Si solar cell (PV Measurement, Inc.). The applied potential and measured cell current were measured using a Keithley model 2400 digital source meter. The current–voltage characteristics of the cells under these conditions were determined by biasing the cell externally and measuring the photocurrent generated. This process was fully automated using Wavemetrics software. IPCE was measured in AC mode (4 Hz) under bias light using a specially designed IPCE system (PV measurement Inc.) equipped with a 75 W xenon lamp as a light source for monochromatic beam and a 75 W–12 V halogen lamp as a bias light source. The IPCE (λ) curve is expressed in the following equation: IPCE (λ) = 1240 (J_{sc}/λ_{ϕ}), where λ is the wavelength, J_{sc} is the current at short circuit (mA cm^{-2}), and ϕ is the incident radiative (W m^{-2}), which can be derived from the measured absorption spectrum of the DSSC for comparison.

3.5.2 Hexavinylester-SubPzs as new electron-acceptor molecules

[(1*E*)-3-Methoxy-3-oxoprop-1-en-1-yl]boronic acid (46)[148]

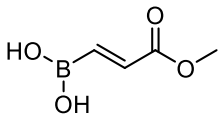

Borane dimethylsulfide complex (5.82 mL, 1.05 equiv) was dissolved in THF and cooled to 0 °C. (1*R*)-(+)-*R*-Pinene (22.56 mL, 2.32 equiv) was added dropwise, and the mixture was stirred at 0 °C for 1 h and at rt for 2 h. The mixture was cooled to -35 °C and ethyl propiolate (6.2 mL, 1 equiv) was added dropwise; the mixture was stirred at -35 °C for 45 min and rt for 3 h. Acetaldehyde (48 mL) was added, and the mixture was heated at rt overnight. The volatile organic components were carefully removed under reduced pressure to give 29 g of a mixture of the product and *R*-pinene. After addition of THF/water (5 mL/5 mL), the mixture was stirred overnight. The solvent was removed under reduced pressure, and 30 mL of pentane were added. The precipitate was filtered and washed several times with pentane, obtaining 3.52 g of a white solid (89 %).

^{1}H NMR (400 MHz, MeOD): δ = 6.87 (d, J = 17.8 Hz, 1H), 6.52 (d, J = 17.8 Hz, 1H), 3.78 ppm (s, 3H).

Phenoxy[2,3,7,8,12,13-hexa(propylthio)subporphyrazinato]boron(III) (47)

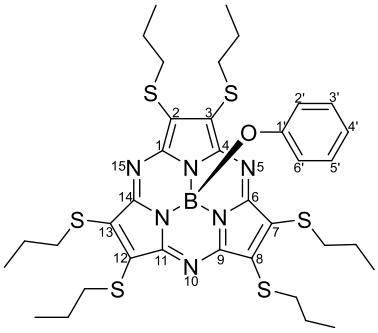

Prepared according to the general procedure for hexasulfanyl-SubPz **2b** (chapter 1); the crude product was chromatographed on silica gel (mixture of n-hexane/ethyl acetate 9:1) giving pure compound **47** (57 mg, 11%) as a red viscous solid.

^{1}H NMR (400 MHz, $CDCl_3$): δ = 6.81 (t, J = 8.0 Hz, 2H; $H^{3',5'}$), 6.70 (t, J = 8.0 Hz, 1H; $^{4'}$), 5.38 (d, J = 8.0 Hz, 2H; $H^{2',6'}$), 4.05 (m, 6H; -S*CH*$_2$Et), 3.57 (m, 6H; -S*CH*$_2$Et), 1.96 (m, 12H; -SCH$_2$*CH*$_2$CH$_3$), 1.17 ppm (t, J = 7.2 Hz, 18H; -SCH$_2$CH$_2$*CH*$_3$).

^{13}C NMR (100.6 MHz, $CDCl_3$): δ = 154.0, 152.6, 131.7, 128.7, 121.7, 119.7, 36.9, 23.8, 13.5 ppm.

MS (APCI, MeOH, +): m/z = 782.2340 $[M]^+$; 720.2188 $[M - OPh^tBu + OMe]^+$.

FT-IR (ATR): ν = 2959, 2928, 2870, 1595, 1477, 1450, 1287, 1235, 1172, 1119, 1029 S*, 895, 838, 749, 579 cm^{-1}.

UV/Vis ($CHCl_3$): λ (log ε/dm^3 mol^{-1} cm^{-1}) = 282 (4.3), 439 (4.4), 557 (4.4) nm.

Fluorescence ($CHCl_3$): λ_{ex} = 552 nm; λ_{em} = 682 nm.

4-*tert*-Butylphenoxy[2,3,7,8,12,13-hexa(methoxycarbonylvinyl) subporphyrazinato]boron(III) (43)

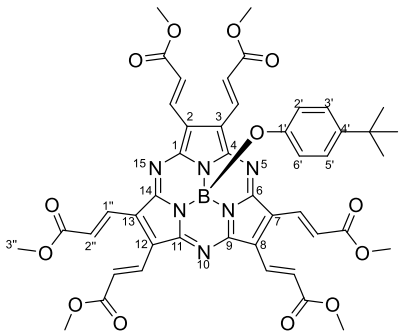

Prepared according to the general procedure for Liebeskind-Srogl cross-coupling of SubPzs (chapter 1); the reaction mixture was stirred at 30 ºC for 20 h under argon atmosphere, cooled to room temperature and passed through a short silica gel column using THF as eluent. The solvent was removed and the residue was purified by silica gel column chromatography (mixture of n-hexane/CH_2Cl_2/ethyl acetate 4:4:2) giving pure compound **43** (6.2 mg, 35%) as a blue solid.

^{1}H NMR (400 MHz, $CDCl_3$): δ = 8.15 (d, J = 16.0 Hz, 6H; $H^{2''}$), 7.99 (d, J = 16.0 Hz, 6H; $H^{1''}$), 6.86 (d, J = 8.0 Hz, 2H; $^{3',5'}$), 5.31 (d, J = 8.0 Hz, 2H; $H^{2',6'}$), 3.94 (s, 18H; -OMe), 1.13 ppm (s, 9H; *t*-Bu).

^{13}C NMR (100.6 MHz, $CDCl_3$): δ = 166.7, 155.6, 149.4, 144.5, 131.6, 131.0, 127.8, 126.0, 117.4, 52.2, 33.9, 31.3 ppm.

MS (APCI, MeOH, +): m/z = 898.3095 $[M]^+$; 899.3065 $[M + H]^+$.

FT-IR (ATR): ν = 2951, 2924, 2853, 1718 S*, 1623, 1502, 1461, 1434, 1271, 1174, 1073, 976, 871, 733 cm^{-1}.

UV/Vis ($CHCl_3$): λ (log ε/dm^3 mol^{-1} cm^{-1}) = 280 (4.8), 426 (4.3), 600 (4.6) nm.

Fluorescence ($CHCl_3$): λ_{ex} = 500 nm; λ_{em} = 621 nm.

Phenoxy[2,3,7,8,12,13-hexa(methoxycarbonylvinyl)subporphyrazinato] boron(III) (44)

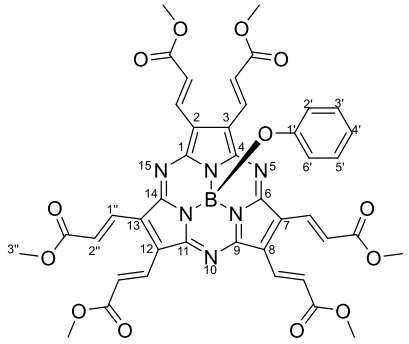

Prepared according to the general procedure for Liebeskind-Srogl cross-coupling of SubPzs (chapter 1); hexa(propylthio)subporphyrazine **47** (44 mg, 52 μmol), boronic acid **46** (136 mg, 1.05 mmol), $Pd(PPh_3)_4$ (36 mg, 31 μmol) and CuTC (178 mg, 0.94 mmol) were added into the flask and purged with argon for 10 min, followed by the addition of anhydrous THF (6 mL) *via cannula*. The reaction mixture was stirred at 30 ºC for 20 h under argon atmosphere, cooled to room temperature and passed through a short silica gel column using THF as eluent. The solvent was removed and the residue was purified by silica gel column chromatography (mixture of n-hexane/CH_2Cl_2/ethyl acetate 4:4:2) giving pure compound **44** (16.6 mg, 38%) as a blue solid.

^{1}H NMR (400 MHz, $CDCl_3$): δ = 8.14 (d, J = 16.0 Hz, 6H; $H^{2''}$), 7.98 (d, J = 16.0 Hz, 6H; $H^{1''}$), 6.86 (t, J = 8.0 Hz, 2H; $^{3',5'}$), 6.73 (t, J = 8.0 Hz, 1H; $^{4'}$), 5.41 (d, J = 8.0 Hz, 2H; $H^{2',6'}$), 3.94 ppm (s, 18H; -OMe).

^{13}C NMR (100.6 MHz, $CDCl_3$): δ = 166.6, 155.5, 151.8, 131.6, 131.0, 129.3, 127.9, 122.2, 118.7, 52.2 ppm.

MS (APCI, MeOH, +): m/z = 841.2285 $[M]^+$; 843.2434 $[M + H]^+$.

FT-IR (ATR): ν = 2951, 2925, 2854, 1715 S*, 1623, 1502, 1460, 1434, 1260, 1173, 1068, 975, 871, 733 cm^{-1}.

UV/Vis ($CHCl_3$): λ (log ε/dm^3 mol^{-1} cm^{-1}) = 280 (4.7), 426 (4.3), 600 (4.6) nm.

Fluorescence ($CHCl_3$): λ_{ex} = 500 nm; λ_{em} = 622 nm.

XRD: Single crystals suitable for X-ray diffraction analysis were obtained by vapor diffusion of isooctane into its 1,2-dichloroethane solution. Crystallographic data and some refining details are summarized in the following table:

Chemical formula	$C_{42.75}H_{36.50}BCl_{0.75}N_6O13$	
Formula weight	879.67 g/mol	
Temperature	200(2) K	
Wavelength	0.71073 Å	
Crystal size	0.015 x 0.124 x 0.164 mm	
Crystal habit	Dark purple plate	
Crystal system	monoclinic	
Space group	C 1 2/c 1	
Unit cell dimensions	a = 41.747(3) Å	α = 90°
	b = 7.8119(7) Å	β = 120.236(3)°
	c = 30.271(3) Å	γ = 90°
Volume	8529.1(13) $Å^3$	
Z	8	
Density (calculated)	1.370 g/cm^3	
Absorption coefficient	0.147 mm^{-1}	
F(000)	3654	

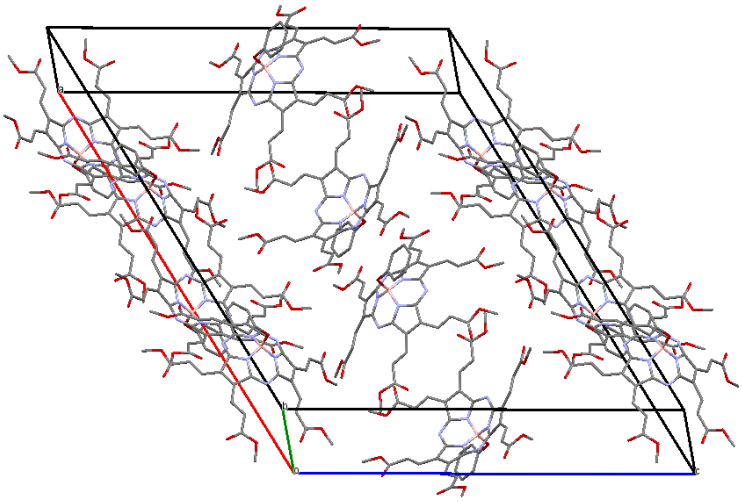

Figure 3.48. Unity cell and crystalline packing of SubPz **44**.

Fluoro[2,3,7,8,12,13-hexa(methoxycarbonylvinyl)subporphyrazinato] boron(III) (45)

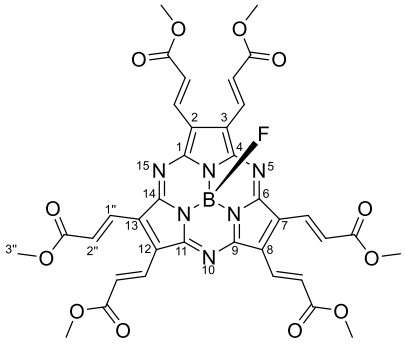

In an oven-dried 10 mL round-bottom flask was charged with hexavinylester-SubPz **44** (25.5 mg, 30 μmol) and dry toluene (5 mL) under argon atmosphere, and the solution was stirred at room temperature for 5 min. Then, $BF_3{\cdot}OEt_2$ (54 mg, 47 μL, 378 μmol) was added and the reaction mixture was stirred at 80 ºC for 20 h. the solvent and excess reagent were evaporated under reduced pressure and the crude was purified by column chromatography on silica gel (mixture of n-hexane/CH_2Cl_2/ethyl acetate 2:1:7 as eluent) to afford **45** (13.5 mg, 60%) as a blue solid.

^{1}H NMR (400 MHz, $CDCl_3$): δ = 8.15 (d, J = 16.0 Hz, 6H; $H^{2''}$), 8.00 (d, J = 16.0 Hz, 6H; $H^{1''}$), 3.95 ppm (s, 18H; -OMe).

^{13}C NMR (100.6 MHz, $CDCl_3$): δ = 166.6, 155.3, 131.9, 130.1, 128.0, 52.3 ppm.

^{19}F NMR (376.7 MHz, $CDCl_3$): δ = –155.58 to –155.80 ppm (m, J = 26.4 Hz, 1F).

MS (APCI, MeOH, +): m/z = 768.2118 $[M]^+$; 769.2086 $[M + H]^+$.

FT-IR (ATR): ν = 2954, 2924, 2852, 1718 S*, 1625, 1461, 1434, 1308, 1274, 1199, 1080, 973, 871, 734 cm^{-1}.

UV/Vis ($CHCl_3$): λ (log ε/dm^3 mol^{-1} cm^{-1}) = 280 (4.7), 426 (4.2), 598 (4.6) nm.

Fluorescence ($CHCl_3$): λ_{ex} = 500 nm; λ_{em} = 617 nm.

3.5.3 Subporphyrazine based molecular sensitizers for DSSCs

4'-*tert*-Butylphenoxy[2,3,7,12,13-penta(propylthio)-8-(4''-ethynylphenylformyl) subporphyrazinato]boron(III) (53)

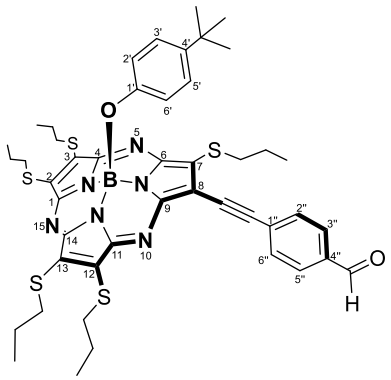

In an oven-dried two-neck round-bottom flask connected to a condenser and held under argon atmosphere was charged with a mixture of previously synthesized sulfanylated-SubPz **2b** and **3b** (345 mg), 4-ethynylbenzaldehyde (112 mg, 0.86 mmol), Cs_2CO_3 (152 mg, 0.86 mmol), DPE-Phos ligand (46 mg, 20% mol,), and $Pd(PPh_3)_4$ (50 mg, 10% mol). The mixture was purged with argon for 10 min, followed by the addition of anhydrous Et_3N (8 mL) and toluene (20 mL) *via cannula*. The reaction mixture was stirred at 80 ºC overnight under argon atmosphere, cooled to room temperature and passed through a short pad of compressed celite with a mixture of

hexanes/ethyl acetate (4:1), and finally the filtrate solvents were removed under reduced pressure. The crude material was chromatographed on a silica gel column using hexanes/ethyl acetate (9:1) as eluent. The product **53** was obtained as a dark red viscous solid (98 mg, 58%).

^{1}H NMR (400 MHz, $CDCl_3$): δ = 10.04 (s, 1H, C*H*O), 7.93 (d, *J* = 8.0 Hz, 2H; $H^{3'',5''}$), 7.83 (d, *J* = 8.0 Hz, 2H; $H^{2'',6''}$), 6.83 (d, *J* = 8.0 Hz, 2H; $^{3',5'}$), 5.32 (d, *J* = 8.0 Hz, 2H; $H^{2',6'}$), 4.24 (m, 1H; -S*CH*$_2$Et), 4.06 (m, 4H; -S*CH*$_2$Et), 3.76 (m, 2H; -S*CH*$_2$Et), 3.58 (m, 3H; -S*CH*$_2$Et), 2.00 (m, 10H; -$SCH_2CH_2CH_2CH_3$), 1.20 (m, 15H; -$SCH_2CH_2CH_2CH_3$), 1.15 ppm (s, 9H; *t*-Bu).

^{13}C NMR (100.6 MHz, $CDCl_3$): δ = 191.3, 156.1, 155.5, 154.6, 153.3, 152.6, 150.0, 144.2, 135.8, 133.5, 132.5, 132.2, 131.5, 131.3, 129.7, 129.2, 125.6, 118.5, 113.1, 101.6, 85.0, 37.0, 36.9, 36.7, 33.9, 31.4, 23.9, 23.7, 13.5 ppm.

MS (APCI, MeOH, +): *m/z* = 892.3024 $[M]^+$; 893.2994 $[M + H]^+$; 774.2247 [M – OPh^{t}Bu + OMe]$^+$; 742.1982 [M – OPh^{t}Bu]$^+$

FT-IR (ATR): ν = 2960, 2928, 2870, 1698, 1599, 1484, 1446, 1351, 1243, 1030, 827, 802 cm^{-1}.

UV/Vis ($CHCl_3$): λ (log ε/dm^3 mol^{-1} cm^{-1}) = 310 (4.6), 445 (4.7), 567 (4.5) nm.

Fluorescence ($CHCl_3$): λ_{ex} = 552 nm; λ_{em} = 682 nm.

General procedure for the synthesis of arylated-SubPzs 54-57

An oven-dried flask was over-dried and purged with argon during 10 minutes. Subsequently SubPz precursor **53** (40 mg, 45 μmol, 1 eq), boronic acid (0.81 mmol, 18 equiv), $Pd(PPh_3)_4$ (31 mg, 50 mol%) and CuTC (86 mg, 0.45 mmol; 10 equiv) were added into the flask and purged with argon for 10 min, followed by the addition of anhydrous THF (6 mL) *via cannula*. The reaction mixture was stirred at 60 ºC for 20 h under argon atmosphere, cooled to room temperature and passed through a short silica gel column using THF as eluent. The solvent was removed and the residue was purified by silica gel column chromatography.

4'-*tert*-Butylphenoxy[2,3,7,12,13-penta(phenyl)-8-(4''-ethynylphenylformyl) subporphyrazinato]boron(III) (54)

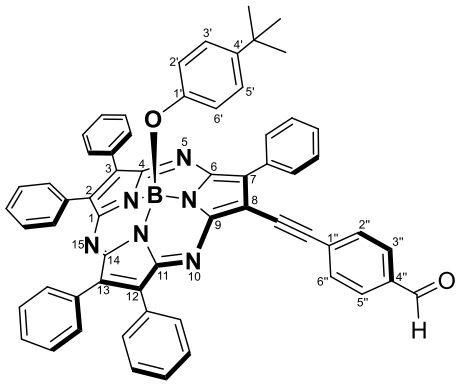

The residue was purified by silica gel column chromatography (hexanes/ethyl acetate 9:1). The product was obtained as a red solid (12.2 mg, 30%).

^{1}H NMR (400 MHz, $CDCl_3$): δ = 10.07 (s, 1H, C*H*O), 8.79 (d, *J* = 8.0 Hz, 2H; $H^{2''',6'''}$), 8.01 (m, 7H; Ph-H), 7.95 (d, *J* = 8.0 Hz, 2H; $H^{3''',5'''}$), 7.90 (m, 9H; Ph-H), 7.82 (d, *J* = 8.0 Hz, 2H; $H^{2'',6''}$), 7.52 (m, 7H; Ph-H), 6.87 (d, *J* = 8.0 Hz, 2H; $^{3',5'}$), 5.38 (d, *J* = 8.0 Hz, 2H; $H^{2',6'}$), 1.12 ppm (s, 9H; *t*-Bu).

^{13}C NMR (100.6 MHz, $CDCl_3$): δ = 191.3, 157.9, 157.3, 157.1, 150.4, 143.3, 135.9, 132.4, 131.7, 131.5, 131.4, 130.5, 129.7, 128.7, 128.5, 125.9, 117.2, 100.3, 87.2, 33.8, 31.3 ppm.

MS (APCI, MeOH, +): *m/z* = 901.3496 $[M]^+$; 903.3614 $[M + H]^+$; 783.2720 [M – OPh^{t}Bu + OMe]$^+$; 751.2459 [M – OPh^{t}Bu]$^+$

FT-IR (ATR): ν = 2956, 2923, 2853, 1697, 1598, 1458, 1441, 1388, 1259, 1110, 1032, 820, 734, 693 cm^{-1}.

UV/Vis ($CHCl_3$): λ (log ε/dm^3 mol^{-1} cm^{-1}) = 306 (4.8), 405 (4.6), 555 (4.7) nm.

Fluorescence ($CHCl_3$): λ_{ex} = 520 nm; λ_{em} = 601 nm.

4'-*tert*-Butylphenoxy[2,3,7,12,13-penta(*p-tert*-butylphenyl)-8-(4''-ethynylphenylformyl) subporphyrazinato]boron(III) (55)

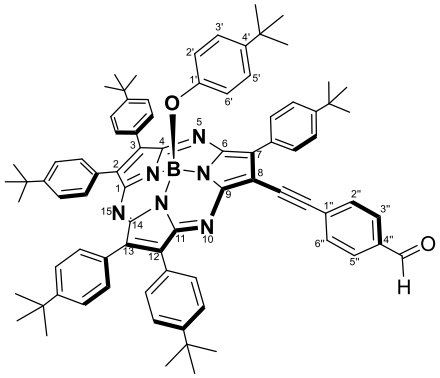

The residue was purified by silica gel column chromatography (hexanes/ethyl acetate 14:1). The product was obtained as a red solid (21.3 mg, 40%).

^{1}H NMR (400 MHz, $CDCl_3$): δ = 10.07 (s, 1H, C*H*O), 8.75 (d, *J* = 8.0 Hz, 2H; $H^{2''',6'''}$), 8.03 (d, *J* = 8.0 Hz, 2H; $H^{3''',5'''}$), 7.92 (d, *J* = 8.0 Hz, 2H; $H^{3'',5''}$), 7.89 (m, 6H; ^{t}BuPh-H), 7.84 (d, *J* = 8.0 Hz, 2H; $H^{2'',6''}$), 7.59 (d, *J* = 8.0 Hz, 2H; ^{t}BuPh-H), 7.54 (d, *J* = 8.0 Hz, 2H; ^{t}BuPh-H), 7.46 (m, 6H; ^{t}BuPh-H), 6.84 (d, *J* = 8.0 Hz, 2H; $^{3',5'}$), 5.37 (d, *J* = 8.0 Hz, 2H; $H^{2',6'}$), 1.42 (m, 45H; *t*-Bu), 1.12 ppm (s, 9H; *t*-Bu).

^{13}C NMR (100.6 MHz, $CDCl_3$): δ = 191.3, 157.7, 157.2, 152.9, 151.8, 151.6, 151.5, 150.6, 132.4, 131.0, 130.8, 130.2, 129.6, 125.8, 125.6, 125.5, 125.4, 117.2, 99.8, 87.7, 34.9, 34.8, 31.4, 31.3 ppm.

MS (APCI, MeOH, +): *m/z* = 1182.6758 $[M]^+$; 1183.6731 $[M + H]^+$; 1033.5689 $[M - OPh^{t}Bu]^+$

FT-IR (ATR): ν = 2958, 2924, 2865, 1702, 1599, 1457, 1388, 1259, 1110, 1032, 837 cm^{-1}.

UV/Vis ($CHCl_3$): λ (log ε/dm^3 mol^{-1} cm^{-1}) = 310 (4.7), 429 (4.6), 568 (4.7) nm.

Fluorescence ($CHCl_3$): λ_{ex} = 520 nm; λ_{em} = 605 nm.

4'-*tert*-Butylphenoxy[2,3,7,12,13-penta(3''-5''-di-*tert*-butylphenyl)-8-(4''-ethynylphenylformyl) subporphyrazinato]boron(III) (56)

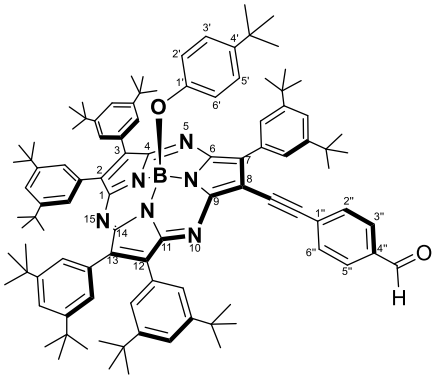

The residue was purified by silica gel column chromatography (hexanes/ethyl acetate 18:1). The product was obtained as a red solid (10 mg, 15%).

^{1}H NMR (400 MHz, $CDCl_3$): δ = 10.07 (s, 1H, C*H*O), 8.32 (d, *J* = 1.8 Hz, 2H; $H^{2''',6'''}$), 8.03 (d, *J* = 8.0 Hz, 2H; $H^{3''',5'''}$), 7.90 (d, *J* = 8.0 Hz, 2H; $H^{3'',5''}$), 7.81 (d, *J* = 8.0 Hz, 2H; $H^{2'',6''}$), 7.60 (d, *J* = 1.8 Hz, 2H; ^{t}BuPh-H), 7.50 (t, *J* = 1.8 Hz, 1H; ^{t}BuPh-H), 7.42 (t, *J* = 1.8 Hz, 1H; ^{t}BuPh-H), 7.41 (t, *J* = 1.8 Hz, 1H; ^{t}BuPh-H), 7.39 (d, *J* = 1.8 Hz, 2H; ^{t}BuPh-H), 7.37 (t, *J* = 1.8 Hz, 1H; ^{t}BuPh-H), 7.35 (d, *J* = 1.8 Hz, 2H; ^{t}BuPh-H), 7.30 (d, *J* = 1.8 Hz, 2H; ^{t}BuPh-H), 6.88 (d, *J* = 8.0 Hz, 2H; $^{3',5'}$), 5.39 (d, *J* = 8.0 Hz, 2H; $H^{2',6'}$), 1.25–1.03 ppm (m, 99H; *t*-Bu).

^{13}C NMR (100.6 MHz, $CDCl_3$): δ = 191.5, 158.4, 157.3, 150.9, 150.7, 150.5, 150.3, 142.9, 135.7, 132.7, 131.1, 130.8, 130.2, 129.4, 125.8, 125.7, 125.3, 122.2, 117.2, 98.2, 87.4, 34.9, 34.7, 33.8, 31.5, 31.4, 31.2 ppm.

MS (APCI, MeOH, +): *m/z* = 1462.9883 $[M]^+$; 1344.9108 $[M - OPh^tBu]^+$

FT-IR (ATR): ν = 2961, 2867, 1703, 1596, 1466, 1392, 1363, 1248, 1204, 1041, 880, 710 cm^{-1}.

UV/Vis ($CHCl_3$): λ (log ε/dm^3 mol^{-1} cm^{-1}) = 302 (4.7), 414 (4.6), 552 (4.7) nm.

Fluorescence ($CHCl_3$): λ_{ex} = 500 nm; λ_{em} = 597 nm.

4'-*tert*-Butylphenoxy[2,3,7,12,13-penta(*p*-methoxyphenyl)-8-(4''-ethynylphenylformyl) subporphyrazinato]boron(III) (57)

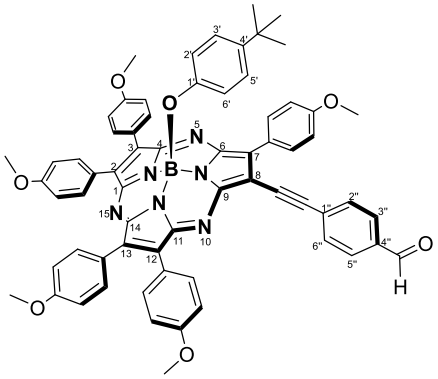

The residue was purified by silica gel column chromatography (hexanes/CH_2Cl2/ethyl acetate 7:2:1). The product was obtained as a red solid (15.2 mg, 32%).

^{1}H NMR (400 MHz, $CDCl_3$): δ = 10.07 (s, 1H, C*H*O), 8.83 (d, *J* = 8.0 Hz, 2H; $H^{2''',6'''}$), 7.98 (d, *J* = 8.0 Hz, 2H; $H^{3'',5''}$), 7.90 (m, 8H; MeOPh-H), 7.83 (d, *J* = 8.0 Hz, 2H; $H^{2'',6''}$), 7.13 (d, *J* = 8.0 Hz, 2H; $H^{3''',5'''}$), 7.05 (d, *J* = 8.0 Hz, 2H; MeOPh-H) 6.99 (m, 6H; MeOPh-H), 6.85 (d, *J* = 8.0 Hz, 2H; $^{3',5'}$), 5.37 (d, *J* = 8.0 Hz, 2H; $H^{2',6'}$), 3.95–3.89 (m, 15H; OMe), 1.11 ppm (s, 9H; *t*-Bu).

^{13}C NMR (100.6 MHz, $CDCl_3$): δ = 191.3, 160.9, 160.0, 158.1, 157.6, 157.1, 156.5, 154.7, 150.7, 143.0, 137.7, 135.7, 132.7, 132.5, 132.0, 129.7, 125.8, 124.3, 117.1, 114.1, 99.7, 87.8, 55.5, 55.3, 33.8, 31.4 ppm.

MS (APCI, MeOH, +): *m/z* = 1052.4190 $[M]^+$; 902.3148 $[M - OPh^tBu]^+$

FT-IR (ATR): ν = 2957, 2923, 2852, 1699, 1602, 1572, 1516, 1453, 1387, 1293, 1205, 1147, 1106, 1027, 832, 729, 577 cm^{-1}.

UV/Vis ($CHCl_3$): λ (log ε/dm^3 mol^{-1} cm^{-1}) = 273 (4.7), 323 (sh), 445 (4.6), 571 (4.5) nm.

Fluorescence ($CHCl_3$): λ_{ex} = 520 nm; λ_{em} = 629 nm.

General procedure for the synthesis of dyes 48 and 49

In an oven-dried 50 mL round-bottom flask was charged with formyl-SubPz **55** or **57** (20 μmol) under argon atmosphere and dissolved with acetone (20 ml). The solution was stirried at 0 ºC for 5 min and $NaClO_2$ (10.8 mg, 120 μmol) was added slowly to a solution. Then, a sulfamic acid solution (13 mg, 120 μmol) in deionized water (5 mL) was added in one portion. The reaction mixture was stirred at 0 ºC until oxidation is complete. The product was extracted with ethyl acetate, washed with 1.0M HCl and dried over anhydrous $MgSO_4$. After filtration and evaporation, the solid residue was purified by silica gel column chromatography.

4'-*tert*-Butylphenoxy[2,3,7,12,13-penta(*p*-*tert*-butylphenyl)-8-(4''-ethynylbenzoic acid) subporphyrazinato]boron(III) (48)

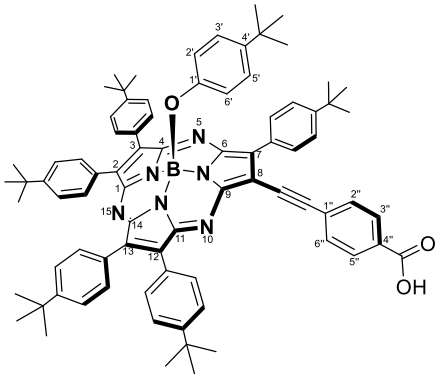

Reaction time: 2h at 0 ºC. The residue was purified by silica gel column chromatography (hexanes/CH_2Cl_2/ethyl acetate/MeOH 4:4:1.7:0.3). The product was obtained as a red solid (16.8 mg, 70%).

^{1}H NMR (400 MHz, $CDCl_3$): δ = 8.75 (d, J = 8.0 Hz, 2H; $H^{2''',6'''}$), 8.16 (d, J = 8.0 Hz, 2H; $H^{3''',5'''}$), 8.02 (d, J = 8.0 Hz, 2H; $H^{3'',5''}$), 7.89 (m, 6H; ^{t}BuPh-H), 7.78 (d, J = 8.0 Hz, 2H; $H^{2'',6''}$), 7.59 (d, J = 8.0 Hz, 2H; ^{t}BuPh-H), 7.59 (d, J = 8.0 Hz, 2H; ^{t}BuPh-H), 7.54 (d, J = 8.0 Hz, 2H; ^{t}BuPh-H) 7.47 (m, 4H; ^{t}BuPh-H), 6.84 (d, J = 8.0 Hz, 2H; $^{3',5'}$), 5.36 (d, J = 8.0 Hz, 2H; $H^{2',6'}$), 1.42 (m, 45H; *t*-Bu), 1.11 ppm (s, 9H; *t*-Bu).

^{13}C NMR (100.6 MHz, $CDCl_3$): δ = 157.7, 155.6, 152.5, 151.5, 151.4, 142.6, 132.9, 132.4, 131.8, 130.6, 130.2, 129.6, 128.7, 128.4, 125.7, 125.3, 116.9, 100.31, 34.9, 34.8, 31.4, 31.3, 30.9 ppm.

HRMS (APCI, MeOH, +): *m/z* = calculated for $C_{81}H_{83}BN_6O_3$ $[M]^+$ 1198.6748; found 1198.6729.

FT-IR (ATR): ν = 3041, 2957, 2861, 2354, 1695, 1605, 1454, 1394, 1260, 1188, 1115, 1024, 839, 714, 559 cm^{-1}.

UV/Vis ($CHCl_3$): λ (log ε/dm^3 mol^{-1} cm^{-1}) = 309 (4.7), 425 (4.6), 566 (4.7) nm.

Fluorescence ($CHCl_3$): λ_{ex} = 500 nm; λ_{em} = 605 nm.

4'-*tert*-Butylphenoxy[2,3,7,12,13-penta(*p*-methoxyphenyl)-8-(4''-ethynylbenzoic acid) subporphyrazinato]boron(III) (49)

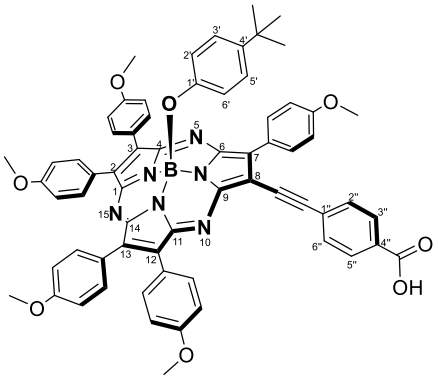

Reaction time: 30 min at 0 ºC. The residue was purified by silica gel column chromatography (hexanes/CH_2Cl_2/ethyl acetate/MeOH 3.5 : 3.5 : 2 :1). The product was obtained as a violet solid (14.5 mg, 68%).

^{1}H NMR (400 MHz, $CDCl_3$): δ = 8.84 (d, *J* = 8.0 Hz, 2H; $H^{2''',6'''}$), 8.17 (d, *J* = 8.0 Hz, 2H; $H^{3'',5''}$), 7.98 (d, *J* = 8.0 Hz, 2H; MeOPh-H), 7.88 (m, 6H; MeOPh-H), 7.77 (d, *J* = 8.0 Hz, 2H; $H^{2'',6''}$), 7.13 (d, *J* = 8.0 Hz, 2H; $H^{3''',5'''}$), 7.05 (d, *J* = 8.0 Hz, 2H; MeOPh-H) 6.98 (m, 6H; MeOPh-H), 6.85 (d, *J* = 8.0 Hz, 2H; $^{3',5'}$), 5.37 (d, *J* = 8.0 Hz, 2H; $H^{2',6'}$), 3.95–3.90 (m, 15H; OMe), 1.11 ppm (s, 9H; *t*-Bu).

^{13}C NMR (100.6 MHz, $CDCl_3$): δ = 160.9, 160.1, 159.9, 158.10, 157.6, 157.0, 156.5, 154.8, 150.7, 143.0, 137.6, 132.6, 132.0, 131.8, 130.2, 1287, 125.8, 124.3, 117.1, 114.1, 111.4, 99.9, 88.1, 55.3, 33.8, 31.3 ppm.

HRMS (APCI, MeOH, –): m/z = calculated for $C_{66}H_{53}BN_6O_8$ $[M]^+$ 1066.3898; found 1066.3981.

FT-IR (ATR): ν = 2955, 2927, 2837, 2543, 1690, 1604, 1572, 1516, 1453, 1388, 1293, 1205, 1175, 1106, 1029, 832, 730, 577 cm^{-1}.

UV/Vis ($CHCl_3$): λ (log ε/dm^3 mol^{-1} cm^{-1}) = 272 (4.7), 312 (sh), 445 (4.6), 571 (4.5) nm.

Fluorescence ($CHCl_3$): λ_{ex} = 520 nm; λ_{em} = 623 nm.

General procedure for the synthesis of dyes 50-52

In an oven-dried 10 mL round-bottom flask was charged with formyl-SubPz **54**, **55** or **56** (30 μmol), cyanoacetic acid (43.4 mg, 510 μmol) and $AcNH_4$ (17.6 mg, 228 μmol) under argon atmosphere. Then, the solid mixture was dissolved with dry toluene. The resulting reaction mixture was heated at 80 ºC for 25 h under argon atmosphere. After cooled at room temperature, the reaction was concentrated under reduced pressure, and the residue was taken up in ethyl acetate. The organic layer was washed with 1M HCl three times and dried over anhydrous $MgSO_4$. After filtration and evaporation, the solid residue was purified by silica gel column chromatography.

4'-*tert*-Butylphenoxy[2,3,7,12,13-penta(phenyl)-8-(4''-ethynylphenylcyanoacrylic acid) subporphyrazinato]boron(III) (50)

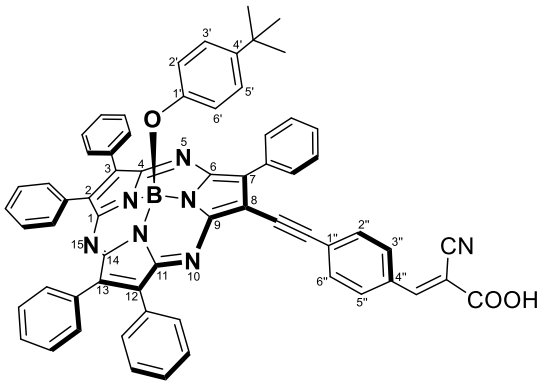

The residue was purified by silica gel column chromatography (hexanes/CH_2Cl_2/ethyl acetate/MeOH 3.5 : 3.5 : 2 :1). The product was obtained as a red solid (17.5 mg, 60%).

^{1}H NMR (400 MHz, DMSO-d_6): δ = 8.70 (d, J = 8.0 Hz, 2H; $H^{2''',6'''}$), 8.02 (m, 7H; Ph-H), 7.91 (d, J = 8.0 Hz, 2H; $H^{3'',5''}$), 7.73 (m, 11H; Ph-H), 7.53 (m, 7H; Ph-H), 6.87 (d, J = 8.0 Hz, 2H; $^{3',5'}$), 5.31 (d, J = 8.0 Hz, 2H; $H^{2',6'}$), 1.06 ppm (s, 9H; *t*-Bu).

^{13}C NMR (100.6 MHz, DMSO-d_6): δ = 159.1, 158.3, 158.1, 157.9, 156.2, 151.2, 133.9, 132.9, 132.1, 132.0, 131.8, 130.8, 129.9, 129.5, 126.6, 119.8, 118.0, 46.6, 34.5, 32.1 ppm.

MS (MALDI-TOF, DCTB): m/z = 969.4 [M]$^+$; 819.3 [M – OPhtBu]$^+$

FT-IR (ATR): ν = 3462, 3054, 3033, 2956, 2924, 2852, 2218, 1690, 1605, 1573, 1454, 1388, 1293, 1251, 1108, 1030, 833, 771, 533 cm^{-1}.

UV/Vis ($CHCl_3$): λ (log ε/dm^3 mol^{-1} cm^{-1}) = 307 (4.6), 352 (4.5), 408 (4.6), 564 (4.8) nm.

Fluorescence ($CHCl_3$): λ_{ex} = 500 nm; λ_{em} = 606 nm.

4'-*tert*-Butylphenoxy[2,3,7,12,13-penta(*p*-*tert*-butylphenyl)-8-(4''-ethynylphenylcyanoacrylic acid) subporphyrazinato]boron(III) (51)

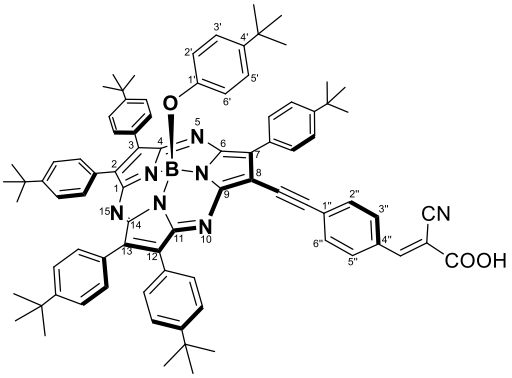

The residue was purified by silica gel column chromatography (hexanes/CH_2Cl_2/ethyl acetate/MeOH 3.5 : 3.5 : 2 :1). The product was obtained as a red solid (30.4 mg, 81%).

^{1}H NMR (400 MHz, DMSO-d_6): δ = 8.69 (d, J = 8.0 Hz, 2H; $H^{2''',6'''}$), 8.02–7.95 (m, 5H; ^{t}BuPh-H), 7.82 (d, J = 8.0 Hz, 2H; $H^{3'',5''}$), 7.76 (m, 6H; ^{t}BuPh-H), 7.67 (d, J = 8.0 Hz, 2H; $H^{2'',6''}$), 7.60–7.50 (m, 7H; ^{t}BuPh-H), 6.85 (d, J = 8.0 Hz, 2H; $^{3',5'}$), 5.28 (d, J = 8.0 Hz, 2H; $H^{2',6'}$), 1.37 (m, 45H; *t*-Bu), 1.05 ppm (s, 9H; *t*-Bu).

^{13}C NMR (100.6 MHz, DMSO-d_6): δ = 157.7, 155.6, 152.5, 151.5, 151.4, 142.6, 132.9, 132.4, 131.8, 130.6, 130.2, 129.6, 128.7, 128.4, 125.7, 125.3, 116.9, 100.31, 34.9, 34.8, 31.4, 31.3, 30.9 ppm.

HRMS (APCI, MeOH, +): m/z = calculated for $C_{84}H_{84}BN_7O_3$ $[M]^+$ 1249.6819; found 1249.6838.

FT-IR (ATR): ν = 3668, 2958, 2924, 2854, 2219, 1721, 1598, 1514, 1457, 1390, 1260, 1182, 1118, 1021, 837, 708, 562 cm^{-1}.

UV/Vis ($CHCl_3$): λ (log ε/dm^3 mol^{-1} cm^{-1}) = 307 (4.6), 355 (sh), 426 (4.7), 570 (4.8) nm.

Fluorescence ($CHCl_3$): λ_{ex} = 520 nm; λ_{em} = 613 nm.

4'-*tert*-Butylphenoxy[2,3,7,12,13-penta(3''-5''-di-*tert*-butylphenyl)-8-(4''-ethynylphenylcyanoacrylic acid) subporphyrazinato]boron(III) (52)

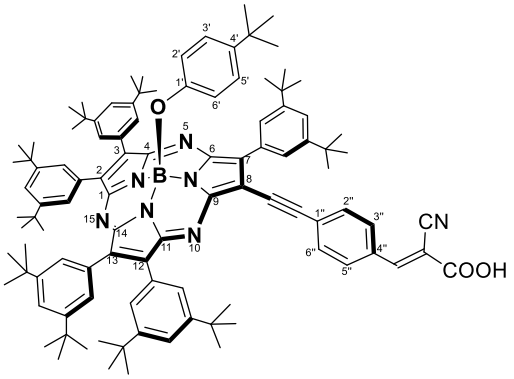

The residue was purified by silica gel column chromatography (hexanes/CH_2Cl_2/ethyl acetate/MeOH 4 :4 : 1.5 :0.5). The product was obtained as a red solid (37.7 mg, 82%).

^{1}H NMR (400 MHz, $CDCl_3$): δ = 8.29 (br s, 2H; $H^{2''',6'''}$), 7.98 (br s, 2H; $H^{3''',5'''}$), 7.72 (d, J = 8.0 Hz, 2H; $H^{3'',5''}$), 7.56 (br s, 2H; ^{t}BuPh-H), 7.43–7.24 (m, 12H; ^{t}BuPh-H), 6.84 (d, J = 8.0 Hz, 2H; $^{3',5'}$), 5.36 (d, J = 8.0 Hz, 2H; $H^{2',6'}$), 1.25–1.03 ppm (m, 99H; *t*-Bu).

^{13}C NMR (100.6 MHz, $CDCl_3$): δ = 157.2, 156.9, 150.8, 150.7, 150.5, 150.3, 132.6, 130.9, 125.7, 125.2, 122.1, 117.2, 98.2, 87.4, 34.9, 34.7, 33.8, 31.5, 31.4, 31.2 ppm.

MS (MALDI-TOF, DCTB): m/z = 1530.0 $[M]^+$; 1379.9 $[M - OPhtBu]^+$

FT-IR (ATR): ν = 3548, 2959, 2904, 2867, 2219, 1628, 1593, 1513, 1466, 1392, 1290, 1201, 1038, 880, 710, 640, 585 cm^{-1}.

UV/Vis ($CHCl_3$): λ (log ε/dm^3 mol^{-1} cm^{-1}) = 307 (4.7), 355(sh), 414 (4.6), 560 (4.7) nm.

Fluorescence ($CHCl_3$): λ_{ex} = 500 nm; λ_{em} = 601 nm.

3.5.4 Activating Intramolecular Singlet Fission on SubPz-Pnc$_2$ conjugate

4-Formylphenoxy[2,3,7,8,12,13-hexa(propylthio)subporphyrazinato]boron(III) (61)

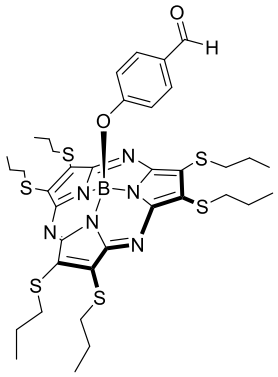

Prepared according to the general procedure for hexasulfanyl-SubPz **2b** (chapter 1); in the first step was used bis(propylthio)maleonitrile **1b** (452 mg, 2.0 mmol), 1.0 M solution of BCl3 in p-xylene (2.0 mL, 2.0 mmol), 4-hydroxybenzaldehyde (1.5 g, 12.0 mmol) and dry toluene (4 mL). In the second step without purification, was employed propanethiol (35 μL), Et_3N (45 μL), and DMI (25 mL). The crude product was chromatographed on silica gel (mixture of n-hexane/ethyl acetate 7:3) giving pure compound **47** (64.9 mg, 12%) as a red viscous solid.

^{1}H NMR (400 MHz, $CDCl_3$): δ = 9.69 (s, 1H; C*H*O), 7.37 (d, J = 8.0 Hz, 2H; $H^{3',5'}$), 5.43 (d, J = 8.0 Hz, 2H; $H^{2',6'}$), 4.04 (m, 6H; -S*CH$_2$*Et), 3.61 (m, 6H; -S*CH$_2$*Et), 1.96 (m, 12H; -SCH$_2$*CH$_2$*CH$_3$), 1.17 ppm (t, J = 7.2 Hz, 18H; -SCH$_2$CH$_2$*CH$_3$*).

^{13}C NMR (100.6 MHz, $CDCl_3$): δ = 190.6, 158.8, 154.1, 132.0, 131.1, 130.2,119.4, 36.9, 23.7, 13.5 ppm.

MS (MALDI-TOF, DCTB): m/z = 809.2 [M]$^+$; 688.1 [M – OPhtBu]$^+$

HRMS (APCI, MeOH, +): m/z = calculated for $C_{37}H_{47}BN_6O_2S_6$ [M]$^+$ 809.2209; found 809.2253.

FT-IR (ATR): ν = 2960.7, 2929, 2870, 2727, 1695, 1597, 1573, 1477, 1450, 1287, 1235, 1172, 1119, 1001 S*, 895, 838, 749, 579 cm^{-1}.

4-Formylphenoxy[2,3,7,8,12,13-hexa(3'',4'',5''-trimethoxyphenyl))subporphyrazinato]boron(III) (62)

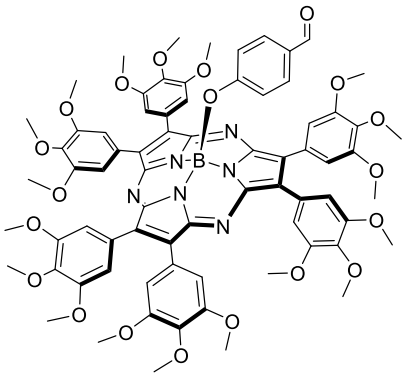

Prepared according to the general procedure for Liebeskind-Srogl cross-coupling of SubPzs (chapter 1); hexa(propylthio)subporphyrazine **61** (47 mg, 58 μmol), boronic acid **4f** (221 mg, 1.6 mmol), $Pd(PPh_3)_4$ (40 mg, 60 %mol) and CuTC (198 mg, 1.0 mmol) were added into the flask and purged with argon for 10 min, followed by the addition of anhydrous THF (5 mL) *via cannula*. The reaction mixture was stirred at 60 °C for 20 h under argon atmosphere, cooled to room temperature and passed through a short silica gel column using THF as eluent. The solvent was removed and the residue was purified by silica gel column chromatography (mixture of n-hexane/ethyl acetate/THF 4:5.6:0.4) giving pure compound **62** (28.5 mg, 36%) as a purple solid.

^{1}H NMR (400 MHz, $CDCl_3$): δ = 9.68 (s, 1H; C*H*O), 7.43 (d, J = 8.0 Hz, 2H; $H^{3',5'}$), 7.15 (s, 12H; Ar-H), 5.55 (d, J = 8.0 Hz, 2H; $H^{2',6'}$), 3.92 (s, 18H; $OMe^{4''}$), 3.62 ppm (s, 36H; $OMe^{3'',5''}$).

^{13}C NMR (100.6 MHz, $CDCl_3$): δ = 190.6, 159.1, 156.8, 153.2, 138.7, 133.3, 132.0, 131.9, 131.5, 129.8, 128.5, 128.4, 126.7, 118.4, 108.6, 61.0, 56.0 ppm

4-(Hydroxymethyl)phenoxy[2,3,7,8,12,13-hexa(3'',4'',5''-trimethoxyphenyl))subporphyrazinato]boron(III) (59)

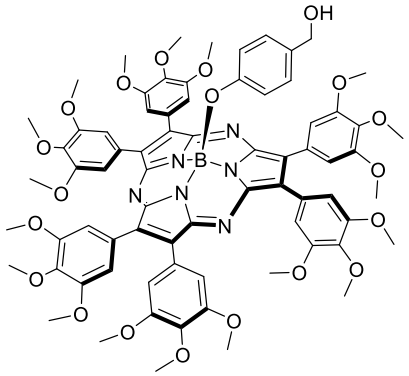

In an oven-dried 5 mL round-bottom flask was charged with formyl-SubPz **62** (17.8 mg, 13 μmol), $NaBH_4$ (1.0 mg, 26 μmol) and CH_2Cl_2 (3 mL) under argon atmosphere. The solution was stirred at 0 °C for 5 min in the dark and MeOH (1.5 mL) was added dropwise. The resulting mixture was stirred for 20 min at 0 °C and quenched by the addition of water (5 mL). The product was extracted with ethyl acetate, washed with brine and dried over anhydrous $MgSO_4$. After filtration and evaporation, the solid residue was purified by silica gel column chromatography (mixture of n-hexane/ethyl acetate/THF 4:5.6:0.4) giving pure compound **59** (13.5 mg, 76%) as a garnet solid.

^{1}H NMR (400 MHz, $CDCl_3$): δ = 7.14 (s, 12H; Ar-H), 6.88 (d, J = 8.0 Hz, 2H; $H^{3',5'}$),5.50 (d, J = 8.0 Hz, 2H; $H^{2',6'}$), 4.42 (s, 2H; CH_2OH), 3.91 (s, 18H; $OMe^{4''}$), 3.62 ppm (s, 36H; $OMe^{3'',5''}$).

^{13}C NMR (100.6 MHz, $CDCl_3$): δ = 156.8, 153.2,152.7, 138.6, 133.3, 133.1, 128.2, 126.9, 118.5, 108.6, 64.8, 60.1, 56.0 ppm

MS (MALDI-TOF, DCTB): m/z = 1363.5 $[M]^+$; 1240.5 $[M - OPhtBu]^+$

HRMS (APCI, MeOH, +): m/z = calculated for $C_{73}H_{73}BN_6O_{20}$ $[M]^+$ 1363.5004; found 1363.4943.

FT-IR (ATR): ν = 3529, 2998, 2926, 2853, 1738, 1672, 1579, 1510, 1477, 1450, 1287, 1235, 1125 S*, 1008, 923, 870, 843, 717 cm^{-1}.

UV/Vis ($CHCl_3$): λ (log ε/dm^3 mol^{-1} cm^{-1}) = 282 (4.8), 446 (4.5), 557 (4.7) nm.

Fluorescence ($CHCl_3$): λ_{ex} = 500 nm; λ_{em} = 672 nm.

SubPz-Pnc$_2$ triad (58)

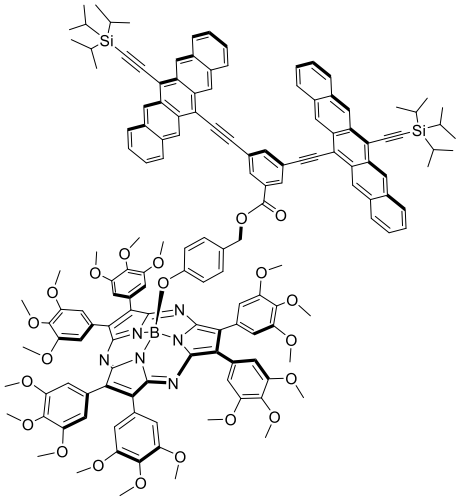

To a solution of hydroxy-SubPz **59** (8.0 mg, 6.4 μmol), Pnc_2-COOH (21.0 mg, 13 μmol), DMAP (0.4 mg, 1.29 μmol) in deoxygenated THF (2 mL), EDC (4.0 mg, 26 μmol) was added under argon atmosphere at 0 ºC, and the reaction mixture was stirred at 0 ºC for 1 h. The mixture was allowed to reach room temperature and kept under stirring overnight. Once the reaction is completed (monotorized by TLC), the solvent was evaporated under reduced pressure, and the residue was passed through a pad of silica gel using a mixture of hexanes/AcOEt/THF (2:6:2). Then, the solvent was evaporated and the residue was purified by column chromatography on Bio-BeadsTM S-X1 (200-400 mesh) using chloroform as the eluent, to give the target material as a dark violet solid (2.8 mg, 9%).

^{1}H NMR (400 MHz, $CDCl_3$): δ = 9.31 (s, 4H) 9.25 (s, 4H), 8.51 (s, 2H), 8.03 (d, *J* = 8.0 Hz, 4H), 7.97 (d, *J* = 8.0 Hz, 4H), 7.44–7.35 (m, 8H), 7.13 (d, *J* = 8.0 Hz, 2H), 7.12 (s, 12H), 5.58 (d, *J* = 8.0 Hz, 2H), 5.29 (s, 2H), 3.88 (s, 18H'), 3.57 (s, 36H), 1.43–.139 ppm (m, 42H).

^{13}C NMR (100.6 MHz, $CDCl_3$): δ = 156.9, 153.2, 138.6, 133.1, 132.3, 130.5, 130.3, 129.8, 128.7, 128.6, 126.8, 126.3, 126.2, 108.6, 61.0, 55.9, 19.0, 11.7 ppm

HRMS (MALDI-TOF, DCTB): m/z = calculated for $C_{150}H_{141}BN_6O_{21}Si_2$ $[M]^+$ 2427.9812; found 2427.9797.

FT-IR (ATR): ν = 2930, 2860, 2128, 1726, 1580, 1510, 1461, 1390, 1313, 1240, 1177, 1011, 875, 842 cm^{-1}.

UV/Vis ($CHCl_3$): λ (log $\varepsilon/dm^3\ mol^{-1}\ cm^{-1}$) = 351 (4.7), 372 (4.7), 440 (4.6), 558 (4.7), 602 (4.5), 660 (4.7) nm.

Fluorescence ($CHCl_3$): λ_{ex} = 540 nm; λ_{em} = 674 nm.

RESUMEN Y CONCLUSIONES

La presente Tesis Doctoral titulada "**Synthesis and Characterization of Subporphyrazines and Subnaphthalocyanines: Optical Properties and Applications in Molecular Photovoltaics**" tiene como objetivo general el desarrollo de diferentes metodologías sintéticas para la preparación de nuevos materiales moleculares basados en subporfirazinas (SubPzs) y subnaftalocianinas (SubNc) como moléculas fronterizas de las bien estudiadas y exploradas subftalocianinas (SubPcs). Esta familia de compuestos, pertenecientes a sistemas porfirínicos contraídos, se presentan como competidores potenciales en varios campos emergentes de la física, lo que significa que la exploración y explotación en la química de estos derivados es una tarea necesaria para satisfacer los requerimientos impuestos por estas posibles aplicaciones.

El primer capítulo de esta tesis se centra en el desarrollo de estrategias sintéticas para extender la deslocalización del sistema electrónico π de la subporfirazina a través de sustituyentes periféricos conjugados. El cromóforo subporfirazínico se funcionaliza con seis unidades de oligofenilenos y vinilenos, como una vía de modular sus propiedades ópticas y redox. La estrategia sintética empleada se basa en reacciones de acoplamiento Liebeskind-Srogl de SubPzs hexasulfuradas, con derivados de ácidos borónicos (Esquema 1).

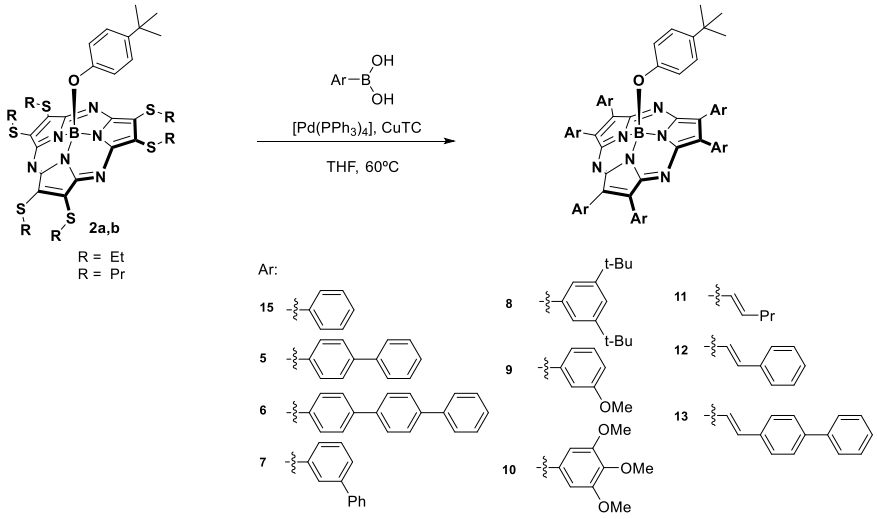

Esquema 1. Síntesis de SubPzs hexafeniladas y hexaviniladas.

Dentro de la serie de SubPzs hexaariladas, los macrociclos *para*-sustituidos con unidades éter o anillos bencénicos muestran un desplazamiento hacia al rojo de las bandas de absorción y emisión. La deslocalización electrónica sobre los fenilos terminales de los sustituyentes periféricos es cada vez menos eficiente a medida que se extiende la longitud de las unidades oligofenileno de uno a tres anillos bencénicos, En contraste, los derivados *meta*-sustituidos sólo producen una ligera perturbación del estado fundamental, aunque su influencia es mayor en el estado excitado. Así, las bandas Q se mantienen inalteradas o se desplazan hacia el azul, mientras que se producen desplazamientos batocrómicos de las bandas de fluorescencia (Figura 1).

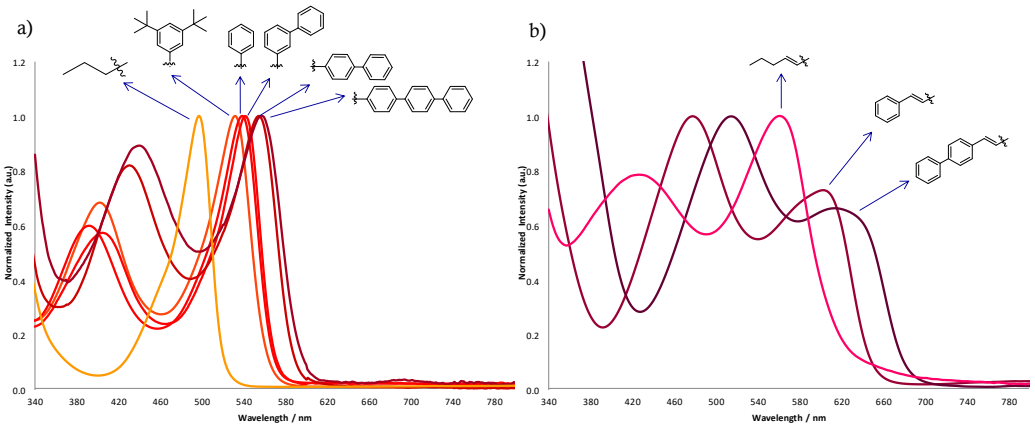

Figura 1. Espectros de absorción UV-Vis de las bandas Q normalizadas en $CHCl_3$ para: (a) Serie SubPzs hexaarilada y (b) serie SubPz hexaviniladas.

Se han llevado a cabo estudios teóricos por DFT y las predicciones concuerdan con los resultados experimentales, de manera que la perturbación de los orbitales HOMO del macrociclo es más significativa cuando los sustituyentes de los grupos arilo periféricos se incorporan en la posición *para*.

Las SubPzs hexasustituidas con unidades vinileno en la periferia presentan una configuración coplanaria de estos sustituyentes con respecto al núcleo aromático de la SubPz. Esto permite una buena comunicación electrónica del macrociclo con otros sistemas enlazados a través de grupos vinileno periféricos, tales como grupos fenilos o bifenilos.

La naturaleza, número y posición de los sustituyentes periféricos determina la organización de los macrociclos en el estado cristalino, que varía desde apilamientos en columna cabeza-cola, con macrociclos dispuestos en zigzag, o paralelos, a una disposición de los macrociclos de tipo cara a cara.

En el segundo capítulo, se ha llevado a cabo la síntesis y caracterización de una nueva familia de subnaftalocianinas dodecafuncionalizadas periféricamente. Con el objetivo de obtener SubNcs sustituidas simétricamente, se prepararon precursores 2,3-naftalendicarbonitrilo tetrasustituidos, que contienen distintos tipos de sustitución. Así, se obtuvieron con buenos rendimientos derivados de 2,3-naftalendicarbonitrilo tetrafluorados, tetraclorados y tetrabromados, mediante reacciones de cicloadición seguidas de aromatización. Estos precursores se utilizaron en reacciones de ciclotrimerización, dando lugar a las correspondientes SubNcs, las cuales se han utilizado en reacciones de sustitución nucleofílica aromática, o reacciones de acoplamiento cruzado catalizadas por paladio, generando una serie de macrociclos con propiedades electrónicas variadas (Figura 2).

Los derivados de SubNc sustituidos axialmente con cloro se obtuvieron directamente por reacción de ciclotrimerización de los precursores 2,3-naftalendicarbonitrilos. La sustitución del cloro por grupos fenoxi se llevó a cabo en una segunda etapa través de la formación de un intermedio axial triflato-SubNc.

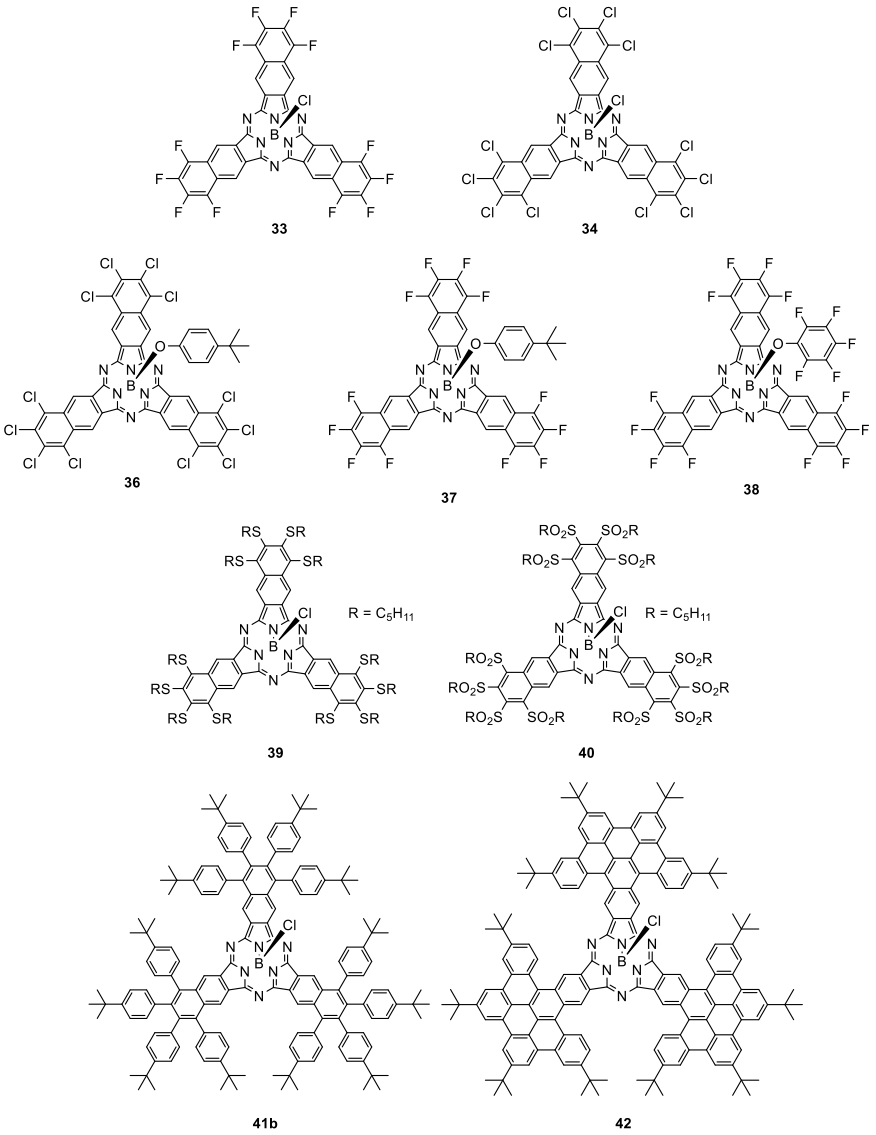

Figura 2. Estructuras químicas de la serie de SubNcs sintetizadas.

Estudios de cristalografía de rayos X muestran la forma cónica que posee el núcleo de las subnaftalocianinas, así como también su tendencia a organizarse en apilamientos columnares al igual que en el caso de las subftalocianinas (Figura 3).

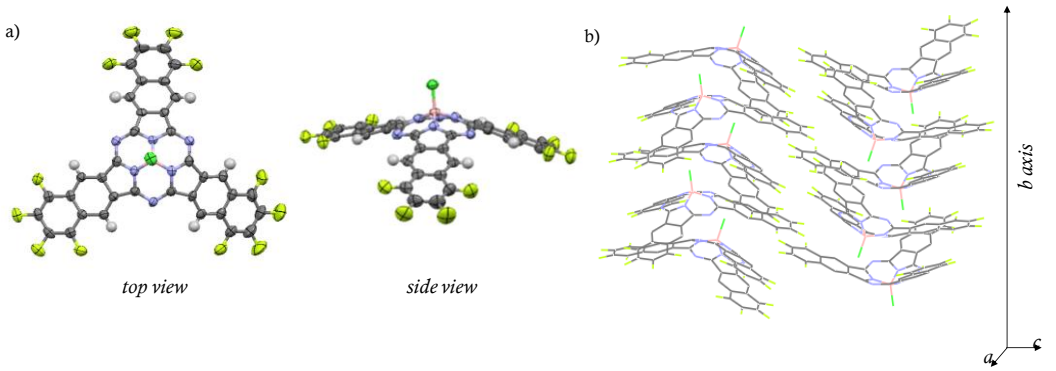

Figura 3. Estructura cristalina de SubNc **33** determinada por difracción de rayos X. (a) Estructura molecular mostrando los elipsoides térmicos a un nivel del 50% de probabilidad. (b) Apilamientos columnares de las estructuras a lo largo del eje *b*.

Se estudiaron las propiedades optoelectrónicas y electroquímicas, así como también los niveles energéticos HOMO/LUMO basados en datos experimentales para toda la serie de SubNcs. Como era de esperar, dependiendo de su funcionalización periférica, estas SubNcs pueden presentar características tanto aceptoras de electrones como dadoras de electrones.

En el tercer capítulo se describen aplicaciones de subporfirazinas y subnaftalocianinas como fotosensibilizadores en células solares orgánicas y fisión de singlete.

Se utilizaron SubNcs con diferentes sustituyentes en posición axial y periférica (SubNc **33**, **34**, **36**, **37** y **40**) por primera vez como materiales aceptores de electrones en células solares poliméricas del tipo de heterounión masiva (BHJ) (Figura 4). La mezcla en el dispositivo con PTB7-Th, un polímero conjugado dador electrónico que presenta un band gap estrecho, produce una respuesta fotovoltaica con contribuciones a la fotocorriente tanto desde el polímero dador, como de las SubNc aceptoras. El máximo valor de eficiencia de conversión de energía solar a energía eléctrica (PCE) fue solamente de un 1.09%. Sus bajas densidades de corriente (Jsc) y fill factor (FF) son el resultado combinado de baja movilidad de carga, transporte de *hole/electron* desequilibrados, y una subóptima morfología en el dispositivo BHJ, contribuyendo con una pérdida de recombinación.

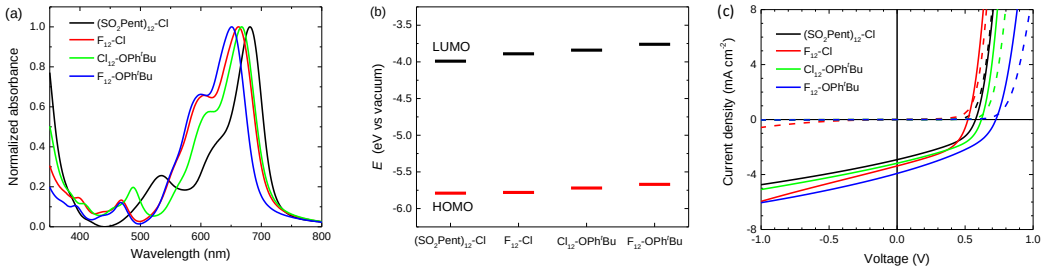

Figura 4. Respuesta óptica de las SubNc en el dispositivo: (a) espectros de absorción óptico, (b) niveles de energías y (c) curvas *J*/*V* de las células basadas SubNc:PTB7-Th en oscuridad (trazos cortos) y bajo iluminación (líneas continuas).

Además, se llevó a cabo la síntesis y caracterización de las propiedades ópticas y electroquímicas de una familia de subporfirazinas funcionalizadas periféricamente con unidades conjugadas viniléster. Estos derivados se han revelado como buenos aceptores de electrones, siendo buenos candidatos para su aplicación células solares del tipo BHJ, como agentes sensibilizadores activos (Figura 5).

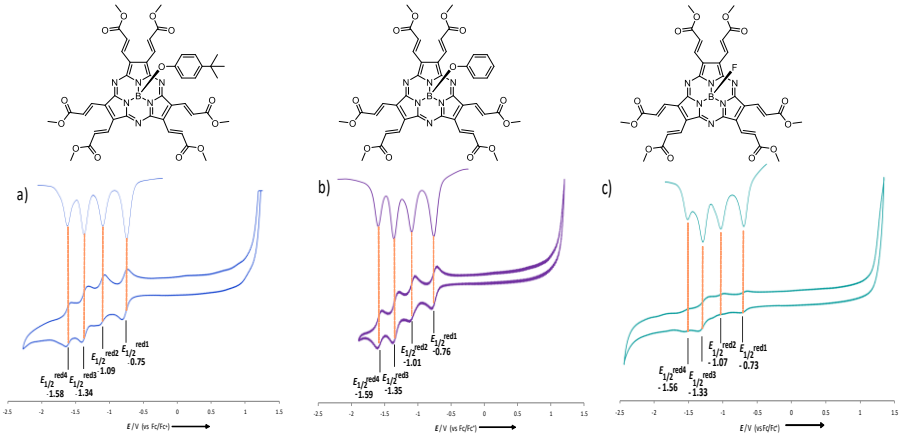

Figura 5. Estructuras químicas de la serie hexaviniléster-SubPz y sus respectivos ciclovoltagramas y SWV vs Fc/Fc^+, mostrando cuatro procesos reversibles de reducción en el rango de -0.5 to -1.6 V.

Por otro lado, se ha llevado a cabo la síntesis, caracterización y estudio de nuevos fotosensibilizadores para DSSCs basados en subporfirazinas. Primero se preparó un precursor de subporfirazina conteniendo un átomo de cloro y cinco sustituyentes tioéter en la periferia. Se incorporó un grupo de anclaje espaciado por un triple enlace

mediante reacción de acoplamiento de Sonogashira. En una segunda etapa, se empleó la metodología desarrollada en el primer capítulo, y se sustituyeron las 5 posiciones periféricas restantes con grupos arilo que dotasen a la SubPz de propiedades dadoras de electrones (Figura 6). La nueva familia de derivados de subporfirazinas se exploraron por primera vez como componentes de células solares de tipo Grätzel (DSSC's). Dadas las bajas eficiencias fotovoltaicas obtenidas, probablemente debidas a las energías de sus orbitales LUMO demasiado bajas para inyectar eficientemente en el TiO_2, se procedió al dopaje del material semiconductor, como una vía para la disminución de la energía de su banda de conducción, ajustándose más al nivel del LUMO del fotosensibilizador. En este caso la fotorespuesta fue mejor.

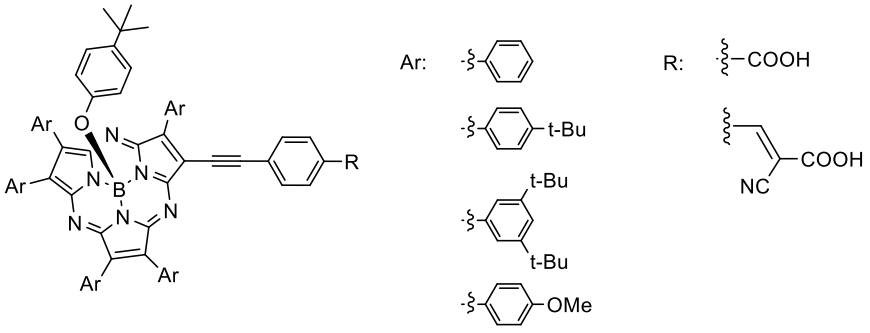

Figura 6. Serie de subporfirazinas aplicadas en DSSC's como sistemas fotosensibilizadores.

Por último, se diseñó, sintetizó y caracterizó una tríada formada por una subporfirazina y una unidad de bispentaceno (SubPz-Pnc2), unidos a través de la posición axial de la SubPz mediante una función éster. Este sistema molecular presenta una absorción pancromática sinérgica, de manera que la SubPz puede actuar como una antena luminosa, y transferir energía (FRET) de manera unidireccional hacia uno de los pentacenos, desencadenando así un proceso de fisión de singlete (Figura 7).

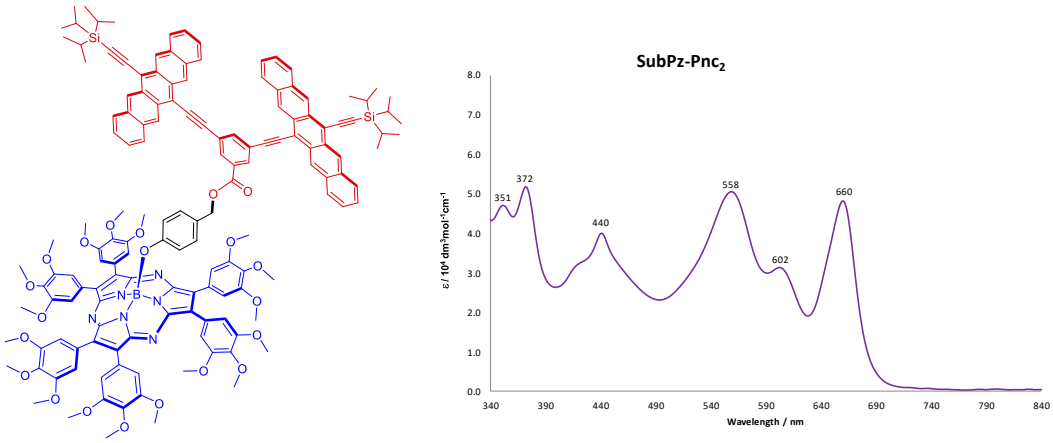

Figura 7. Sistema tríada SubPz-Pnc_2 y su espectro de absorción UV/Vis en $CHCl_3$.